1118

TRANSPORTATION RESEARCH RECORD

Bridge Needs, Design, and Performance

TRANSPORTATION RESEARCH BOARD
NATIONAL RESEARCH COUNCIL
WASHINGTON, D.C. 1987

Transportation Research Record 1118
Price $13.00
Typesetting and Layout: Joan G. Zubal

modes
1 highway transportation
3 rail transportation

subject areas
25 structures design and performance
34 general materials

Transportation Research Board publications are available by ordering directly from TRB. They may also be obtained on a regular basis through organizational or individual affiliation with TRB; affiliates or library subscribers are eligible for substantial discounts. For further information, write to the Transportation Research Board, National Research Council, 2101 Constitution Avenue, N.W., Washington, D.C. 20418.

Printed in the United States of America

Library of Congress Cataloging-in-Publication Data
National Research Council. Transportation Research Board.

Bridge needs, design, and performance.

p. cm.—(Transportation research record, ISSN 0361-1981 ; 1118)
Reports presented at TRB's 1987 Annual Meeting in Washington, D.C.
1. Bridges—Maintenance and repair—Congresses. I. National Research Council (U.S.). Transportation Research Board. Meeting (66th : 1987 : Washington, D.C.) II. Series.
TE7.H5 no. 1118
[TG315]
380.5 s—dc 19
[624'.28] 87-30169
CIP

Sponsorship of Transportation Research Record 1118

GROUP 2—DESIGN AND CONSTRUCTION OF TRANSPORTATION FACILITIES
John M. Hanson, WISS Janney, Elstner & Associates Inc., chairman

Structures Section

Committee on General Structures
Clellon Lewis Loveall, Tennessee Department of Transportation, chairman
John J. Ahlskog, Dan S. Bechly, Neal H. Bettigole, Edwin G. Burdette, Martin P. Burke, Jr., Fernando E. Fagundo, Dah Fwu Fine, Richard S. Fountain, Frederick Gottemoeller, J. Leroy Hulsey, Walter J. Jestings, Robert N. Kamp, John M. Kulicki, Andrew Lally, Richard M. McClure, Roy L. Mion, Andrew E. N. Osborn, Kantilal R. Patel, William J. Rogers, David R. Schelling, Arunprakash M. Shirole, Stanley W. Woods

Committee on Steel Bridges
Albert D. M. Lewis, Purdue University, chairman
Pedro Albrecht, Chester F. Comstock, William F. Crozier, Harry B. Cundiff, David A. Dock, Jackson L. Durkee, Nicholas M. Engelman, John W. Fisher, Louis A. Garrido, Geerhard Haaijer, Theodore H. Karasopoulos, Abba G. Lichtenstein, Joseph M. McCabe, Jr., W.H. Munse, Charles W. Roeder, Robert H. Scanlan, Frank D. Sears, Charles Seim, Stephen R. Simco, Frederick H. Sterbenz, Carl E. Thunman, Jr., Carl C. Ulstrup, Stanley W. Woods, Chris S. C. Yij

Committee on Concrete Bridges
Robert C. Cassano, California Department of Transportation, chairman
Craig A. Ballinger, John A. Belvedere, Ronald A. Brechler, Stephen L. Bunnell, John H. Clark, W. Gene Corley, C.S. Gloyd, Allan C. Harwood, H. Henrie Henson, James J. Hill, Ti Huang, Roy A. Imbsen, H. Hubert Janssen, Heinz P. Koretzky, John M. Kulicki, R. Shankar Nair, Walter Podolny, Jr., Alex C. Scordelis, Frieder Seible, John F. Stanton, Adrianus Vankampen, Julius F. J. Volgyi, Jr., Donald J. Ward, W. Jack Wilkes

GROUP 3—OPERATION, SAFETY, AND MAINTENANCE OF TRANSPORTATION FACILITIES
James I. Taylor, University of Notre Dame, chairman

Maintenance Section

Committee on Sealants and Fillers for Joints and Cracks
Egons Tons, University of Michigan, chairman
Chris Seibel, Jr., Consulting Engineer, secretary
Craig A. Ballinger, Delmont D. Brown, John W. Bugler, Martin P. Burke, Jr., William T. Burt III, Robert A. Cameron, Robert L. Carper, John P. Cook, Frank D. Gaus, C. W. Heckathorn, Jerome M. Klosowski, Starr D. Kohn, T. J. Larsen, Arthur A. Linfante, Jr., Louis G. O'Brien, Roger C. Olson, William G. Prince, Guy S. Puccio, Anthony L. Shloss, Charles V. Slavis, J.B. Thornton, Ronald J. Watson

George W. Ring III and Adrian G. Clary, Transportation Research Board staff

Sponsorship is indicated by a footnote at the end of each paper. The organizational units, officers, and members are as of December 31, 1986.

NOTICE: The Transportation Research Board does not endorse products or manufacturers. Trade and manufacturers' names appear in this Record because they are considered essential to its object.

Transportation Research Record 1118

The **Transportation Research Record** series consists of collections of papers on a given subject. Most of the papers in a Transportation Research Record were originally prepared for presentation at a TRB Annual Meeting. All papers (both Annual Meeting papers and those submitted solely for publication) have been reviewed and accepted for publication by TRB's peer review process according to procedures approved by a Report Review Committee consisting of members of the National Academy of Sciences, the National Academy of Engineering, and the Institute of Medicine.

The views expressed in these papers are those of the authors and do not necessarily reflect those of the sponsoring committee, the Transportation Research Board, the National Research Council, or the sponsors of TRB activities.

Transportation Research Records are issued irregularly; approximately 50 are released each year. Each is classified according to the modes and subject areas dealt with in the individual papers it contains. TRB publications are available on direct order from TRB, or they may be obtained on a regular basis through organizational or individual affiliation with TRB. Affiliates or library subscribers are eligible for substantial discounts. For further information, write to the Transportation Research Board, National Research Council, 2101 Constitution Avenue, N.W., Washington, D.C. 20418.

Contents

Foreword

This Record contains 14 papers related to design, needs, and performance of bridges. Two papers report on evaluations of expansion joints, four papers on fiber-reinforced resin structural elements. Topics of the remaining eight papers range from bridge design and fatigue behavior to bridge strengthening needs and techniques.

In his paper, Dunker examines recommendations for improvements by the inspectors of 15 bridge types in the National Bridge Inventory and responses to a questionnaire to identify bridge strengthening needs sent to FHWA field offices, state departments of transportation, and other agencies. An inspection of Iowa load-restricted bridges supported the conclusion that many steel-stringer, steel-truss bridges were in average-to-good condition and were good candidates for strengthening rather than reconstruction.

Tiberio et al. document preliminary findings and recommendations as well as the development status of research to design a software system capable of performing computer-aided design and drafting (CADD) of certain simple-span bridges. The study involved the interfacing of new or existing analytical computer programs with computer-aided graphics display technology. The software design required evaluation of existing analytical programs as well as state-of-the-art applications of CADD in bridge designs.

Performance of four types of modular expansion joints, four types of metal-reinforced expansion joints, and nine types of strip seal and armored expansion joints on existing bridges in Pennsylvania was evaluated by Dahir and Mellott. None of the joint systems provided ideal performance, and the study detected serious problems with anchorage systems. As judged by a rating system used by the researchers, some of the joint systems provided better performance than others. Recommendations are provided for obtaining better performance by existing systems.

Zhou and Nowak present a procedure for flexural and torsional analysis of simply supported highway bridges. The structures are modeled as orthotropic plates. A finite difference method is used to calculate the nonlinear bridge responses.

In the paper by Kennedy it is shown that a waffle slab concrete bridge can efficiently provide the required resistance moments in two orthogonal directions through its geometry of cross-section. Results from a feasibility study indicate that a waffle slab bridge *(a)* can be more economical than solid slab and slab-on-girder bridges; and *(b)* can provide excellent access to prestressing cables for inspection and maintenance purposes. Tools are presented for design and analysis of waffle slab bridges for serviceability and ultimate-limit states.

Wesgerber et al. conducted a field study in Ohio that consisted of rating about 316 seals in eight categories, based on visual inspection. Twenty-four different types of sealing systems were included, ranging in age from less than 1 month to 15 years or more. A significant number of seals were not preventing passage of water or intrusion of debris. Few of the rated performance items showed significant correlation with either age or traffic count. Some reasons for poor performance are given in the paper.

Selective stiffening of steel bridges can be used to attract stress away from critical regions, that is, to adjust minor weaknesses, thus reducing the total strengthening requirements. This technique is examined by Dunker et al. for both simple- and continuous-span bridges. Changes in stress range associated with selective stiffening need to be checked for fatigue.

Wagner et al. show that unstiffened web plate at gaps between flanges, connection plates, stiffeners, or gusset plates is susceptible to out-of-plane distortion-induced fatigue cracking. The distortion can be reduced by positive attachment of component parts. This requirement has been incorporated into design specifications.

Keating and Fisher are conducting fatigue tests of welded bridge details in the high-cycle, long-life regime. Large-scale plate girders with coverplate, web attachment, and web stiffener

details are subjected to fatigue loading that simulates actual truck traffic. The test specimens allowed for a detailed study of distortion-induced fatigue cracking at a connection plate web gap detail. Results indicated that the retrofit method of drilled holes at the crack tips was inadequate at high levels of distortion. A summary of proposed revisions to the specifications is given.

The effect of overloads on concrete bridges is discussed by James et al. These overloads induced cracking in the concrete more than that normally expected, and observations indicated that cracking sometimes occurred at tensile stresses below 6 to 7.5 $\times$ $(F_c')^{1/2}$. Increased cracking often resulted in increased deterioration due to corrosion effects. More cracking occurred on steel-supported concrete decks than on prestressed concrete girders.

In his paper, Green notes the advantages in corrosion resistance, electrical nonconductivity, and formability of fiberglass resin composites in structural applications. Design of structural elements with these materials is mainly controlled by their deflection and stability characteristics (i.e., their resistance to buckling and creep). A sample case study is presented of a design application for nonconductive framing for an electronic test facility building.

Preis and Bell describe the development of a fiberglass tendon and anchorage system for use as post-tensioning elements in concrete construction. These elements have been incorporated into a bridge outside of Düsseldorf the performance of which is being monitored.

The design and manufacturing of a glass fiber and vinylester resin composite tanker truck body is described by Plecnik. Structural calculations were performed with the SAP IV finite element program for static analysis and the BOSOR4 finite element program for various buckling conditions. A U.S. Department of Transportation permit was obtained for the composite tanker truck allowing it to transport many different hazardous materials.

In his paper, McCormick describes predicted behavior and measured behavior of the superstructure of a pedestrian bridge fabricated from glass-reinforced plastic under a field load test. The overall structural behavior of the bridge and resistance to handling abuse exceeded expectations.

Bridge Strengthening Needs in the United States

KENNETH F. DUNKER, F. WAYNE KLAIBER, AND WALLACE W. SANDERS, JR.

Large numbers of bridges in the United States are structurally deficient or are nearing the ends of their useful lives. Replacing these bridges in the near future is not economically feasible; therefore, rehabilitation and strengthening techniques are needed to extend the useful lives of bridges. Records from the National Bridge Inventory, responses from questionnaires to bridge engineers and other bridge specialists, and site inspections of load-restricted bridges were used to determine bridge types for which strengthening methods are most urgently needed. Steel stringer, timber stringer, and steel through-truss bridges have a particularly critical need for strengthening, because large numbers of these bridge types, if left unstrengthened, will have to be taken from service or retired in the near future. Other bridge types needing strengthening because of anticipated retirements are concrete slab, concrete tee, concrete stringer, steel girder-floor beam, and concrete deck arch. If strengthening and rehabilitation methods are not developed or made available for these bridge types in the near future, large numbers of bridge replacements will be required.

Many bridges in the United States have reached or are approaching the end of their useful lives. Design lane widths and design and legal loads have increased since most existing bridges were built. Since the 1940s, salt and other deicing chemicals have been applied to highways and bridges, and inadequate maintenance funding has led to deterioration of the strength of many bridges. For all of these reasons, the need for large-scale rehabilitation, strengthening, widening, and replacement of bridges has become critical.

In recognition of this problem, AASHTO has sponsored research through the NCHRP. NCHRP Project 12–28(4), "Methods of Strengthening Existing Highway Bridges," was specifically directed toward the strengthening alternative for coping with deficient bridges. A beginning task in the project was to determine which bridge types could be effectively and economically strengthened. For this task, strengthening was viewed as a means to extend the lives of bridges that are in fair to excellent condition but require additional load-carrying capacity to meet current design or legal load specifications.

Ideally, strengthening needs should be determined from a comprehensive bridge management system with consideration of such factors as actual bridge capacity versus required capacity for the route, functional adequacy, and long-term economic planning. Because such a comprehensive system is not available for the entire United States at this time, three approaches were taken to determine which bridge types could be effectively strengthened. The collective experience and expertise of the bridge inspectors who have evaluated the nation's bridges were employed to examine the pertinent data contained in the National Bridge Inventory (NBI), current as of January 23, 1986. Needs perceived by bridge engineers and other bridge specialists in government offices and private consulting practices were solicited in late 1985 by means of a questionnaire, and the responses were tabulated. Site inspections of Iowa bridges, many of which were load restricted, were conducted in 1986. Each of these three approaches will be discussed in the following sections.

Bridge Engineering Center, Department of Civil Engineering, Engineering Research Institute, 416 Town Engineering, Iowa State University, Ames, Iowa 50011.

NATIONAL BRIDGE INVENTORY

Reliability of Bridge Records

The NBI, now essentially complete, contains records on more than 575,000 highway bridges having spans of 20 ft or greater, culverts of bridge length, and tunnels. The records are prepared according to a coding guide *(1)* from the FHWA, which often is supplemented by a guide from state or local authorities such as that of the Iowa Department of Transportation (Iowa DOT) *(2)*.

Each NBI bridge record can contain up to 90 items, some of which may not be used because of local policies or lack of information. Those items judged most relevant and reliable for determining bridge strengthening needs are

- Year built, Item 27;
- Structure type—main, Item 43;
- Superstructure condition rating, Item 59;
- Substructure condition rating, Item 60;
- Estimated remaining life, Item 63;
- Inventory rating, Item 66;
- Structural condition rating, Item 67; and
- Type of work (proposed improvement), Item 75.

These items were further combined to determine bridge life (sum of age in 1985 determined from Item 27, and Item 63) and structural adequacy and safety (the S1 portion of the FHWA sufficiency rating formula, determined from Items 59, 60, and 66).

Questions that need to be asked with regard to such a large database as the NBI are "How reliable are the data?" and "How can interpretation errors be minimized?" A review of the first 50 bridge records from each state or reporting governmental unit showed few obvious coding errors but many blanks, often apparently as a result of state or local policies. In

TABLE 1 FIFTEEN COMMON BRIDGE TYPES, NBI

NBI Item 43	Main Structure Type	Number of Bridges	Percentage of Bridges
302	Steel stringer	130,892	27.2
702	Timber stringer	58,012	12.0
101	Concrete slab	42,450	8.8
402	Continuous steel stringer	36,488	7.6
310	Steel through truss	31,206	6.5
104	Concrete tee	26,798	5.6
502	Prestressed concrete stringer	26,654	5.5
201	Continuous concrete slab	21,958	4.6
102	Concrete stringer	16,884	3.5
505	Prestressed concrete multiple box	16,727	3.5
303	Steel girder-floor beam	9,224	1.9
204	Continuous concrete tee	7,467	1.6
111	Concrete deck arch	6,245	1.3
501	Prestressed concrete slab	5,561	1.2
504	Prestressed concrete tee	4,687	1.0
	Total	441,253	91.8

order to avoid misinterpretations of the bridge records, all computer sort runs were programmed to reject any records containing blanks or unauthorized characters in items to be examined in a particular sort.

Those records containing correctly coded bridge types for Item 43 were examined by means of a matrix with row headings for the design material portion of the type and column headings for the construction design portion of the type. The number of masonry through-trusses, steel slabs, or other unusual or fictitious bridge types in the matrix were less than 1 percent. So that work was done with the most reliable portions of the data, only the 15 most common bridge types were selected as types for further study. Those bridge types are listed and ranked by number of records in the NBI in Table 1. The 15 bridge types represent approximately 92 percent of the more than 481,000 highway bridge records in the NBI. The remainder of the 575,000 NBI records are for tunnels and culverts.

A table prepared for the common bridge types and years built indicated either errors in the coding for some bridges or an inadequacy in the type classification for the NBI. Approximately 5 percent of the prestressed bridges are coded showing year built before the 1950s. Some of the apparent errors may be caused by insertion of 00 when year built was unknown; the category for bridges built in 1900 and earlier accounted for more than an average share of the 5 percent. It is also quite possible that older bridges, which have been recently widened with prestressed concrete or which have had main spans replaced with prestressed concrete, were classified as prestressed concrete structures using original date of construction for the year built. No conclusions could be reached regarding the apparent errors, and those errors could pervade data for all bridge types. The data, therefore, were not screened to eliminate bridges with unusual year built coding.

Overall, the NBI data are relatively free of obvious errors. There are some definite and some probable coding errors, but those errors did not exceed 5 percent and often were less than 1 percent for the NBI items checked. So that the NBI records could be analyzed most accurately, records with obvious errors or with significant omissions were rejected.

Bridge Strengthening Needs

The most direct approach to determining bridge types in need of strengthening from the NBI is to examine Item 75, the improvements recommended by the bridge inspectors. These inspectors' recommendations generally are tempered by local policies, consideration of functional obsolescence, knowledge of funding programs, and knowledge of rehabilitation and strengthening methods. In the 15 common bridge types, inspectors recommended some improvement for more than 49 percent of the bridges. For the bridges for which improvements were recommended, the types of improvements are ranked in Figure 1.

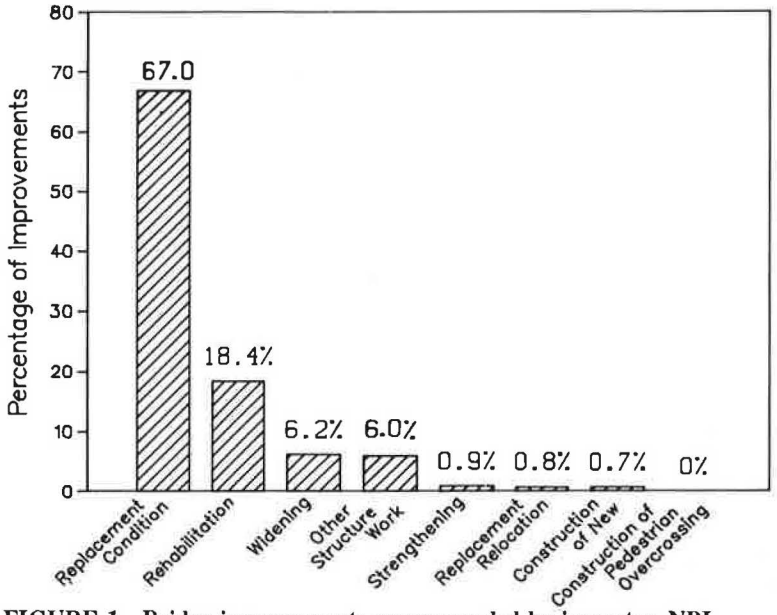

FIGURE 1 Bridge improvements recommended by inspector, NBI.

The overwhelming choice of improvement, accounting for two-thirds of the recommendations, was replacement due to condition, which, of course, means that one-third of the nation's bridges would be replaced in the near future if inspectors' recommendations were followed.

Figure 1 also shows that only 0.9 percent of the recommendations were for strengthening of bridges. There are probably several reasons for the few strengthening recommendations. Some inspectors may not recognize that strengthening is a means to prolong bridge life, and in some states inspectors may not have the option of strengthening. Another possible reason that strengthening is seldom suggested could be the limitations in the NBI coding. An inspector cannot code both strengthening and widening, for example, and instead would be forced to code either replacement or rehabilitation. An additional reason for the large number of replacement recommendations could be the inspectors' intent to make known the urgency of bridge safety problems. Or, perhaps federal and state bridge funding programs are configured in ways that make replacement much more attractive than any type of strengthening or rehabilitation.

For those bridges for which strengthening was recommended, the responses are ranked by number, for bridge types

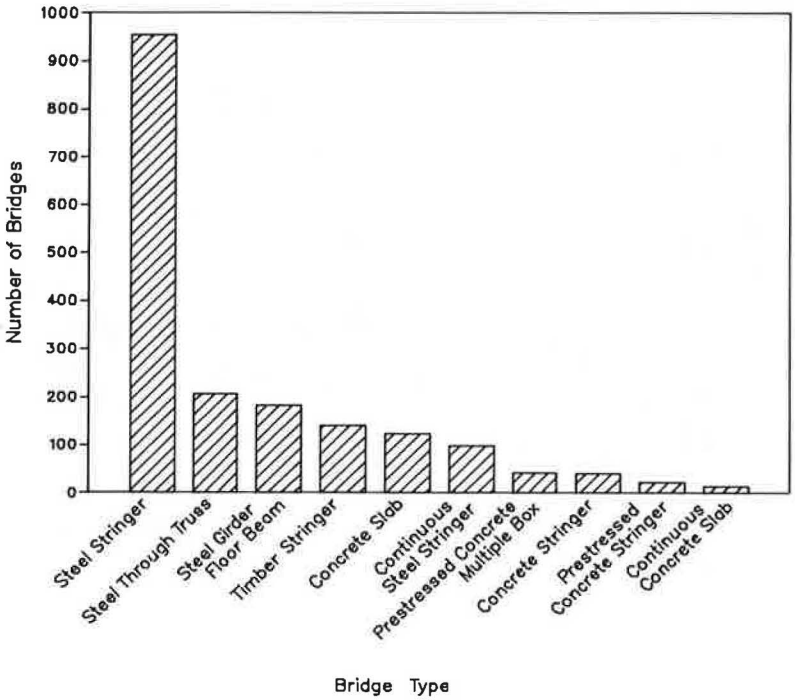

FIGURE 2 Strengthening recommended by inspector, ranked by bridge type, NBI.

in Figure 2. The recommendations for strengthening steel stringer bridges account for more than one-half of the recommendations. The next four bridge types in the ranking are steel through-truss, steel girder-floor beam, timber stringer, and concrete slab.

A less direct approach is to consider the bridge types for which some type of structural work—replacement, rehabilitation, widening, other structure work, and strengthening—was recommended by the inspector. It is quite possible that strengthening could be used instead of replacement or as a part of rehabilitation, widening, or other structure work.

The bridge types for which some type of structural work was recommended are ranked by number of recommendations in Figure 3. If the bridge types ranked in the first five in Figure 3 are compared with the bridge types ranked in the first five in Figure 2, it is apparent that the rankings are similar. Four of the

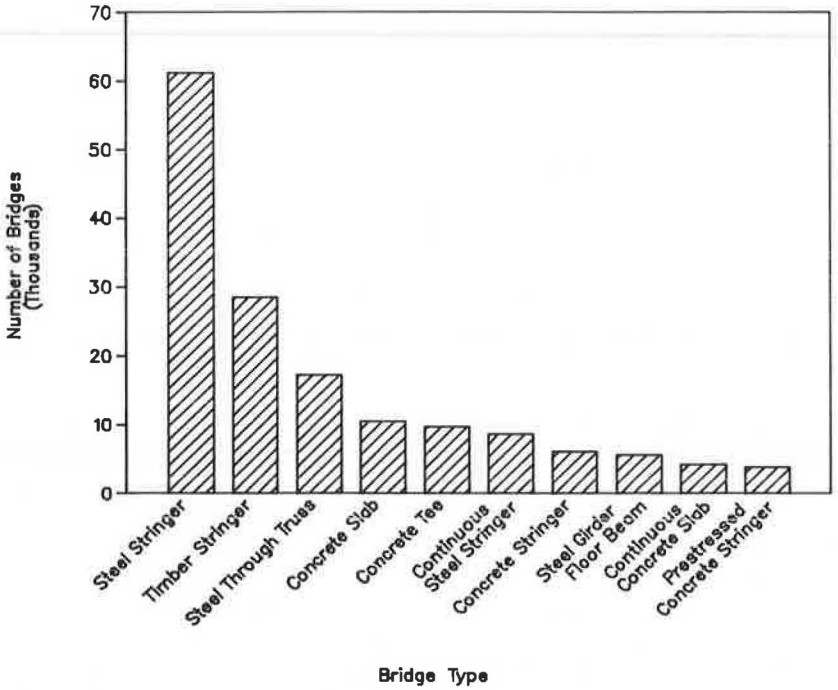

FIGURE 3 Structural work recommended by inspector, ranked by bridge type, NBI.

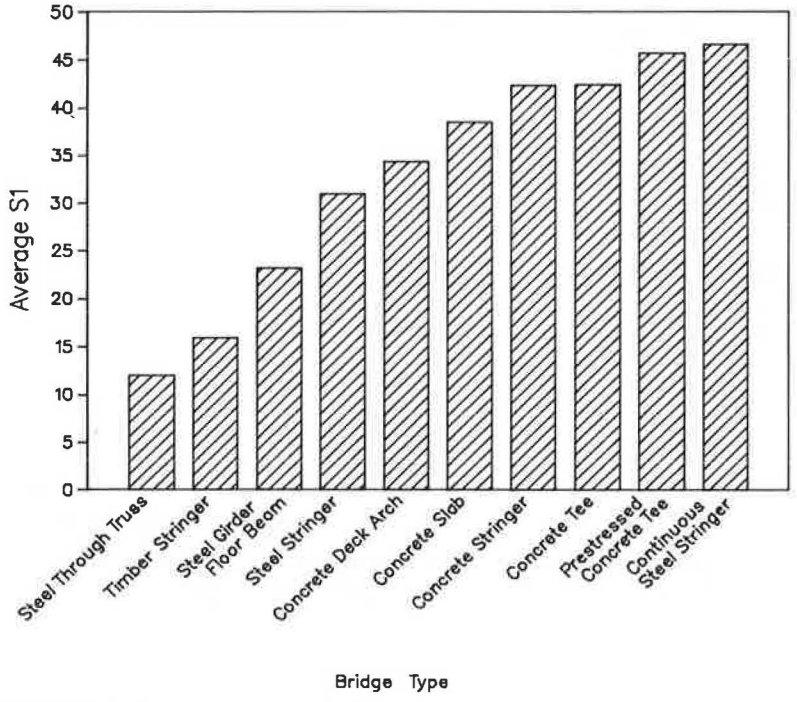

FIGURE 4 Average structural adequacy and safety ranked by bridge type, NBI.

first five in each figure are the same. The steel girder-floor beam type, included in the first five for strengthening, is replaced by the concrete tee type for structural work.

Another approach, which is more general and accounts for almost all of the bridges in the NBI, is to examine the structural adequacy and safety factor (S1) determined from the superstructure condition rating; substructure condition rating and inventory rating, as detailed in the FHWA guide for bridges *(1)*; remaining life; and anticipated retirement; all of which can be obtained directly or by simple computations from the bridge records. If the characteristics of bridges for which inspectors recommended strengthening are compared with the characteristics of average bridges, low structural adequacy and safety often correlate well with a need for strengthening.

The average S1 value then was computed for the 15 common bridge types, and the 10 bridge types with the lowest S1 values,

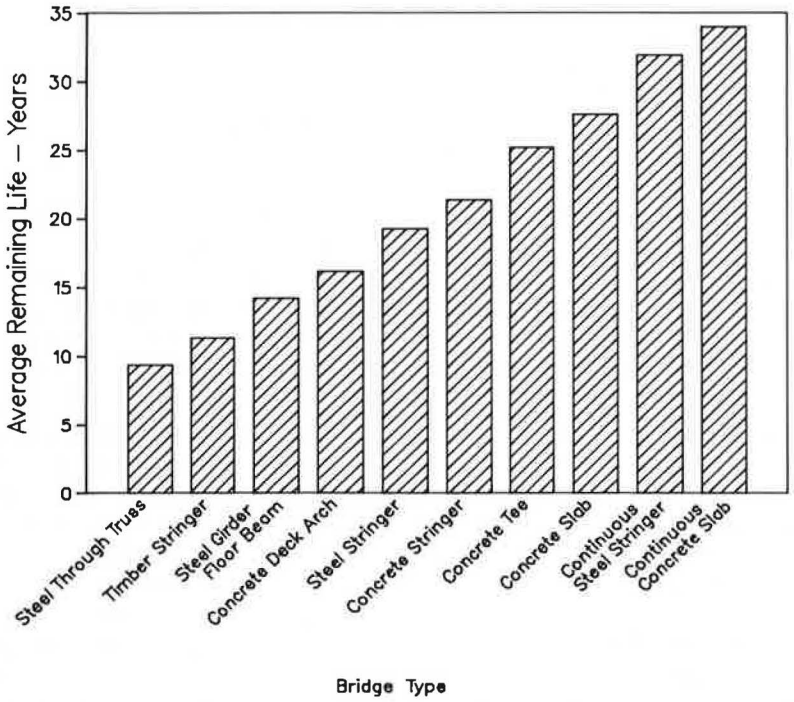

FIGURE 5 Average remaining life ranked by bridge type, NBI.

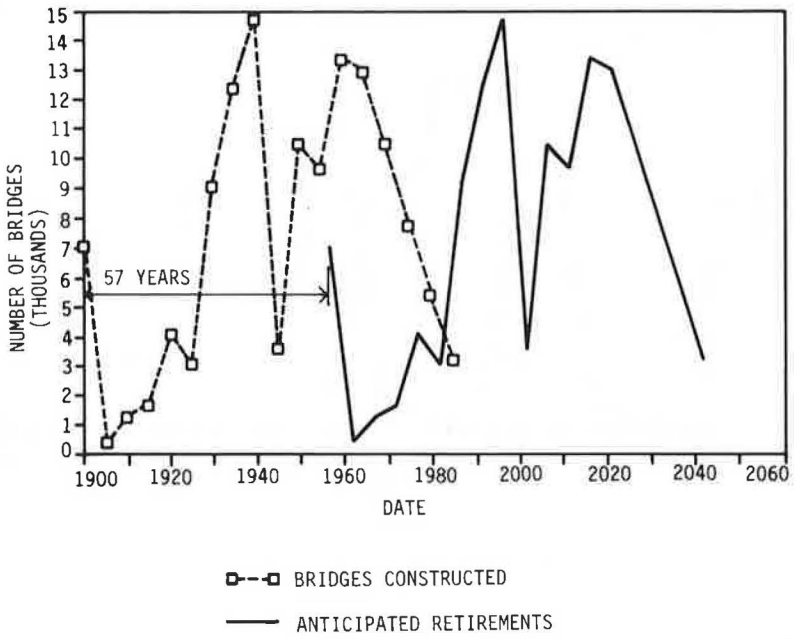

FIGURE 6 Numbers of steel stringer bridges constructed, and anticipated retirements by 5-year periods, NBI.

which indicate low-strength bridges, are ranked in Figure 4. The first five rankings based on S1 are similar to those in Figures 2 and 3 and are identical to those for structural condition, Item 67. The only new type in the first five is the concrete deck arch type.

Remaining life also can give some evidence of need for strengthening. Those bridge types for which inspectors estimated a relatively low remaining life are often candidates for strengthening. The average remaining lives are ranked for 10 bridge types in Figure 5. No bridge types different from those identified in previous figures appear in the first five rankings.

Either specific inspector recommendations or more general measures of the potential needs for strengthening point to the same bridge types. So that some concept of the urgency of the strengthening needs could be developed, the number of anticipated bridge retirements was examined for all of the 15 common bridge types.

In Figures 6–8, the numbers of bridges constructed in each 5-year period are plotted for steel stringer, timber stringer, and steel through-truss bridges, respectively. The first point in each figure is for the number of bridges constructed in 1900 or earlier, and the other points are for numbers constructed during 5-year periods such as 1901–1905. The average life was computed from NBI data for each bridge type, and a solid line was plotted in each figure by using the numbers for the construction points but extended into the future by the average life. The solid line in each figure, then, represents anticipated bridge retirements. For those bridge types having large numbers of anticipated retirements in the near future, there is a definite need for effective strengthening methods.

Those bridge types with large numbers of anticipated retirements in the near future, ranked in order by maximum number in any 5-year period, are steel stringer, timber stringer, steel through-truss, concrete slab, concrete tee, concrete stringer, steel girder-floor beam, and concrete deck arch. The graphs for those bridge types are all similar to Figures 6–8, and all show a similar urgency. As of 1985, the number of anticipated retirements is either small with a large projected increase in the near future, or as in Figure 8, the number of anticipated retirements is at a high level that will continue in the near future.

The bridge records in the NBI are quite consistent in identifying steel stringer, timber stringer, and steel through-truss bridge types as the primary types for which strengthening, as a means to prolong bridge life, is required. Secondary needs involve concrete slab, concrete tee, concrete stringer, steel girder-floor beam, and concrete deck arch bridge types.

Questionnaire

The NCHRP project research team *(3)* sent a questionnaire to FHWA offices, state departments of transportation, selected county engineers, selected bridge design consultants, and others considered to have expertise and experience in bridge strengthening. The questionnaire contained a variety of questions relating to the performance and economics of bridge strengthening. Responses to the following question were of interest: "For what types of bridges do you see a need for the development of a design procedure for strengthening?"

The responses are organized and plotted in Figure 9. Because the response format was open (not tied to the NBI), bridge types were not as accurately specified as in the NBI. General responses, which furnish little insight as to bridge type, are omitted from the categories in Figure 9, which gives results similar to those from the NBI. Obviously, many bridge engineers and management personnel see the need for strengthening methods for steel truss, steel stringer, and steel girder-floor beam bridges. Questionnaire respondents generally see less need for strengthening methods for timber and concrete

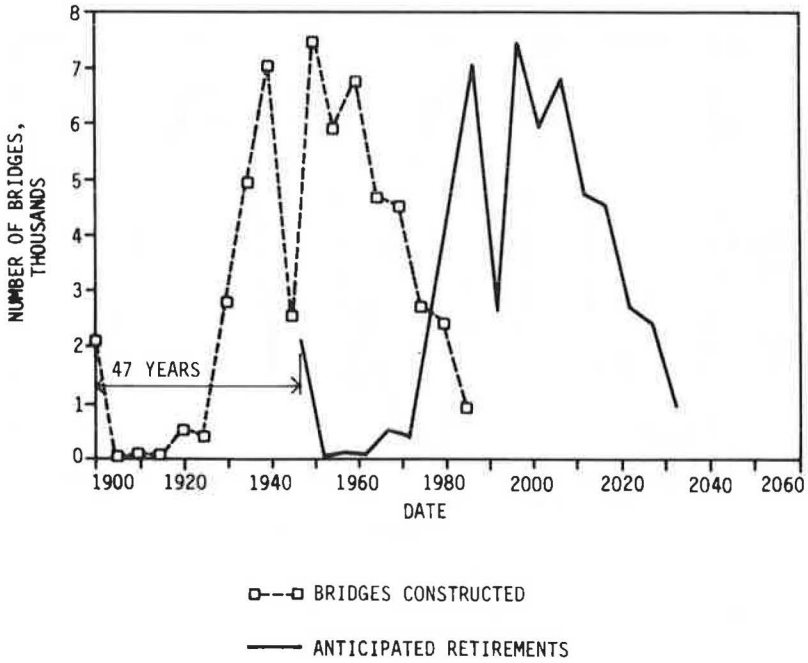

FIGURE 7 Numbers of timber stringer bridges constructed, and anticipated retirements by 5-year periods, NBI.

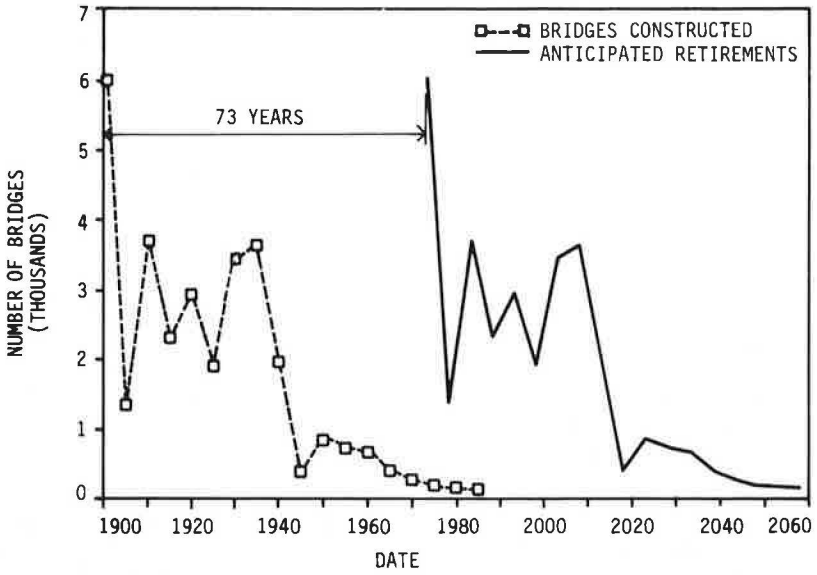

FIGURE 8 Numbers of steel through-truss bridges constructed, and anticipated retirements by 5-year periods, NBI.

bridges. Concrete slab and tee bridge types were mentioned, but other timber and concrete responses related only to material and not to specific designs or constructions.

Site Inspections

The Iowa DOT regularly prepares the "Iowa Bridge Embargo Map" for load-restricted bridges on all federal and Iowa highways. The map was used as a guide for site inspections of more than 40 bridges. About half of the 40 bridges were load restricted either by the Iowa DOT or by county or local authorities.

Of the load-restricted bridges, which would have a low S1 rating under the NBI, approximately one-third were in poor condition and obviously require replacement in the near future. Another one-third were in average condition and could be strengthened along with rehabilitation, if functional and economic considerations were favorable. The last one-third of the bridges were in good condition, well maintained, and good

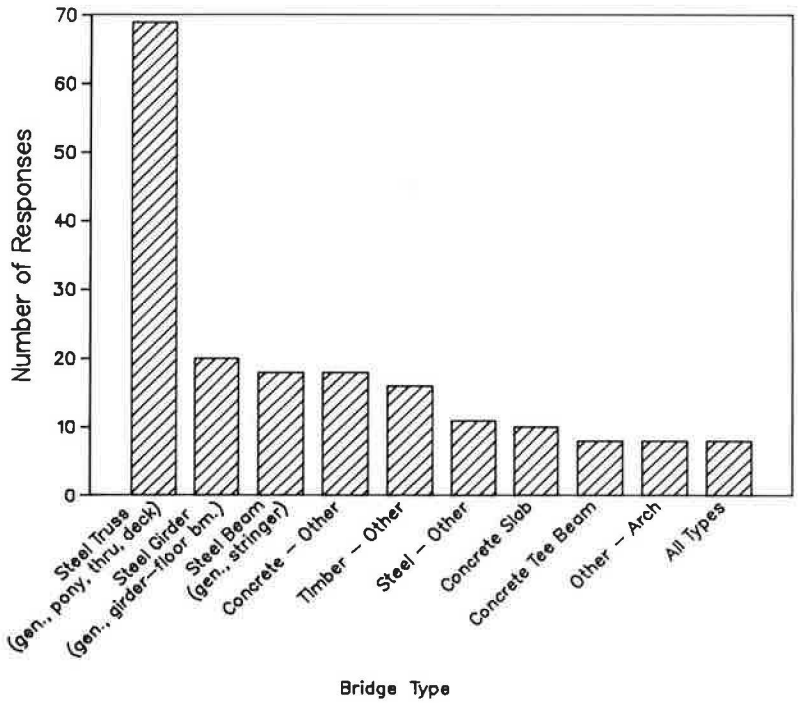

FIGURE 9 Questionnaire responses for strengthening needs ranked by bridge type.

candidates for strengthening without significant rehabilitation if functional and economic considerations were favorable. Most of the load-restricted bridges in average to good condition were steel stringer, continuous steel stringer, steel through-truss, or steel pony truss bridges. Even though the site inspections were quite random, they tend to support conclusions that can be drawn from the NBI records and the NCHRP strengthening questionnaire.

SUMMARY AND CONCLUSIONS

Direct and indirect examination of NBI bridge records indicate that the bridge types with greatest potential for strengthening are steel stringer, timber stringer, and steel through-truss. If rehabilitation and strengthening cannot be used to extend their useful lives, many of these bridges will require replacement in the near future. Other bridge types for which there also is potential for strengthening are concrete slab, concrete tee, concrete stringer, steel girder-floor beam, and concrete deck arch.

Questionnaire responses from bridge engineers and bridge specialists strongly support the need for development of strengthening methods for steel truss and steel stringer or steel girder-floor beam bridges. There is less interest in strengthening methods for timber bridges, quite possibly because some engineers do not perceive timber as a permanent material. Questionnaire responses also support the need for strengthening of the concrete bridge types identified through the NBI, but the responses are not confined to the specific NBI classifications for bridge type.

Inspection of Iowa load-restricted bridges, even though these inspections were for a small number of the nation's bridges, tend to support previous conclusions for bridge types in need of strengthening. Although some of the load-restricted bridges will have to be replaced, others could be strengthened, if functional and economic considerations were favorable, to extend their useful lives with minimal additional rehabilitation.

ACKNOWLEDGMENTS

Research for this paper was sponsored by AASHTO in cooperation with FHWA, and was conducted by NCHRP. Data from the NBI were provided by the Bridge Division of FHWA. The authors also wish to thank T. J. Wipf and graduate assistants D. Eberline and M. Hall for their help in developing the NCHRP questionnaire and in tabulating responses.

REFERENCES

1. *Recording and Coding Guide for the Structure Inventory and Appraisal of the Nation's Bridges.* Design and Inspection Branch, Bridge Division, FHWA, U.S. Department of Transportation, 1979.
2. *Manual of Instructions for Completing the Structure Inventory and Appraisal Form—State-County-Municipal.* Office of Transportation Inventory, Division of Planning and Research, Iowa Department of Transportation, Ames, 1978.
3. F. W. Klaiber, K. F. Dunker, T. J. Wipf, and W. W. Sanders, Jr. *Methods of Strengthening Existing Highway Bridges.* Preliminary Draft of Final Report for NCHRP 12–28(4), ISU-ERI-Ames-87049, 1986.

Publication of this paper sponsored by Committee on General Structures.

A Bridge Automated Design and Drafting System (BRADD–2)

TERRENCE J. TIBERIO, JOHN C. HAYWARD, MAHENDRA G. PATEL, AND RICHARD M. MCCLURE

This paper contains the preliminary findings, recommendations, and development status of the BRADD–2 system research project. The objective of the initial phase of the research was to design a software system capable of performing computer-aided design and drafting of certain simple span bridges. This design involves the interfacing of new or existing analytical computer programs with computer-aided graphics display technology. Evaluation of existing analytical programs as well as state-of-the-art applications of computer-aided design and drafting (CADD) in bridge designs were also required.

This paper documents the preliminary findings, recommendations, and development status of the BRADD–2 system research project sponsored by the Pennsylvania Department of Transportation (PennDOT) *(1)*. The objectives of the research were to design and develop a software system capable of performing computer-aided design and drafting of certain simple-span bridges. These objectives involve the interfacing of new or existing analytical computer programs with computer-aided graphics display technology. The software design required evaluation of existing analytical programs as well as state-of-the-art applications of the computer-aided design and drafting (CADD) system in bridge designs.

The basic capabilities of the software include the following:

1. The system allows interactive input of basic geometric and engineering data needed to perform structural analysis and design of pertinent bridge components and to prepare complete bridge design drawings. The bridge components include the various superstructure and substructure types, as follows:

Substructure types
a. Stub abutment on spread and pile footings,
b. Reinforced concrete cantilever abutment on spread and pile footings,

Superstructure types
a. Precast channel beams,
b. Adjacent prestressed concrete box beams,
c. Spread prestressed concrete box beams,
d. Prestressed concrete I-beams, and
e. Steel multibeams and girders.

T. E. Tiberio and J. C. Hayward, Michael Baker, Jr., Inc., 4301 Dutch Ridge Road, Beaver, Pa. 15009. M. G. Patel, Pennsylvania Department of Transportation, Harrisburg, Pa. 17120. R. M. McClure, The Pennsylvania State University, University Park, Pa. 16082.

2. Quantity and cost estimate calculations are automatically generated for desired bridge types. This procedure allows comparison and value engineering studies to be performed and conclusions to be drawn before final design drawings are generated.

3. The design drawings generated by the proposed system are to the appropriate scale and orientation typical of designs that are conventionally drafted. The drawings are generated in graphic design files and therefore accessible through the graphics workstation for review, modification, and additions as they normally occur during the design process.

4. The system has the ability to provide hard copy documentation of all required quantity, cost, analysis, and design calculations and full-size design drawings as requested by the user.

5. The system can be used as a design tool for separate bridge components without using drafting routines if desired.

6. Routines to partially draft bridge components designed separately are available.

BACKGROUND

In 1981, PennDOT retained a consultant, Buchart-Horn, Inc., to develop ready-to-use standardized bridge plans for simple-span steel, prestressed concrete, concrete, and wood structures. Development of "Bridges Low-Cost" (BLC) standards was completed in January 1985. The preengineered design and preprinted plans made it possible for a designer to greatly reduce the time required for generating contract documents even though the process relied on conventional manual computational techniques.

In 1983, PennDOT contracted Michael Baker, Jr., Inc., as a subcontractor to Intergraph Corp., to automate these standards in conjunction with the installation of an Intergraph CADD system. The new system was the bridge automated design and drafting (BRADD) system. The manual procedure of basic data entry, straight forward equation computations, and tabular lookups was replaced with a CRT data entry, interactive computations, alternative cost evaluations, and automatically produced drafted documents. Two out of six series of the BLC standards were completely automated, reducing design and drafting time to a few hours.

The BLC standards and the initial BRADD system (BRADD–1) proved that development of preengineered and predrafted systems was both feasible and practical and could save a substantial amount of design time. However, the obvious

limitations of the initial work, such as lack of scaled drawings, limited bridge types, foundation restrictions, and so forth, indicated the need for further improvement in the automation of bridge design and drafting.

The PennDOT evaluated two basic alternatives for improvement: the first was to expand the BLCs to remove geometric, structural, and foundation limitations, incorporating the expansion in CADD; and the second was to develop an interactive bridge design and drafting system. It was envisioned that in the long run the interactive bridge design and drafting system would be more cost-effective and more versatile, and could more easily permit future expansion than the BLCs.

Initially (in the spring of 1984), it was thought that development of a new interactive system should include simple, multiple, and continuous bridges using basically steel, concrete, and prestressed concrete construction materials. However, preliminary cost estimates indicated that a substantial investment of funding, time, and effort would be required to develop such a system. The interactive design and drafting (to scale) technology for civil engineering application is still in its infancy. The risks in going to such a broad system were considered to be great. Hence, it was decided to limit the development to single-span structures, expanding to multiple and continuous spans on success of the initial effort and availability of funding.

The success of BRADD–1 indeed led to a major expansion of the concept involving a second project (BRADD–2) to develop more sophisticated bridge design and drafting software. The later activities were projected to result in an automated system of analysis and drafting routines that allow the designer to consider a wider array of bridge types and have substantially more flexibility in the creation of contract documents than before.

Highway planning and research funding was secured, and with the concurrence of the FHWA, PennDOT retained a researcher, Michael Baker, Jr., Inc., who started the BRADD–2 project in early January 1985.

The initial phase (Task 1) of BRADD–2 was completed in October 1985; a report was published in November 1985 *(2)*. The software development phase (Task 2), underway since July 1985, was scheduled to be completed by October 1986. System acceptance and availability of the software to other transportation departments was expected during the first quarter of 1987.

PROJECT DESCRIPTION

The overall objective of BRADD–2 was to develop an integrated software system that would combine and automate the design, analysis, and drafting steps for certain types of highway bridges. The system was to fully use state-of-the-art computer-aided design and drafting (CADD) technology in order to improve design productivity and reduce the time required to produce contract documents. It was envisioned that the software system would be expandable, permitting a wider array of bridge alternatives to be added to it in future projects.

Anticipated Results and Product Description

The general result of the BRADD–2 research program was to be computer software developed to run on an Intergraph CADD system. The Intergraph system was rapidly becoming the standard for highway design purposes, having been chosen by many of the leading state transportation agencies and the FHWA. The software was to be developed on the contractor's Intergraph system and then installed on the PennDOT system for actual production use.

The operation of the software was to be interactive in nature. A designer, by interactive dialog with the computer, enters appropriate information, span length, deck width, elevations, loading type, and desired superstructure and substructure types, as prompted by an alphanumeric terminal. The software processes the input information necessary to make an informed decision regarding general bridge type and specific structural components. Documentation of the input information, analytical results, and cost estimates is supplied to the user in printed form if requested. On selection of a bridge design, the user can instruct the computer system to create a set of design documents within a specific CADD graphics file. These drawings can be edited or enhanced at an interactive graphics workstation using normal CADD drafting techniques available with the Intergraph equipment. Final plots, suitable as finished contractor documents, can be created for subsequent construction procurement processes on user request.

Research Methodology

The work for BRADD–2 was to be accomplished *(3)* in three major tasks covering system design (Task 1), actual software development (Task 2), and system installation on PennDOT equipment (Task 3). A lesser task (Task 4) was included for report production, documentation, and user manual creation. The precedence diagram (Figure 1) depicts the general work flow; each major task is briefly outlined in the following paragraphs.

Task 1—Evaluations, Recommendations, and Design of a Proposed Computer-Aided Design and Drafting System

Included in this task was a survey of existing bridge analysis and design software and CADD drawing generation routines. The purpose of the task was to investigate the feasibility of developing the proposed system and if feasible to design such a system. The result of Task 1 was a final report including an outline of a software system design presented for client review and approval.

Task 2—Development of the Proposed Computer-Aided Bridge Design and Drafting System

Task 2 began in July 1985 with the purpose of transforming the conceptual system design prepared in Task 1 into a functional software system. To provide practical limits to the project, specific superstructure and substructure types were identified. Engineering development such as the preparation of designs or design procedures for specific bridge components generally precedes actual software programming. Existing and acceptable bridge analysis and design routines were to be used

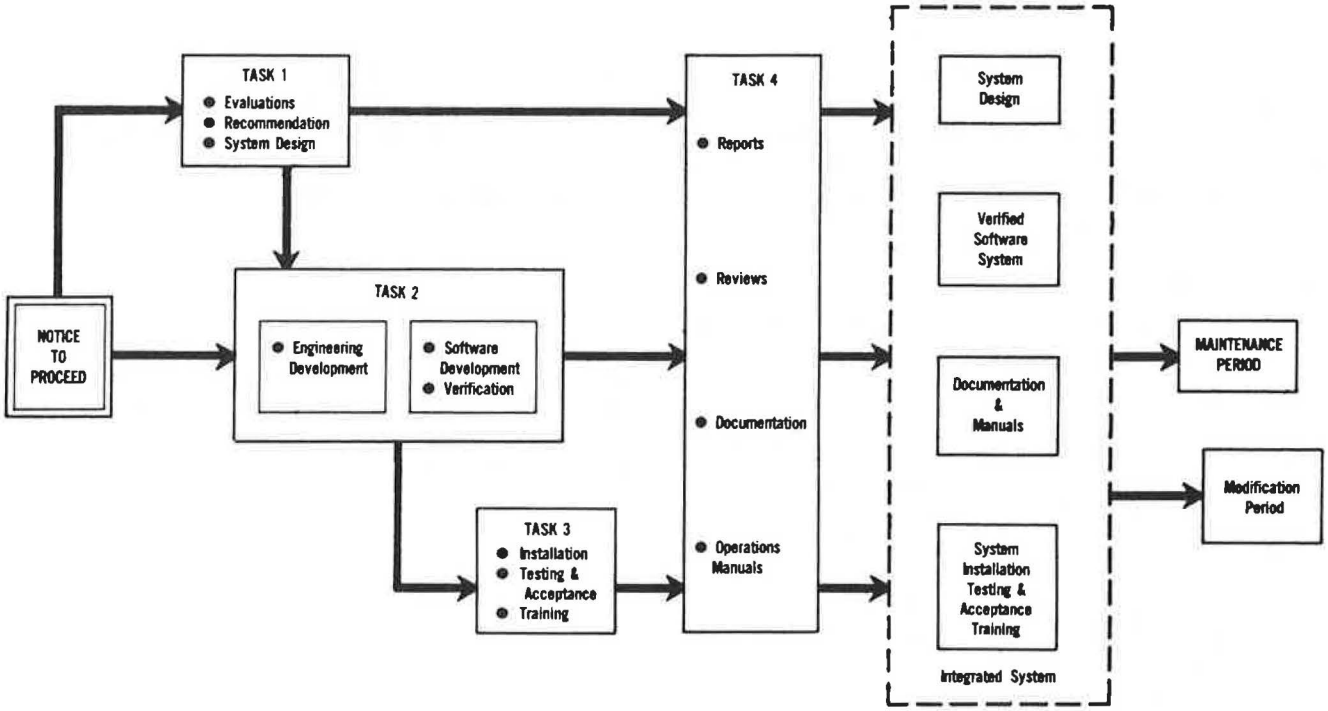

FIGURE 1 Precedence diagram—bridge automated design and drafting (BRADD–2) system development.

wherever possible so that the programming effort would be integration and interface oriented. Actual coding, testing, debugging, and verification were to be conducted at the consultant's computer facilities. The product of Task 2 was to be a working computer software system for bridge design, analysis, and drafting. The completion of this task was scheduled for October 1986.

Task 3—Installation of the Bridge Design and Drafting Software onto the PennDOT Intergraph System

This task entails installation of the software onto the department's system, testing and acceptance, training of PennDOT staff in its use, and a maintenance and modification period of 2 years. Testing and system acceptance are expected to be completed sometime during the first quarter of 1987.

Task 4—Preparation of Quarterly Reports, Final Report, Software Documentation, and Operational Manuals

In addition to quarterly reports documenting the general progress of the research, it was proposed that four documents be prepared. At the completion of Task 1, a final report was prepared *(2)*. Following software development, the team was to produce a project summary, a system documentation manual, a procedural manual, and an operations manual. The system documentation and operations manuals were to be directed toward programming staff and to provide information necessary for program modifications and maintenance. The procedural manual was to be oriented to the bridge engineer or designer who actually uses the system.

Michael Baker, Jr., Inc., served as the prime contractor on the BRADD–2 project. Buchart-Horn, Inc., provided engineering support through a subcontract arrangement. These two firms brought together a staff with considerable experience in the development of standard bridge design components and procedures and the automation of those procedures using Intergraph equipment. Overall direction of the Michael Baker, Jr., Inc., work effort was assumed by J. C. Hayward. Project management of the software development was the responsibility of T. J. Tiberio.

GENERAL CONCLUSIONS OF TASK 1

Survey Evaluation

The highway survey of CADD *(2)* usage indicates that there is a strong interest to supplement computer-aided design programs with computer drafting packages. Some industries have already accomplished this link for special applications. The extent of computer-aided drafting varies for each application. In general, some packages assist operators in producing graphics files interactively whereas others produce them automatically.

The automotive industry uses specialized software to assist operators in creating graphics files interactively. This system suits automotive needs because of the large numbers of automobile components, each of which has numerous variations. Standard details are impractical because of the wide range of component configurations encountered in automobiles. Automated drafting of scaled details has a low priority because of the need for an operator to create custom drawings and the lack of standard details.

The survey indicated that building, highway, and bridge designs are well suited for automated drafting applications.

Designs for these applications are time-consuming and produce design drawings that are unique and useful for single projects only. These areas of design engineering lend themselves well to standard details. Reduction in the design and drafting effort, uniform plan presentation, use of standard details, and elimination of repetitious information during the design and drafting stages are some of the benefits that can be realized from automated drafting software.

Feasibility Study

Some examples of computer-automated drafting applications that have been integrated with computer-aided design include the following.

In 1972, the Oklahoma DOT developed a design and drafting package for prestressed I–beam superstructures, abutments, and piers. This comprehensive package produced complete design drawings and could be considered a forerunner of the BRADD system. This software package was developed before CADD systems were widely available.

Butler Buildings Systems developed a software system for analysis, design, and drafting of one-story steel buildings. This system designs structural members and connections. Final drawings are produced to scale complete with an erection diagram and materials list.

Westinghouse Corporation developed an integrated system for the design of pipe support systems in nuclear plants. This system allows an engineer to design the pipe support interactively using a finite element program. Final construction drawings can be generated from the output of the finite element analysis.

The CANDID program developed by Louis Berger International, Inc., provides automated drafting for highway geometry, earthwork, culverts, bridges, and buildings. Bridge drawings produced by this system include plan and elevation, abutments, and piers. This software produces generic drawings using data read from cards. The generic drawings require operator interaction to add details that are unique to each client.

As demonstrated by the preceding systems, integrated design and automated drafting systems are feasible. They have been developed for a variety of applications and provide an efficient means of designing bridges.

Development Requirements

In the development of the BRADD–2 system, it was important to consider certain limitations and requirements.

For example, development of an automated design and drafting package had to be followed by continued maintenance to update the system to current codes and standards. Failure to do so would result in an obsolete program and a loss of the initial investment. For example, the Oklahoma DOT bridge design system became obsolete because it was not updated for code changes and revisions to the standard details. The BRADD–2 system was to be modular, making future changes and enhancements easier and preventing the system from becoming obsolete.

Development Feasibility

An automated bridge design and drafting system was feasible; some versions had already been developed. Detail standardization, uniform plan presentation, and reduction in design and drafting effort were some of the benefits. The ability to efficiently modify and update designs, and perform cost comparisons made the system even more attractive. A state-of-the-art bridge design and drafting system enables highway industry users to achieve more benefits from their CADD investments.

BRADD–2 SYSTEM DESIGN

Overview

The BRADD–2 system consists of five major subsystems, input, design, reports, generation, and plot. These subsystems are connected as shown in Figure 2 and further detailed in Figure 3. The input subsystem controls the interaction of the user with the other BRADD–2 subsystems. The input subsystem gathers input data from the user for input to the database.

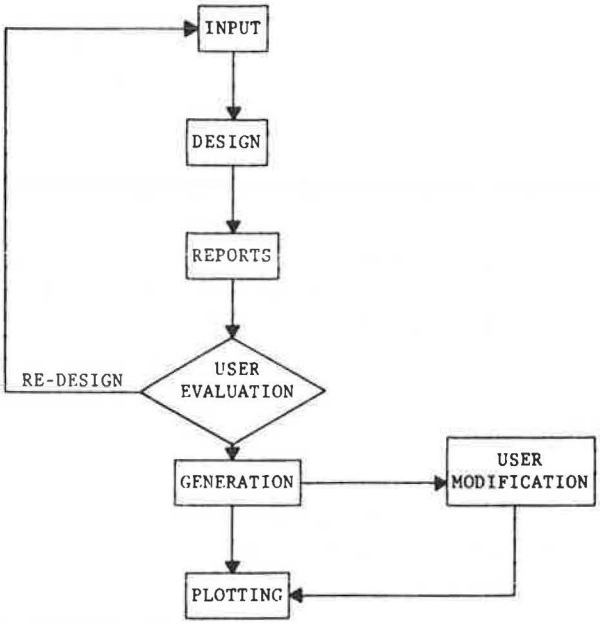

FIGURE 2 BRADD–2 subsystem flow chart.

From the input subsystem, the user can choose to proceed to the design subsystem. This subsystem contains all of the programs for the design of each component of the bridge. From the design subsystem, the user can proceed to the report subsystem. This subsystem generates additional data as requested by the user to help the user evaluate the design. After the report subsystem, the user may elect to execute the generation subsystem. This subsystem generates graphics design files containing the design drawing in standard scales and showing proper orientation and skew. The final subsystem is the plot subsystem. This subsystem generates plots from the graphics design files. This subsystem primarily consists of the standard Intergraph plotting package plus routines to automate the generation of the plots.

System Outline

The following gives a more detailed description of each of these subsystems.

Input Subsystem

This portion of the system consists of menus and prompts modification programs. The prompts programs cue the user for input data and store it in the BRADD–2 database. Prior to saving the data, the program checks the validity of the input and rescues the user when necessary.

The prompts modification program allows the user to modify input data and default parameters encountered in the design process. This program displays a current summary of the input data and permits the user to select the parameter to be changed. On selection, the user is prompted for the new information. Then the new data is validated and updated in the BRADD–2 database.

The BRADD–2 system has the flexibility of using simple interactive menus and prompting for input for the less experienced user but also allows abbreviated commands that permit more rapid movement through the system by the more experienced user.

Design

The design subsystem consists of three types of programs: preprocessor programs, component application programs, and postprocessor programs. Each type of program actually is a battery of programs for each design component.

Preprocessor Programs. Preprocessors extract data from the BRADD–2 database file to generate the input data necessary for each component design program. Data required for the design but not defined in the database are requested from the terminal. Temporary input files are generated for each design program.

Component Design Programs. The component design programs perform the actual engineering design required for

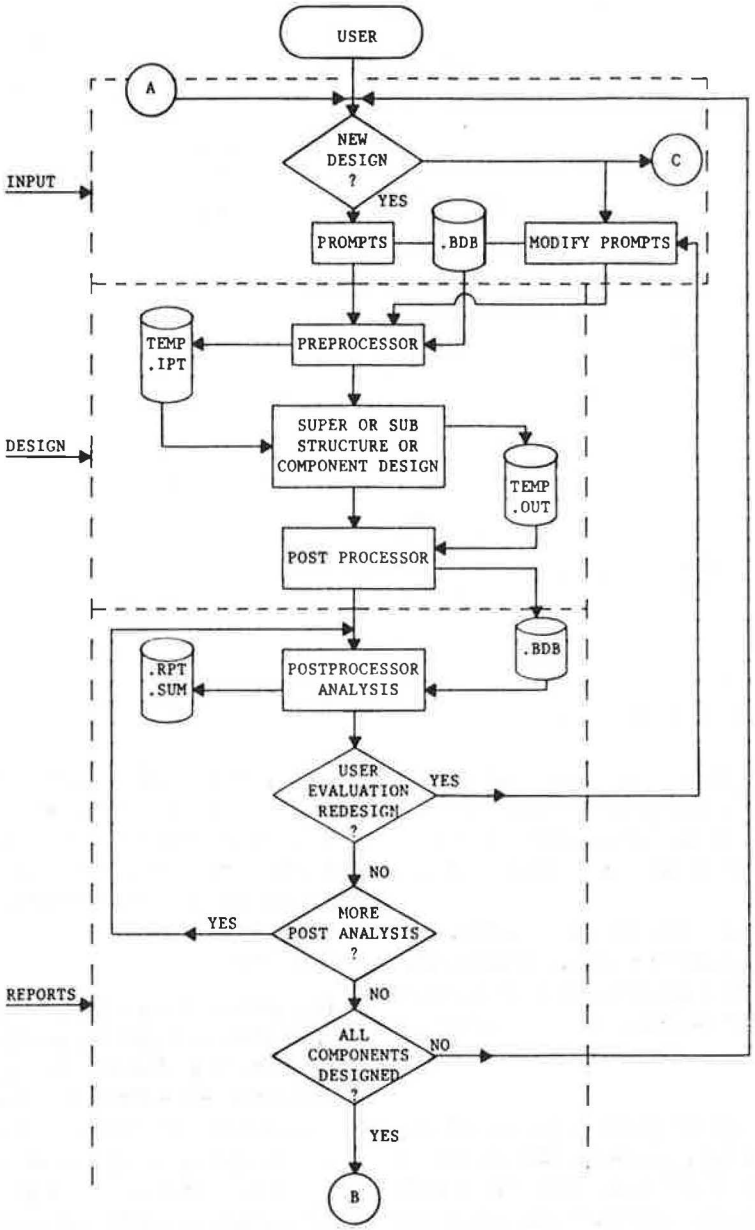

FIGURE 3 Detailed BRADD–2 flow chart.

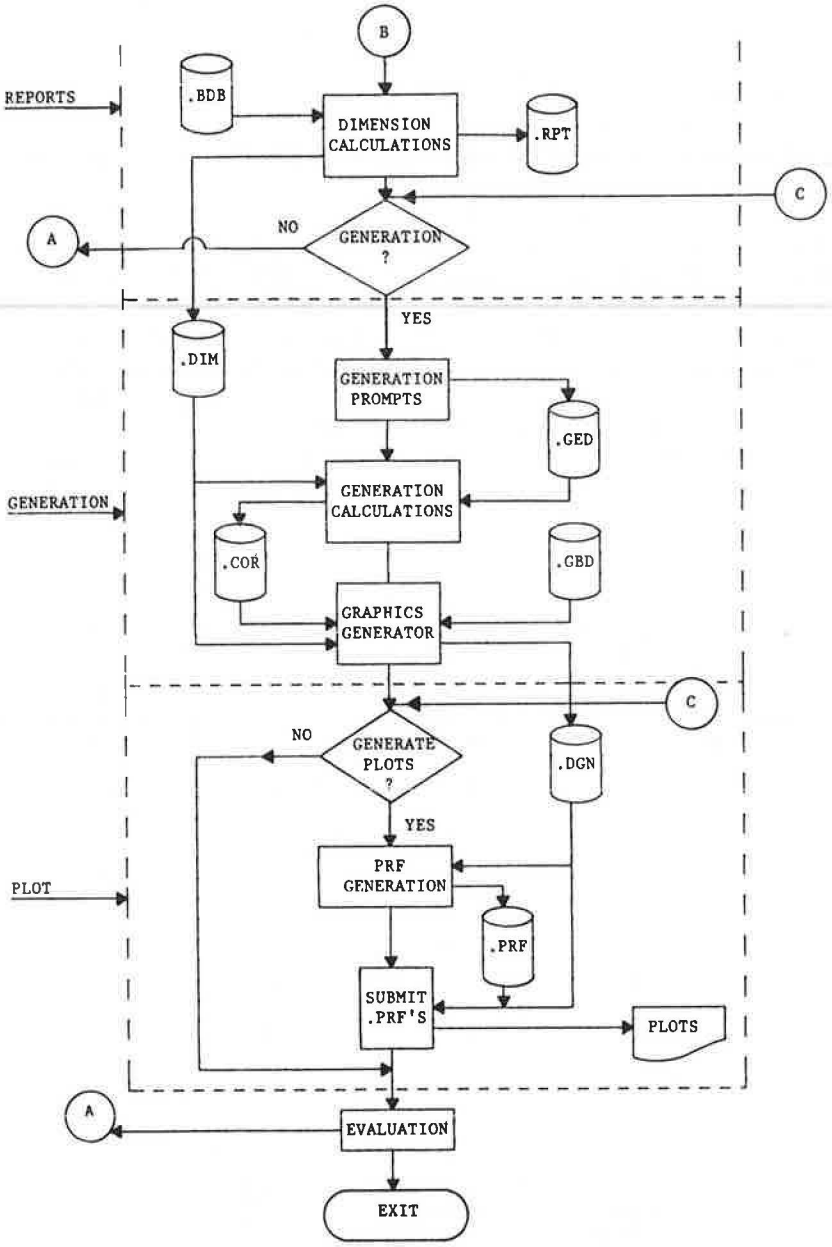

FIGURE 3 *continued.*

each component. These programs depend on the software selected from any survey of available programs. Some programs may design a large percent of the superstructure or the substructure whereas other programs may design smaller portions of the structure.

Postprocessor Programs. Postprocessors examine the output data from the design programs and place all needed data into the database file. Some data placed in the database may be from simple calculations made from the data in the output file.

Report

This part of the BRADD–2 system performs the detailed analysis of the results of the design programs. This analysis includes, for example, moment and shear output for a girder design, required area of steel for a concrete deck design, and quantity of prestressing strand for a prestressed beam. Another analysis performed by the programs in this subsystem is detailed dimension calculations used for computing quantities, costs, and scaling data. The amount of postprocessing analysis is controlled by the user; more analysis may be requested to help the user evaluate the design.

Generation

This portion of the system, consisting of generation prompts, generation calculations, and graphics generation programs, generates final drawings in a graphics design file. The final drawings contain details placed at a specific engineering scale.

Generation Prompts. The generation prompts allow the user to specify the generation desired. Options include type, size, and location (TSL) drawings, superstructure drawings, substructure drawings, and a complete drawing set. These options allow the user to generate the drawings for only a portion

of the design. Redesign and generation of an abutment do not require the superstructure to be regenerated. The generation option selected by the user would be stored in a generation database to be accessed by other programs.

Generation Calculation. The generation calculation program computes necessary parameters to place each detail to scale. These parameters include node coordinates, detail location in the file, and detail scale value. These parameters are stored for retrieval in generating the design file.

Graphics Generation Programs. The graphics generator generates scaled design files using information from the dimension database, the coordinate database, and the graphics database. Elements read from the graphics database are placed in the design file at the coordinates specified in the coordinate database. Dimensions are then placed as defined in the dimension database.

Plot

This portion of the system generates plot request forms and submits them to the batch queue for plots. This portion consists of PRF generation and submit programs. The PRF generation searches the design file for drawing locations and creates PRF for these sheets. Then the submit program submits the PRFs into a queue to produce electrostatic plots.

MODULE FILE NOTATIONS

.BDB—BRADD Database
.IPT—Input
.OUT—Output
.RPT—Report
.SUM—Summary
.DIM—Dimensions
.GED—Generation Database
.GDB—Graphic Database
.COR—Coordinates
.DGN—Design
.PRF—Plotting Request

ACKNOWLEDGMENTS

This project was sponsored by the PennDOT and the FHWA. The overall project was under the direction of M. G. Patel of PennDOT, Bureau of Design. The Project Review Panel included the following PennDOT personnel and an FHWA representative: F. W. Bowser, Director, Bureau of Design; A. A. Wagner, Bureau of Design; R. M. McClure, The Pennsylvania State University; S. R. Simco, Chief Bridge Engineer; H. M. Lathia, Fiscal and Systems Center; J. E. O'Melia, District Bridge Engineer—District 2–0; M. G. Patel, Assistant Chief Bridge Engineer; R. C. Arner, District Bridge Engineer—District 3–0; J. Szivos, Bureau of Bridge and Roadway Technology; and W. E. Williams, FHWA.

REFERENCES

1. F. W. Bowser, J. C. Hayward, and M. G. Patel. *Development of a Bridge Automated Design and Drafting System* (BRADD–2). Pennsylvania Department of Transportation, Harrisburg, May 1985.
2. J. C. Hayward and T. J. Tiberio. *Task 1 Final Report for Development of a Bridge Automated Design and Drafting System* (BRADD–2). HPR–84–30. FHWA–PA–85–021. U.S. Department of Transportation, Nov. 1985.
3. *Proposal for Development of a Computer-Aided Bridge and Drafting System* (HPR-84-30). Michael Baker, Jr., Inc., in association with Buchart-Horn, Inc., Beaver, Pa., Nov. 1984.

Publication of this paper sponsored by Committee on General Structures.

Bridge Deck Expansion Joints

SABIR H. DAHIR AND DALE B. MELLOTT

The ability of a bridge deck expansion joint to be smooth riding, durable, and waterproof is essential to the performance of the bridge superstructure. Recent developments in the design, manufacture, and installation procedures for expansion dam systems have indicated a potential ability to meet these requirements. In this study, the characteristics and field performance of modular expansion joint systems, metal-reinforced elastomeric expansion dam systems, and gland-type bridge expansion dam systems were evaluated. Results of the field study are summarized and recommendations made on continued use of some systems, including neoprene seals for small movements (<2 in.), strip seals for intermediate movements (up to 4 in.), and finger dams with neoprene troughs for large movements (>4 in.).

In 1984, the Pennsylvania Department of Transportation (PennDOT) entered into a cooperative agreement with the Federal Highway Administration (FHWA) to conduct a comprehensive statewide evaluation of all types of bridge deck expansion joints used in Pennsylvania.

Previous studies *(1–4)* conducted by the PennDOT on expansion joint systems have revealed varied performance and snow plow damage. Increased deterioration was caused by chloride contamination that attacks the concrete and substructure steel, and additional damage was caused by heavy truck traffic as the vehicle loads were transferred from one deck slab to the next. A recent study by the PennDOT's Operation Review Group revealed that 76 percent of the expansion joints were either completely open or leaking water onto the superstructure.

This research effort has been directed to the evaluation of the performance capabilities of a variety of expansion joint systems, including those of common and traditional specifications, as well as a number of recently developed systems. Several different proprietary and nonproprietary expansion joint types were reviewed and evaluated for their relative design, construction, and performance aspects. This report covers the results of the joint systems review and evaluation effort.

SCOPE

Bridge deck expansion joints are divided into the following three groups.

1. Modular expansion joint systems including finger and sliding plate dams, with 2 to 16 in. of movement, but generally more than 13 in. of movement.
2. Metal-reinforced expansion joint systems, with 1½ to 13 in. of movement, but generally 2 to 13 in. of movement.
3. Strip seals and armored expansion joint systems, including preformed neoprene seals, with ½ to 4 in. of movement.

The bridge deck expansion joint systems that were evaluated in Pennsylvania are listed and abbreviated in this report as follows:

1. Modular expansion joints—

ACMA	AM
Wabo-Maurer	WM
Delastiflex	DE
Finger dam	FD

2. Metal-reinforced expansion joints—

Transflex	TF
Waboflex	WF
Unidam	UD
Fel Span	FS

3. Strip seal and armored expansion joints—

ACMA	AM
Wabo-Maurer	WM
Delastiflex	CP
Onflex	OF
Pro Span	PS
Armored neoprene	AR
Preformed neoprene	PN
Strip seals	SS
Harris	HS

Most of these types have two or more models, depending on the movement width or modification of the initial design.

Evaluating each joint type or system on at least three structures in various parts of the state was proposed. An inventory and comprehensive information package available for evaluating most of the systems was used to select the structures.

A code universally used and accepted by engineers was provided to personnel by AASHTO. It is quoted here for ready reference:

> The design shall be such as to allow for total thermal movement at the rate of 1¼ inches in 100 feet. Provisions shall be made for changes in length of span resulting from live load stresses. In spans more than 300 feet long, allowance shall be made for expansion and contraction in the floor. The expansion end shall be secured against lateral movement.

It has been stipulated that a good expansion joint should

S. H. Dahir, Pennsylvania State University, Middletown, Pa. 17057. D. B. Mellott, Bureau of Bridge and Roadway Technology, Pennsylvania Department of Transportation, Harrisburg, Pa. 17120.

1. Accommodate all movements of the structure,
2. Withstand all loadings,
3. Have good riding qualities,
4. Not present a danger to cyclists or other types of traffic,
5. Not impart undue stress to the structure unless the structure has been designed accordingly,
6. Be reasonably silent and vibration free,
7. Give reliable service throughout the expected temperature range,
8. Resist corrosion,
9. Facilitate maintenance and repair, and
10. Control deck drainage to prevent damage to structure below.

PROCEDURE

The bridge structures were selected from a listing of structures included in research work of the Bureau of Construction Quality Control *(1, 3)* and from a listing compiled by the Bureau of Bridge and Roadway Technology as the result of a request for bridge deck expansion systems used in the various engineering districts. FHWA supplied an evaluation form for joint ratings. The rating system was based on a scale of 5 (excellent) to 0 (failure) for each of the following joint parameters:

A. General appearance,
B. Condition of anchorage,
C. Debris accumulation,
D. Watertightness,
E. Surface damage,
F. Noise under traffic, and
G. Ease of maintenance.

Four engineers were chosen and worked in two-person teams to inspect and evaluate the joints on the selected structures using the FHWA rating system.

Rating joints for watertightness required inspecting below the joint under the bridge for evidence of water leakage. The teams performed this inspection wherever possible without elaborate arrangements. As a result, the teams were not able to evaluate this parameter on every installation. However, a sufficient number of the joint systems were inspected to reflect the degree of watertightness of the joint type of system.

One rating item was not clear to the inspection and rating team—namely, ease of maintenance. Strictly speaking, ease of maintenance is a characteristic of the joint design and construction. Therefore, it could not be adequately evaluated by the inspection team. Instead of *ease of maintenance*, the *need for maintenance* was rated. Accordingly, the rating figures shown under Item G on the performance record sheets reflect the degree to which the joint needed maintenance at the time of inspection.

The rating system proposed by FHWA was discussed by a project review team assembled explicitly for the purpose of reviewing and analyzing the data collected. The use of a weighted system was recommended based on the consideration of which items were most important relative to joint performance. These weighted rating factors were used to calculate the final rating. The following weighted percentages were developed as the result of the voting by all the review team members.

Characteristic	*Percentage*
General appearance	9
Condition of anchorage	26
Debris accumulation	9
Watertightness	27
Surface damage	12
Noise under traffic	8
Need for maintenance	9
Total	100

Although bridge deck drainage was not considered as a part of the joint evaluation process, it was noted that in many cases lack of deck drainage maintenance may have contributed to joint problems. This needed maintenance was not included in the rating of the joints.

The PennDOT project review team reviewed the data, data analysis, and results of the study, and recommended improvements and refinements to the anchorage system and future rating procedures.

GENERAL DISCUSSION OF SYSTEMS EVALUATED

The inspection and evaluation teams collected data on 57 systems on 146 bridges throughout Pennsylvania. Schematic drawings typical of each system are listed in Figures 1–4.

Pennsylvania Standard Joint Systems

These systems basically consist of *(a)* open joints protected by armored neoprene or preformed neoprene compression seals, *(b)* metal plates with neoprene strips known as "strip seals" and anchored to the bridge deck, and *(c)* toothed bearing

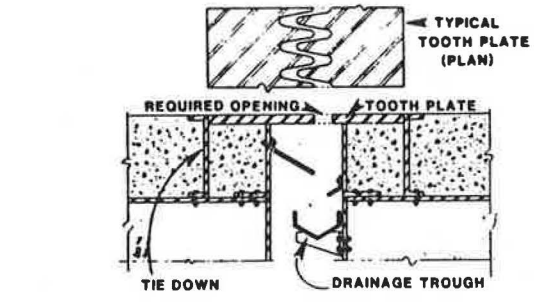

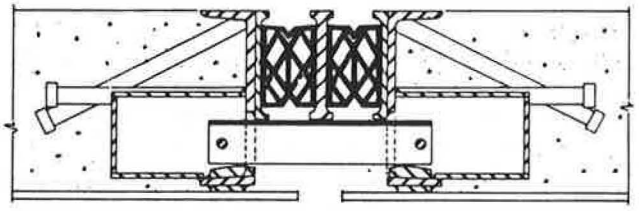

FIGURE 1 Typical finger dam and modular dam systems.

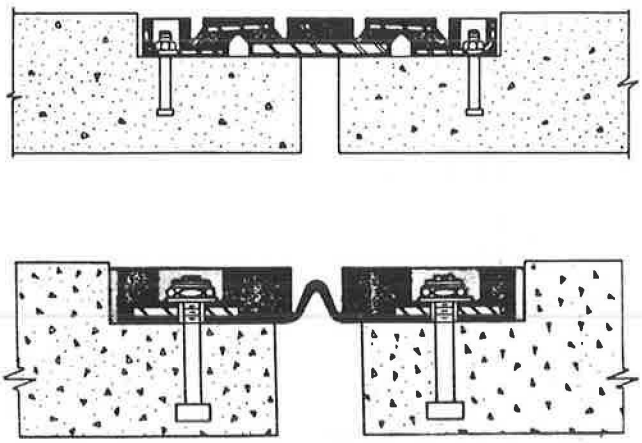

FIGURE 2 Typical metal-reinforced and continuous-belt dam systems.

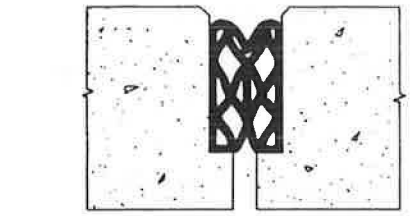

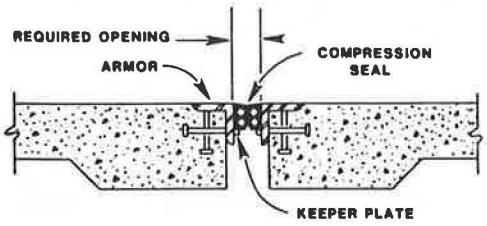

FIGURE 3 Typical conventional seal systems.

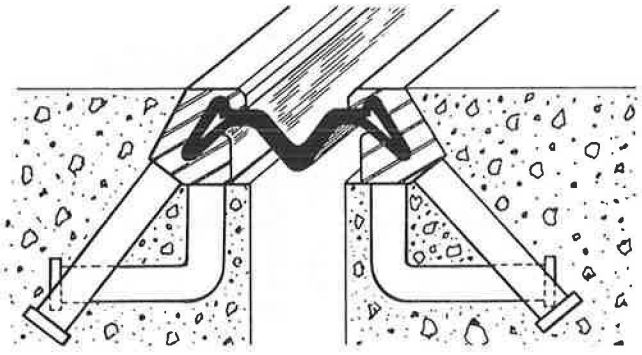

FIGURE 4 Strip seal system.

supports (finger dams) to transmit traffic loads across the joints. The armored neoprene and standard unarmored neoprene compression seals are typically used with prestressed beam construction and are used for movements up to 2 in.; the strip seals are used for movements up to 4 in. The tooth, or finger, dams are used for movements exceeding 4 in., although they also may be used for movements of 4 in. or less. Figures 5–7

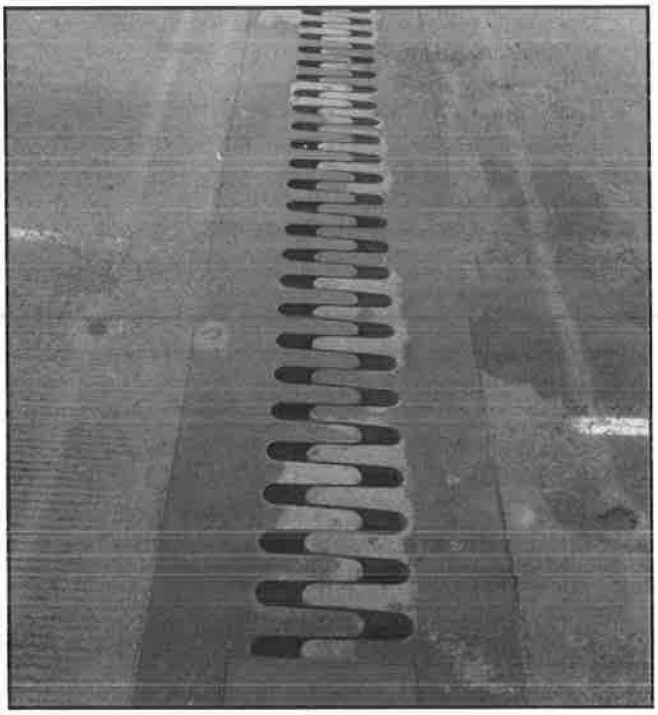

FIGURE 5 A typical finger dam.

FIGURE 6 A typical neoprene dam.

show photographs of a finger dam system, an armored neoprene, and a preformed compression seal, respectively. Finger joints may be equipped with neoprene troughs to direct contaminated water away from the bridge abutments or piers, or they may allow water to fall directly into the area below the joint if the area is not adversely affected by the drainage water.

The armored neoprene, the preformed neoprene compression seal, and the finger dam are the standard joint systems commonly used in Pennsylvania. They have been generally satisfactory in their performance but have had some problems related mostly to poor construction or lack of maintenance.

FIGURE 7 A typical neoprene compression seal dam.

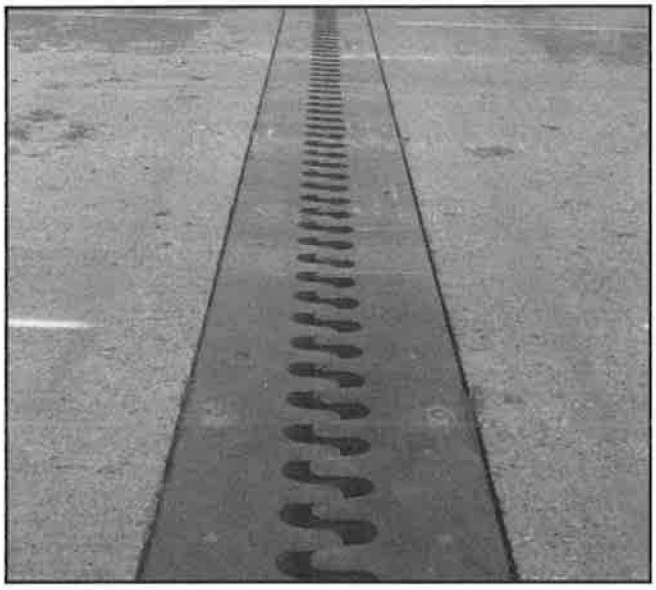

FIGURE 8 A finger dam with horizontal and vertical finger misalignment.

The most common problems are

1. Misalignment during construction, especially in the finger dam systems. The misalignment can be either horizontal, causing the fingers to jam on expanding, or vertical, causing rough riding, noise, and sometimes bending or breaking of some fingers. Figure 8 shows a finger dam having both horizontal and vertical misalignment.
2. Blockage of dams by debris accumulation. This problem arises when the dam or trough does not have sufficient slope to drain the contaminated water and flush the loose debris before it has a chance to accumulate and harden, or when the dams having small slopes are not maintained periodically. It was reported by the Arkansas Department of Transportation *(5)* that when a finger dam had a trough sloping at 8 percent, there was no debris accumulation 6 years after placement, but when the trough had a slope of 1 percent, it was filled with debris in 6 months. Obviously, the problem of debris accumulation, which can inhibit the drainage of contaminated water that accelerates the rebar corrosion and concrete deterioration, can be greatly alleviated by design (i.e., providing a steep trough slope), where possible, or by periodic maintenance (flushing of the dam) as needed.
3. Some of the cantilever fingers can be bent or even broken under the continuous pounding of heavy truck traffic unless they are designed with sufficient tensile strength and are well aligned and properly anchored during construction. During construction and bridge deck maintenance, care must be taken to have the finger dam system well anchored and at the proper elevation with the adjacent pavement surface, and not partially covered by paving concrete.
4. In the case of armored neoprene and preformed neoprene compression seals, problems may arise if the concrete around the armored channels is not adequately consolidated (Figure 9) or if the neoprene becomes twisted during construction (Figure 10). Obviously, these problems can be avoided if strict construction controls are applied. A problem that can be alleviated by maintenance is the rusting of the plates that occurs unless the plates are painted periodically.

Strip Seal or Gland Type Systems

These devices provide movements up to 4 in. (Figure 11). Several of these systems have been used in Pennsylvania on an experimental basis. They are listed at the beginning of this section in the grouping of the joint dam systems. Generally, their performance has ranged from fair to quite good, as may be seen in the summary of performance averages in Table 1.

Some of the problems encountered when using these systems include debris accumulation, leakage, and noise under traffic (Figure 12).

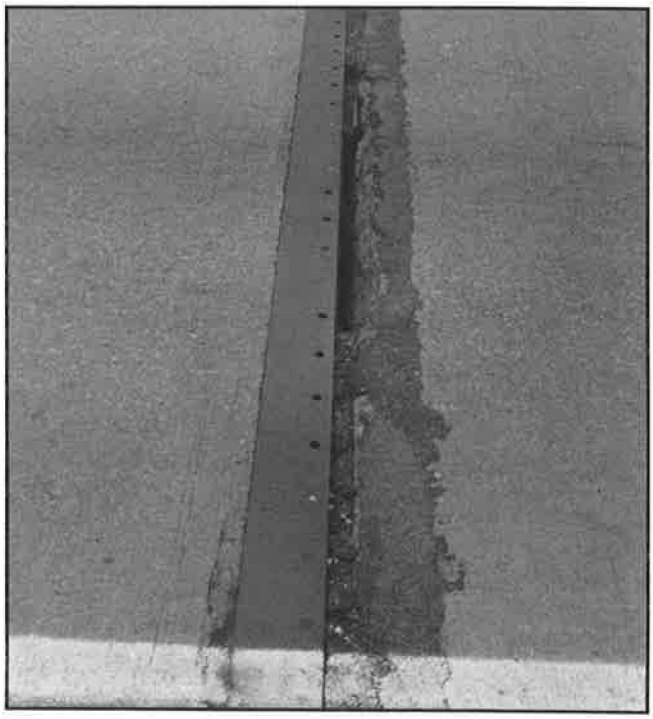

FIGURE 9 Damaged concrete adjacent to armored channels—concrete has not been well consolidated.

TABLE 1 SUMMARY OF RATINGS BY JOINT SYSTEM TYPE

Model Name	Condition No.	A	B	C	D	E	F	G	Unadjusted Avg	Weighted Avg
Compression seals (neoprene)										
Armored (AR)	54	211	208	196	129	201	210	208	3.79	4.15
Preformed (PN)	5	20	20	20	20	20	20	20	4.00	4.00
Strip Seals										
Strip seals (SS)	7	28	28	12	26	28	26	23	3.49	3.63
Harris (HA)	1	3	4	2	4	4	4	4	3.57	3.73
Prospan (PS)	4	16	16	14	8	16	18	16	4.00	4.54
Wabo-Maurer (WM)	35	134	140	108	56	140	138	137	3.82	4.54
Elastomeric Dams										
Delastiflex (CP)	21	58	70	69	59	72	63	46	3.07	3.40
Fel Span (FS)	48	161	178	187	148	174	167	145	3.49	3.56
Onflex (OF)	17	57	68	39	67	63	58	56	3.43	3.63
Transflex (TF)	65	182	205	254	132	191	199	173	3.02	3.11
Unidam (old) (UD)	10	35	42	40	22	32	38	29	3.61	4.11
Unidam (new) (UD)	3	10	12	12	4	12	12	10	3.52	3.92
Waboflex (WF)	29	96	103	116	46	106	97	88	3.40	3.81
Modular										
Acme (AM)	17	66	68	68	30	68	59	65	3.31	3.91
Delastiflex (DE)	3	9	12	12	9	9	12	6	3.29	3.34
Wabo-Maurer (WM)	35	139	143	108	108	143	117	134	3.77	4.13
Finger dams (FD)	22	83	88	87	72	86	86	82	3.98	4.36

NOTE: Ratings were as follows: poor, <3.50; fair, 3.50–3.84; satisfactory, 3.85–4.19; good, 4.20–4.59; excellent, >4.60.

Metal-Reinforced Elastomeric and Continuous-Belt Dam Systems

These systems were intended to replace the finger dam system, accommodating movements between 4 and 13 in. with no need for maintenance. They included the Transflex (Figure 13), the Waboflex, the Fel Span and the Unidam joint systems. Figure 2 shows an example of each of these systems. The performance of these systems has varied from poor to fair to barely satisfactory as may be seen from Table 1. Generally, these systems were expensive and performance has been disappointing.

Problems associated with the use of these systems have ranged from poor anchorage to wear and tear by traffic pounding and snow plows. Obviously, when the neoprene surface is torn or the anchorage becomes loose, the joint will leak contaminated water and allow debris to filter through the dam.

FIGURE 10 Preformed neoprene is twisted—probably a construction defect.

FIGURE 11 A typical strip seal dam.

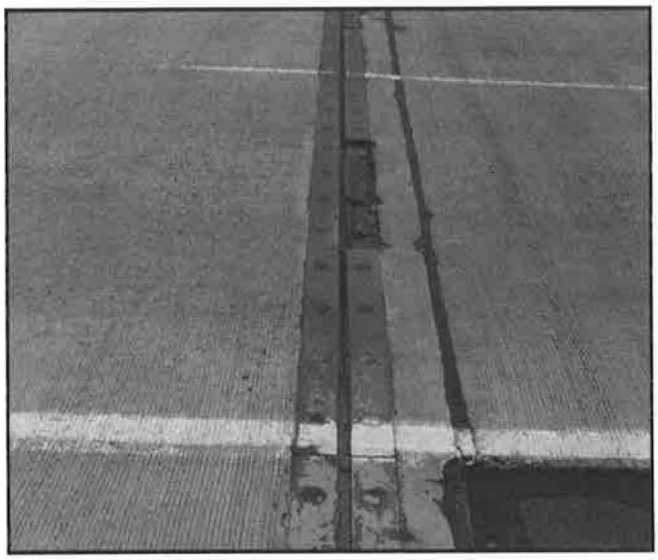

FIGURE 12 A strip seal dam having missing reinforcing strips and debris accumulation.

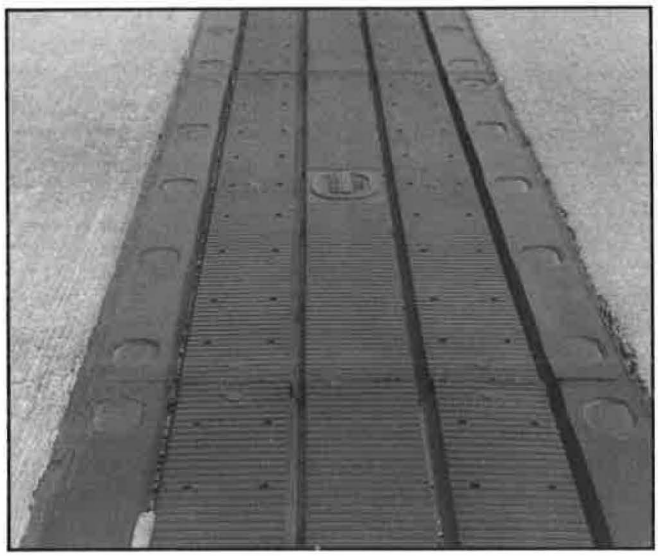

FIGURE 13 A typical Transflex dam.

Of the four systems in this group, the Transflex systems were generally most subject to tear and loosening of anchorage, followed by the Fel Span and Waboflex systems. The Unidam system generally performed better than the Transflex and other systems in this group; nevertheless, they were not completely satisfactory, as may be seen in Figure 14. The Fel Span dam system has since been modified to use a continuous belt anchored to the concrete deck by neoprene blocks or hold-down members that put it in the same group as the strip seal and gland type systems. The old version would leak where the segmented sections were joined in the field.

The Modular Expansion Dam Systems

These systems provide movements up to 26 in. or more through a prefabricated assembly or module that consists of one or more preformed neoprene elastomeric elements secured between contoured transverse load distribution members that bear on custom-designed support beams. The entire module is installed between end dams anchored into the concrete superstructure.

FIGURE 14 A Unidam joint showing severe damage and debris accumulation.

These systems were intended to accommodate wide joint movements while permanently (over the life of the bridge deck) sealing the joints so as to prevent infiltration of contaminated water and debris, thereby alleviating the problems of steel corrosion and concrete deterioration that are accelerated by these contaminants. In short, they were supposed to be durable, leak proof, and maintenance free. Three proprietary types of these systems were used in Pennsylvania. They are known as ACMA, Delastiflex, and Wabo-Maurer modular systems. Figure 15 shows an example of a typical modular system.

Unfortunately, experience with these systems in Pennsylvania and elsewhere *(6, 7)* shows that although some of these expensive systems have performed fairly well, most have had problems, no less troublesome than those they were supposed to eliminate when using the conventional finger dam systems. Snow plow damage and debris accumulation are typical problems with the modular systems (Figure 16).

The ACMA modular system performance has been fairly good in Pennsylvania, but it often becomes deformed, leaks, and is fairly noisy under traffic. The ACMA system has been modified to the new ACMA Beta series, but this series has not been used long enough to determine if the performance has been substantially improved. The Delastiflex modular system has had anchorage problems, leakage, noise, and debris accumulation, and is subject to damage by snow plows. The snow plow damage associated with the excessive exposed rubber surface has made the Delastiflex system unsuitable for installation in Pennsylvania. The Wabo-Maurer system has had fewer performance problems than the other modular systems; however, the Wabo-Maurer modular has had problems with the

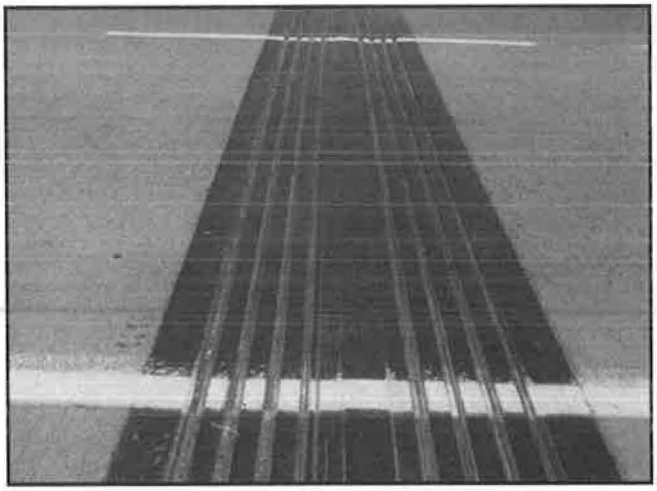

FIGURE 15 A typical modular dam.

FIGURE 16 A modular joint showing debris accumulation.

expansion mechanism that maintains the neoprene elements in their proper place, and with the support members in the modular system.

SYSTEM RATINGS AND ANALYSIS OF DATA

In the early stage of data collection, from criteria discussed in the Procedure section of this report, if a bridge deck had several joint devices of the same type, all the joints were inspected but only the average ratings and the number of joints were reported. Later, it was decided that it was more appropriate to record and report the data for each individual joint device.

The data indicate that there is no joint device that gives the ideal performance as measured by the seven rating criteria, nor does any joint device fail to meet all minimum performance requirements. With these data, one can only attempt to determine which of these systems are providing satisfactory, marginal, or less-than-satisfactory overall performance relative to each other.

Two different approaches for determining an overall rating of each joint type were considered. The first was based on an unadjusted average rating of the seven rating categories. The results according to this approach are listed in Table 1.

The second and probably more appropriate approach was to assign weights to each rating category. Weights were suggested by the researchers and were later revised by the project review team. Preliminary weighted evaluations are also shown in Table 1. For the table, qualitative descriptors assigned to each rating range were reviewed by the project review team. The consensus that emerged as a result of this review is as follows: A weighted average below 3.5 is considered poor; 3.50–3.84, fair; 3.85–4.19, satisfactory; and 4.20–4.59 good. On an aggregated basis, no joint systems were rated excellent, as indicated by an average greater than 4.59. Only newly installed single-joint systems exhibited excellent performance. Based on the weighted averages in Table 1 and comments from members of the project review team and the engineering districts, it appears that the minimum acceptable weighted average should be in the range of 3.85–3.90.

As mentioned earlier in the report, watertightness was not evaluated for every joint rated. This posed a problem when computing overall averages for each system. When entering the data in the computer, a zero (100% failure) was assigned to those joints where watertightness was not rated. This reduced the average from what it would have been had watertightness been rated because it is safe to assume that the rating would have been one or better had watertightness been rated. To eliminate this error and provide more accurate averages for both unadjusted and weighted ratings, the following was done:

- All joints not rated for watertightness were separated from the joints with complete ratings.
- The 27 percent original weighted percentage (OWP) for watertightness was then divided among the other parameters by the ratio method [(27 × OWP) divided by (73 × z), where z is the percentage value added to the OWP.]
- The totals of the rating for each parameter for the joints not rated for watertightness were multiplied by the adjusted weighted percentages (AWP).
- The remaining totals for the joints completely rated were multiplied by the OWPs.
- These two totals were added together and divided by the total number of joints rated, except watertightness, which was divided only by the number of joints rated for watertightness.
- All seven parameter totals were added to get the final weighted averages that appear in Table 1.

The unadjusted average was obtained from the following steps:

- Divide the total of each parameter by the number of joints rated. Again, watertightness is divided by the number of joints rated for watertightness.
- Add the seven quotients and divide by seven to get the unadjusted average. See Table 1.

Even new systems exhibited defects due to poor design or construction. In such cases, the joint system is likely to deteriorate rapidly and fail prematurely. This effect may explain why an otherwise satisfactory system displays less than satisfactory

performance in one or more installations. Proper installation during construction and periodic maintenance are critical to the performance of any joint device and cannot be overemphasized.

In this study, it was also observed that poor maintenance of the drainage facility, that is, not cleaning the debris, may have contributed to less than satisfactory performance and poor ratings. The inspection team noted that on most structures, drainage inlets were either partially or totally blocked by debris and mud, and some of the joints needed flushing and cleaning. In some cases, grass or even shrubbery grew in the mud accumulated in the system. Such conditions burden the joint component to the point that it may not be capable of performing as intended, at least not for the life it was expected to serve. Furthermore, accumulation of deicing chemicals and water containing the chemicals causes bridge steel corrosion and concrete spalling and deterioration *(8)*.

Another problem that was observed is that of joint systems on skew angles. Many skewed joints having acute angles approximately between 30 and 70 degrees had buckling or folding of the neoprene and damage caused by the snow plows and truck traffic. Exact measurements or counts were not made of the skewed joints or of the damage effects. However, it was observed that generally the smaller the angle of skew was, the more severe was the damage or distortion, especially where truck traffic was heavy. The joint types that appeared to be most susceptible to damage include unprotected neoprene compression seal joints (unarmored), Fel Span, and the elastomeric joint types. Edge anchoring of the neoprene appeared to be difficult to maintain on these joints. Obviously, distortions because of skew drastically reduce the life expectancy of the joint.

In a study of the allowable movement ratings of various proprietary bridge deck expansion joint systems at various skew angles in Michigan *(9)*, it was concluded that for the majority of the expansion joint systems evaluated,

> As the angle of crossing becomes more severe, the total perpendicular movement a system can adequately provide decreases due to the inability of the system to fully extend to its maximum recommended perpendicular width, or fully close to its minimum recommended perpendicular width, or both.

Another important observation was the effect of heavy truck traffic on the damage caused to most of the joint systems. It was obvious that the heavier the truck traffic the greater the expansion joint damage, especially on the exposed neoprene, as in the case of the Transflex systems. Even some finger dam joints that were misaligned had some of the steel fingers bent where there was heavy truck traffic. Sufficient specific data were not available for correlating truck traffic with the degree of damage.

CONCLUSIONS

In rating the performance of the joint systems using the criteria suggested by FHWA, it appears that most of the joint systems in the study fail to meet an average rating high enough to make it acceptable. Ostensibly, a weighted average rating in the range of 3.85–3.90 would place a joint system in a truly satisfactory bracket. Table 1 shows that armored neoprene and preformed neoprene compression seals fall into the satisfactory range. Also in the satisfactory range would be the Unidam (old and new models) and the ACMA and Wabo-Maurer modular systems. The finger dam, ProSpan, and Wabo-Maurer (the latter both strip seal) systems are in the good range of 4.20–4.59. All other systems have averages that vary from 3.11 to 3.81, indicating a wide range of level of performance. The criteria that have been used may not sufficiently bring out the true level of performance of each joint system in the study. However, the suggested ranges do separate the better performing systems from those that have inferior performance. The systems that clearly have shown inferior performance and, therefore, should not be used include the Transflex, Waboflex, Unidam (LK-series), Delastiflex (DE and CP), and Fel Span systems. The other systems that do not fall into either the most satisfactory or the unsatisfactory groupings must be judged on the basis of recent improvements, as in the case of improved anchorage for the strip seals, and on their relative cost over the expected performance life of the system.

In rating the performance of the joint systems as shown in Table 1, other considerations should be taken into account. These include the following:

1. Can the system stand the continuous pounding of traffic, particularly truck traffic, without undergoing surface damage or structural damage in the system? Also, is the system protected against snow plow damage?
2. Is the system designed such that water contaminated with deicing chemicals, sand, and other debris will not collect in it long enough to affect its performance adversely?
3. How will the system perform when maintenance is neglected for a period exceeding expected maintenance schedules?
4. How easily can the system be maintained with minimal traffic delay and without elaborate maintenance procedures?

This study has revealed serious problems with the present anchorage systems. Numerous installations are listed as failures because the anchorage failed. In some cases, the anchor size contributed to the failure by allowing movements in the anchor slots. This movement eventually caused the anchor system to loosen and the added movements then contributed to excessive wear of the anchor fasteners that either failed because of enlarged anchor slots or a reduction in the fastener section to the point that yield failure occurred. In many instances, the anchors were pulled out from the bridge deck concrete. Therefore, systems with poor anchorage are not acceptable and should not be used unless the anchorage system is improved.

Cost-effectiveness of each system over the expected life of the structure should be investigated thoroughly, and these costs and impact on traffic delays should be considered in selecting a system. A cost analysis of the expansion joint systems was beyond the scope of this study, and in general actual maintenance costs for each system are extremely difficult to obtain precisely. However, comparison of the available first costs and the general performance of the joint systems indicates that the most cost-effective systems appear to be the conventional specification systems that are currently used by PennDOT, namely *(a)* compression seals up to 2-in. movements, *(b)* neoprene strip

seals with improved anchorage up to 4-in. movements, and *(c)* finger dams for movement greater than 4 in. The survey teams observed that these systems had the least damage occurrence and the least need for maintenance.

RECOMMENDATIONS

Until better maintenance-free systems or procedures are found, it is recommended that the joint systems to be implemented should be only those systems that have a weighted average rating of 3.85 or more, or have been found highly satisfactory by the engineering districts. Of these systems, preference should be given where possible to those with the least need for maintenance and to those that can be maintained easily. Systems with a satisfactory rating of 3.85 or more may be used selectively where conditions and cost justify their use, provided that improvements on weaknesses are made where possible and strict adherence to installation details during construction is observed. Obviously, joint systems with ratings of poor and fair (less than 3.85) should not be used.

Furthermore, until a system is developed that would require minimal maintenance, a maintenance schedule should be established to include periodic maintenance of the bridge deck drainage system and cleaning of the expansion joint system. Even with the present systems, scheduling of bridge deck maintenance is just as important as roadway joint sealing or roadside mowing of the grass. This maintenance schedule should be included as a part of the bridge deck expansion joint system requirements at the outset, that is, when the system is installed. Thus far, there appears to be no perfect, truly maintenance-free expansion joint system, especially for the larger movements. Like most other systems, without proper maintenance these systems will not meet all the requirements they are designed to achieve. Maintenance costs over the life of the system, including traffic delays, should be included when comparing service life costs of the systems. As previously stated, strict adherence to installation detail is of paramount importance for both the proper function of the system and reduced maintenance costs.

The presence of anchor-related modes of failure suggests that the anchors should be cast as a part of the concrete construction and securely fastened to the reinforcement steel in the concrete. The problem can be directly attributed to a design that did not use the proper size of anchor or the failure to require the proper securing of the anchor, that is, locking devices were not used or the bolt torque requirement was not correct. These deficiencies should be corrected by proof load testing or by using adhesive anchors.

Manufacturer's designs and PennDOT's specified designs for expansion joint systems need to be improved with regard to performance. Systems whose performance is decreased greatly by small deviations from ideal or design installation techniques should be identified and improved, or their use should be prohibited.

ACKNOWLEDGMENTS

This project was sponsored in part by FHWA under Special Experimental Features Program, Experimental Project No. 5, "Bridge Deck Expansion Joints" in cooperation with PennDOT.

The evaluation was conducted under the general supervision of the project manager Gerald J. Malaskeskie. The evaluation study and report editing were completed with the assistance of K. A. McManigle and J. L. Williams, civil engineers assigned to the Bureau of Bridge and Roadway Technology. One of the latter served on each of the two evaluation teams that conducted the actual inspection and evaluation of the bridge deck expansion joints. Members of the project review team who assisted in the evaluation process are the following PennDOT professional engineers: R. McClure, F. Sankey, W. Scott, J. Ebersole, C. Reed, D. Casner, H. Wels, G. Dorsch, and S. Dadhania.

REFERENCES

1. D. B. Mellott. Transflex Bridge Expansion Joints. Research Project 69–23. Pennsylvania Department of Transportation, Harrisburg, March 1970.
2. R. J. Brunner and D. B. Mellott. A Summary Report on the Installation and Performance of Pavement and Bridge Joint Sealants. Pennsylvania Department of Transportation, Harrisburg, Nov. 1973.
3. D. B. Mellott. Transflex Bridge Expansion Joints. Research Project 69–23. Final Report. Pennsylvania Department of Transportation, Harrisburg, Nov. 1977.
4. D. B. Mellott. Status of Bridge Deck Expansion Dam Systems. Research Projects 73–15, 73–16, and 74–20; Pennsylvania Department of Transportation, Harrisburg, Nov. 1978.
5. *ASSHTO Design Practices, Standard Specifications for Highway Bridges.* 11th ed., AASHTO, Washington, D.C., 1973, p. 128.
6. *Watertight Bridge Deck Joint Seals.* National Experimental and Evaluation Program, Final Report, Project 11, FHWA, U.S. Department of Transportation, July 1977.
7. Bridge Inspection and Rehabilitation. *Transportation Research Record 899*, TRB, National Research Council, Washington, D.C., 1983, 76 pp.
8. *Departmental Bridge Maintenance—1985.* Operations Review, Pennsylvania Department of Transportation, Harrisburg, Nov. 1985.
9. F. J. Bashore, A. W. Price, and D. E. Branch. Determination of Allowable Ratings for Various Proprietary Bridge Deck Expansion Joint Devices at Various Skew Angles. Michigan Transportation Commission, Lansing, Mich., May 1980.

Publication of this paper sponsored by Committee on General Structures.

Nonlinear Analysis of Highway Bridges

JIANHUA ZHOU AND ANDRZEJ S. NOWAK

A nonlinear procedure is developed for the derivation of the load-deflection relationship for highway bridges. The approach is based on the finite difference method. The algorithm is described. A closed-form expression is developed to model behavior of a girder section. The procedure is demonstrated on a composite steel girder bridge.

There is a growing need for more accurate methods of bridge evaluation. Live-load spectra have changed, with amounts of load usually increased. Bridges are subjected to deterioration. On the other hand, costs of repair or strengthening are often prohibitively high. Therefore, a tool to reveal the actual strength of a bridge and to predict its serviceable life time is useful.

A procedure was developed for the flexural and torsional analysis of simply supported highway bridges. The structure is modeled as an orthotropic plate. The finite difference method is used to calculate the nonlinear bridge responses.

The objective of the paper is to present the developed procedure. The general steps and formulas are described; the approach is also demonstrated on a composite steel girder bridge. The method is simple to use and requires less computing time than the FEM or grillage method.

SECTION ANALYSIS

The purpose of the section analysis is to develop force-deformation relationships for the bridge elements considered. In particular, moment-curvature (M–ϕ) and torque-twist relationships are considered.

The M–ϕ curve can be determined using the computer program developed by Tantawi *(1)*. In his approach, the section is idealized as a set of uniform layers, as shown in Figure 1. Strain is increased gradually in increments. At each strain level, the corresponding moment is calculated using nonlinear stress-strain relationships for materials such as steel and concrete.

To simplify the calculations, a closed-form expression was derived to represent M–ϕ curves for the slab and composite girder section:

$$\phi = M/EI_e + C_1(M/M_y)^{C_2} \quad (1)$$

where

EI_e = elastic bending rigidity,
M = applied moment, and
M_y = yielding moment.

Department of Civil Engineering, University of Michigan, Ann Arbor, Mich. 48109.

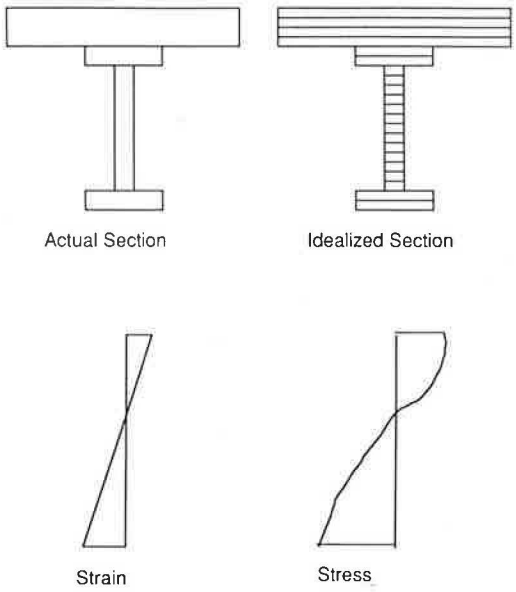

FIGURE 1 Typical composite section and strain diagram.

C_1 and C_2 are constants determined by solving the following two equations:

$$\phi_y = M_y/EI_e + C_1 (M_y/M_y)^{C_2} \quad (2)$$

$$\phi_u = M_u/EI_e + C_1 (M_u/M_y)^{C_2} \quad (3)$$

The resulting C_1 and C_2 are

$$C_1 = \phi_y - M_y/E_{Ie} \quad (4)$$

$$C_2 = \ln[(\phi_u EI_e - M_u)/(\phi_y EI_e - M_y)]/\ln(M_u/M_y) \quad (5)$$

in which

M_u = ultimate moment,
ϕ_y = curvature at yielding, and
ϕ_u = curvature corresponding to ultimate strength.

For composite girders, C_2 ranges from 20 to 24 and C_1 from 25 to 28 $\times$ 10^{-5} ft^{-1}. For slabs, C_2 is about 22 to 26 and C_1 27 to 30 $\times$ 10^{-5} ft^{-1}.

An M–ϕ curve for a typical composite girder is presented in Figure 2. For comparison, an M–ϕ curve calculated using Tantawi's program *(1)* is also shown in Figure 2. A torsion-twist curve for the same composite girder is shown in Figure 3.

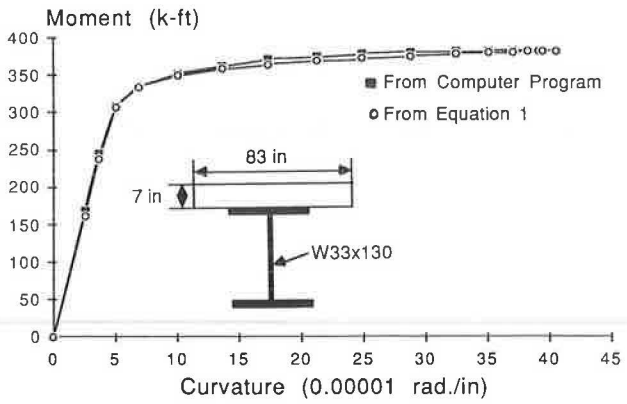

FIGURE 2 M–ϕ curve for a typical composite section.

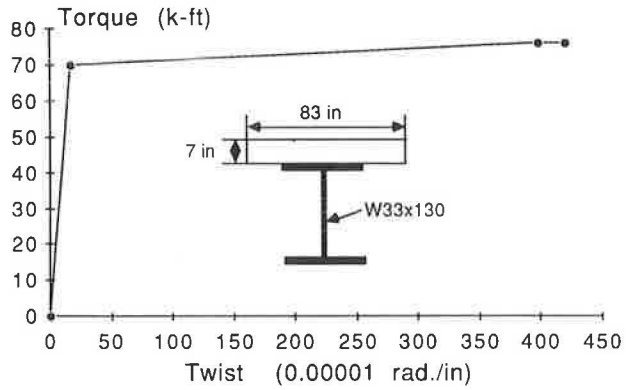

FIGURE 3 Torsion-twist curve for a typical composite section.

FINITE DIFFERENCE ANALYSIS

Based on the assumptions made by Heins and Yoo *(2)* and Heins and Kuo *(3)*, the system of girders, diaphragms, and slab is represented by an orthotropic plate. Segments of the longitudinal and transverse members and slab are shown in Figure 4. The corresponding plate elements are also shown in Figure 4. In Figure 4, m_x, m_{xy} and q_x are the bending moment, torsional moment, and shear, respectively, exerted on the transverse member and slab; m_y, m_{yx} and q_y are the bending moment, torsional moment, and shear, respectively, exerted on the longitudinal member and slab. The equilibrium differential equation for the plate element is

$$-P(x, y) = \partial^2 M_x/\partial x^2 + \partial^2 M_{xy}/\partial x \partial y + \partial^2 M_{yx}/\partial y \partial x + \partial^2 M_y/\partial y^2 \quad (6)$$

where

M_x = the bending moment per unit width of the section in x direction,
M_y = the bending moment per unit width of the section in y direction,
M_{xy} = the twisting moment per unit width of the section in x direction,
M_{yx} = the twisting moment per unit width of the section in y direction, and
$P(x, y)$ = the applied load per unit area.

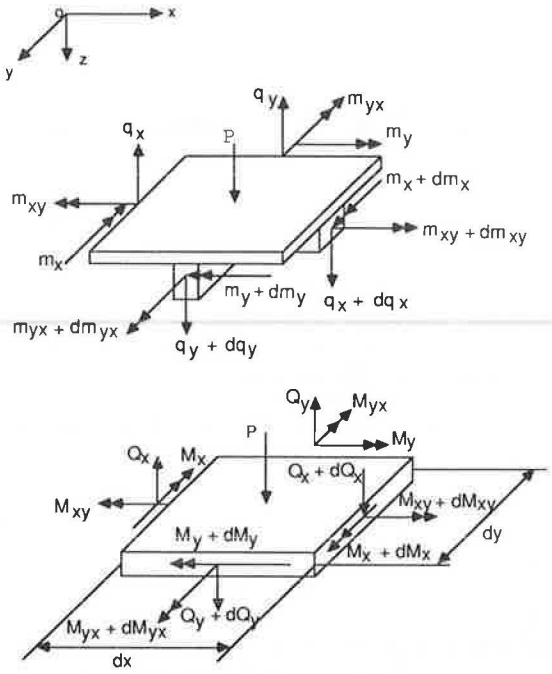

FIGURE 4 Orthotropic plate element.

The total load per plate element P_T can be divided into three components exerted on the girder, diaphragm, and slab.

A system of differential equations was developed that expresses the compatibility conditions in force and displacement equations between plate elements. This system can be expressed in the following matrix form:

$$[K]\{w\} = \{P\} \quad (7)$$

where

$[K]$ = stiffness matrix,
$\{w\}$ = vector of grid point deflections, and
$\{P\}$ = vector of loads.

From these equations, the unknown grid point deflections $\{w\}$ were calculated. Then moments (M_x, M_y, M_{xy}, M_{yx}) and shear forces (Q_y, Q_x) were derived from the following equations:

$$M_x = -D_x \partial^2 w/\partial^2 x \quad (8)$$

$$M_y = -D_y \partial^2 w/\partial^2 y \quad (9)$$

$$M_{xy} = -D_{xy} \partial^2 w/\partial x \partial y \quad (10)$$

$$M_{yx} = -D_{yx} \partial^2 w/\partial y \partial x \quad (11)$$

$$Q_y = \partial M_{xy}/\partial x + \partial M_y/\partial y \quad (12)$$

$$Q_x = \partial M_{yx}/\partial y + \partial M_x/\partial x \quad (13)$$

where the various order derivatives can also be evaluated using the finite difference method.

In the finite difference analysis, special mesh patterns were developed that allow for a considerable reduction of computing time. The details of these patterns are given by Zhou and Nowak (unpublished).

BRIDGE STRENGTH EVALUATION

Based on the finite difference formulation, a procedure was developed to evaluate the ultimate capacity of bridge structures. The evaluation involves a considerable nonlinear structural analysis. The available procedures, such as the Newton-Raphson algorithm and the modified Newton-Raphson algorithm or incremental method *(4)*, require excessive computational effort. Therefore, a special computer time saving procedure was developed for this study.

The developed incremental-iterative approach includes seven major steps. First, elastic stiffness is used to evaluate bridge responses under dead loads. Then truck load is increased by increments. The incremental load ΔP_j is determined as a function of the initial load increment ΔP_0 and number of iterations n_{j-1} in the previous load increment,

$$\Delta P_j = \Delta P_0 / n_{j-1} \tag{14}$$

Using Equation 1, the tangent stiffness matrix is formed, corresponding to the deflections $\{w_j\}$ due to truck load level P_j. The tangent stiffness $K_t(w_j)$ is defined in Figure 5.

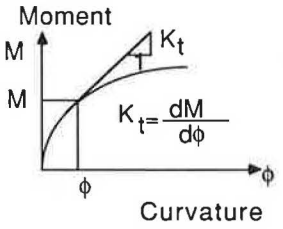

FIGURE 5 Evaluation of tangent stiffness.

Iterations are carried out to compute deflections and curvatures corresponding to the increased load level using the finite difference formulas

$$\{w_{i+1}\} = [K_t(w_j)]^{-1}\{\delta_i\} + \{w_i\} \tag{15}$$

where $\{\delta_i\}$ is the unbalanced force resulting in the previous iteration.

Then the secant stiffness corresponding to deflections $\{w_{i+1}\}$, $K_s(w_{i+1})$, is derived, as shown in Figure 6. The unbalanced force resulting in this iteration is evaluated, see Figure 7 as

$$\{\delta_{i+1}\} = \{P_j\} + \{\Delta P_j\} - [K_s(w_{i+1})]\{w_{i+1}\} \tag{16}$$

If the unbalanced force is not close to zero, the next iteration is carried out. The tangent stiffness, as in the first iteration, is used. This process significantly reduces computation time. The calculations are continued until convergence criteria are satisfied and the unbalanced force is close to zero.

After each load increment, failure criteria are checked. The calculations are terminated when the permanent deflection exceeds 1 percent of span length or concrete crush occurred. Otherwise another cycle of iteration is carried out using a next load increment. The algorithm is presented in Figure 8.

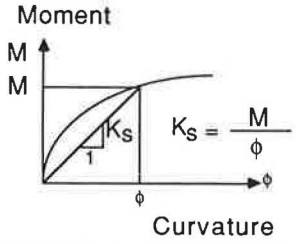

FIGURE 6 Evaluation of secant stiffness.

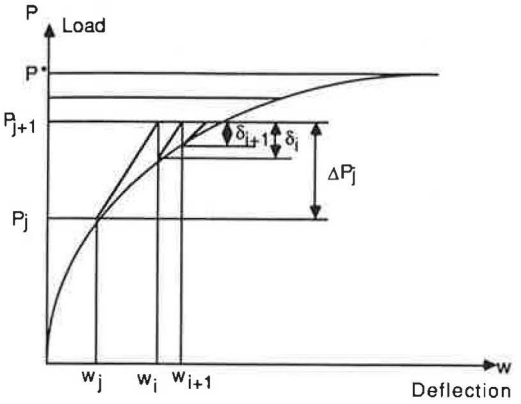

FIGURE 7 Solution process using incremental-iterative method.

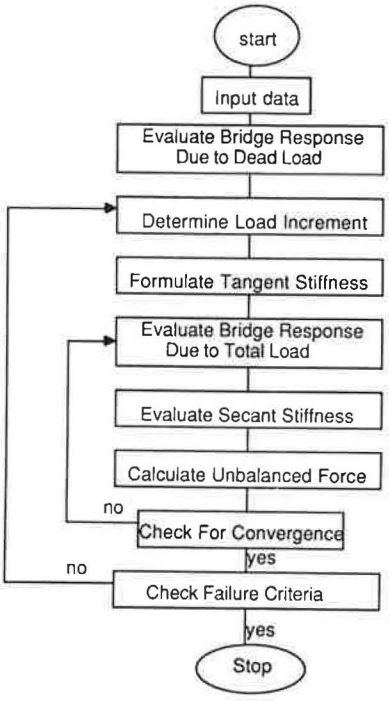

FIGURE 8 Flowchart for incremental-iterative method.

NUMERICAL EXAMPLE

The developed procedure is demonstrated on a composite steel girder bridge designed according to AASHTO guidelines *(5)*. The span is 60 ft; the cross section is shown in Figure 9.

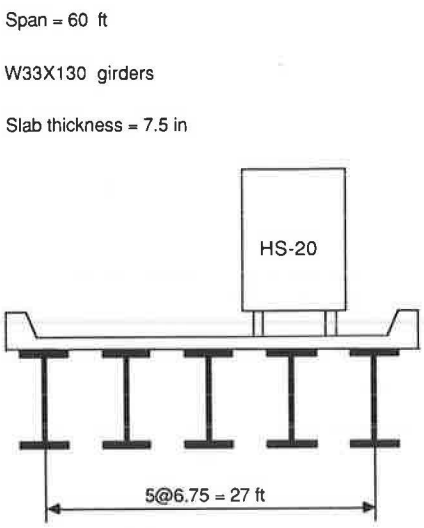

FIGURE 9 Cross section for a typical composite girder bridge.

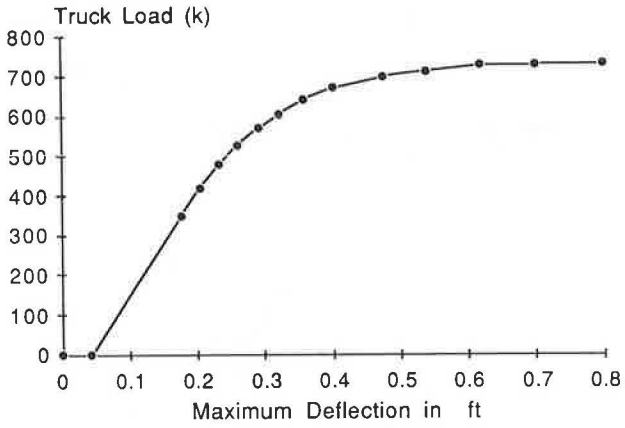

FIGURE 10 Load-deflection curve for a typical composite girder bridge.

AASHTO *(5)* truck HS–20 wheel configurations and load proportions were used, with the transverse position as shown in Figure 9. The curve for the resulting live load of total truck weight versus deflection is presented in Figure 10.

CONCLUSIONS

A numerical procedure was developed for nonlinear analysis of girder bridges. The approach based on the finite difference method allowed for evaluation of the ultimate strength of the structure.

A closed-formula expression was developed to model M–ϕ curves for composite girder or slab sections. The formula permitted considerable computing time saving compared to other available methods.

A load-deflection curve was calculated for a typical composite steel girder bridge to demonstrate the developed procedure.

ACKNOWLEDGMENTS

The present research was sponsored by the National Science Foundation under Grant ECE–8413274, with program director John B. Scalzi.

REFERENCES

1. H. M. Tantawi. *Ultimate Strength of Highway Girder Bridges.* Ph.D. thesis. Department of Civil Engineering, University of Michigan, Ann Arbor, 1986.
2. C. P. Heins and C. H. Yoo. *Grid Analysis of Orthotropic Bridges.* International Association for Bridge and Structural Engineering, Vol. 30/I, 1970, pp. 73–91.
3. C. P. Heins and J. T. C. Kuo. Ultimate Live Load Distribution Factor for Bridges. *Journal of the Structural Division*, ASCE, Vol. 101, No. ST7, July 1975, pp. 1481–1495.
4. W. J. Anderson. *Finite Elements in Mechanical and Structural Design.* Video Lecture Series 1002: Dynamic and Nonlinear Analysis, Automated Analysis Corp., Ann Arbor, Mich., May 1985.
5. *Standard Specifications for Highway Bridges.* AASHTO, Washington, D.C., 1983.

Publication of this paper sponsored by Committee on General Structures.

Prestressed Waffle Slab Bridges

JOHN B. KENNEDY

Design engineers intuitively regard the two-way structural system of a waffle slab to be incompatible with the one-way load-transferring action of a bridge. However, in relatively wide bridges, in bridges on isolated supports, and in skew bridges, large twisting and transverse moments are present. In this paper it is shown that a waffle slab bridge through its geometry of cross section can provide efficiently the required resistance moments in two orthogonal directions. Results from a feasibility study indicate that a waffle slab bridge *(a)* has the potential of being a more economical alternative to solid-slab and slab-on-girder bridges; and *(b)* provides excellent access to prestressing cables for both inspection and maintenance purposes. Tools for design and analysis of waffle slab bridges for both serviceability and ultimate limit states are presented.

Solid-slab bridges are economical for spans up to about 50 ft; however, for longer spans the redundant dead weight makes these bridges less economical. To enhance structural efficiency, voided-slab bridges were introduced. Observations of the performance of voided-slab bridges have revealed several disadvantages, namely: accessibility to the inside of the voids is poor making it difficult to assess any damage to prestressing steel because of corrosion from exposure to deicing salts; the structure does not lend itself to readily applicable remedial measures; and the structure is quite prone to cracking *(1)*, requiring expensive repairs and maintenance. Such cracking is caused mainly by tensile stresses arising from a combination of *(a)* splitting stresses due to longitudinal prestress, *(b)* transverse bending, *(c)* local stress concentration at void formers, and *(d)* restricted shrinkage around the void formers. In contrast, a bridge in waffle slab (two-way ribbed slab) construction, a portion of which is shown in Figure 1, would not be handicapped by these disadvantages; furthermore, because of its geometric shape such a bridge does not carry any redundant dead-weight concrete as does the solid-slab bridge.

Although waffle slab construction has been used regularly in buildings, its use in bridges has so far been limited. In the published literature, the only example appears to be that reported by Lin et al. *(2)*. The reason for this neglect is that many bridge engineers intuitively regard the two-way structural system of a waffle slab to be incompatible to the one-way transferring action of a bridge. However, a close scrutiny of the load distribution behavior of bridges shows that not all bridges transfer loads to their supports in distinctly one direction. For example, in wide, skew, and irregularly shaped bridges, especially those with randomly spaced, isolated intermediate supports, the transfer of loads to the supports is complex. In such bridges, a major proportion of the load is transferred by means of large torsional or transverse moments. It has been shown *(3)* that the most efficient way of designing for these large moments is by providing moments of resistance of similar magnitude in two perpendicular directions. The geometry of a waffle slab, where the lever arm for the steel is large in both directions, is an ideal structural form to accommodate the required moments of resistance in the two perpendicular directions. Besides its structural efficiency, a waffle slab bridge has the additional advantage of pleasing esthetics. This paper is a state-of-the-art report on recently developed tools for the analysis and design of prestressed waffle slab bridges.

Department of Civil Engineering, University of Windsor, Windsor, Ontario, Canada, N9B 3P4.

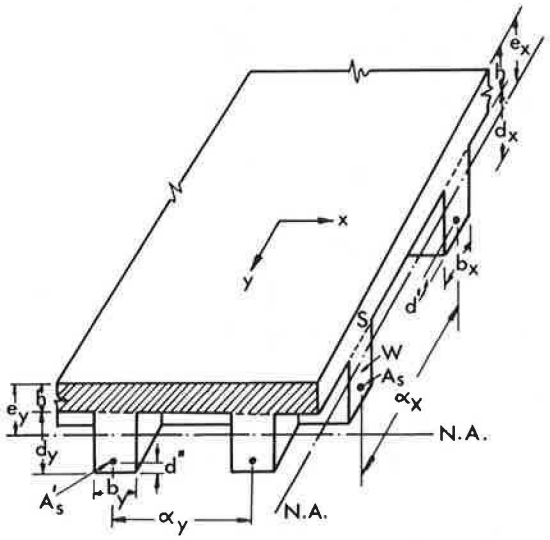

FIGURE 1 Geometry of a waffle slab.

FEASIBILITY STUDY

Recently, a feasibility study *(4)* was undertaken to investigate the structural efficiency of a waffle slab bridge system in comparison with conventional alternatives, namely the solid-slab bridge and the slab-on-girder (one-way, ribbed-slab) bridge. The following three categories of bridges were considered:

1. *Category I Bridges*: These were two-span, continuous bridges (Figure 2*a*) with skew ranging from 0° to 45°; the volume of concrete was kept constant in the three aforementioned alternatives (Figure 2*c*).
2. *Category II Bridges*: These bridges had the same planform as bridges in Category I, but were continuous over two isolated supports (Figure 2*b*); again, the volume of concrete was kept constant (Figure 2*c*).

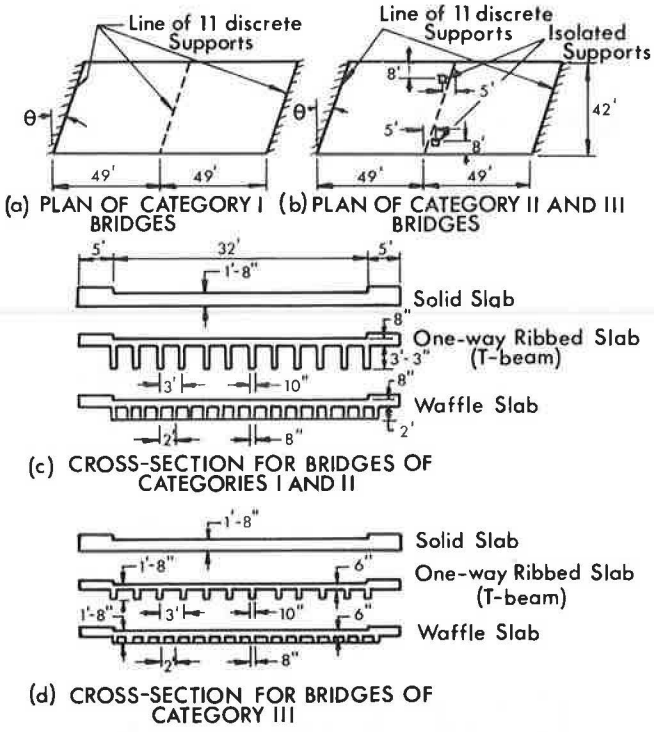

FIGURE 2 Details of bridges in feasibility study.

3. *Category III Bridges*: The planform of these bridges was similar to that of Category II (Figure 2*b*), except that cross sections of the three alternatives were so chosen that the depth of construction remained the same in all cases (Figure 2*d*).

All bridges were designed as three-lane bridges; they were analyzed and designed by STRAND, a group of elastic linear programs *(5)* based on the finite element technique and following Wood's procedure for design *(3)*. The orthotropic rigidities required by the program were calculated according to the method proposed by Kennedy et al. *(6, 7)*. Some of the analytical results were compared with experimental test results on waffle slab bridge models *(7)*.

In order to show the economic advantage of waffle slab bridges, an estimate of cost of each of the various bridges studied was determined. The cost estimates were based on *(a)* the volume of concrete in the bridge superstructure, *(b)* the amount of prestressing steel required, and *(c)* the cost of formwork. The estimate did not include the cost of *(a)* pier and abutments; *(b)* scaffolding to support the formwork; *(c)* approaches to the bridge; or *(d)* site works, excavation, pavements and curbs, finishes, and painting. The following 1983 Canadian unit prices were used: \$1.85/lb for prestressing steel, \$58.30/yd^3 for concrete, and \$0.12/ft^2 of bridge deck area for grouting. Formwork costs were as follows: \$2.80/ft^2 of deck area for the solid-slab bridge; \$3.50/ft^2 of the surface area formed in the one-way ribbed-slab (T–beam) bridge; and \$2.75/ft^2 of deck area for the waffle slab bridge. The latter price was based on a reuse factor of 4 for the molded fiberglass pans (domes); recent advances in technology make it possible to increase the reuse factor to 24 in some construction-using modules. The results of the cost estimates are summarized in Table 1. This table presents the ratio of the estimated total cost of each bridge in solid-slab or one-way, ribbed-slab (T–beam) constructions to the estimated total cost of the corresponding bridge in waffle slab construction. From the results in Table 1, the waffle slab bridge is more economical than the two other alternatives.

ELASTIC ANALYSIS

The linear elastic response of prestressed waffle slab bridges can be readily predicted by use of several computer programs, such as STRAND *(5)* and SAP IV *(8)*. However, for an accurate prediction of such a response it is essential that the designer use realistic estimates of the orthotropic rigidities of the bridge. Formulas derived for the rigidities were based on extensive theoretical and experimental studies *(6)*. The usual assumptions in the analysis of orthotropic plates *(9)* as well as the following were made: *(a)* the number of ribs is large enough for the real bridge to be replaced by an idealized one with continuous properties, and *(b)* the area of the deck is magnified by the factor $1/(1 - \mu^2)$ to allow for the influence of the Poisson ratio μ of the concrete. Thus, referring to Figure 1, the orthotropic rigidities D_x and D_y and the coupling rigidities D_1 and D_2 of an uncracked section are expressed as

$$D_x = D + [Eh(e_x - h/2)^2/(1 - \mu^2)] + EI_x'/\alpha_x$$

$$D_y = D + [EH(e_y - h/2)^2/(1 - \mu^2)] + EI_y'/\alpha_y$$

$$D_1 = \mu D_x'$$

$$D_2 = \mu D_y' \qquad (1)$$

where

TABLE 1 RATIO OF ESTIMATED COST OF PRESTRESSED CONCRETE BRIDGES IN SOLID SLAB OR ONE-WAY RIBBED SLAB (T–BEAM) CONSTRUCTION TO THAT IN WAFFLE SLAB CONSTRUCTION

Bridge Category[a]	Type of Construction	Bridge Skew Angle θ			
		0°	15°	30°	45°
I	Solid slab	1.09	1.12	1.11	1.16
	One-way ribbed slab (T–beam)	1.62	1.61	1.59	1.68
II	Solid slab	1.18	1.33	1.30	1.29
	One-way ribbed slab (T–beam)	2.07	2.20	2.02	2.28
III	Solid slab	1.10	1.20	1.15	1.28
	One-way ribbed slab (T–beam)	1.22	1.46	1.45	1.51

[a] See Figure 2.

D = $Eh^3/12(1 - \mu^2)$ = flexural rigidity of the deck with respect to its middle plane;
h = thickness of the deck;
E = modulus of elasticity of the concrete;
α_x (α_y) = spacing of longitudinal (transverse) ribs;
e_x (e_y) = depth of the neutral plane from the top fiber for bending in the x (y) direction, given in Appendix A; and
I_x' (I_y') = moment of inertia of longitudinal (transverse) rib with respect to the assumed neutral axis, given in Appendix A.

The torsional rigidity of an uncracked section of a concrete waffle slab is estimated by means of the membrane analogy method with a modification that accounts for the stiffening effect afforded by the ribs (beam stems) in the direction orthogonal to the one under consideration.

Referring to Figure 1 and considering the geometry of the deflected membrane, the torsional constants for deck, stem, and concrete equivalent area for the steel are calculated and added to yield the torsional constant J. Thus, for a section normal to the y-axis (Figure 1),

$$J = J_1 + J_2 + J_3 \tag{2}$$

in which J_1, J_2, and J_3, the contributions of areas of the deck, stem, and concrete equivalent, respectively, to the steel, are defined as

$$J_1 = \frac{1}{2} K_1 \alpha_y h^3;$$

$$J_2 = K_1 d_y b_y^3, \quad \text{for } d_y \geq b_y;$$

$$J_2 = K_1 b_y d_y^3, \quad \text{for } b_y \geq d_y; \text{ and}$$

$$J_3 = 4K_1(n - 1)(A_s')^2/\pi \tag{3}$$

where K_1 is the usual constant for rectangular sections in torsion *(10)*. The contribution J_3, being relatively small, can be ignored in a practical design. The modification for J_1 is by means of the reduction factor of 1/2, which accounts for the continuity of the deck, it being distinct from the top flange of an isolated T–section. Because a waffle slab is stiffened by ribs in two orthogonal directions, the torsional contribution J_1 of the deck in one direction (see hatched area in Figure 1) is augmented by the stiffening rib in the orthogonal direction. Considering the section normal to the x-axis (Figure 1), the presence of the transverse rib W increases the torsional contribution J_s of the deck S to a value denoted by $J_{(S+W)}$. Hence, the augmented value of J_1 for the hatched area (normal to the y-axis) becomes

$$(J_1)_{\text{modified}} = J_1 J_{(S+W)}/J_S \tag{4}$$

Thus, Equation 2 becomes

$$J = (J_1)_{\text{modified}} + J_2 + J_3 \tag{5}$$

The torsional rigidity D_{yx} can now be calculated from

$$D_{yx} = GJ/\alpha_y \tag{6}$$

where $G = E/2(1 + \mu)$ = shear modulus. Similarly, the torsional rigidity D_{xy} of a section normal to the x-axis (Figure 1) can be calculated mutatis mutandis.

For a *cracked section*, the flexural rigidities can be expressed as

$$D_x = E[I_{sx} + I_{cx}/(1 - \mu^2)]/\alpha_x$$
$$D_y = E[I_{sy} + I_{cy}/(1 - \mu^2)]\alpha_y$$
$$D_1 = \mu D_x'$$
$$D_2 = \mu D_y' \tag{7}$$

where

I_{cx} (I_{cy}) = moment of inertia of the concrete and $(n - 1)$ times the area of compression steel, if any, in compression about the neutral axis for bending in the x (y) direction (expressions for I_{cx} and I_{cy} are given in Appendix A);
I_{sx} (I_{sy}) = moment of inertia of the transformed steel section about the neutral axis for bending in the x (y) direction, given in Appendix A; and
D_x' (D_y') = flexural rigidity of the deck with respect to the neutral plane of the gross cracked section associated with bending in the x (y) direction.

The torsional rigidity for a cracked section can be calculated from

$$D_{xy} = \alpha(D_x D_y)^{1/2} \tag{8}$$

where D_x and D_y are determined from Equation 7, and the torsional parameter $\alpha = D_{xy}/(D_x D_y)^{1/2}$, in which D_x and D_y are found from Equation 1 and D_{xy} is derived from Equation 6.

The designer should be aware that the calculated rigidities are affected by creep, which also influences the modular ratio n; these influences can be readily accounted for by adjusting E_c to a time-dependent modulus of deformation *(11)*, as well as augmenting the value of n according to the adopted code of practice.

ULTIMATE LOAD ANALYSES

The ultimate load analyses of waffle slab bridges were based on assumed yield line patterns of failure; the justification for these failure patterns were *(a)* test results from two post-tensioned waffle slab bridge models, continuous over two isolated interior column supports *(12)*; *(b)* test results from five simply supported waffle slab bridge models *(7)*; and *(c)* results from an extensive parametric study of a progressive failure analysis *(13)*. The customary assumptions in yield line analysis *(14)* were made. The analyses are applied to relatively wide waffle slab bridges with relatively weak edge beams. The predicted collapse load has been found to be invariably lower than the actual collapse load; the reason for this is that some load-enhancing factors such as strain hardening of the prestressing steel, torsional resistance of the waffle slab, and to a lesser extent membrane action in the slab are ignored in order to

simplify the analysis. The following cases of loadings were examined.

Uniformly Distributed Load Plus Concentrated Load

A skew waffle slab bridge, continuous over two isolated column supports C is shown in Figure 3. The two parallel ends of the bridge are simply supported and the angle of skew is θ. The inclination of the column line *CC* is α_1 in the range $0 \leq \alpha_1 < \theta$. The special case $\alpha_1 = \theta$ will be treated separately. It should be noted that a bridge geometry having $\alpha_1 > \theta$ is not economical because such a column arrangement increases the critical length of the bridge between the highly stressed obtuse corners and the column line; for this reason this case is not considered herein.

To conform to a possible deformation condition, a failure pattern is assumed where the yield lines *fg* and *oo'* are positive corresponding to a sagging moment condition and where the yield line *cd* is negative corresponding to a hogging moment condition. The yield line *fg* passes through the intersection of the two axes of rotation *cd* and *c'd'*. At collapse, it is assumed that the center *o* of the span deflects downward a distance δ; furthermore, from the extensive results obtained from the progressive failure analysis *(13)* the deflection at the center *o'* of the column line *CC* can be taken as $(c/l)^2\delta$ where *c* is the *x* distance between the two columns and *l* is the width of the bridge. In the design of a continuous bridge, the total dead load is generally more critical than the live load, and therefore the failure pattern is influenced by the former rather than by the latter. Denoting q_u as the ultimate superimposed load including dead load on the bridge per unit area and P_f as the factored concentrated live load at the center *o*, then equating the external and internal virtual works yields

$$q_u = \left\{R_1\left[R_2m_1 + R_3m_3 + \frac{2}{l}(2M_{BB} + M_{BT})\right] + \left(\frac{c}{l}\right)^2 R_4m_4 - P_f\right\} \div \left\{R_9 + \left(\frac{c}{l}\right)^2 R_{10}\right\} \quad (9)$$

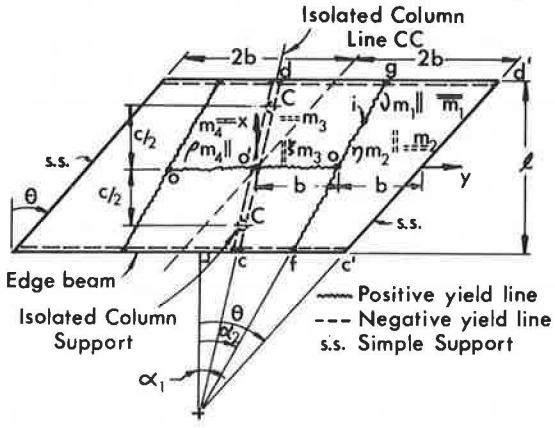

FIGURE 3 Assumed yield line pattern for continuous-skew bridge with $\alpha_1 \neq \theta$.

where

$m_1(\upsilon m_1)$ = ultimate positive moment of resistance per unit width (length) about the *x* (*y*) axis in the region of the span center *o*;
$m_3(\xi m_3)$ = ultimate negative moment of resistance at the column line *CC* per unit width (length) about the *x* (*y*) axis;
ρm_4 = ultimate positive moment per unit length about the *y* axis in the region of the column line *CC*;
$M_{BB}(M_{BT})$ = ultimate moment of resistance of the edge beam resisting a sagging (hogging) moment;
R_1–R_{10} = constants defined in Appendix B; and
$\tan \alpha_2$ = $\frac{1}{2}(\tan\theta + \tan\alpha_1)$, with α_1 always less than α_2, from the deformation geometry shown in Figure 5.

For a bridge subjected to a uniformly distributed load only, the ultimate collapse load q_u can be readily deduced from Equation 9 by putting $P_f = 0$. Equation 9 can be used for the following bridge geometries by making the following substitutions:

1. Two-span, continuous, skew bridge whose pier line is perpendicular to the direction of traffic. Put $\alpha_1 = 0$; $\tan\alpha_2 = \frac{1}{2}\tan\theta$.
2. Two-span, continuous, rectangular bridge. For $\alpha_1 \neq 0$, put $\theta = 0$, $\tan\alpha_2 = \frac{1}{2}\tan\alpha_1$; for $\alpha_1 = 0$, put $\theta = 0$, $\alpha_1 = \alpha_2 = 0$.
3. Two-span, continuous bridge with continuous pier line support. Put $c = 0$; $m_4 = \rho m_4 = 0$. This applies also to the previous bridge geometries 1 and 2.
4. Single-span bridge with nonparallel abutments. Put $m_3 = 0$; $M_{BT} = 0$; $\tan\alpha_2 = \frac{1}{2}(\tan\theta + \tan\alpha_1)$; $c = 0$; $m_4 = \rho m_4 = 0$, where θ and α_1 are the inclinations of the right and left abutments to the *x*-axis, respectively.

Collapse Load of a Bridge with Column Line Inclination $\alpha_1 = \theta$

For such a bridge the failure pattern is shown in Figure 4, with $\alpha_1 = \theta$ and $\alpha_2 = \theta/2$. Equating the external and internal virtual works yields the following expression for the ultimate uniformly distributed load,

$$q_u = \left\{R_{11}m_1 + R_{12}m_3 + R_{13}(2M_{BB} + M_{BT}) + \left(\frac{c}{l}\right)^2 R_{14}m_4 - P_f\right\} \div \left\{bl + \left(\frac{c}{l}\right)^2 R_{19}\right\} \quad (10)$$

in which R_{11}–R_{19} are defined in Appendix B. Equation 10 can be used for the following bridge geometries:

1. Two-span, continuous, skew bridge with continuous pier line support. Put $c = 0$, $m_4 = \rho m_4 = 0$.
2. Single-span bridge with parallel abutments. Put $m_3 = 0$, $M_{BT} = 0$, $\alpha_2 = \theta/2$, $c = 0$, $m_4 = \rho m_4 = 0$.

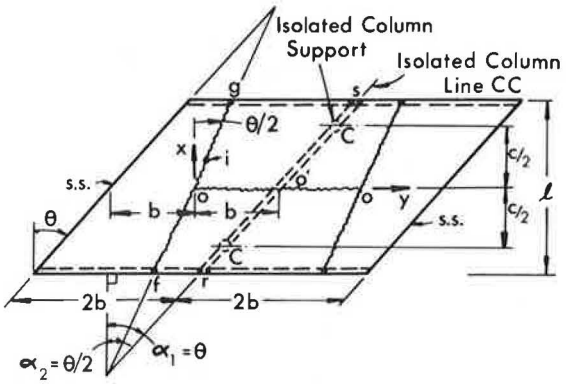

FIGURE 4 Assumed yield line pattern for continuous-skew bridge with $\alpha_1 = \theta$.

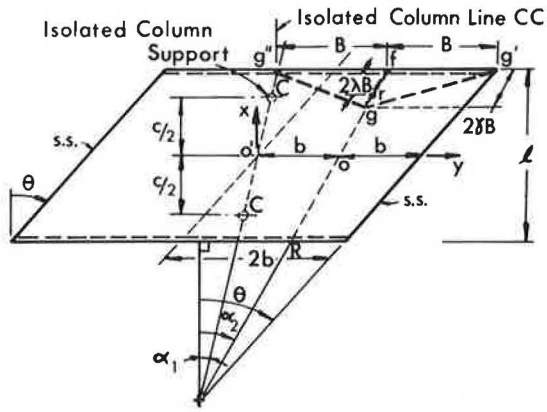

FIGURE 5 Assumed yield line pattern for continuous-skew bridge subjected to concentrated load near edge beam.

Concentrated Load Near an Edge Beam

It has been shown *(12)* that for such a loading the failure pattern can be assumed as shown in Figure 5. In this figure the concentrated load P is applied at a known distance $2\lambda B$ from the center of the edge beam along the skew centerline fR, which makes an angle α_2 with the x axis; $2B$ is the long span of an edge beam; fg is a positive yield line, whereas gg' and gg'' are negative yield lines. It is assumed that at failure the collapse load P_u and the uniformly distributed load q cause point f to deflect a distance δ. By equating the external and internal virtual works, it can be shown that the collapse load is

$$P_u = \left\{(4 \cos \alpha_2)\left[m_1 + m_2 + (\upsilon m_1 + \eta m_2) \tan^2 \alpha_2 - \frac{B^2}{6} q\right] \times \gamma^2 + \frac{(2M_{BB} + M_{BT})\,\gamma}{B} + \frac{\eta m_2}{\cos \alpha_2}\right\} + (\gamma - \lambda) \quad (11)$$

in which m_2 (ηm_2) = ultimate negative moment of resistance in the slab per unit width (length) about the x (y) axis in the region of the edge beam; m_2 (ηm_2) are not necessarily equal to m_3 (ξm_3) (see Figure 3); and $2\gamma B$ is the unknown length of the yield line fg. The nondimensional quantity γ is given in Appendix B.

From the bridge geometries,

$$B = b + \frac{l}{4}(\tan \theta - \tan \alpha_1), \text{ and}$$

$$\tan \alpha_2 = \tfrac{1}{2}(\tan \theta + \tan \alpha_1) \quad (12)$$

When the concentrated load P is close to the center of the edge beam, a conservative value for the collapse load can be deduced by putting $\lambda = 0$ in Equation 11,

$$P_u = \frac{(2M_{BB} + M_{BT})}{B} + 4\left\{\eta m_2\left[m_1 + m_2 + (\upsilon m_1 + \eta m_2) \times \tan^2 \alpha_2 - \frac{B}{6} q\right]\right\}^{1/2} \quad (13)$$

The expressions for B and $\tan \alpha_2$ (Equations 12) simplify according to the following bridge geometries:

1. Two-span, continuous, skew bridge with pier line perpendicular to the direction of traffic (i.e., $\alpha_1 = 0$): $B = b + (l/4) \tan \theta$, $\tan \alpha_2 = \frac{1}{2} \tan \theta$.
2. Two-span, continuous, skew bridge with pier line parallel to the abutments (i.e., $\alpha_1 = \theta$): $B = b$, $\alpha_2 = \theta$.
3. Two-span, continuous, rectangular bridge with pier line inclined an angle α_1 to the x axis: $B = b + (l/4) \tan \alpha_1$, $\tan \frac{1}{2}\alpha_2 = \tan \alpha_1$.
4. Two-span, continuous, rectangular bridge with $\alpha_1 = 0$: $B = b$, $\alpha_2 = \theta$.
5. Simple-span, skew bridge with nonparallel abutments: $M_{BT} = 0$; B and α_2 are given by Equations 12.
6. Simple-span, skew bridge with parallel abutments: $M_{BT} = 0$; $B = b$, $\alpha_2 = \theta$.

Treatment of Truck Loads

The desired Equations 9–13 can be used to deal with AASHTO truck live loads, for example, the AASHTO HS 20 truck *(14)*. Figure 6 shows a longitudinal section of a two-span, continuous, rectangular bridge loaded by a concentrated load P at the center O of one span through which a yield line passes, Figure 6*a*; an AASHTO HS 20 truck with the heaviest axle acting at O, Figure 6*b*; and an AASHTO HS 20 truck causing a yield line to form under the heaviest axle at a distance y from the right

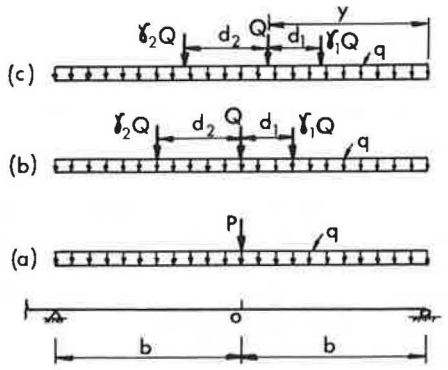

FIGURE 6 Longitudinal section of a continuous rectangular bridge under three loadings *(a)*, *(b)*, and *(c)*.

abutment, Figure 6c. The internal works due to the action of the loadings in Figures 6a and 6b are equal, and hence at failure their external works must be equal. Thus,

$$P = \left[1 + \frac{\gamma_1(b - d_1)}{b} + \frac{\gamma_2(b - d_2)}{b} + \left(\frac{c}{l}\right)^2 \times \left(1 - \frac{2|x|}{c}\right)\frac{\gamma_2 d_2}{b}\right] Q \quad (14)$$

in which d_1 and d_2 = distances of the wheel loads $\gamma_1 Q$ and $\gamma_2 Q_2$, respectively, from the wheel load Q, and $|x|$ is the x component of the distance of the center of the truck from the longitudinal centerline of the bridge. For an AASHTO HS 20 truck *(14)*, $\gamma_1 = 1/4$ and $\gamma_2 = 1$; introducing the live load factor $(\gamma\beta_L)$ for Q, the factored equivalent concentrated load P_f becomes from Equation 14:

$$P_f = \left[2.25 - \frac{(d_1 + 4d_2)}{4b} + \left(\frac{c}{l}\right)^2 \times \left(1 - \frac{2|x|}{c}\right)\frac{d_2}{b}\right](\gamma\beta_L)Q \quad (15)$$

For one-lane loading of the type shown in Figure 6b on a continuous rectangular bridge, equating the external and internal works for one span yields

$$q_u = \left\{\frac{l}{b}\left[2m_1 + m_3 + \frac{2}{l}(2\bar{M}_{BB} + \bar{M}_{BT})\right] + 2\rho m_4 \times \left(\frac{bc}{l^2}\right) - P_f\right\} \div \left[bl + bc\,\frac{(2c - l)}{4l}\right] \quad (16)$$

which is identical to Equation 9 for a continuous rectangular bridge ($\theta = 0$) with $\alpha_1 = \alpha_2 = 0$. Equation 16 leads to an overestimate of the ultimate load q_u because it is assumed that the positive yield line passes through the span center O in Figure 7; the ultimate load q_u, based on the true location of the yield line for the loading in Figure 6c, can be shown to be *(12)*

$$q_u = \left\{l(2bm_1 + m_3 y) + 2(2bM_{BB} + yM_{BT}) + 2\rho m_4 \frac{c}{l^2} y\,(2b - y)^2 - \left[(2b - y)(9y - d_1) - 4yd_2 + y\left(\frac{c}{l}\right)^2\left(1 - \frac{2|x|}{c}\right)d_2\right]\frac{\gamma\beta_L Q}{4}\right\} \div \left\{\left[bl + (2b - y) \times (2c - l)\frac{c^2}{4l}\right] y\,(2b - y)\right\} \quad (17)$$

where y, the distance of the positive yield line from the right abutment as shown in Figure 6c, is determined from Appendix B.

Because the resistance moment along the column line support has the greatest influence in shifting the positive yield line, Equations 16 and 17 can be used to obtain a better estimate for the collapse loads of continuous skew bridges. The procedure for analysis is as follows. Multiply the value of q_u obtained from Equations 9 or 10 by the ratio [(q_u from Equation 17)/(q_u from Equation 16)]. The procedure for design is the same as before, except for using the reciprocal of the preceding ratio, that is, [(q_u from Equation 16)/(q_u from Equation 17)].

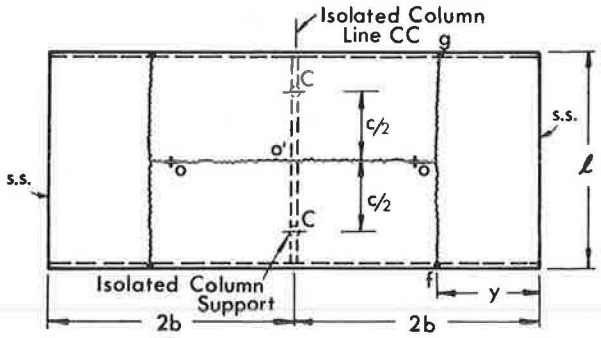

FIGURE 7 Assumed yield line pattern for continuous rectangular bridge.

For the edge loading discussed earlier, the most critical location of an AASHTO truck is close to the edge beam, that is, hypothetically $\lambda = 0$, where the differences $(B - d_1)$ and $(B - d_2)$ are the largest, resulting in the least collapse load. In such a case, the factored equivalent concentrated load P_f at the center of the edge beams is deduced from Equation 15 by replacing b with B and putting $c = 0$.

$$P_f = \left[2.25 - \frac{(d_1 + 4d_2)}{4B}\right](\gamma\beta_L)Q \quad (18)$$

Because m_3 does not contribute to P_u in Equations 11 and 13 and the influence of M_{BT} in shifting the yield line fg off center is relatively small, it can be assumed without too much error that the positive yield line remains at the center under an AASHTO truck loading. Thus, for a given factored value for q_D in Equation 13 and known moments of resistance, a value for P_u can be derived; equating P_u to P_f in Equation 18 yields the actual live load factor $(\gamma\beta_L)$; for design the reverse procedure is followed.

For multilane truck loading of bridges, the deflection at any point i on the positive yield line fg is necessary. For continuous bridges under concentrated loads at the center of each span (Figure 3),

$$\text{Deflection at } i = \delta_i = \frac{\delta}{2b}\,[2b + (\tan\theta - \tan\alpha_1)x] \quad (19)$$

in which $-l/2 \le x \le +l/2$, and δ is the deflection at the span center O. For continuous bridges with pier line inclination $\alpha_1 = \theta$ (Figure 4),

$$\delta_i = \text{constant} = \delta \quad (20)$$

Therefore, for multilane AASHTO truck loading, equivalent concentrated loads P_f acting along the positive yield line passing through the span center O are first deduced from Equation 15. Thus, as a result of multilane loading, P_f in Equation 9 (or 10) is replaced by $m\sum_{k=1}^{N} P_{f_k}\,(\delta_{i_k}/\delta)$, whereas $(\gamma\beta_L)Q$ in Equation 17 is replaced by $Nm(\gamma\beta_L)Q$. Here N = number of loaded lanes; m = load modification factor *(15)*; δ_{i_k}, = deflection of the equivvalent concentrated load P_{f_k}, given by Equation 19 or 20; and the term $(1 - 2|x|/c)$ in Equation 17 is replaced by

$$\frac{1}{N}\left[\sum_{k=1}^{N}\left(1-\frac{2|x_k|}{c}\right)\right]$$

The term $|x_k|$ is the x component of the distance between the longitudinal centerline of an AASHTO truck loading and the longitudinal centerline of the bridge.

For loads applied near an edge beam, it is reasonable to expect that only one AASHTO truck loading can be accommodated in that region; therefore, for this case multilane loading is not applicable.

As a worked design example, it is required to estimate the longitudinal positive moment m_1, at midspan for a two-span, continuous, skew, waffle slab bridge having a continuous pier line support (i.e., $c = 0$). The plan of the bridge is similar to the plan of Category I bridges shown in Figure 2*a*, with the following data: $\alpha_1 = 45°$; $\theta = 45°$; length of each span $2b = 90$ ft (27.43 m); three 12-ft traffic lanes with a total bridge width l = 42 ft 3 in. (12.88 m). Consider $q_D = 0.34$ kip/ft^2 (16.27 kPa); AASHTO HS 20 truck loading with $d_1 = d_2 = 14$ ft (4.27 m). Assume the following moment ratios: $\upsilon = 0.6$; $\eta = 1.0$; $\xi = 0.6$; $\rho = 0.6$; $m_1/m_2 = 1.5$; $m_1/m_3 = 0.8$; $m_1/m_4 = 2.0$. Take M_{BB} = 760 kip-ft (1.03 MN-m) and M_{BT} = 850 kip-ft (1.15 MN-m). The factored dead load $q_u = 1.3\ (0.34) = 0.44$ kip/ft^2 (21.75 kPa); the live load factor $(\gamma\beta_L) = 1.3[1.67(1 + \text{impact factor})] = 2.17[1 + 50/(125 + 90)] = 2.67$. From Equation 15 (with $c = 0$) and $Q = 32$ kip (142.2 kN), $P_f = [2.25 - 70/180](2.67)(32) = 159$ kip (707.6 kN). For a three-lane loading, P_f is replaced by

$$m\sum_{k=1}^{3} P_{f_k}\ (\delta_{i_k}/\delta)$$

with $m = 0.90$. Because $\alpha_1 = \theta$, Equation 20 yields

$$\delta_{i_1} = \delta_{i_2} = \delta_{i_3} = \delta;$$

and, because $c = 0$,

$$P_{f_1} = P_{f_2} = P_{f_3} = P_f.$$

Therefore, the term

$$m\sum_{k=1}^{3} P_{f_k}\ (\delta_{i_k}/\delta) = 0.9(P_f\delta + P_f\delta + P_f\delta)/\delta = 2.70P_f = 429.3 \text{ kip } (1{,}910 \text{ kN}).$$

Using Equation 10 (because $\alpha_1 = \theta$), with $q_D = q_u = 0.44$ kip/ft^2 (21.75 kPa), $P_f = 429.3$ kip (1,910 kN) and the other relevant data, yield $m_1 = 310$ kip-in./in. (1.38 MN-m/m). For a more refined solution, $q_D = 0.44$ kip/ft^3 is first augmented by the ratio [(q_u from Equation 16)/(q_u from Equation 17)] = 1.01 with y = 35.9 ft (10.95 in.). Using $q_u = (0.44)(1.01)$ in Equation 10 leads to $m_1 = 313$ kip-in./in. (1.39 MN-m/m). Applying a performance factor of $\phi = 0.9$, then m_1 becomes 348 kip-in./in. (1.55 kN-m/m). Hence, the other moments can now be estimated from m_1 and the assumed ratios. Preliminary calculations show that the following bridge geometry is adequate to provide the specified moments of resistance: 8 in. (200 mm) deck; 33 in. deep × 8 in. wide ribs; 6-ft spacing for longitudinal ribs; 8-ft 6-in. spacing for transverse ribs; ratio of prestressing steel = 0.5 percent; additional mesh steel reinforcing is required for local bending in the deck.

As illustrated in the preceding example, it is necessary in design to assume realistic values for the moment ratios υ, η, ρ, m_1/m_2, m_1/m_3, and m_1/m_4, based on previous experience, and on available results from an elastic analysis. It is recommended that in the longitudinal direction, ratios of negative to positive ultimate moments of resistance per unit width between 1 and 1.3 should be used; ratios of the ultimate moments of resistance per unit width in the transverse and longitudinal directions may vary from 0.5 to 1.0 depending on the aspect ratio of the bridge, edge support conditions, and the location on the bridge. In order to minimize cracks and crack widths, it is necessary also to vary the distribution of the required steel along the yield lines, following the elastic bending moments as closely as possible, for example, more negative steel near the column strips than in the middle strips. Furthermore the ultimate load method of design does not recognize the presence of large torsional moments and hence steep strain gradients at the corners and support regions of such bridges; therefore, these regions require special attention in design. Other construction details for this type of bridge structure include layouts of the prestressing steels and anchorage, provisions for the obtuse and acute corners, type of supports, and reinforcing the deck. These issues will be addressed in a forthcoming paper.

In the analysis of a bridge that has been designed elastically, the equations derived here can be used to estimate the values of the collapse load q_u or P_u, and hence the corresponding load factors $(\gamma\beta_D)$ and $(\gamma\beta_L)$ on the design loading. Although these equations are for two-span bridges, they can also be used to give conservative results for bridges with three or more spans.

ORTHOGONAL VERSUS NONORTHOGONAL RIB CONSTRUCTION

Although it is obvious that an orthogonal rib design (i.e., ribs orthogonal to the flow of traffic) is the correct configuration for rectangular bridges, it may not be so for skew bridges. To investigate this problem, tests were carried out on three bridge models *(16)* each having the same skew angle, self-weight, span, and width; the three structures were of the orthogonal-nonorthogonal-rib waffle slab constructions and solid-slab construction. The test results revealed that the orthogonal rib waffle slab construction for skew bridges can be expected to have the following advantages over the other two constructions: *(a)* a better load distribution characteristic; *(b)* a superior stiffness and ultimate load-carrying capacity; and *(c)* less severe stress concentration at the critical obtuse corners.

DYNAMICS OF WAFFLE SLAB BRIDGES

The dynamic response of waffle slab bridges was studied recently *(17)*. The analytical study was verified and substantiated by experimental results from tests on prestressed and reinforced waffle slab bridge models. The study showed that by increasing the stiffness by means of prestressing, the natural frequencies of the bridge are significantly enhanced; this phenomenon helps in avoiding resonance under low-frequency excited sources of vibration. Furthermore, to demonstrate the advantage of using waffle slab versus solid-slab construction the dynamic responses of the two types of construction having the same self-weight and planform geometry were compared. The natural frequency of the waffle slab bridge was 65 percent

greater than the one for the solid-slab bridge; this result was expected because the longitudinal and transverse rigidities of the waffle slab bridge were much greater than those of the solid-slab bridge. Furthermore, the first natural frequency of a waffle slab bridge appears to be greater than any vehicle frequencies, which are in the range 2–5 Hz, thus leading to a much lower dynamic load allowance used in design.

OTHER OBSERVATIONS

The presence of transverse ribs in the waffle slab bridge has additional advantages regarding the serviceability limit states. First, the transverse ribs make it possible to locate the prestressing steel at varying levels of eccentricity, leading to better control, possible elimination of longitudinal cracking of the deck, and reduced final deflections. Second, the transverse ribs are also important for providing crack control around the obtuse corners of skewed concrete bridge structures where complicated stress fields exist. Third, the transverse ribs help in reducing local deformation due to heavy wheel loads on the bridge deck for better live-load distribution. Furthermore, the shallower cross-sectional depth in waffle slab construction in comparison to the one-way ribbed-slab (T–beam) construction would result in smaller cost for bridge approaches.

Although construction details of this type of bridge will be addressed elsewhere, some brief comments on practical design are in order here. While prestressing in two directions may eliminate all tensile stresses in a waffle slab rectangular bridge, the same may not be possible in a waffle slab skew bridge. In the latter bridge, the direction of the top-surface principal stresses deviate considerably from those of the bottom-surface principal stresses as well as from the direction of prestress; this is especially so around the obtuse corners. To eliminate all tensile stresses in such cases requires excessively high levels of prestress and hence a heavier cross section, which may not be economical. It is more practical instead to provide untensioned reinforcement to resist local stresses when they occur. This refinement may be calculated in a similar way as in reinforced-concrete construction; the axial forces induced by the prestress in the steel reinforcement are ignored. It is suggested that, for crack control, the minimum percentage of untensioned steel in the transverse direction should be about 0.15 percent *(1)*. It is also important to remember to reduce the maximum compressive stress around the acute corners of waffle slab skew bridges by curtailing alternate prestressing cables in those regions.

It is usual practice to make the waffle solid over column supports; furthermore, shear requirements dictate the use of tapered pans near the exterior supports. In cases where moment connections are not necessary, low-friction pads such as Teflon or Tetron are suggested for bearings. Such bearing details normally provided in bridges to permit thermal changes are well suited to accommodate elastic shortening and rotation due to posttensioning.

Finally, one can expect prestressed waffle slab bridges to be much stiffer and stronger than similar bridges in reinforced concrete construction and with a smaller amount of secondary stress produced by sustained loads. In general, prestressed concrete construction also becomes more attractive in situations where construction depth is at a premium.

CONCLUSION

This study has shown that waffle slab bridges have the potential of being an economical alternative to other types of bridges. This economic advantage becomes greater with increase in width-to-span ratio or in skew angle of the bridge. The waffle slab construction, besides affording excellent access for inspection and maintenance of salt damage to prestressing steel, also reduces the dead load moment and deflection; these effects minimize the amount of secondary stresses produced by sustained loads. Furthermore, such bridges have a much superior dynamic response. The results presented herein provide the designer with aids for design and analysis of simple- and continuous-span waffle slab bridges.

REFERENCES

1. P. Csagoly and M. Holowka. *Cracking of Voided Post-Tensioned Concrete Bridge Decks*. Research Report 193. Ministry of Transportation and Communications, Downsview, Ontario, Canada, 1975.
2. T. Y. Lin, F. Kulka, and Y. C. Yang. *Post-Tensioned Waffle and Multispan Cantilever System with Y-Piers Composing the Hegenberger Overpass*. Concrete Bridge Design, SP23–27. American Concrete Institute, Detroit, Mich., 1969. pp. 495–506.
3. R. H. Wood. The Reinforcement of Slabs in Accordance with a Predetermined Field of Moments. *Concrete*, Vol. 2, No. 2, 1968, pp. 69–76.
4. J. B. Kennedy and B. Bakht. Feasibility of Waffle Slabs for Bridges. *Canadian Journal of Civil Engineering*, Vol. 10, No. 4, 1983, pp. 627–638.
5. *Suite of Bridge Design and Analysis Program HECB/B/13 STRAND (Version 1) User: Parts 1 and 2*. Department of the Environment, London, England, 1974.
6. J. B. Kennedy and S. K. Bali. Rigidities of Concrete Waffle Slab Structures. *Canadian Journal of Civil Engineering*, Vol. 6, No. 1, 1979, pp. 65–74.
7. J. B. Kennedy and I. S. El-Sebakhy. Waffle Slab Concrete Bridges: Ultimate Behaviour. *Journal of the Structural Division*, ASCE, Vol. 108, No. ST6, 1982, pp. 1285–1301.
8. K. J. Bathe, E. L. Wilson, and F. E. Paterson. *A Structural Analysis Program for Static and Dynamic Response of Linear System (SAP IV)*. Report EERC 72–11. Earthquake Engineering Research Center, University of California at Berkeley, April 1974.
9. H. T. Huber. Die Theorie der Kreuzweise Bewehrtren Eisenbetonplatten Nebst Anwendungen auf Mehrere Bautechnisch Wichtige Aufgaben uber Rechteckige Platten. *Der Bauingenieur*, Vol. 4, 1923, pp. 354–360.
10. S. Timoshenko and J. N. Goodier. *Theory of Elasticity*. McGraw-Hill Book Co., New York, 1970, p. 312.
11. M. A. Saeed and J. B. Kennedy. *Time-Dependent Deformation in Prestressed Concrete*. Symposium on the Design of Concrete Structures for Creep, Shrinkage, and Temperature Changes, International Association for Bridge and Structural Engineering, Madrid, Spain, 1970, pp. 217–227.
12. J. B. Kennedy and I. S. El-Sebakhy. Ultimate Loads of Orthotropic Bridges Continuous Over Isolated Interior Supports. *Canadian Journal of Civil Engineering*, Vol. 12, No. 3, 1985, pp. 547–558.
13. I. S. El-Sebakhy and J. B. Kennedy. Progressive Failure Analysis of Orthotropic Bridges. *Journal of Structures and Computers*, Vol. 24, No. 3, 1986, pp. 401–411.
14. K. W. Johansen. *Yield-Line Theory*. Translation, Cement and Concrete Association, London, England, 1962.
15. *Standard Specifications for Highway Bridges*, 12th ed., AASHTO, Washington, D.C., 1977.

16. J. B. Kennedy. Orientation of Ribs in Waffle-Slab Skew Bridges. *Journal of Structural Engineering*. Vol. 109, No. 3, March 1983, pp. 811–816.
17. N. F. Grace. *Free Vibration of Prestressed Continuous Composite Bridges and Skew Orthotropic Plates*. Ph.D. dissertation, University of Windsor, Ontario, Canada, 1986.

APPENDIX A

The following define the terms introduced in the section Elastic Analysis:

$$\begin{aligned} e_x &= [b_x d_x(h + d_x/2) + (n-1)A_s \\ &\quad \times (h + d_x - d') + \alpha_x h^2/2(1-\mu^2)] \\ &\quad \div [b_x d_x + (n-1)A_s + \alpha_x h/(1-\mu^2)] \\ e_y &= [b_y d_y(h + d_y/2) + (n-1)A_s' \\ &\quad \times (h + d_y - d'') + \alpha_y h^2/2(1-\mu^2)] \\ &\quad \div [b_y d_y + (n-1)A_s' + \alpha_y h/(1-\mu^2)] \\ I_x' &= b_x d_x[(h + d_x/2) - e_x]^2 \\ &\quad + (n-1)A_s[(h + d_x - d') - e_x]^2 \\ &\quad + b_x d_x^3/12 \\ I_y' &= b_y d_y[(h + d_y/2) - e_y]^2 \\ &\quad + (n-1)A_s'[(h + d_y - d'') - e_y]^2 \\ &\quad + b_y d_y^3/12 \end{aligned}$$

where

n	=	modular ratio;
b_x (b_y)	=	width of longitudinal (transverse) rib;
d_x (d_y)	=	depth of the longitudinal (transverse) rib;
d' (d'')	=	concrete cover to the center of the longitudinal (transverse) prestressing steels;
A_s (A_s')	=	area of prestressing steel in the longitudinal (transverse) rib; and
D_x' (D_y')	=	flexural rigidity of the deck with respect to the neutral plane of the gross cross section associated with bending in the x (y) direction.

$$I_{cx} = \alpha_x(kd_x)^3/3$$

$$I_{cy} = \alpha_y(kd_y)^3/3$$

$$I_{sx} = nA_s[(h + d_x - d') - kd_x]^2$$

$$I_{sy} = nA_s'[(h + d_y - d'') - kd_y]^2$$

The location of the neutral axis kd_x (or kd_y) is determined by equating the tension force to the compression force on the section. Thus, by assuming that the neutral axis lies in the deck, kd_x is given by

$$nA_s[(h + d_x - d') - kd_x] - \alpha_x(kd_x)^2/2(1-\mu^2) = 0$$

and kd_y by

$$nA_s'[(h + d_y - d'') - kd_y] - \alpha_y(kd_y)^2/2(1-\mu^2) = 0$$

APPENDIX B

The following terms appear in the section Ultimate Load Analysis.

$$R_1 = \frac{l}{b} \text{ (in which } 2b \text{ is the length of each span)}$$

$$R_2 = 2 + \frac{\upsilon(\tan\theta + \tan\alpha_1)^2}{2}$$

$$R_3 = 1 + \xi \tan^2 \alpha_1$$

$$R_4 = \frac{\rho}{b \sin\alpha_2 \tan\alpha_2}\,[R_5 \ln R_6 + R_7 \ln R_8]$$

[Note: When $R_7 \le 0$, put $R_7 \ln R_8 = 0$.]

$$R_5 = -b \sin\alpha_2 - \left(\frac{c}{2}\right)(\cos\alpha_2 + \tan\alpha_1 \sin\alpha_2)$$

$$R_6 = 1 + \frac{b \sin\alpha_2}{R_5}$$

$$R_7 = b \sin\alpha_2 - \left(\frac{c}{2}\right)(\cos\alpha_2 + \tan\alpha_1 \sin\alpha_2)$$

$$R_8 = 1 - \frac{b \sin\alpha_2}{R_7}$$

$$R_9 = \frac{[48b^2 + l^2(\tan\theta - \tan\alpha_1)^2]l}{48b}$$

$$R_{10} = \frac{bl}{2} - \frac{l^2}{8b \cos\alpha_2 \sin^2\alpha_2}\,(R_5 \ln R_6 + R_7 \ln R_8)$$

$$R_{11} = 2\left(\tan\frac{\theta}{2}\right)^{-1}\left(\cos^2\frac{\theta}{2} + \upsilon \sin^2\frac{\theta}{2}\right) \times \left[\ln\left(2b\cos\theta + l\tan\frac{\theta}{2}\right) - \ln\left(2b\cos\theta - l\tan\frac{\theta}{2}\right)\right]$$

[Note: When $\theta = 0$, put $R_{11} = \frac{2l}{b}$.]

$$R_{12} = \left(\tan\frac{\theta}{2}\right)^{-1}\left(\cos^2\theta + \xi \sin^2\theta\right) \times \left\{\ln\left[2b\cos^2\theta + (b\sin^2\theta + b)\tan\frac{\theta}{2}\right] - \ln\left[2b\cos^2\theta + (b\sin^2\theta - l)\tan\frac{\theta}{2}\right]\right\}$$

[Note: When $\theta = 0$, put $R_{12} = \frac{l}{b}$.]

$$R_{13} = \frac{8b\cos^2\theta}{4b^2\cos^2\theta - l^2\tan^2\frac{\theta}{2}}$$

$$R_{14} = \frac{\rho}{b \sin\frac{\theta}{2} \tan\frac{\theta}{2}} [R_{15} \ln R_{16} + R_{17} \ln R_{18}]$$

[Note: When $R_{17} \leq 0$, put $R_{17} \ln R_{18} = 0$.]

$$R_{15} = \left(-2b \cos\theta \sin\frac{\theta}{2} - c \cos\frac{\theta}{2}\right) \div 2 \cos\theta$$

$$R_{16} = \left[1 + \left(\frac{2b}{c}\right) \cos\theta \tan\frac{\theta}{2}\right]^{-1}$$

$$R_{17} = \left(2b \cos\theta \sin\frac{\theta}{2} - c \cos\frac{\theta}{2}\right) \div 2 \cos\theta$$

$$R_{18} = \frac{1}{\left[1 - \frac{2b}{c} \cos\theta \tan\frac{\theta}{2}\right]}$$

$$R_{19} = \frac{l^2}{8b \cos\frac{\theta}{2} \sin^2\frac{\theta}{2}} [R_{15} \ln R_{16} + R_{17} \ln R_{18}]$$

The nondimensional quantity γ in Equation 11 is derived from the stationary condition $\partial P/\partial\gamma = 0$, namely

$$\gamma^2 - (2\lambda)\gamma \cdot C = 0$$

where

$$C = \left\{\frac{\lambda}{B}(2M_{BB} + M_{BT}) + \frac{\eta m_2}{\cos\alpha_2}\right\} + \{4 \cos\alpha_2[m_1 + m_2(\upsilon m_1 + \eta m_2) \times \tan^2\alpha_2 - (B^2/6)q]\}$$

The distance y of the positive yield line from the right abutment, shown in Figure 6c, is determined from the stationary value of q_u in Equation 17, that is, $\partial q_u/\partial y = 0$, resulting in the following equation for y:

$$R_{20}y^4 + R_{21}y^3 + R_{22}y^2 + R_{23}y + R_{24} = 0$$

in which

$$\begin{aligned} R_{20} &= [c_3 + (2b)c_4 + c_5]c_9 - c_4c_8 \\ R_{21} &= 2[c_2 - (2b)c_5 - c_6 + c_7]c_9 + (4b)c_4c_8 \\ R_{22} &= [3c_1 - (2b)(c_2 - 2bc_5 - c_6 + 4c_7)]c_9 \\ &\quad + [c_2 + (2b)c_3 - c_6 + c_7]c_8 \\ R_{23} &= [2c_1 - (4b)c_7][c_8 - (2b)c_9] \\ R_{24} &= (-2b)[c_1 - (2b)c_7]c_8 \end{aligned}$$

where

$$c_1 = 2b(lm_1 + 2M_{BB})$$

$$c_2 = lm_3 + 2M_{BT} + 8\rho m_4 cb^2/l^2$$

$$c_3 = -8\rho m_4 cb/l^2$$

$$c_4 = 2\rho m_4 c/l^2$$

$$c_5 = 2.25(\gamma\beta_L)Q$$

$$c_6 = d_2\left\{\left[\frac{c}{l}\right]^2\left[1 - \frac{2|x|}{c}\right] - 1\right\}(\gamma\beta_L)Q$$

$$c_7 = -d_1(\gamma\beta_L)Q/4$$

$$c_8 = bl + \frac{bc(2c - l)}{2l}; \text{ and}$$

$$c_9 = \frac{(l - 2c)c}{4l}$$

Publication of this paper sponsored by Committee on Concrete Bridges.

Observations from a Field Study of Expansion Joint Seals in Bridges

FRANK E. WEISGERBER, ISSAM A. MINKARAH, AND STEPHAN R. MALON

Expansion joint seals in bridges continue to be a problem in that their success rate is far from an acceptable level. In a recent field study in Ohio, a significant percentage of seals were observed to be performing poorly in preventing passage of water and intrusion of debris into the expansion joint. The field study included rating of about 360 seals in eight rating categories based on visual inspection. Twenty-four different types of sealing systems were included, ranging in age from less than 1 month to 15 years or more. The resulting data were subjected to statistical analysis to determine average rating for each type of seal, correlation factors, and so forth. The calculated correlations were much weaker than intuitively expected and in some cases nonexistent. Few of the rated items showed significant correlation to either age or traffic count, which was attributable to several factors. This study by its nature included only those seals that survived long enough to be included. Some groups of seals included products of several different manufacturers. The seals were also operated under varying environmental conditions. Poor workmanship in installation was observed in many cases, causing poor performance at an early age. Several cases of faulty design details were observed. At least 5 percent of the observed seals suffered abuses that would not normally be expected or considered in the design, such as being covered over when the adjacent pavement was overlaid.

Attempts have been made to seal the expansion joints in bridges since 1914 *(1)*. Permitting water and debris to enter the expansion joints is detrimental to the structural components located below the bridge deck.

Special expansion joint seal designs have been patented as early as 1936. Today there are at least 30 different basic types of sealing systems being placed *(2)*, ranging from simple applications of poured-in-place asphalt-based compounds that are inexpensive but short lived and not very effective to rather complex and often expensive configurations composed of metal and elastomeric materials.

Tens of thousands of bridge expansion joint seals are now in place throughout the United States. Of course, all expansion joints in bridges are not sealed. Based on interviews with Ohio Department of Transportation (ODOT) bridge engineers, it is estimated that less than 10 percent of all bridge joints in the state system have been sealed. But it is not common to routinely specify particular sealing systems for new bridge pavements or those being overlaid or restored.

Experience has shown that installing successful expansion joint seals could be routinely accomplished. However, recent field observations suggest that expansion joint seals should not be taken for granted and at times actually obtaining a successful seal may be due cause for celebrating. The problems with expansion joint seals can be quite significant, leading the state of Tennessee, for example, to begin designing jointless bridges *(3)* despite the difficulties introduced in dealing with thermally induced stresses.

There are two main objectives in sealing expansion joints in bridges: to prevent the passage of water through the deck to the bridge components below and to prevent the intrusion of debris into the joint itself, which may render it inoperative. Additionally, there are many secondary but important objectives to be met in specifying, detailing, and installing these seals. The first cost, useful life, ease of maintenance, vulnerability to damage, esthetics, ride quality, and other factors must be considered in selecting a seal for a specific project. Certainly, too, the sealing system design process should include consideration of the specific circumstances of the application such as expected joint movement, skew angle, and traffic count.

The intent of this paper is to share some of the observations of a recent study of bridge expansion joint seals. This study, funded through a contract with ODOT, involved over 360 seals installed in about 120 bridges. Twenty-four different types of seals were observed. A few of the seals were less than 1 month old when inspected and a few had been in place for over 15 years. This set of seals constitutes a reasonably broad cross section of the seals in place in Ohio bridges.

The observations and data summary recounted in this paper may be useful to those concerned with expansion joint seals in bridges located in many geographic regions. A full account of the project, including study procedures and all data on the seals observed, is available in the project report.

SUMMARY OF STUDY PROCEDURES

It is necessary to briefly summarize the procedure used in the study in order to put the following presentation of results and the subsequent discussion in perspective.

The fundamental goals of this project were the following:

- Inspect a large variety of seals in place in a wide variety of circumstances,
- Rate the effectiveness and condition of the seals in several categories,
- Compare the types of seals to correlate seal effectiveness and site conditions, and
- Make observations and draw conclusions useful to future specifications of seals.

Department of Civil and Environmental Engineering, University of Cincinnati, Cincinnati, Ohio 45221.

Based on visual inspection, each seal was rated in each of seven categories: general appearance, condition of anchorage, debris accumulation, watertightness, surface damage, noise under traffic, and ease of maintenance. The ease of maintenance category was further divided into ease of cleaning and ease of replacement to make a total of eight categories. In the subsequent discussions, the categories are referred to in similar terms but are renamed to reflect desirable attributes. For example, debris accumulation became debris exclusion.

In each category the seal was rated numerically from 5 to 0, with 5 indicating perfect condition or effectiveness and 0 indicating failure. Detailed definition of the intermediate ratings 1–4 is outside the scope of this paper, but in general 4 indicates satisfactory condition, 3 represents marginal acceptability, 2 indicates unacceptable condition, and 1 indicates severe deficiency. The rating range of 5 to 0 has been used in studies conducted in several other states by other investigators, but it must be noted that the meaning of a particular value, for example, 3 in watertightness, varies from study to study. Moreover, composite ratings have been calculated differently in different studies in that some use an unweighted average of the seven main categories whereas others use a weighted average. Consequently, it is not appropriate to directly compare numerical results among studies conducted in different states.

Also, the rating scheme is prone to include subjectivity. In order to maintain consistency within the present study, the three investigators involved performed practice observations and ratings in the field until consistency was maintained, performed most ratings in teams of two, and occasionally repeated the rating for certain seals by a different team of investigators.

All of the data obtained, including the ratings just discussed and the parameters such as traffic counts, skew angles, and age of the seal were maintained in computer files. This process made it convenient to obtain statistical information using the SPSSx statistical analysis package *(4)*. The statistical analysis included finding the average rating in each category for each type of seal, an overall average for each type of seal, averages with respect to type and age of seal, standard deviations, and so forth. Also, correlation factors were calculated in order to determine how strongly the various items were related. Some of the results of this analysis are presented in the following section.

In addition to gathering data on the seals from site visits and from the plans and other records kept on file in the ODOT district offices, information was gathered from interviewing a bridge engineer in each of the 12 districts in Ohio. The authors take this opportunity to note their appreciation for the cooperation they received from these gentlemen. Many of the bridge engineers accompanied the investigators on inspection visits and were able to provide much valuable background and insights relative to the expansion joint seals.

SUMMARY OF RESULTS

The field study includes neoprene troughs, elastomeric compounds poured into sliding-plate joints, metal-faced joints, foam strips, and others. But three general types of seals together account for about 75 percent of all the seals observed in this study: compression seals (45%), strip seals (8%), and steel-reinforced modular seals (22%). Each of these three types includes the products of several different manufacturers grouped together. Figure 1 shows example illustrations of the seals included in each group. The two profiles shown to represent steel-reinforced modular seals are combined in one group because they both include steel reinforcement and both are typically installed in segments.

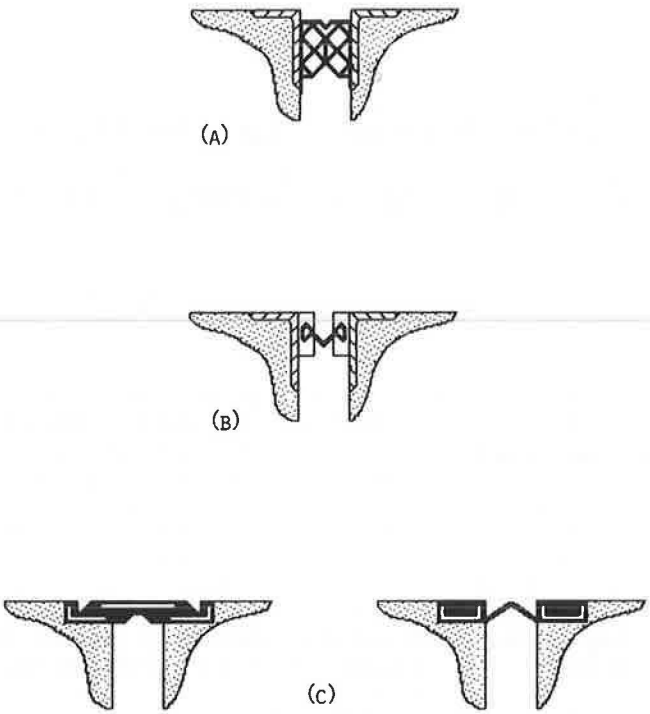

FIGURE 1 General types of bridge expansion joint seals: *(a)* compression seals, *(b)* strip seals, and *(c)* steel-reinforced modular seals.

Table 1 gives the average rating in each category for each general type of seal along with a composite rating average and the average age. In most items, the differences in average rating are small and probably of small significance. However, the differences in watertightness are large enough to be considered significant and seem to give the advantage to the strip seal over both the compression seal and the modular seal. The modular seals, on the other hand, are significantly better with respect to debris accumulation and ease of replacement. Compression seals are also easy to replace and the deck construction at the

TABLE 1 AVERAGE RATING BY GENERAL TYPE OF SEAL

Category	Strip Seals	Compression Seals	Steel-Reinforced Seals
General appearance	3.83	3.71	3.25
Condition of anchorage	3.83	3.96	3.66
Debris accumulation	3.20	3.15	3.76
Watertightness	3.93	3.44	3.11
Surface damage	3.93	3.79	3.35
Noise under traffic	3.93	3.61	3.79
Ease of cleaning	3.63	3.87	3.76
Ease of replacement	3.33	3.77	3.76
Straight average	3.70	3.66	3.56
Age (years)	8.27	6.83	8.73

TABLE 2 CORRELATION FACTORS FOR COMPRESSION SEALS

	TRAF	SKEW	MVT	AGE	ANCH	DEBR	WAT	DAM	SAVG
ANCH	–0.08	–0.02	–0.02	–0.18	1.00	0.37	0.50	0.62	0.81
DEBR	–0.17	–0.44	–0.05	0.09	0.37	1.00	0.33	0.22	0.47
WAT	–0.04	–0.48	–0.05	0.06	0.50	0.33	1.00	0.47	0.69
DAM	–0.11	–0.18	–0.22	–0.13	0.62	0.22	0.47	1.00	0.78
SAVG	–0.19	–0.32	–0.20	–0.07	0.81	0.47	0.69	0.78	1.00

NOTE: TRAF = average daily truck traffic; SKEW = skew angle of expansion joint; MVT = theoretical joint movement; AGE = age of seals in years; ANCH = condition of anchorage; DEBR = debris accumulation; WAT = watertightness; DAM = surface damage; and SAVG = unweighted average of all eight categories.

TABLE 3 CORRELATION FACTORS FOR STEEL-REINFORCED SEALS

	TRAF	SKEW	MVT	AGE	ANCH	DEBR	WAT	DAM	SAVG
ANCH	–0.29	–0.20	0.08	–0.25	1.00	0.12	0.36	0.69	0.74
DEBR	0.34	0.17	0.13	–0.08	0.12	1.00	0.49	0.11	0.46
WAT	0.01	0.00	–0.01	–0.29	0.36	0.49	1.00	0.51	0.81
DAM	–0.32	–0.22	0.03	–0.35	0.69	0.11	0.51	1.00	0.84
SAVG	–0.17	–0.16	0.05	–0.35	0.74	0.46	0.81	0.84	1.00

TABLE 4 CORRELATION FACTORS FOR STRIP SEALS

	TRAF	SKEW	MVT	AGE	ANCH	DEBR	WAT	DAM	SAVG
ANCH	0.25	0.05	0.01	–0.64	1.00	0.31	0.60	0.37	0.76
DEBR	–0.14	–0.01	–0.38	–0.32	0.31	1.00	0.45	0.16	0.64
WAT	0.25	–0.13	0.15	–0.78	0.60	0.45	1.00	0.47	0.76
DAM	0.55	0.23	–0.28	–0.39	0.37	0.16	0.47	1.00	0.71
SAVG	0.38	0.03	–0.28	–0.71	0.76	0.64	0.76	0.71	1.00

edge of the compression seal (the condition of anchorage) is least likely to deteriorate. The straight average, which is simply the average of all eight rating categories with equal weight, differs little between the types.

In an effort to discern which seal types might be more effective in certain circumstances, correlation factors were calculated. Two parameters with a correlation factor equal to 0 are totally unrelated. A correlation factor equal to 1 indicates a perfect relationship; a correlation factor equal to –1 a perfect inverse relationship.

Table 2 gives the correlation factors calculated for compression seals; Table 3, the correlation factors for seal-reinforced modular seals; and Table 4 the factors for strip seals.

In some regards, the results shown are disturbing. Correlations that were expected are in many instances much weaker than expected or virtually nonexistent. For example, Table 2 indicates that for compression seals both watertightness and surface condition are practically unrelated to traffic count (correlation factors of –0.04 and –0.11, respectively) although one might intuitively guess that some significant inverse relationship should exist. Table 3 indicates there is no correlation (0.01) between watertightness and traffic count for steel-reinforced modular seals, but there is some slight inverse correlation (–0.32) between traffic count and surface damage—that is, surface condition degenerates with increased traffic as expected. More disturbingly, Table 4 indicates that watertightness of strip seals slightly increases, in general, with traffic count (0.25) and further that the surface damage rating improves significantly (0.55) with traffic count.

Some calculated correlation factors do conform to expectations. In general, the strip seal watertightness strongly degenerates (–0.78) with age; condition of anchorage is at least moderately correlated to watertightness (0.50, 0.36, and 0.60); and watertightness and debris exclusion are somewhat related for all three types of seal. Nevertheless, overall the correlations appear to fail to substantiate some intuitive expectations.

DISCUSSION AND INTERPRETATION OF RESULTS

It is, for example, highly unlikely that surface condition or watertightness could actually improve with age or higher traffic count. However, in looking closely several factors were revealed that could at least partially explain why intuitive correlations did not manifest themselves in the data collected.

One major factor is that by and large this study included, as it must by its nature, only the surviving expansion joint seals. As previously noted, only a small percentage of all bridge joints are sealed. But once a given expansion joint is sealed, there is at least some effort made to keep it sealed; if a seal fails it is replaced or restored. Thus the only aged seals included in the study are ones that ought to have a decent rating in most categories—they are survivors. Seals that would have shown significant deterioration with age had been replaced. This situation tended to deemphasize correlations between condition and age. Interestingly, strip seals, the seal type judged most difficult of the three to replace, displayed the nearest to the expected

condition of correlation with age, tending to confirm this explanation.

Another factor that conceivably influences the data is that there is an observed geographic clumping of seal types. Some seal types are used frequently in some districts and rarely in others. Although Ohio is not one of the largest states in terms of area, its geologic and climatic circumstances differ significantly from corner to corner. Consequently, in some ways, the different types of seals were compared under different service conditions. This variation should be expected to influence the data in an unpredictable manner.

Also each of the three general types of seals for which average data are given actually includes several varieties of seals as produced by different manufacturers. It is possible, indeed likely and expected, that a strip seal produced by one firm will behave better or worse than one produced by another firm. Statistical analysis has been performed to compare the various brands of the seal types but the results are not given here. In several cases only two or three samples of a specific brand were included in the study, an insufficient number to give statistically reliable results; thus to show preference for or against a specific brand would not be justified, especially in view of the other observations made in this paper.

The factors most responsible for the distributing features of the numerical data were related to the following three field observations:

1. The workmanship associated with installing the various seals was obviously poor in 5 to 10 percent of the cases and suspect in many more. Seals were set higher than the deck surface, joints between modular seals were sloppily made, some seals were cut too short, and so forth. This poor workmanship lead to poor performance and therefore low ratings even though the seal system itself was apparently capable of very good performance.
2. In some cases the seals were installed with care just as detailed, but the details themselves were faulty. In a few cases the seals themselves appeared impervious to water but the runoff from the deck was directed to the berm area from which it was permitted to fall directly on the shelf on which the bearings were placed. This water then ran along the shelf and caused considerable deterioration in the bearings and spalling of the headwalls. There were also several other details that lead to similarly undesirable results.
3. In some cases, seals that may have been detailed well and installed with care performed poorly and thus received lower ratings because they had been abused after installation. Some 12 steel-reinforced modular seals in one stretch of pavement were covered over when the adjacent pavement was overlaid. It is difficult to say how much effect this had on watertightness, but it hurt the rating for general appearance significantly.

CONCLUSION

It would be inappropriate to draw hard and fast conclusions directly from the correlation factors shown here because of the points brought up in the foregoing discussion, and because the data are based on grouping the products of many manufacturers.

Despite the nature of some of the statistical data noted, the study has yielded results that should help future attempts at sealing the expansion joints in bridges. Observations on the workmanship and details indicates closer attention must be paid to these factors. Some of the numerical data suggest certain seals should be reconsidered before further use.

This study also suggests that further investigation is desirable and helps to direct future work, in which better general control should be maintained on the specimens observed, as implied by the discussion on the age-versus-performance data. This might be done by permitting certain test seals to deteriorate further before replacement or by maintaining long-term records including replacement data. Long-term records of failed joints in the present study could not be readily retrieved, if they existed at all. Obviously a follow-up study that reexamines the present subject seals periodically over a number of years should be initiated. It is also desirable to study more seals of certain types to gain statistical significance.

Because this study is quite recent, additional work is planned but not yet completed. Scheduled to be completed soon is performance of the statistical analysis described herein on data collected in similar studies conducted in other states.

The most important general observation made during this study is that the condition of the bridge structure located below the deck, including headwalls, bearings, girders, and other structural members, was directly dependent on the watertightness of the expansion joint. Good expansion joint seals save a great deal in terms of deterioration of the structures.

ACKNOWLEDGMENT

The research on which this paper is based was funded by the Ohio Department of Transportation and FHWA, U.S. Department of Transportation.

REFERENCES

1. W. Koster. *Expansion Joints in Bridges and Pavements.* Maclaren and Sons, London, England, 1969.
2. J. J. Hill and A. M. Shirole. Bridge Joint Systems—A Performance Evaluation. In *Transportation Research Record 990*, TRB, National Research Council, Washington, D.C., 1984, pp. 1–4.
3. C. L. Loveall. Jointless Bridge Decks. *Civil Engineering Journal of ASCE*, Vol. 55, No. 11, Nov. 1985.
4. *SPSSx User's Guide.* 2nd ed., SPSS Inc., Chicago, Ill., 1986.

Publication of this paper sponsored by Committee on Sealants and Fillers for Joints and Cracks.

Strengthening of Steel Stringer Bridges by Selective Stiffening

KENNETH F. DUNKER, F. WAYNE KLAIBER, AND WALLACE W. SANDERS, JR.

When indeterminate structures such as steel stringer bridges are strengthened by the addition of material, they are also stiffened at the locations where material is added. Under elastic conditions, this stiffening has the effect of attracting stress away from other parts of the structure. For steel stringer bridges in need of strengthening, it may be possible to add material selectively in order to strengthen and stiffen some critical locations and at the same time reduce the stresses at other critical locations. Reasonable amounts of stiffening can be achieved by addition of diaphragms, by addition of composite action in noncomposite bridges, and by addition of coverplates or angles to stringers. This stiffening, which can affect live-load moments by as much as 20 percent, can be used to increase the rating of bridges. Strengthening of a stringer bridge by selective longitudinal stiffening under allowable stress design generally increases the flexural strength of the bridge. Because selective stiffening may have positive or negative effects on fatigue-critical details, the effects must be checked.

The two major classifications of structures, determinate structures and indeterminate structures, behave differently when modified; these differences need to be considered if and when one of these structures needs to be strengthened. Elastic shears and moments in determinate structures are independent of structure stiffness, whereas elastic shears and moments in indeterminate structures are dependent on structure stiffness. One strategy for strengthening determinate structures is to add material at locations of overstress. If the same strategy is applied to indeterminate structures, the additional material has the effect of stiffening locations of overstress. The stiffened locations attract additional stress, and some of the benefits of the additional material are lost.

An alternate strategy for strengthening indeterminate structures is to add material that is chosen primarily for its stiffening effects. With this strategy, material can be placed to attract stress away from critical regions. The material can then have the dual effect of strengthening the locations where it is placed and of strengthening other locations by relieving stress. This alternate strategy cannot be used to overcome major weaknesses in a structure but can be used to adjust minor weaknesses, thus reducing the total strengthening requirements. It is quite possible that strengthening by selective stiffening offers some additional options in terms of construction accessibility and economics.

Bridge Engineering Center, Iowa State University, 416 Town Engineering, Ames, Iowa 50011.

Selective stiffening is one of the numerous strengthening methods investigated under the NCHRP Project 12–28(4), *Methods of Strengthening Existing Highway Bridges (1).*

SIMPLE-SPAN BRIDGES

In the United States, simple-span, steel stringer bridges are usually analyzed and designed as determinate structures. In reality, however, a simple-span bridge is indeterminate because modifications in transverse stiffness, longitudinal stiffness, and plan geometry of the bridge affect distribution of live load to stringers. So that simple-span bridges can be designed as determinate structures, the indeterminacy must be considered through use of the wheel load fractions in the AASHTO bridge design specifications *(2).*

One common strategy for strengthening a simple-span stringer bridge is to add material to each stringer over the center of the span, where overstress occurs. Material may be added by making the bridge deck composite with the stringers. This is done by using shear connectors or by bolting steel angles to each stringer web near top and bottom stringer flanges. This strategy is necessary when strengthening is required to overcome major weaknesses. When only minor weaknesses need to be overcome, an alternate strategy is to increase the transverse stiffness of the bridge with the goal of distributing live loads away from the overloaded stringers, in order to use the longitudinal strength of the bridge more effectively.

Finite element analyses performed by the United States steel industry *(3)* for steel stringer bridges having spans of 100 to 400 ft have indicated potential reductions of 20 to 45 percent in live-load moments for interior stringers. The finite element analyses indicated little potential for reduction in live-load moments for exterior stringers. These analyses cover relatively long-span bridges but neglect the many short-span steel stringer bridges in existence.

In order to determine the potential benefits of transverse stiffening for short-span bridges, a series of computations was performed for typical two-lane and three-lane bridges. The bridges are from the FHWA standard bridge plans for noncomposite steel stringer bridges *(4).* The bridges vary in span from 20 to 70 ft in 10-ft intervals, have an 8-in.-thick deck, and are designed for HS20–44 loading. For the two-lane study, the minimum-width 28-ft roadway was chosen, for which the bridges have four wide-flange steel stringers spaced 8 ft apart. The relatively heavy concrete curbs and guard rails on the FHWA plans were neglected so that the bridges in this study do not have stiffened edges. Transverse stiffening effects of steel

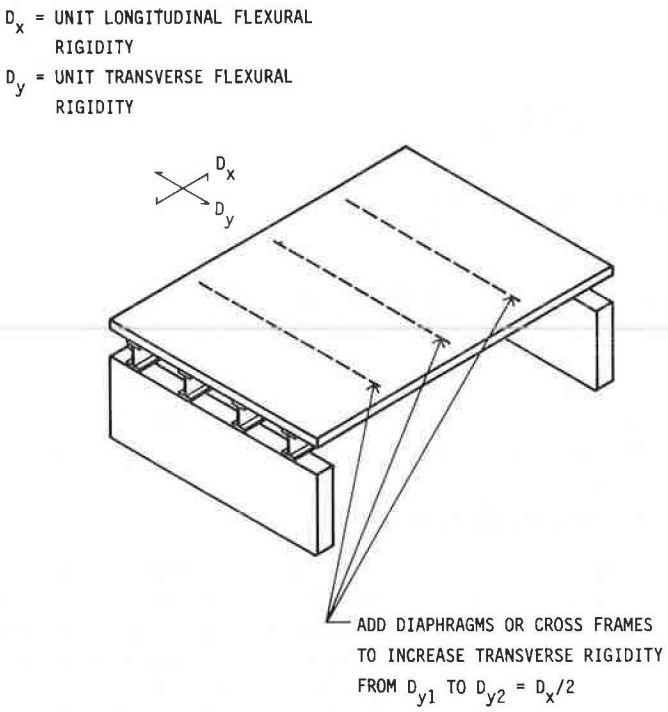

FIGURE 1 Transverse stiffening of simple-span bridges.

diaphragms, which would be small, were neglected so that the transverse stiffness of the bridges depends only on the deck.

The basic concept of transverse stiffening is illustrated in Figure 1. Diaphragms or cross frames are added to the bridge in order to increase the unit transverse flexural rigidity D_y to half the longitudinal flexural rigidity D_x. The required increase in transverse stiffness varies from a factor of approximately 4 to approximately 40, depending on design load and span. This transverse stiffening could theoretically be achieved by means of concrete or steel cross members spaced 8 to 16 ft apart. In the two-lane and three-lane studies, this transverse stiffening was performed for both the FHWA bridges designed for HS20–44 loading and similar bridges having reduced steel stringer sizes for H15–44 loading.

All bridges were analyzed for load distribution by means of the method presented by Bakht and Jaeger *(5)*. Based on orthotropic plate theory, this method accounts for transverse and longitudinal plate stiffnesses, is quite easy to use, and meets AASHTO requirements for a more accurate analysis. The method had been verified by grillage analysis for stringer bridges with at least two diaphragms at third points or three diaphragms at quarter points *(6)*.

In Figure 2, the horizontal line at the value of 1.0 represents the constant AASHTO wheel loading fraction $S/(4.0 + 0.25S)$, where S is the 8-ft stringer spacing. All of the wheel load fractions computed by the method based on orthotropic plate theory are less than the AASHTO fraction because the lines representing computed values never increase above 1.0. Figure 2 shows little difference between the unstiffened HS20–44 and H15–44 bridges and between the stiffened HS20–44 and H15–44 bridges. The beneficial effect of the transverse stiffening is about 1 percent for the 20-ft-span bridges and increases to about 5 percent for the 70-ft-span bridges.

The horizontal line at 1.0 in Figure 3 represents the constant AASHTO wheel load fraction for interior stringers of $S/5.5$, where S is the 8-ft stringer spacing. Except for the 20-ft span, the AASHTO fraction is conservative for the four cases in the figure. For an interior stringer, differences exist between the

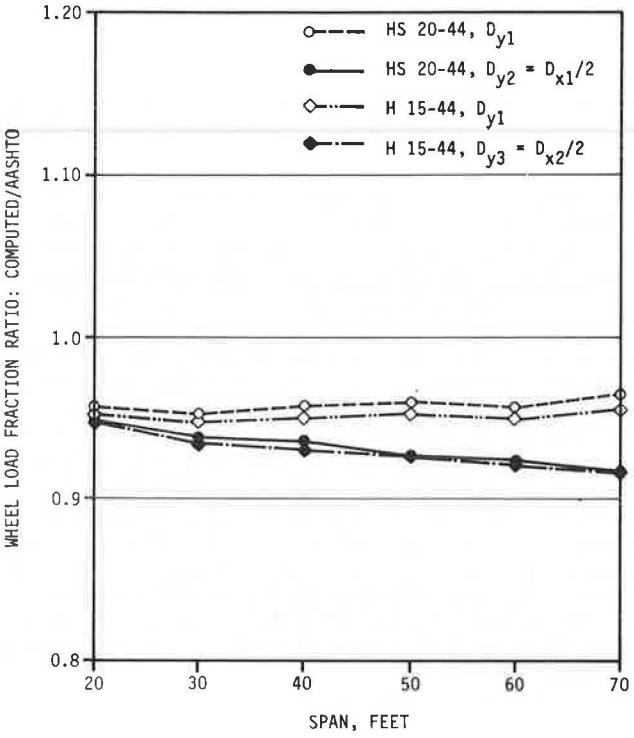

FIGURE 2 Effect of transverse stiffening on exterior stringer for two-lane bridges, 28-ft roadway.

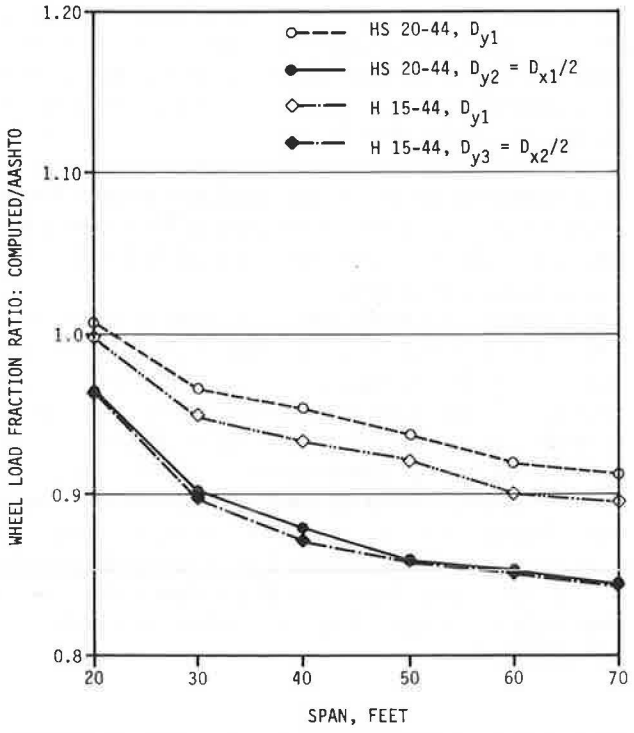

FIGURE 3 Effect of transverse stiffening on interior stringers for two-lane bridges, 28-ft roadway.

unstiffened HS20–44 and H15–44 bridges and between the stiffened HS20–44 and H15–44 bridges, and generally more variations occur in load fractions with a change in span. Beneficial effects of transverse stiffening range from 5 percent for a 20-ft-span bridge to 8 percent for a 70-ft-span bridge.

The two-lane bridges considered up to this point are relatively narrow and arguably not as likely to benefit from transverse stiffening as wider bridges. In order to examine the effects of transverse stiffening on wider bridges, four series of three-lane bridges with 44-ft roadway widths, based on the FHWA standard plans *(4)*, were examined. All of the bridges in the series have six stringers spaced at eight feet. Computations were again performed for unstiffened and stiffened HS20–44 and H15–44 bridges.

The analysis results illustrated in Figure 4 are very similar to the results illustrated in Figure 2 for two-lane bridges. The results plotted in Figure 5, however, show more variation from those plotted in Figure 3. Most of the wheel load fractions computed by the Bakht-Jaeger method exceed the AASHTO interior stringer fraction, indicating that the AASHTO fraction is unconservative. The transverse stiffening does have more effect on three-lane bridges than on two-lane bridges. The beneficial effects of transverse stiffening range from 3 to 15 percent.

Increasing the transverse stiffness of a steel stringer bridge can reduce live-load moments to stringers by as much as 15 percent and thereby increase the rating of a bridge. Maximum reductions occur for interior stringers in wider and in longer-span bridges. If all stringers are of the same size, as required by the current AASHTO specifications, the relatively minimal benefit for exterior stringers may not be a limiting factor, because the exterior stringers usually will be oversized in the original design.

CONTINUOUS-SPAN BRIDGES

In usual practice, individual stringers in continuous-span bridges are analyzed and designed as indeterminate members, neglecting the additional indeterminacy of the transverse stiffness of the deck. The stiffnesses of stringers often change as coverplates are added or as stringers are made composite with the bridge deck. Because these changes in stiffness significantly alter the design moments in the various positive and negative moment regions, these changes need to be considered when strengthening a continuous-span bridge by adding material to the stringers.

In order to demonstrate the effects of selectively stiffening noncomposite steel stringers, a series of stiffening experiments was conducted on a three-span stringer having spans of 64, 80, and 64 ft as shown in Figure 6. These span lengths are from one of the standard bridge designs *(4)*. The selective stiffening was applied as a doubling of the moment of inertia in positive- and negative-moment regions. The increased moment of inertia could easily be achieved in positive-moment regions by making the stringer composite with the bridge deck. (This assumes that bond between the deck and stringers is broken, which is not necessarily true.) In either the negative- or the positive-moment regions, the increased moment of inertia could be obtained by addition of coverplates or by addition of angles bolted to the stringer web near top and bottom flanges.

Five stiffening cases used for the analysis experiments are illustrated in Figure 6. The three-span stringer with constant

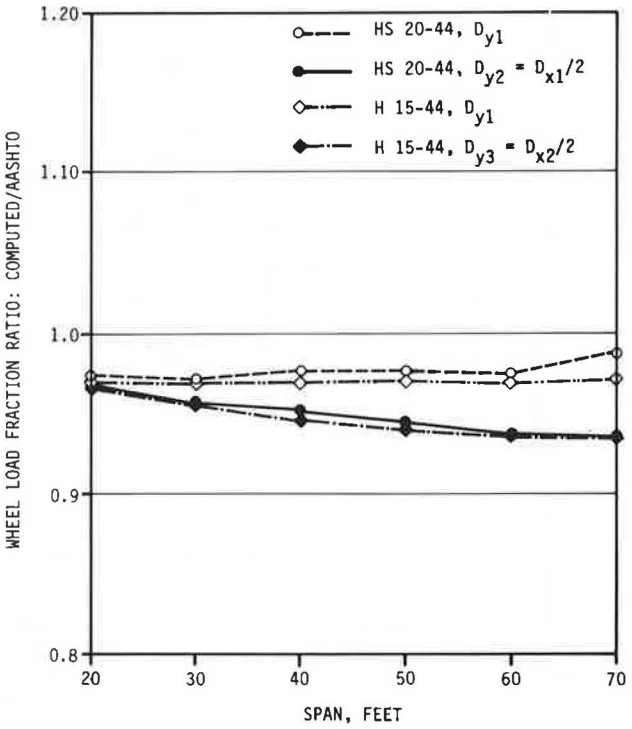

FIGURE 4 Effect of transverse stiffening on exterior stringers for three-lane bridges, 44-ft roadway.

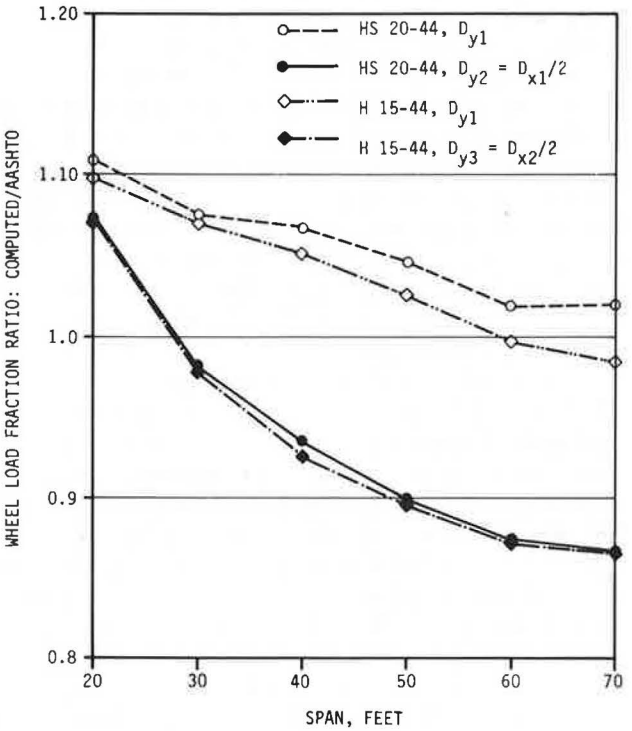

FIGURE 5 Effect of transverse stiffening on interior stringers for three-lane bridges, 44-ft roadway.

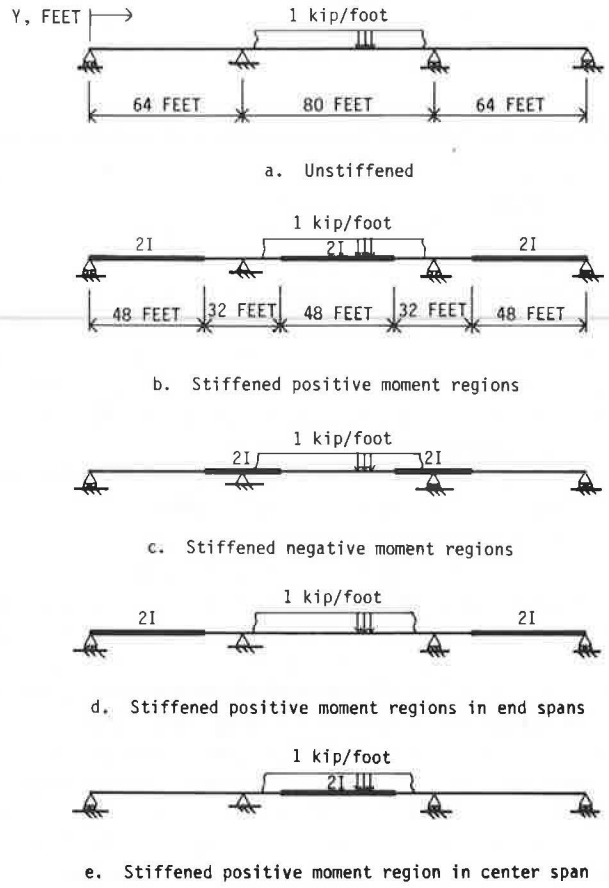

FIGURE 6 Longitudinal stiffening cases for three-span continuous stringer.

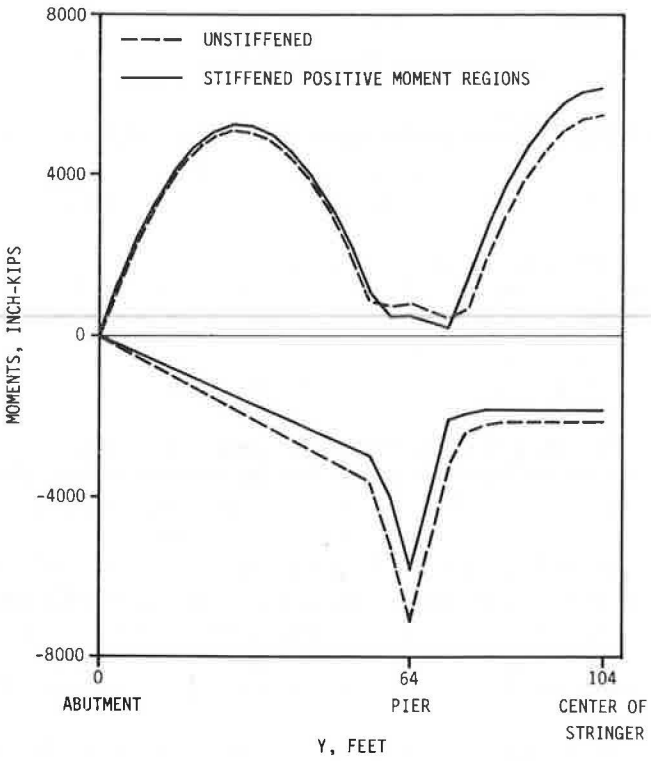

FIGURE 7 Moment envelopes for three-span continuous stringer.

moment of inertia in Figure 6*a* is the basis for all comparisons. In Figure 6*b* the moment of inertia has been doubled in all positive-moment regions, and in Figure 6*c* the moment of inertia has been doubled in all negative-moment regions. Figures 6*d* and 6*e* represent positive-moment stiffening for selected spans. In Figure 6*d*, the end spans are stiffened, and in Figure 6*e* the center span is stiffened.

A uniform load, which would simulate a lane load without concentrated loading, was applied to the various spans individually and in combinations to produce positive- and negative-moment envelopes for all stringers. The envelopes for Figures 6*a* and 6*b* are plotted in Figure 7 for the left-end span and the left half of the center span. The total envelopes are symmetrical with respect to the middle of the center span.

Stiffening of the positive-moment regions in Figure 6*b* has the effects of significantly decreasing negative moments near the continuous support, of significantly increasing positive moments near the middle of the center span, and of very slightly increasing the positive moments near the middle of the end spans. This same effect is shown in Figure 8, where the ratio of the positive-moment envelope for Figure 6*b* over the positive-moment envelope for Figure 6*a* and the ratio of the negative-moment envelopes have been plotted. The positive-moment envelope ratios in the end span are nearly 1.0, indicating little change from unstiffened to stiffened stringer. The negative-moment envelope ratio near the first interior support is approximately 0.8, which indicates that stiffening of the positive-

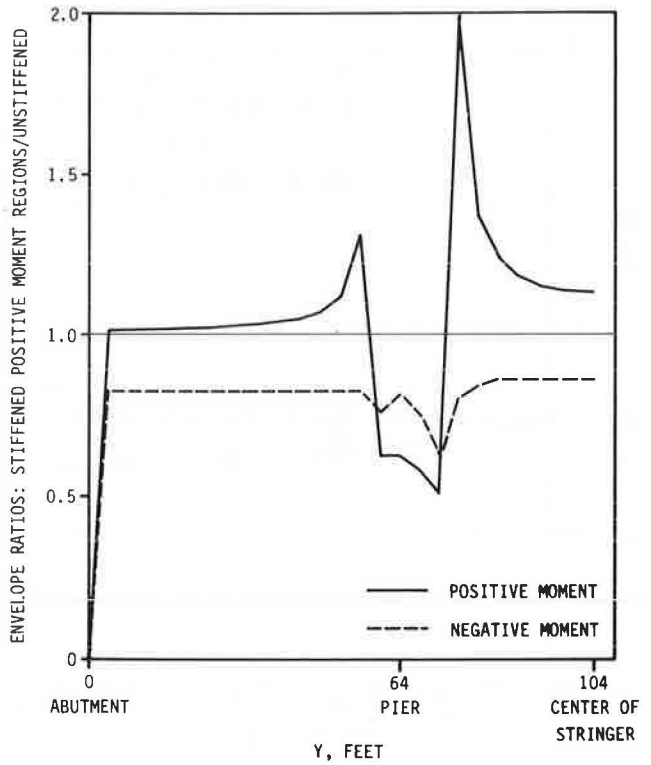

FIGURE 8 Moment envelope ratios for three-span continuous stringer.

TABLE 1 MOMENT RATIOS FOR THREE-SPAN CONTINUOUS STRINGERS

Stiffening Case	Moment Sign	Moment Ratio: Stiffened/Unstiffened Case		
		End Span Y = 25.6 ft	Pier Y = 64 ft	Center Span Y = 104 ft
	Positive	1.02	0.62	1.13
	Negative	0.83	0.81	0.86
	Positive	0.98	1.50	0.87
	Negative	1.16	1.19	1.13
	Positive	1.05	0.78	0.94
	Negative	1.08	0.93	0.68
	Positive	0.96	0.78	1.19
	Negative	0.75	0.90	1.24

Note: Underline indicates usual design criterion.

moment regions has reduced the critical support moments by about 20 percent. The positive-moment envelope ratios near the middle of the center span are about 1.15, which indicates a 15 percent increase in positive moment with positive-moment region stiffening. The large variations in ratios near inflection points have little effect on allowable stress design in most cases because those moments are relatively small, but the variations would have an effect on any fatigue-critical details.

The effects of stiffening positive moment regions are given again at the top of Table 1, for locations on the spans and at the pier typically used as critical moment locations in design or rating of a bridge. The effects of negative-moment region stiffening, also given in Table 1, are in the opposite directions, as can be expected. The negative moment increases 19 percent near the pier and positive moments decrease about 13 percent near the middle of the center span.

Table 1 also illustrates the effects of stiffening the positive-moment regions only in the end spans. The critical positive moment in the end spans increases by 5 percent, the critical negative moment at the support decreases by 7 percent, and the critical positive moment at the middle of the center span decreases by 6 percent. Stiffening the positive-moment region of the center span has a more dramatic effect in attracting moment. The critical positive moment for that span increases by 19 percent. The critical negative moment at the support decreases by 10 percent, and the critical positive moment in the end spans decreases by 4 percent.

The various stiffening patterns can be used to attract moment away from negative-moment regions or certain positive-moment regions. It may be possible to strengthen a continuous stringer bridge adequately by increasing the stiffness in positive-moment regions and taking advantage of the additional material at those locations and the reduced moments near supports.

The longitudinal stiffening effects just discussed quite possibly can be combined with the transverse stiffening effects discussed for simple-span bridges. Bakht and Jaeger *(5)* suggest that lengths between inflection points can be used to determine equivalent orthotropic plates for purposes of determining wheel load fractions. With selective longitudinal stiffening and transverse stiffening it may be possible to compound live-load stress reductions. Studying these combined effects for certain strengthening applications would be worthwhile, and the combined effects should be verified experimentally before being used in design or rating computations.

FATIGUE AND STRENGTH

Fatigue stresses are dependent on the stress ranges for live loads at specific critical locations. Selective longitudinal and transverse stiffening also alter those stress ranges. Those changes need to be considered in modifying the stiffness of a stringer bridge for strengthening purposes.

Transverse stiffening can increase the rating of a bridge but does not increase the overall longitudinal moment strength of a bridge. Transverse stiffening, therefore, may not be an option if moment strength is critical. Selective longitudinal stiffening generally increases the flexural strength of continuous stringers at the stiffened locations. If these locations are plastic hinges, selective stiffening increases the flexural strength of the stringers.

SUMMARY AND CONCLUSIONS

The usual strategy of strengthening a structure by adding material at overstressed locations is an excellent strategy for increasing the rating of determinate structures. The stiffening

effects of that material, however, can have both beneficial and nonbeneficial effects for indeterminate structures such as steel stringer bridges. Stiffening effects are most obvious for continuous-stringer bridges but are also present in simple-span bridges with respect to the transverse direction. A reasonable amount of transverse stiffening can reduce wheel load fractions by up to 15 percent for noncomposite, wide-flange steel stringers in short-span bridges. Selective longitudinal stiffening of continuous-span steel stringers can have the effect of increasing or decreasing live-load moment by as much as 20 percent at critical locations. It may be possible to compound live-load stress reductions for transverse and longitudinal stiffening in continuous-span bridges.

Because fatigue is associated with live-load stress ranges, any transverse and longitudinal stiffening associated with strengthening of stringer bridges must be planned carefully so as not to aggravate any existing fatigue problems or create new problems. Transverse stiffening does not increase the longitudinal flexural strength of a bridge; however, longitudinal stiffening generally increases flexural strength.

ACKNOWLEDGMENT

Research for this paper was sponsored by AASHTO, in cooperation with FHWA, and was conducted by NCHRP.

REFERENCES

1. F. W. Klaiber, K. F. Dunker, T. J. Wipf, and W. W. Sanders, Jr. *Methods of Strengthening Existing Highway Bridges.* Preliminary Final Report for NCHRP 12–28(4), ISU–ERI–Ames 87049. Ames, Iowa, 1986.
2. *Standard Specifications for Highway Bridges.* 13th ed. AASHTO, Washington, D.C., 1983.
3. *Steel Bridges, The Best of Current Practice.* American Institute of Steel Construction, Inc., Chicago, 1985.
4. *Standard Plans for Highway Bridges, Vol. II, Structural Steel Superstructures.* FHWA, U.S. Department of Transportation, 1982.
5. B. Bakht and L. G. Jaeger. *Bridge Analysis Simplified.* McGraw-Hill, New York, 1985.
6. M. S. Cheung, R. Jategaonkar, and L. G. Jaeger. Effects of Intermediate Diaphragms in Distributing Live Loads in Beam-and-Slab Bridges. *Canadian Journal of Civil Engineering*, Vol. 13, No. 3, June 1986, pp. 278–292.

Publication of this paper sponsored by Committee on Steel Bridges.

Review of Field Measurements for Distortion-Induced Fatigue Cracking in Steel Bridges

JOHN W. FISHER, BEN T. YEN, AND DAVID C. WAGNER

Through a review of existing field inspection results and bridge details, many bridges have been identified as susceptible to out-of-plane, distortion-induced fatigue cracking. The review includes floor beam girder, multiple-girder diaphragm, and floor beam tie girder box systems. Consideration is given to primary live-load stresses on the global scale, whereas live-load stress ranges, rotations, and out-of-plane distortions are investigated at the local level. The details of plate attachment, the manner of force transmittal between components, and the specific geometry at gaps are shown to be influential factors in determining the magnitude of out-of-plane distortions and corresponding stresses. Cases are cited in which secondary members imposing out-of-plane displacements of only thousandths of an inch have resulted in cyclic bending stresses at the level of allowable stresses at details. Specific behavior for each detail is discussed.

Forces in secondary members such as cross bracing can cause lateral deflection in steel girder webs, resulting in fatigue cracking. Cracks have also developed in the webs of girders due to differential deflection of parallel girders and end rotations of transverse floor beams. These out-of-plane deflections and rotations generate high-magnitude secondary plate-bending stresses. Furthermore, when secondary stresses are directly superimposed over the primary stresses in steel members, fatigue cracking occurs quite early.

These secondary stresses are not calculated in normal design and rating procedures; thus fatigue provisions have not been applied to this type of cracking. The effect of out-of-plane distortion on a few structural details is presented with the review of case study results.

FLOOR BEAM CONNECTION PLATES

Extensive cracking has developed in girder web plates at the ends of floor beam connection plates. Results of studies indicate the cracking to be the direct result of cyclic, secondary bending stresses that are generated through relative out-of-plane movement. These displacements, though often less than 0.005 in. (0.130 mm), concentrate in gaps between the floor beam connection plate and the girder tension flange. Figure 1 shows the crack developed in a web gap at a floor beam-to-girder connection plate in the girder's negative moment region. As is common practice, the connection plate is cut short of the tension flange. The gap containing the crack is bounded by the web-to-flange and connection plate-to-web fillet welds.

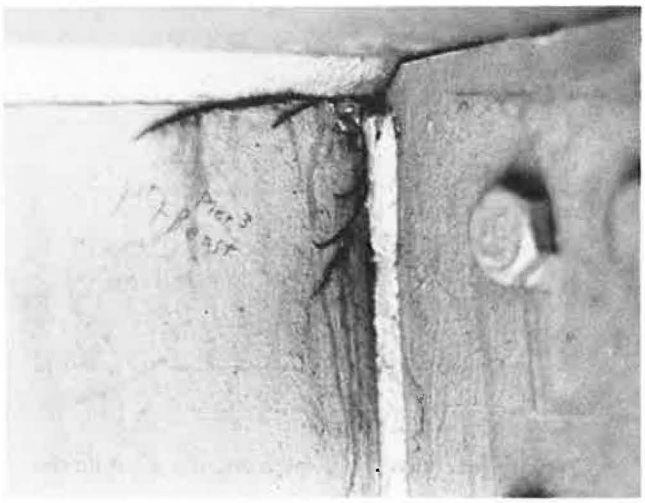

FIGURE 1 Typical cracks in web at floor beam-to-girder connection.

This mode of fatigue cracking was found at numerous gaps on the web of main girders on the Woodrow Wilson Bridge *(1)*. The structure consists of 19 continuous multiple-girder spans ranging from 62 ft (18.9 m) to 212 ft (64.6 m) in length. Floor beams are 25.7 ft (7.8 m) and 36 in. (914 mm) deep. No positive attachment was made between either flange and the connection plate. The deck slab was cast directly on the outside main girders and supported by stringers and floorbeams in the interior. Thus, the deck restrained movement of the top flange of the main girders and, as the transverse floor beam deformed, caused out-of-plane distortion of the web within the web gap. The stress gradients from measured strains next to the gap are shown in Figure 2. The gradient shows that double-curvature web plate deflection exists in the short gap length. When extrapolated, a stress of 10.6 ksi (68.9 MPa) is expected at the longitudinal weld toe at the top. Within the gap, the surface stress at the weld toe can be two to three times greater than those recorded just outside the local region, as calculated by finite element analysis.

The stress range spectrum for the first gauge at the gap is shown in Figure 3. Also shown are the maximum and effective stress ranges at the weld toe, by adjusted extrapolation. Results of case studies indicate that the maximum stress range often

Fritz Engineering Laboratory No. 13, Lehigh University, Bethlehem, Pa. 18015.

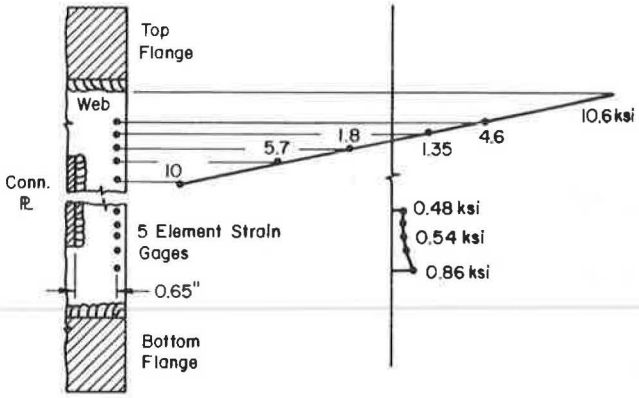

FIGURE 2 Measured and extrapolated stress gradient on web surface.

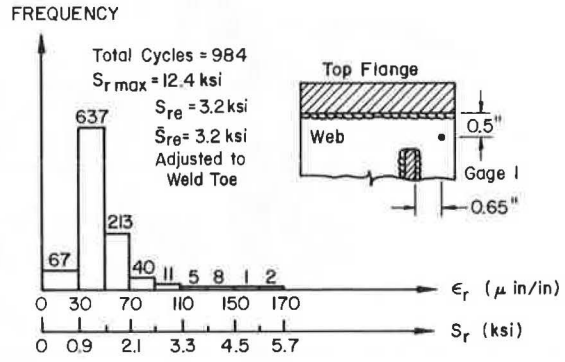

FIGURE 3 Stress range spectrum of a point on the web.

exceeds 12 ksi (82.7 MPa) and a Miner's effective stress range of 3 ksi (20.7 MPa) is quite common. These out-of-plane deflection-induced stress ranges are high enough for fatigue cracking in the web plate.

Similar cracking prevailed in main girder webs at the floor beam connection plates of the Poplar Street Bridge *(2)*. The multiple girder structure has six straight or curved continuous spans of 75 to 100 ft (22.9 to 30.5 m) length. In the negative-moment region, the floor beam connection plates are attached to the compression flange. The corresponding stiffener on the exterior face of the girder is only fitted to the compression flange and cut $^5/_8$ in. (16.0 mm) short of the tension flange. The floor beam attachment in the positive moment region of the girder is similar except that the bottom flange is in tension. At piers, floor beams are connected directly to bearing stiffeners, which are tightly fitted to both top and bottom flanges and welded only to the girder web. Cracks developed in the web at each of these three types of connection plates.

Typical cracking at the base of a bearing stiffener and within the gap of an adjacent transverse stiffener is shown in Figure 4. Nine bearing stiffener-to-floor beam connections were monitored. Cracking prevailed at the toe of the longitudinal flange-to-web weld and through the throats of the transverse connection plate-to-web welds. Representative stresses at the top flange of one connection are plotted in Figure 5. The back-to-back gauges "N" and "25" had stresses of –6.0 ksi (–41.4 MPa) and 4.2 ksi (28.9 MPa), respectively. These magnitudes

FIGURE 4 Cracking at base of bearing stiffener and adjacent transverse stiffener.

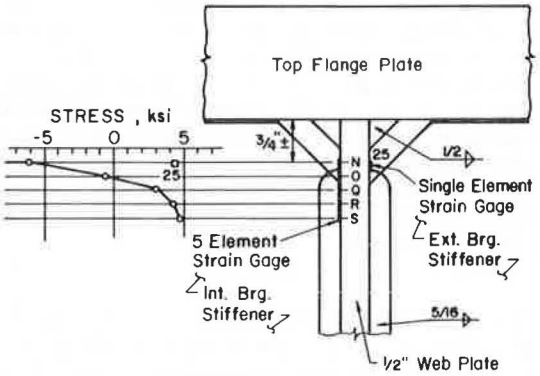

FIGURE 5 Typical stress gradient of web at bearing stiffener gap.

TABLE 1 RESULTS OF MEASUREMENTS AT BEARING STIFFENER, POPLAR STREET BRIDGE

Maximum Out-of-Plane Displacement		Web Stresses			
		Random Trucks		Maximum	
(in.)	(mm)	(ksi)	(MPa)	(ksi)	(MPa)
>0.001	>0.025	9.8–13.0	67.6–89.6	14.0	96.5
0.001	0.025	5.6–8.2	38.6–56.5	10.5	72.4
0.0005	0.013	4.2–5.1	28.9–35.2	6.50	44.8
0.001	0.025	2.6–4.2	17.9–28.9	4.90	33.8
>0.0005	>0.013	1.0	6.90	1.40	9.70

and the stress gradient indicate that the web was undergoing out-of-plane bending. The maximum measured out-of-plane displacement was approximately 0.001 in. (0.0254 mm) within this region.

For the case of Figure 5, the projected stress was –14.0 ksi (–96.5 MPa) at the longitudinal weld toe. A list of selected results from field measurements at some bearing stiffeners is presented in Table 1. The web stresses have been adjusted to the flange-to-web weld toe by linear extrapolation.

Cracking also developed in the web at the connection plates of floor beams. Typical web behavior is best represented by the

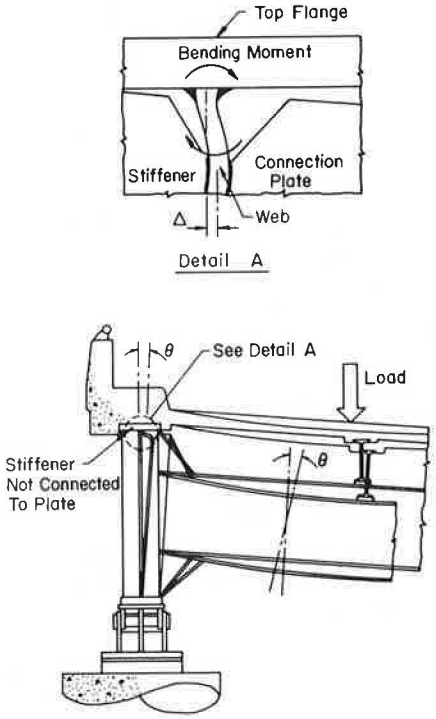

FIGURE 6 Representation of floor beam end rotation and web behavior.

TABLE 2 RESULTS OF MEASUREMENTS AT FLOOR BEAM CONNECTIONS, POPLAR STREET BRIDGE

Crack Length		Maximum Out-of-Plane Displacement	
(in.)	(mm)	(in.)	(mm)
7.0	177.8	0.043	1.09
6.0	152.4	0.030	0.76
4.5	114.3	0.025	0.64
3.5	88.9	0.020	0.51
3.25	82.6	0.021	0.53
3.0	76.2	0.021	0.53
2.75	69.9	0.025	0.64
2.5	63.5	0.008	0.20
1.875	47.6	0.024	0.61
1.75	44.5	0.022	0.56
1.5	38.1	0.028	0.71
Uncracked		0.001	0.03
Uncracked		>0.001	>0.03
Uncracked		0.000	0.00

schematic in Figure 6 for the negative moment region of the girders. The connecting plates are tightly fit to, or cut short of, the top (tension) flange. Floor beam end rotations introduce out-of-plane displacement in the web of girders and cause cracking of the web plate. A listing of crack length and the maximum out-of-plane displacement measured under normal traffic loads is presented in Table 2. There appears to be a direct relationship between the displacement and the length of the crack. The displacements at the 1/2-in. (12.7-mm) gaps with cracks were 10 to 20 times larger than those at the bearing stiffeners.

Review of field data indicates that a displacement of about 0.025 in. (0.64 mm) and a surface stress on the order of 20 ksi (138 MPa) at the flange-to-web weld toe are typical of floor beam connection plate gaps 1/4 to 3/4 in. (6.4 to 19.1 mm) long. Connection plates tightly fit to the tension flange have smaller out-of-plane displacements but the plate-bending stresses could still be relatively high. Stresses of 22 ksi (151.7 MPa) with a displacement of only 0.008 in. (0.20 mm) have been recorded at such sites.

MULTIPLE GIRDER DIAPHRAGM CONNECTION PLATES

A similar condition of cracking exists in the gap at the junction of longitudinal girder flanges and the transverse connection plates of diaphragms or cross-bracing in multigirder bridges. As the girders deflect unevenly under load, the diaphragms transfer lateral forces that cause the connection plate to displace and rotate. Such movement results in out-of-plane distortion of the web plate and the development of fatigue cracks in the gap.

Cracks in the web plate at the gap develop along the toe of the flange-to-web weld and at the weld across the ends of the transverse connection plate in both the positive- and negative-moment regions of girders. Figure 7 shows a crack in the positive-moment region of a simple-span structure. Figure 8 shows cracks at the stiffener weld and at the web-to-flange weld at a diaphragm connection plate in the negative-moment region of the continuous-span Beaver Creek Bridge *(3)*.

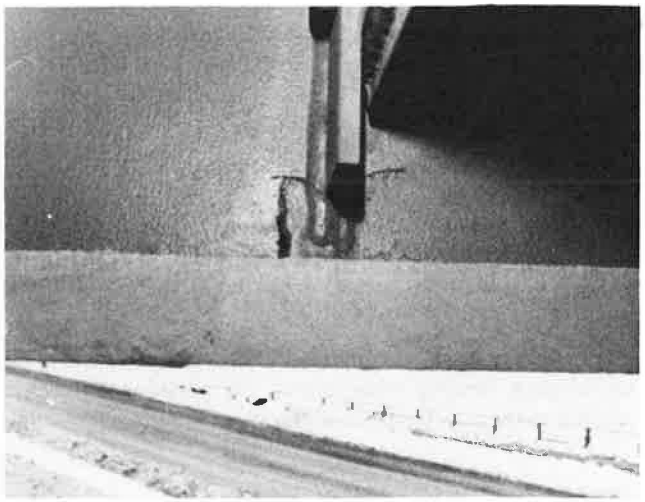

FIGURE 7 Cracking across transverse welds at diaphragm connection plate in the positive-moment region.

This type of fatigue cracking in welded multigirder bridges was detected in the I–79 Bridge 2680 over Big Sandy Creek *(4)*. The bridge has two 108-ft (32.9-m) side spans and two 130-ft (39.6-m) interior spans, with six continuous girders of 5 ft (1.5 m) depth. The diaphragms are equally spaced and the configurations are shown in Figure 9. Small cracks were found in the web along both the flange-to-web weld and the connection plate weld in many diaphragm connection plate gaps. The gap lengths ranged from 1/2 to 5/8 in. (12.8 to 15.9 mm). The cracks were parallel to the primary stresses in the web plate. The maximum measured vertical stress on the web surface was 20 ksi (138 MPa). At all locations, measured strains revealed

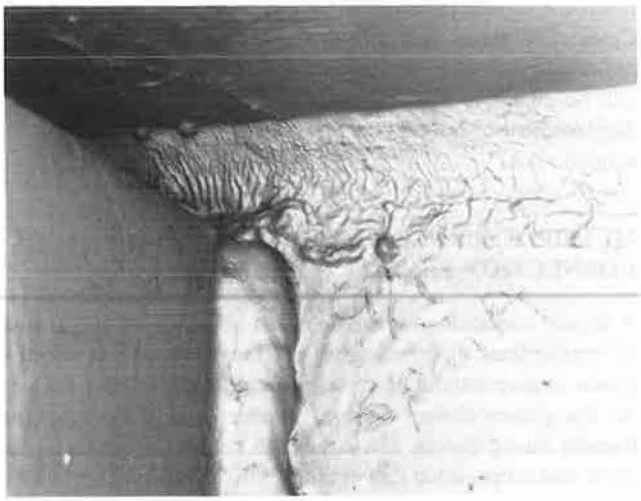

FIGURE 8 Cracking at the diaphragm connection plate gap in the negative-moment region.

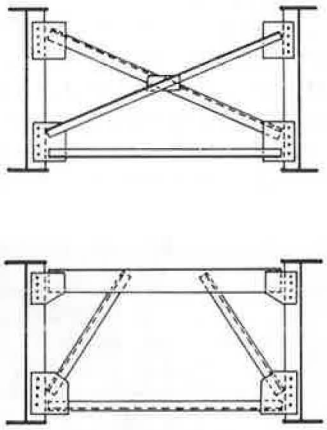

FIGURE 9 Diaphragm connection details for Bridge 2680.

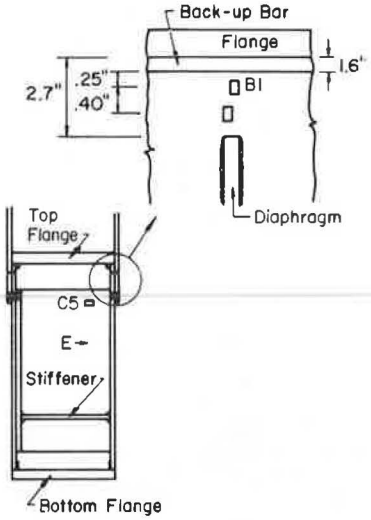

FIGURE 10 Typical box section and expanded detail, I–79 box girder.

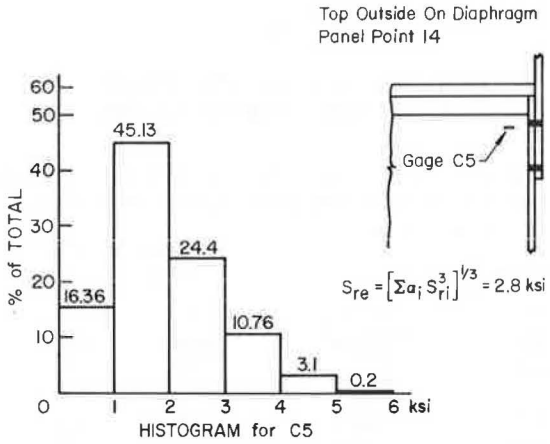

FIGURE 11 Stress range histogram of box diaphragm.

that the diaphragm was distorting the web and inducing cyclic, out-of-plane bending stresses with the passage of live load, leading to the development of cracks.

BOX MEMBER DIAPHRAGMS

Cracks have been detected in web plates of box girders at gaps of internal diaphragms opposite floor beams attached to the box girder. When the diaphragm plate is not connected to the top or bottom flanges of the box, unstiffened web portions or gaps are formed. Furthermore, backup bars are often used at the junction of a web plate and the flange. Lack of fusion at the backup bar is a common phenomenon and constitutes a discontinuity at the weld. The combination of out-of-plane displacement and rotation within the gap, and the existence of relatively large initial flaws can cause fatigue cracking in the gap.

This type of distortion-induced cracking has developed in the 750-ft (228.6-m) box girder of the tie arch structure at Neville Island *(5)*. Cracks were found to exist in the welded connections between diaphragm plates and the outside web of the 42- × 150-in. (1,067- × 3,810-mm) box. A typical box section and expanded detail are shown in Figure 10. The strain-time data from the strain gauges show that major stress cycles occur when trucks pass over the 8-ft (2.44-m) floor beam. The diaphragm and web plate in all four gaps are subjected to high-magnitude stress cycles that include stress reversal.

A stress range histogram from a gauge on the diaphragm is shown in Figure 11. The maximum range of stress is 5.6 ksi (38.6 MPa) and the equivalent constant-amplitude stress range is 2.8 ksi (19.3 MPa). The stress range histogram from a gauge on the web is given in Figure 12. The maximum stress range within such gaps varies between 8 and 11 ksi (55.2 to 75.8 MPa), with effective stress ranges of 3 to 4 ksi (20.7 to 27.6 MPa). These stresses cause cracking in the web on both inner and outer surfaces of the web plates, similar to the condition at floor beam connection plates with out-of-plane displacements.

Out-of-plane displacement generates a stress gradient within the gap. Stress gradients at the instant of maximum and minimum stress in gauge B1 during a high-magnitude stress cycle are constructed in Figure 13. The difference between the maximum and minimum is the stress range for this cycle of

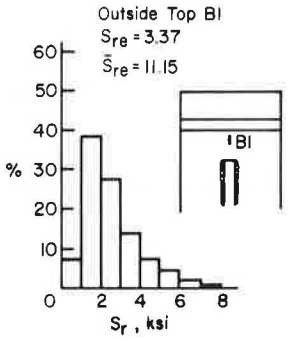

FIGURE 12 Stress range histogram of box girder web.

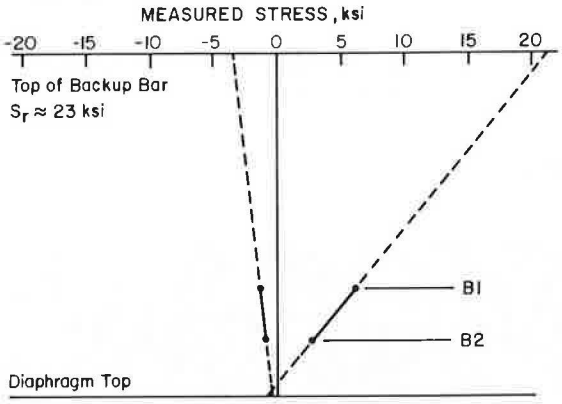

FIGURE 13 Stress gradients at top outside gap of box.

instantaneous stress excursion. Extrapolation (dashed lines) to the backup bar root shows that stress ranges could be on the order of 23 ksi (159 MPa). Such a magnitude of live-load stress can cause cracking at the root of the backup bar.

Throughout the review of the cases involving box distortion and subsequent fatigue cracking, double curvature has always been detected in the web plate at the gaps. This curvature and the corresponding cyclic bending stresses were induced by the restraint between floor beams and the tie-girder with its diaphragms. At each floor beam connection, the distortion of the box girder rendered all four gaps at the corners susceptible to fatigue cracking. When lack of fusion areas existed behind the backup bar and served as notches perpendicular to the direction of stresses, development of cracks occurred with a low number of stress cycles. Furthermore, when the crack propagation changes direction in accordance with the stress field around the diaphragm-to-web connection, a crack perpendicular to the primary tension of the tie box could result. Early detection of these cracks is therefore of paramount importance.

LATERAL BRACING GUSSET PLATES

Lateral bracing is often placed between adjacent girders at a level above the bottom flanges. The attachment is made through gusset plates connected to the web plates. Thus, any force or displacement of the bracing members causes out-of-plane movements and corresponding stresses in the web.

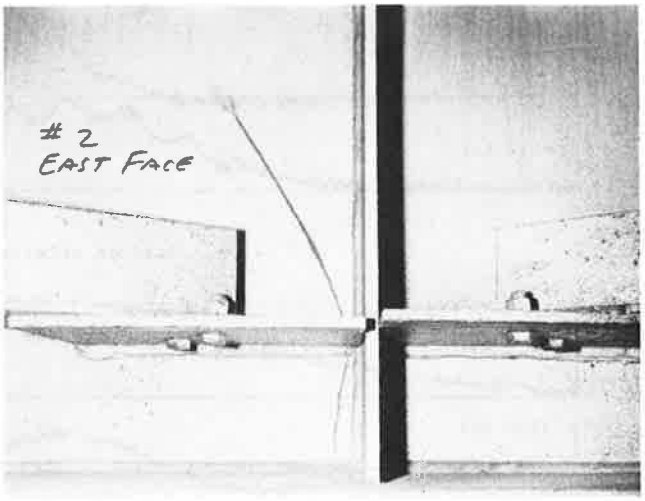

FIGURE 14 Typical crack growth from gusset plate gap.

The gusset plate may be welded, bolted, or cut free of the transverse stiffener in addition to being connected to the web. Figure 14 shows one case of two separate gusset plates welded to the web only. The gap bounded by the weld toe of the transverse stiffener and the near end of the gusset plate is less than 1/4 in. (6.4 mm) in length. The out-of-plane displacement and cyclic bending stresses have caused the crack development and growth.

Cracking in web plates at the lateral gusset plate gaps has developed in I–79 Bridge 2682 over Big Sandy Creek *(4)*. The twin bridge is supported by two main steel girders with four stringers resting on transverse floor beams. The continuous girders have three spans of 120, 130, and 120 ft (36.6, 39.6, and 36.6 m). The lateral bracing members at a floor beam location are bolted to a gusset plate welded to the girder web, but not to the floor beam connection plate, forming gaps such as that shown in Figure 15. The gaps vary from 1/4 to 1 in. (6.4 to 25.4 mm) in length. The prevailing condition has resulted in the formation of vertical cracks on the outside surface of the web plate along weld toes of the transverse stiffener.

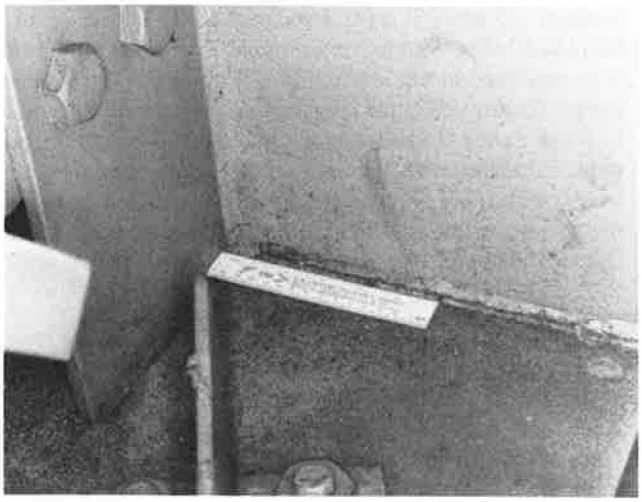

FIGURE 15 I–79 Bridge 2682 lateral gusset plate connection detail.

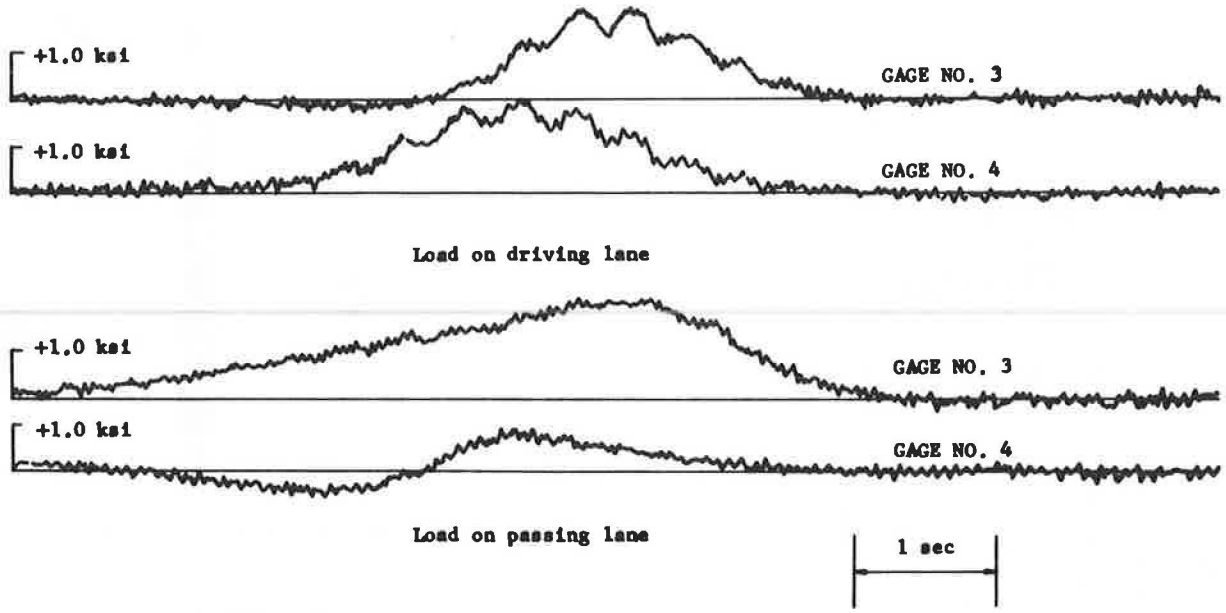

FIGURE 16 Time-dependent strain response of the lateral bracing.

Strain measurements indicated a maximum flexural bending stress range of 3 to 5 ksi (20.7 to 34.5 MPa) in girder flanges and a maximum stress range of 2 to 3 ksi (13.8 to 20.7 MPa) in the lateral bracing members framing into a gusset plate. Figure 16 shows the time response of the two laterals as a truck crossed the bridge. The time lag in the development of tensile stresses and the difference in magnitudes imply rotation of the lateral connection plate in addition to transverse displacement.

Strains were measured at the weld toe of a transverse connection plate in the gusset plate gap and at the weld toes of the outside (facia) stiffener. Stress ranges of 8 to 12 ksi (55.2 to 82.7 MPa) were obtained at the weld toe on the outer surface of the web directly opposite the gusset plate gap. The stress range at the transverse weld in the gap was revealed to be closer to 7 ksi (48.3 MPa). Maximum stresses of 9 to 15 ksi (62.1 to 103.4 MPa) were induced at the transverse weld in the gap.

Similar cracking was investigated on the Canoe Creek Bridge *(6)*. This six-span structure has five spans with lengths between 135 and 162 ft (41.1 and 49.4 m). Stress ranges of 18 ksi (124.2 MPa), with maximum stresses of 12 ksi (42.8 MPa), were measured in the 1½-in. (38.1-mm) gaps at lateral gusset plates. The stresses in the laterals were of opposite sign and out of phase during the passage of vehicles. This condition again implies that the lateral connection plate was forced to rotate as well as deflect out of plane. Such rotations reduced the stress at one weld toe, but elevated the stress at another and induced cracking thereon.

INTERMEDIATE TRANSVERSE STIFFENERS ADJACENT TO FIELD SPLICES

Numerous cases of cracking at intermediate transverse stiffeners of girder webs have been reported with the causes traced to the transportation of the girders. One such crack that was investigated is shown in Figure 17. The crack initiated at the termination of the transverse stiffener welds and extended

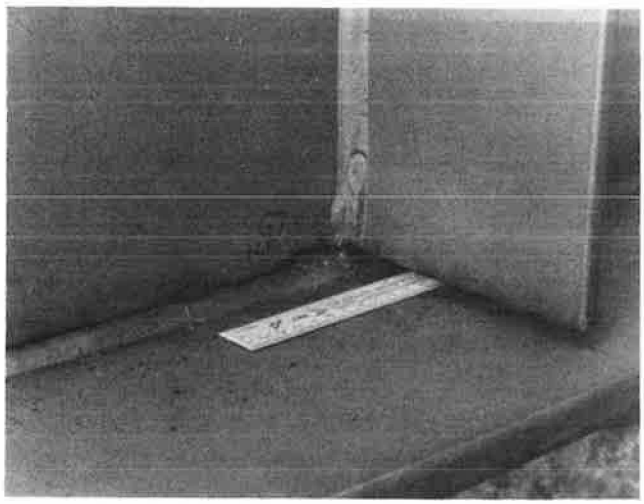

FIGURE 17 Cracking at a transverse stiffener web gap adjacent to a field splice.

along the web-to-flange weld parallel to the longitudinal axis of the girder. Because of the comparatively slender and flexible web, there may often be a relative movement between the top and bottom flanges during transportation. The support points of girder segments during transportation are usually directly under intermediate transverse stiffeners. At these locations, the lateral movement is accommodated by the flexible gap between the stiffener and flange. Hence, the out-of-plane lateral deformation and corresponding stresses are again introduced in the gap. This condition has led to cracking at the end of transverse stiffener welds and at the web-to-flange fillet weld. These cracks are often unnoticed until an in-service inspection is performed.

This type of cracking has been found in I–79 Bridges 2680 and 2682 over Big Sandy Creek *(4)*. The intermediate stiffeners with cracks are not serving as floor beam or diaphragm

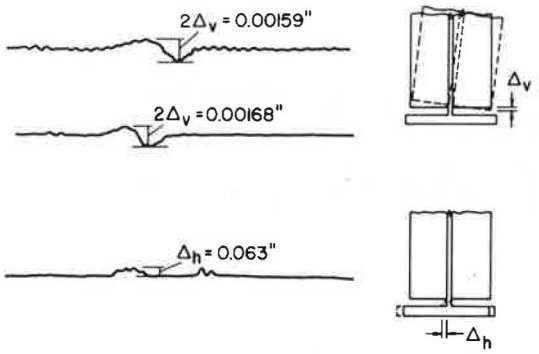

FIGURE 18 Displacement-time response of gaps at stiffener adjacent to a field splice.

connection plates but are adjacent to bolted field splices. Careful inspection of the crack surfaces showed the presence of both the red primer paint and the final finish coat, indicating that the cracks existed at the time of application of the primer coat. Continued propagation of the crack along the web-to-flange weld is considered to be the result of lateral movement during transportation, with little in-service extension.

Two cracked locations were monitored during normal random truck traffic. Figure 18 shows the displacement-time responses. At one location, the presence of a long horizontal crack allowed a relative horizontal displacement to occur between the flange and stiffener. The rotation of the stiffener with respect to the flange below the gap is minimal. The other location had only a short crack. Truck loads induced relative rotation between the stiffener and the flange with little relative horizontal movement. The distortions were compatible with the small out-of-plane bending stresses measured on the web at the gap. At the ends of these cracks, the in-service, out-of-plane cyclic stresses were always less than 1 ksi (6.9 MPa). Such stress levels should not produce a threat to the life of the structure.

SUMMARY AND CONCLUSIONS

Numerous common bridge details have been noted as susceptible to out-of-plane distortion-induced fatigue cracking. Though the details serve different functions in the overall behavior of the structure, a single feature is common to all. This feature is a short length of unstiffened web plate at a gap between flanges, connection plates, stiffeners, or gusset plates. When lateral forces or displacements are induced by bridge components at or nearby the gap, this length of web plate absorbs the majority of out-of-plane displacements. The local distortion in a gap is often in the form of double curvature and results in high secondary bending stresses that are not accounted for in present design procedures. Fatigue cracks could develop.

Cracking in the gap usually extends along the weld toes and perpendicular to maximum stresses. In the cases where the in-plane flexural bending stresses of the web plate are in the same direction as the out-of-plane secondary stresses, the growth of the crack could be relatively rapid. Thus, cracks in horizontal gaps at lateral gusset plate connections could pose a serious threat to the serviceability of the bridge, as vertical cracks could propagate toward the tension flange.

It has been shown that distortion in gaps can be reduced by positive attachment of component parts. The review of available measurements indicates that a positive connection should be made between the girder flanges and the transverse connection plates for diaphragms and floor beams. This requirement has been incorporated into design specifications. Furthermore, a study is in progress to develop schemes for connections of lateral bracing members and transverse stiffeners.

REFERENCES

1. J. W. Fisher. *Report on Strain Measurements on Woodrow Wilson Bridge*. FHWA, U.S. Department of Transportation, 1983.
2. M. J. Koob, P. D. Frey, and J. M. Hanson. *Evaluation of Web Cracking at Floor Beam to Stiffener Connections of the Poplar Street Bridge Approaches*. Illinois Department of Transportation, Springfield, Sept. 1985.
3. J. J. Lee, C. Castiglioni, et al. *Displacement Induced Stresses in Multigirder Steel Bridges*. Fritz Engineering Laboratory Report 500–1(86). Lehigh University, Bethlehem, Pa., Feb. 1986.
4. J. W. Fisher, A. W. Pense, et al. *Final Report on Cracking of I–79 Bridges 2680 and 2682*. Fritz Engineering Laboratory Report 501–1(85). Lehigh University, Bethlehem, Pa., May 1985.
5. J. W. Fisher, A. W. Pense, et al. *Final Report on I–79 Tied Arch Cracking—Neville Island Bridge*. Fritz Engineering Laboratory Report 494–1(84). Lehigh University, Bethlehem, Pa., Dec. 1984.
6. J. W. Fisher, C. A. Menzemer, et al. *Distortion Induced Stresses in a Floorbeam-Girder Bridge: Canoe Creek*. Fritz Engineering Laboratory Report 500–2(86). Lehigh University, Bethlehem, Pa., April 1986.

Publication of this paper sponsored by Committee on Steel Bridges.

Fatigue Behavior of Variable Loaded Bridge Details Near the Fatigue Limit

PETER B. KEATING AND JOHN W. FISHER

The findings of the current NCHRP Project 12–15(5), "Fatigue Behavior of Variable Loaded Details Near the Fatigue Limit," are highlighted. The main focus of the research is the examination of welded bridge details in the high-cycle, long-life regime. Large-scale plate girders with coverplate, web attachment, and web stiffener details are subjected to fatigue loading that simulates actual truck traffic. A Rayleigh type stress spectrum is used with the inclusion of an occasional overload exceeding the constant-amplitude fatigue limit. The frequencies of occurrence being considered for the overloads are 0.1, 0.05, and 0.01 percent. Prior research indicated that fatigue crack propagation occurred even when the effective stress range was below the constant-amplitude fatigue limit and the exceedance rate of the limit was as low as 0.1 percent. The current test specimens also allow for a detailed study of distortion-induced fatigue cracking at a connection plate web gap detail. Results indicate that the retrofit method of drilled holes at the crack tip is inadequate at high levels of distortion. In addition to the experimental work, a review of fatigue test data generated around the world since the AASHTO fatigue provisions were adopted in 1974 was completed. This study has allowed for a reassessment of the provisions. A summary of the proposed revisions to the specifications is given.

In order to fully understand the fatigue behavior of welded steel bridge members and details, test data resulting from full-scale test specimens must be generated and analyzed. The NCHRP Project 12–15(5) entitled "Fatigue Behavior of Variable Loaded Bridge Details Near the Fatigue Limit," concerns itself with several aspects of full-scale fatigue testing. The primary objective of the research program is to study the fatigue behavior of welded bridge details subjected to variable-amplitude, high-cycle fatigue loading. This type of loading is more representative of what an actual bridge is subjected to than the constant-amplitude loading that has been used to generate almost all of the data that forms the database for the current AASHTO fatigue provisions. In addition, the fatigue behavior of web connection plate details is investigated.

This experimental work is unique in that both crack development and the adequacy of retrofit methods can be examined under variable-amplitude loading and in a laboratory environment. No previous research of this type has been performed. As a supplement to the project, a reassessment of the current fatigue design criteria has been completed. This study involved the compilation of full-scale fatigue test data generated since the introduction of the AASHTO fatigue provisions in 1974. The test data were evaluated to determine the adequacy of the fatigue provisions. Recommendations for change to the fatigue design specifications have been set forth so that the specifications may better reflect the expanded fatigue test database.

Fritz Engineering Laboratory, Lehigh University, Bethlehem, Pa. 18015.

HIGH-CYCLE FATIGUE TESTS

Fatigue cracks developed at the ends of the coverplated bridge beams that were only infrequently subjected to stress ranges that exceeded the fatigue limit of AASHTO's Category E' *(1)*. This suggests that severe fatigue problems could result if bridges become subjected to heavier loads in the future, and that the consequences of occasional overloads from permits and other sources may be more critical than previously assumed. The consequence of initiating fatigue crack growth in existing bridges as a result of increased loads could have a major impact on the life expectancy and safety of bridges on high-volume arteries where large numbers of random variable-stress cycles are expected. The available test data in the high-cycle region of behavior are sparse and do not provide an adequate basis on which to assess this problem. The principal objective of NCHRP Project 12–15(5) is to extend the findings of Project 12–15(4) [NCHRP Report 267 *(2)*] by providing additional information on the fatigue behavior of welded bridge members under randomly applied, variable-amplitude loading near the fatigue limit of the extreme-life region.

Background

Fatigue test results from several studies before the NCHRP 12–15(5) project indicated that fatigue cracks develop in test specimens even though the effective stress range is well below the crack growth threshold or fatigue limit *(3, 4)*. The types of specimens tested varied from small-scale attachment details to full-scale coverplated beams. The percentage of cycles exceeding the constant-amplitude fatigue limit for these tests ranged from 100 percent to as few as 0.24 percent. However, these studies were limited in scope in that only a few detail types were tested, and with those, a limited number of tests were run. This procedure resulted in little or no replication of data.

The NCHRP Project 12–15(4) test program was initiated with the objective to expand the existing database through the use of full-scale beams. Eight rolled W18 × 50 beams of A588 steel with a span length of 15 ft were used. Two types of welded attachments were incorporated: 1- × 4½-in. partial-length coverplates and 1.0-in.-thick by 12.0-in.-long fillet-welded web attachments. All beams were tested in their as-welded state. A Rayleigh type distribution was used for the

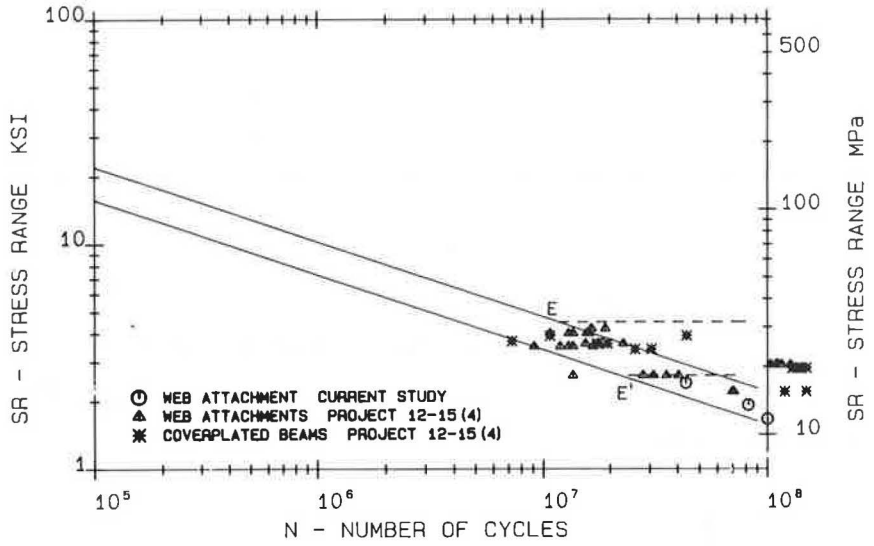

FIGURE 1 Fatigue test data, NCHRP Projects 12–15(4) and 12–15(5).

stress range spectrum. Fatigue limit exceedance rates, held constant for a given test, varied from 0.10 to 11.72 percent for the program.

The test results from Project 12–15(4) are shown in Figure 1. The data are plotted by using the effective stress range as calculated from the root mean cubed (RMC) (Miner's) rule:

$$S_{re} = (\Sigma\, \alpha_i \cdot S_{ri}^3)^{1/3} \quad (1)$$

where S_{re} is the effective stress range, S_{ri} is the stress range at the ith interval of the frequency-of-occurrence histogram, and α_i is the fraction of stress range within the ith interval. All stress cycles in the spectrum are assumed to contribute to fatigue crack propagation. As indicated in the figure, the test data plot consistently with the straight-line extension of the Categories E and E′ design curves even though the calculated effective stress ranges are below the constant-amplitude fatigue limit. The results were revealed to be independent of the exceedance rate. The study concluded that the existence of a fatigue limit below which no fatigue crack propagation occurs is assured only if none of the stress cycles exceed this constant-amplitude fatigue limit.

Research Approach

The current NCHRP Project 12–15(5) involves the fatigue testing of eight full-scale welded plate girders. All webs, flange plates, and attachments are A36 steel. Each girder is 26 ft long; girders are tested in pairs on a 25-ft span under four-point loading. A view of the test setup is shown in Figure 2. The girders are 36 in. deep with 1- × 12-in. flanges and a 3/8-in.-thick web plate. Three detail types are fillet welded to the girders: partial-length coverplates, web attachments, and transverse web stiffeners. The coverplates are 1- × 9-in. plates, either with or without the transverse end weld. This detail provides a Category E′ classification because the flange thickness is greater than 0.8 in. The web attachments consist of 1.0-in.-thick by 12-in.-long plates with longitudinal fillet welds only. These are also Category E′ due to their thickness. The 3/8- ×

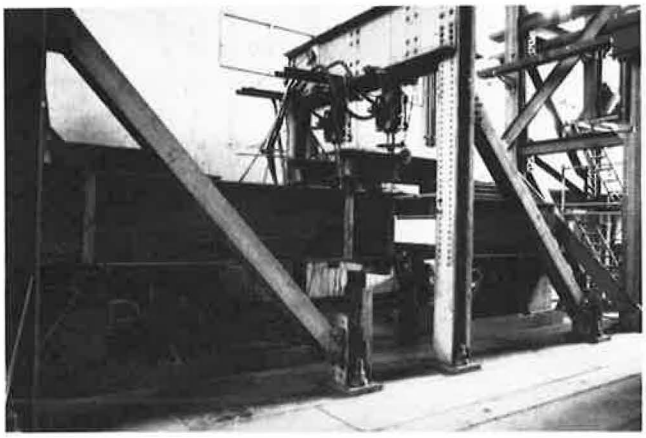

FIGURE 2 View of test setup of full-scale plate girders.

3.0-in. transverse web stiffeners (Category C) are cut short of the tension flange with a 1 1/2-in. web gap. The girder and attachment configurations are shown in Figure 3. Each test girder has 16 possible detail failure locations.

As with previous test programs, a Rayleigh type stress spectrum is used. The variable-amplitude stress spectrum is generated by repeatedly applying a block of 1,000 randomized loads of 10 different magnitudes. The details are arranged on the girder so that each reaches its respective constant-amplitude fatigue limit at the same applied load. The web attachments were arranged in the shear span to provide a range in the assumed constant-amplitude fatigue limit from 4.2 to 2.3 ksi. The 10th or highest load in the spectrum corresponds to the fatigue limit of the detail. A normalized stress range spectrum, which results in an effective stress range 58 percent of the detail fatigue limit, is shown in Figure 4. Overloads are included into the spectrum at set exceedance rates. For the first pair of girders, this rate is 0.1 percent. Subsequent rates will be 0.05 and 0.01 percent. The magnitudes of the overloads result in stress ranges at each detail that are between 7/6 and 3/2 of the assumed constant-amplitude fatigue limit.

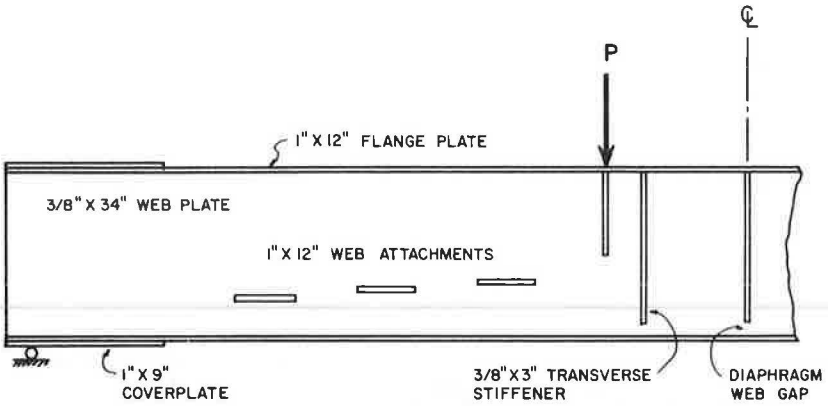

FIGURE 3 Plate girder with welded details.

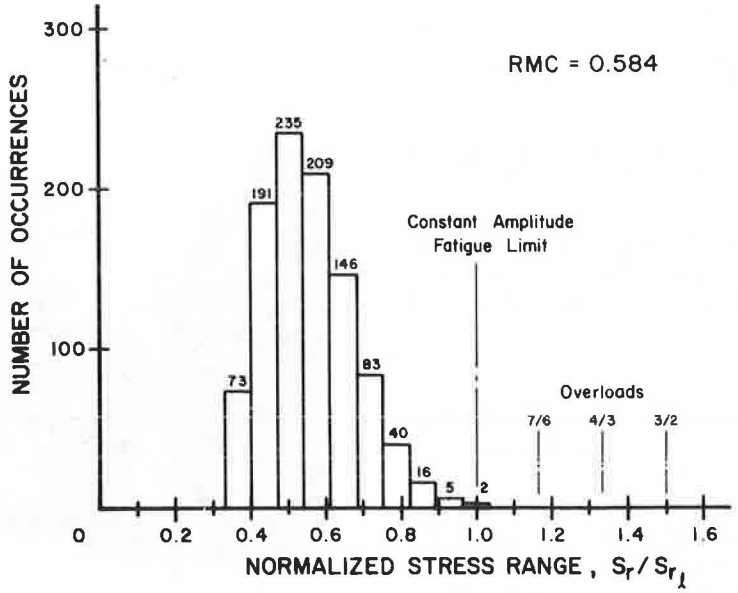

FIGURE 4 Normalized stress range histogram.

Results and Evaluation of Experimental Data

The fatigue test has yielded three failure points, which occurred at the weld end of three web attachments (Figure 5), through the first quarter of 1987. One detail, with an effective stress range of 2.4 ksi, failed at $43.6 \cdot 10^6$ cycles. While the constant amplitude fatigue limit of Category E′ is 2.6 ksi, the position of this particular detail gave an assumed fatigue limit of 4.2 ksi for a 0.1 percent exceedance rate. Using the Category E′ fatigue limit results in an exceedance rate of 14.6 percent. Fatigue crack growth was detected at a second web attachment detail at $81.7 \cdot 10^6$ cycles. At this location, the load spectrum results in an effective stress range of 2.2 ksi with a peak value of 4.3 ksi. The third crack was detected at $100.7 \cdot 10^6$ cycles, at an effective stress range of 1.4 ksi and a maximum stress range of 3.5 ksi. These data points are plotted in Figure 1, as the open circle symbols.

Further fatigue crack growth at this detail was prevented by the placement of holes through the web plate at the crack tips. Different-sized holes were used at each end because the crack resided in a moment stress gradient. Diameters were 1.0 in. for the top and 2.0 in. for the bottom hole. These sizes were selected on the basis of the relationship

$$\Delta K/\sqrt{\rho} = 4\sqrt{\sigma_y} \quad (2)$$

where ΔK ($\sqrt{\text{ksi-in.}}$) is the stress intensity factor range, ρ (in.) is the diameter of the hole, and σ_y (ksi) is the yield stress of the steel *(5)*.

DISTORTION-INDUCED FATIGUE CRACKING

As a secondary study on NCHRP Project 12–15(5), distortion-induced fatigue cracking at a connection plate web gap detail is also being examined under variable-amplitude loading. The current test program presents an opportunity to examine and evaluate this type of fatigue cracking and possible retrofit methods under long-life conditions. Before the project, no other laboratory study of distortion-induced fatigue cracking had simulated in-service loading conditions, that is, both in-plane and out-of-plane stresses simultaneously.

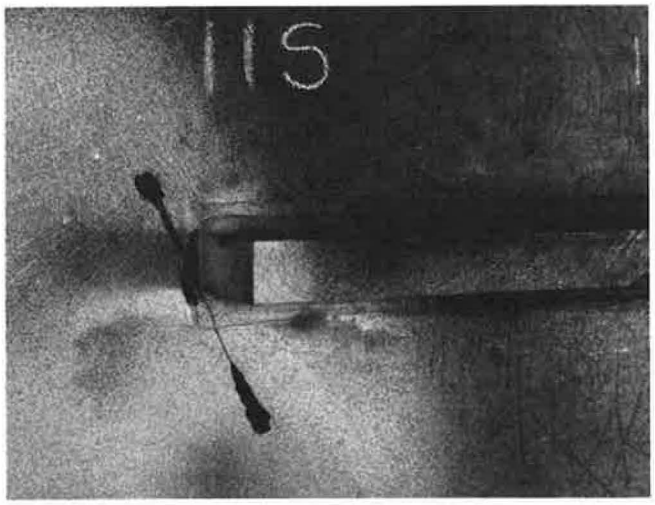

FIGURE 5 Fatigue crack at web attachment.

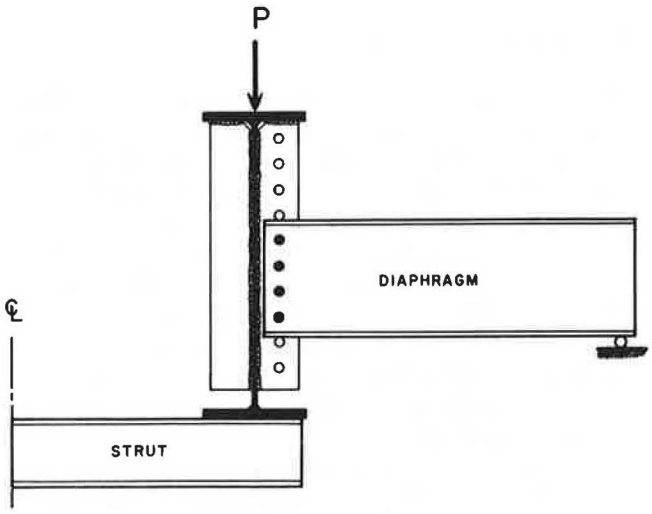

FIGURE 6 Test setup for distortion-induced web gap fatigue cracking.

As shown in Figures 2 and 3, each test girder contains a web gap detail at midspan. The connection plate is cut short of the tension flange by either 1½ or 4 in. A diaphragm consisting of a W14 × 22 rolled section is bolted to the connection plate with its free end supported against vertical motion at the test frame column. This configuration is shown schematically in Figure 6. The bottom flange of the test girder is restrained against rotation by means of a rolled section strut, simulating a flange embedded in a concrete deck or the restraint found at a support. The in-plane vertical deflection of the girder from the applied loads causes the connection plate to be forced out-of-plane by the resisting moment developed at the diaphragm connection. This setup models the differential displacement of bridge girders and the resulting distortion at diaphragm locations in the negative-moment region and at supports.

Strain measurements taken during static tests, before the variable-amplitude loading, indicated that the vertical web gap membrane stresses were high. At the static load that produced an in-plane stress at the connection plate end equivalent to the constant amplitude fatigue limit (12 ksi), a strain corresponding

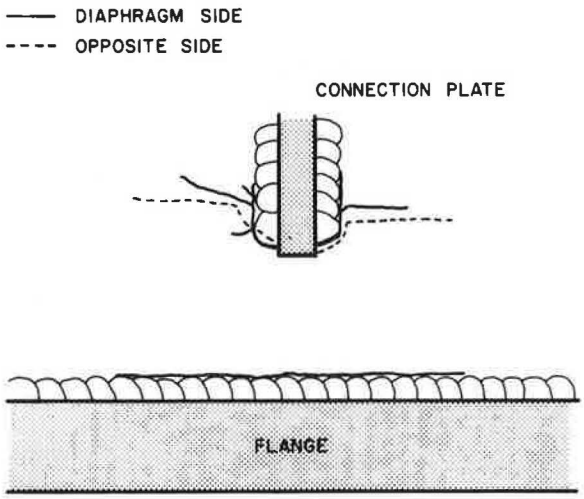

FIGURE 7 Map of the web gap fatigue cracking.

to 43 ksi was measured. This distortion-induced stress is approximately 20 percent greater than the nominal yield stress of the steel. Varying the vertical bolted position of the diaphragm resulted in no significant changes in the measured web gap stresses.

With the onset of variable-amplitude loading, fatigue cracks developed quickly in the web gaps. The initial cracking was first detected at approximately 50,000 cycles, with extensive cracking at 100,000 cycles. The distortion-induced fatigue cracks developed at both the toe of the web-to-flange fillet weld and at the connection plate end as shown schematically in Figure 7.

At approximately 1 million random variable-load cycles, the web gap cracking was retrofitted by means of drilled holes at the crack tips. Figure 8 shows the progression of fatigue cracking in stages at one of the web gap details. Holes of 1½-in. diameter were used to core out the cracking at the connection plate end and ¾-in.-diameter drilled holes were used at the tips of the web-to-flange cracks (Stage I). Within 500,000 cycles, crack reinitiation occurred at the toe of both the connection plate weld and the web-to-flange weld. The crack tips were again arrested by drilling and testing was resumed (Stage II). At $2.1 \cdot 10^6$ cycles (Stage III), and again at $2.9 \cdot 10^6$ cycles (Stage IV), a crack reinitiated at the drilled hole along the stiffener fillet weld toe.

At this point in the test, the diaphragms were permanently removed from the test girders to prevent further distortion-induced fatigue damage and avoid the possible loss of the girders due to fracture at the connection plate detail. Strain measurements taken at the top of the uppermost hole (Stage IV) indicated that the in-plane web stresses were elevated 10 percent because of the presence of the web cracks. Subsequently, a crack reinitiated at the perimeter of the drilled hole at $9.4 \cdot 10^6$ cycles (Stage V). The test was run an additional 20 million cycles before a toe crack reinitiated at the top hole (Stage VI). The crack tip was drilled out and the toe of the vertical fillet weld was peened to help prevent additional cracking. At $47 \cdot 10^6$ cycles (Stage VII), fatigue cracks initiated at the perimeter of the uppermost hole and at one of the web-to-flange holes. The second crack represented a situation that would

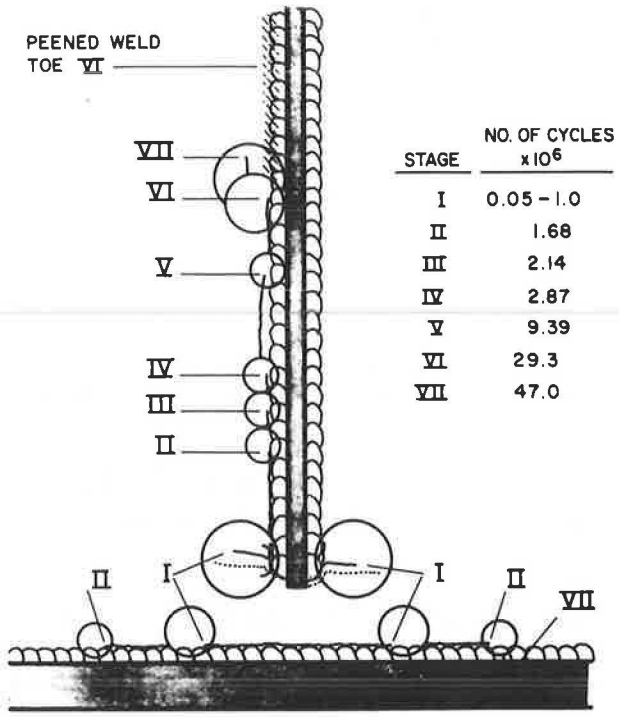

FIGURE 8 Schematic history of web gap fatigue cracking.

eventually jeopardize the test. Strain measurements on the flange plate gave an increase of 12 percent over the nominal stress without the web cracking. The crack front was drilled on both sides of the web plate and the flange plate clamped to help reduce the level of stress in the flange, minimizing the probability of continued cracking. A view of the final stage of web and flange cracking and retrofit holes is given in Figure 9.

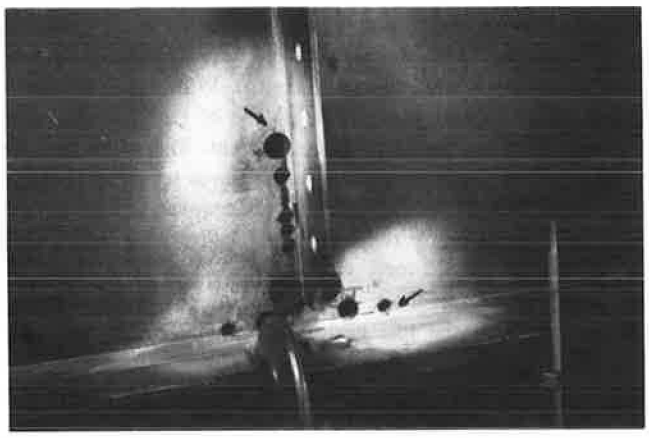

FIGURE 9 Retrofitted distortion-induced web cracking.

This discussion illustrates the difficulty in retrofitting web gap cracking when it is induced by high levels of out-of-plane deformation. Even though holes were drilled at the crack tips, the level of stress from the out-of-plane motion of the diaphragm remained at such an elevated state that cracks quickly reinitiated. When the diaphragms were removed and the in-plane loading continued, the detail had previously sustained such a large magnitude of damage that cracks continued to develop and propagate. Eventually, the web cracks caused the stresses in both the web and flange plates to increase enough to initiate cracking at the perimeter of the holes. Peening stopped the crack from initiating at the weld toe.

FATIGUE DATA REVIEW

A fatigue data review and reassessment of the current fatigue specifications has been conducted *(6)*. Since the AASHTO specification fatigue resistance provisions were developed from test data reported in NCHRP Reports 102 and 147 *(7, 8)*, several major fatigue studies have been conducted around the world. By compiling and reviewing all available full-scale test data, the existing fatigue specifications could be reevaluated and appropriate changes made so that the specifications more accurately reflect the current state of knowledge. In addition, the review provides an opportunity to provide fatigue criteria consistent with applications in other countries.

Background

Before NCHRP Project 12–7 [NCHRP Reports 102 and 147 *(7, 8)*] only approximate fatigue design relationships were in use because of the limitations of the test data available at the time. NCHRP Project 12–7 was developed to provide a statistically designed experimental program under controlled conditions. The program involved some 530 test beams and girders with various welded details that are commonly used in the design of bridges. Large-size beam specimens were used to overcome some of the limitations of smaller, simulated specimens, such as reduced residual-stress fields and limited initial-weld defect distributions. All specimens were tested under constant cycle loading.

The results from the regression analyses of the generated test data indicated that only two variables significantly influenced the fatigue strength of the welded details: stress range and the detail type. Steel type and minimum and maximum stress levels were found to be not significant. This simplification resulted from the presence of residual stresses that exist in welded steel structures from the welding process. A stress–range–cycle–life relationship was defined using six different design categories to classify the fatigue strength of the details used in the test program. This procedure led to the provisions now used in the current AASHTO fatigue design specifications *(9)*.

Research Approach

Data were collected from many different sources around the world, including Japan, Switzerland, East Germany, Office of Research and Experiments of the International Union of Railways—ORE (West Germany, Poland, England, and Holland), as well as the United States. These additional studies evaluated the applicability of the NCHRP test program to fabrication conditions elsewhere in the world and were used to develop similar fatigue codes. The additional tests augmented the NCHRP findings and often defined the fatigue strength of details that were not examined under the NCHRP program.

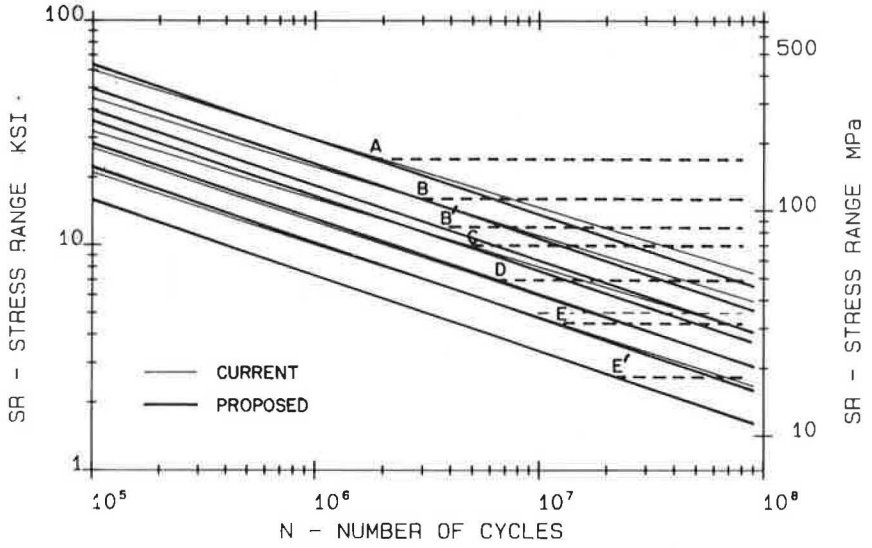

FIGURE 10 Comparison of current and proposed AASHTO design curves.

A major effort of the fatigue test review was the development of a computerized database containing fatigue test results of varying detail types *(10)*. Included in the database were the data from both the original NCHRP test program (to 1972) and from all the new sources. The development of this database allowed for the systematic analysis of the large amount of fatigue data compiled from various references.

The database was limited to test data that could be used to define the fatigue resistance of welded steel details. This limitation meant the inclusion of test data resulting from large-scale test specimens. As was extensively addressed in NCHRP Reports 102 and 147 *(7, 8)*, small-scale specimens always provide higher cycle lives than large-scale beam type specimens. Small-scale specimens were used in the review where no alternative existed, though reliance on these data has been minimal. No attempt was made to evaluate the fatigue strength of riveted and bolted connections. Nor was the adequacy of weld improvement techniques evaluated. While these processes tend to increase the fatigue resistance of certain details, the objective of the review was to accurately define the lower bound resistance for as-welded details, or the minimum level of fatigue strength that would be obtained provided that standard fabrication and inspection procedures were employed.

Each new source of test data was first compared with the appropriate AASHTO fatigue curves to determine if the results from the recent tests were consistent with the findings of the original NCHRP studies or if the fatigue resistance of a particular detail had possibly been misrepresented by the current specifications. A regression analysis was performed using all the data for a given detail type to determine if any significant differences arose. Once the new data were properly categorized, all data, both old and new, for each detail type were compared with the appropriate fatigue resistance curve.

Findings

The reassessment of the fatigue provisions provided an opportunity to have the AASHTO fatigue criteria consistent with

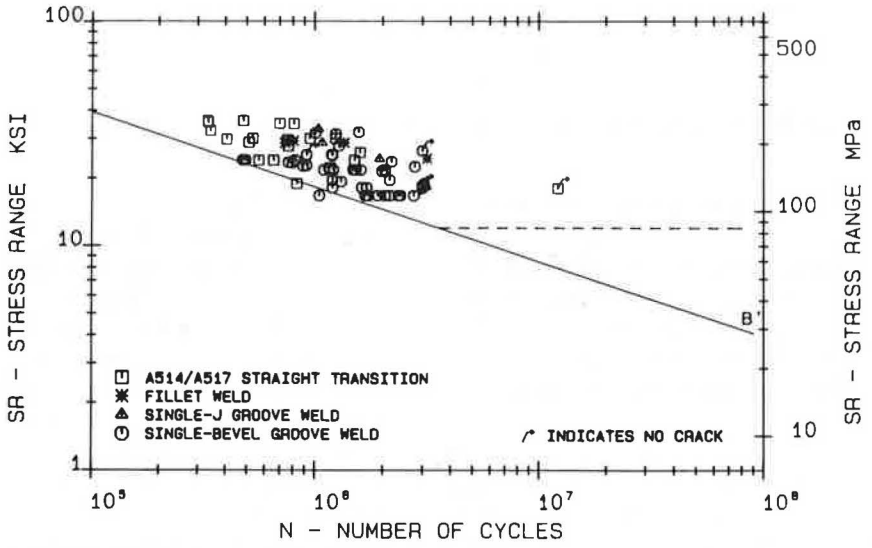

FIGURE 11 Category B′ fatigue test data.

TABLE 1 PROPOSED ALLOWABLE STRESS RANGE VALUES FOR REDUNDANT MEMBERS

Redundant Load Path Members				
	Allowable Range of Stress F_{sr}, ksi			
Category	For 100,000 Cycles	For 500,000 Cycles	For 2,000,000 Cycles	For over 2,000,000 Cycles
A	63	37	24	24
B	49	29	18	16
B	39	23	14.5	12
C	35.5	21	13	10 12
D	28	16	10	7
E	22	13	8	4.5
E′	16	9.2	5.8	2.6
F	15	12	9	8

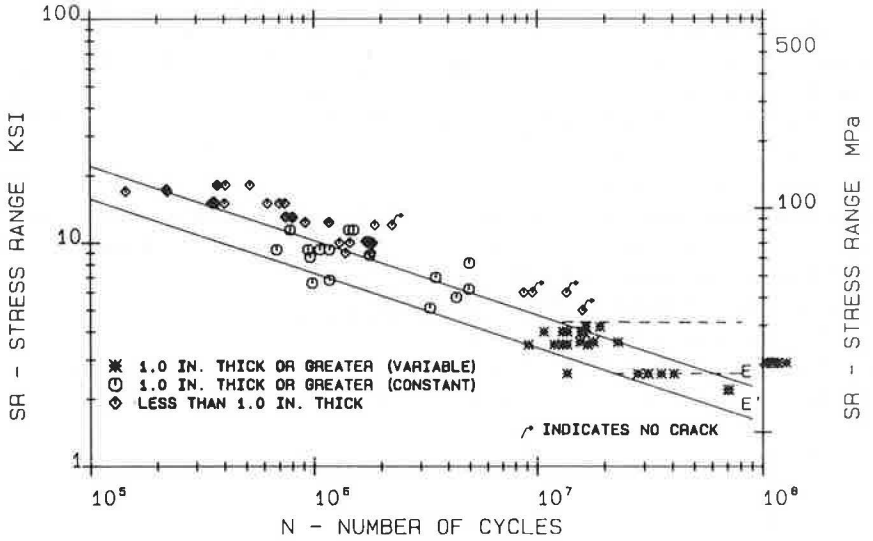

FIGURE 12 Web attachment test data with Category E and E′.

other applications in other countries. As the database for a given detail has increased it has generally been observed that the slope of the S–N curve tends to stabilize to a value of –3.0. Also, recognition of the relationship between crack growth and the experimental results on welded details has led to the adoption of a slope of –3.0 for other design S–N curves, such as those adopted by the European Convention Constructional Steelwork (ECCS) *(11)*.

The results of the present fatigue data review suggested that minor adjustments to the existing AASHTO fatigue design curves were desirable. The slopes of the proposed curves were all established at –3.0. A comparison between the existing and proposed fatigue design curves is shown in Figure 10. With the exception of Category A, the proposed curves were developed by using the current stress range intercept values at $2 \cdot 10^6$ cycles. The constant-amplitude fatigue limit for each curve, with the exception of Category E, corresponds to its current value, as the review of the data did not indicate a need to change these values. A new category, B′, has been added because the review indicated that Category B overestimated the fatigue strength of certain longitudinal groove welds. The stress range intercept values for 100,000, 500,000, and 2,000,000 cycles as well as the constant-amplitude fatigue limits for each proposed curve are given in Table 1.

Fatigue test data obtained from full-scale box girder specimens with longitudinal partial-penetration groove welds indicated a

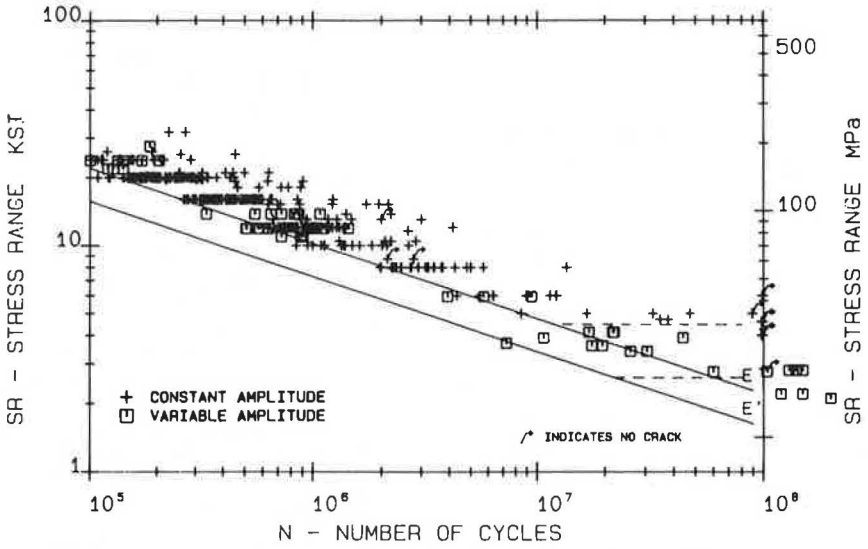

FIGURE 13 Coverplated beam test data with Category E and E′.

TABLE 2 PROPOSED ALLOWABLE STRESS RANGE VALUES FOR NONREDUNDANT MEMBERS

Non-Redundant Load Path Members				
	Allowable Range of Stress F_{sr}, ksi			
Category	For 100,000 Cycles	For 500,000 Cycles	For 2,000,000 Cycles	For over 2,000,000 Cycles
A	50	29	24	24
B	39	23	16	16
B	31	18	11	11
C	28	16	10 12	9 11
D	22	13	8	5
E	17	10	6	2.3
E	12	7	4	1.3
F	12	9	7	6

fatigue strength consistently below Category B *(12–14)*. In Figure 11, these data are plotted with the proposed Category B′ design curve. The decreased resistance is due to the geometry at the detail. Large initial defects were found to occur in the large-scale sections as a result of blowholes and root gap flaws. These defects appear to be larger than the discontinuities observed in full-penetration groove welds and fillet welds. This same condition has been observed in longitudinal groove welds with backing bars left in place. Category B′ has also been recommended to define the fatigue strength of full-penetration groove-welded splices at transitions in width or thickness when the base metal is of A514/A517 steel. These data points are also plotted in Figure 11. Previously, the use of flange splices in A514/A517 steel was permitted only with a 2.0-ft radius transition.

The analysis of the test data for web attachments indicated that the plate thickness has an influence on the fatigue strength of this type of detail *(2, 15)*. Shown in Figure 12 are data for this type of detail, plotted with both the proposed Category E and E′ design curves. The web attachment details with a plate thickness of 1.0 in. or greater resulted in a fatigue resistance that was below Category E. It was revealed that Category E′ gave a more reasonable lower bound estimate of the fatigue resistance of this detail.

High-cycle, long-life fatigue tests of coverplated beams *(16)* indicated that 5.0 ksi overestimated the constant-amplitude fatigue limit for this type of detail. The minimum-stress range value at which fatigue failure occurred was found to be 4.7 ksi. It was concluded that a stress range value of 4.5 ksi was a better estimate of the constant-amplitude fatigue limit for Category E.

The complete database for coverplated beams with a flange thickness less than 0.8 in. is shown in Figure 13.

Concern where failure of a single element could cause collapse of a structure resulted in a more conservative fatigue design requirement in order to minimize the possibility of fatigue crack growth in fracture critical members. In order to provide a rational and consistent criterion for nonredundant members, a uniform reduction of 20 percent has been applied to the allowable stress range values at 100,000, 500,000, and 2,000,000 design cycles. The 20 percent reduction provides uniformly the minimum reduction that was used in the earlier versions of the AASHTO specifications. The reduced allowable stress range values are analogous to designing the structure for a 25 percent higher load. The allowable stress range values for nonredundant load path members are given in Table 2.

Summary

The review of the test data that has been produced since NCHRP Reports 102 and 147 were published has significantly increased the database for welded steel details. New types of details that were not previously covered in the original provisions have been added to the database. The comparison of the test data with the current AASHTO fatigue provisions did not result in any major deviation between the design fatigue strength and the test results. The findings that were reported in the original NCHRP reports have been supported by the subsequent test programs. No indications were given in the more recent studies that the NCHRP results were in error.

CONCLUSIONS

NCHRP Project 12–15(5) has provided the opportunity to study several important aspects of the behavior of welded bridge details using full-scale specimens. The results from the high-cycle fatigue tests allow for a rational assessment of the variable loadings that cross bridge structures so that existing structures can be assessed for possible fatigue damage. The results will be used to assess the adequacy of existing AASHTO fatigue design specifications. The full-scale test specimens have also allowed for the examination of distortion-induced fatigue cracking under variable-amplitude loading at a web gap detail. Preliminary results have indicated that holes drilled at the crack tip are ineffective in arresting the crack propagation at high stress levels. The fatigue data review has resulted in proposed changes to the current AASHTO fatigue design specifications that better reflect the expanded database for fatigue test data of full-scale welded bridge details.

REFERENCES

1. J. W. Fisher, R. E. Slockbower, H. Hausamman, and A. W. Pense. Long Time Observation of a Fatigue Damaged Bridge. *Journal of the Technical Councils of ASCE*, Vol. 107, No. TC1, April 1981, pp. 55–71.
2. J. W. Fisher, D. R. Mertz, and A. Zhong. *NCHRP Report 267: Steel Bridge Members Under Variable Amplitude Long Life Fatigue Loading*. TRB, National Research Council, Washington, D.C., 1983.
3. C. G. Schilling, K. H. Klippstein, J. M. Barsom, and G. T. Blake. *NCHRP Report 188: Fatigue of Welded Steel Bridge Members Under Variable-Amplitude Loading*. TRB, National Research Council, Washington, D.C., 1978.
4. P. Albrecht and I. M. Friedland. Fatigue Limit Effect on Variable-Amplitude Fatigue of Stiffeners. *Journal of the Structural Division, ASCE*, Vol. 105, No. ST12, Dec. 1979, pp. 2657–2675.
5. J. W. Fisher, B. M. Barthelemy, D. R. Mertz, and J. A. Edinger. *NCHRP Report 227: Fatigue Behavior of Full-Scale Welded Bridge Attachments*. TRB, National Research Council, Washington, D.C., 1980.
6. P. B. Keating and J. W. Fisher. *NCHRP Report 286: Evaluation of Fatigue Tests and Design Criteria on Welded Details*. TRB, National Research Council, Washington, D.C., 1986.
7. J. W. Fisher, K. H. Frank, M. A. Hirt, and B. M. McNamee. *NCHRP Report 102: Effects of Weldments on the Fatigue Strength of Steel Beams*. TRB, National Research Council, Washington, D.C., 1970.
8. J. W. Fisher, P. A. Albrecht, B. T. Yen, D. J. Klingerman, and B. M. McNamee. *NCHRP Report 147: Fatigue Strength of Steel Beams with Welded Stiffeners and Attachments*. TRB, National Research Council, Washington, D.C., 1974.
9. *Standard Specifications for Highway Bridges*, 13th ed., AASHTO, Washington, D.C., 1983.
10. P. B. Keating, S. A. Halley, and J. W. Fisher. *Fatigue Test Database for Welded Steel Bridge Details*. Fritz Engineering Laboratory Report 488.2(86). Lehigh University, Bethlehem, Pa., May 1986.
11. *Recommendations for the Fatigue Design of Structures, Committee TC6 Fatigue*, 1st ed., European Convention for Constructional Steelwork, Brussels, Belgium, 1985.
12. C. Miki, T. Nishimura, J. Tajima, and A. Okukawa. Fatigue Strength of Steel Members Having Longitudinal Single-Bevel-Groove Welds. *Trans. of Japan Welding Society*, Vol. 11, No. 1, April 1980, pp. 43–56.
13. C. Miki, F. Nishino, J. Tajima, and Y. Kishimoto. Initiation and Propagation of Fatigue Cracks in Partially-Penetrated Longitudinal Welds. *Proc. of Japan Society of Civil Engineers*, No. 312, Aug. 1981, pp. 129–140.
14. *ORE Report D 130—Fatigue Phenomena in Welded Connections of Bridges and Cranes*. Reports D130/RP 1/E through D130/RP 10/E. Office of Research and Experiments of the International Union of Railways, Paris, France.
15. J. W. Fisher, H. Hausamman, M. D. Sullivan, and A. W. Pense. *NCHRP Report 206: Detection and Repair of Fatigue Damage in Welded Highway Bridges*. TRB, National Research Council, Washington, D.C., 1979.
16. R. F. Slockbower and J. W. Fisher. *Fatigue Resistance of Full Scale Cover-Plated Beams*. Fritz Engineering Laboratory Report 386–9(78), Lehigh University. Bethlehem, Pa., 1978.

Publication of this paper sponsored by Committee on Steel Bridges.

Effects of Overloads on Deterioration of Concrete Bridges

R. W. JAMES, R. A. ZIMMERMAN, AND C. R. MCCREARY, JR.

An overview of the problem of predicting the effects of overloads on highway bridges is presented, with emphasis on understanding the mechanisms responsible for progressive overload-induced damage to concrete decks. Interaction between physical damage directly attributable to wheel loads and other damage mechanisms such as corrosion is discussed. Existing methods of linear and nonlinear analysis of bridges and rating methods are reviewed. The rapidly developing field of fracture mechanics of concrete and its application to concrete bridge decks is discussed.

The most important economic issue facing the transportation community today is the deterioration of the roadways and structures comprising the nation's highway system. The significance of this problem is emphasized by Turner *(1)*, who also proposes a solution to the perceived rapid deterioration. To reduce the rate of traffic-induced deterioration, primarily of pavements, Turner proposes a redesign of the nation's truck fleet over a 10-year period to reduce the equivalent single-axle loading (ESAL) of the various vehicles by reducing the legal single- and tandem-axle limits to 15,000 and 25,000 lb, respectively. To maintain transportation productivity, Turner proposes an increase in gross vehicle weights to approximately 112,000 lb, with a corresponding increase in the length and number of axles to accomplish the reduced ESAL. This proposal has considerable merit; however, rational assessment of the economic impact of changes in the nation's truck fleet is not a simple matter. The effects of changes in ESAL on flexible and rigid pavements can be evaluated by techniques and data originating in the 1960 Illinois Road Test; however, the effects of heavy vehicles on highway bridges, particularly on bridge decks, are not so well understood. There is considerable economic pressure to increase transportation sector productivity by increasing legal vehicle weights. A recent study *(2)* has resulted in a recommended change in the formula regulating vehicle and axle weights, the so-called bridge formula, to allow longer and heavier vehicles, but to reduce the legal weights of some shorter vehicles, independent of changes in single- and tandem-axle weight limits.

Methods and data to quantify the effects of heavy-truck traffic on highway bridges have not been available in sufficient detail to provide meaningful analyses. Brown et al. *(3)* were forced to omit consideration of the increased cost of maintenance associated with a hypothetical scenario of increased weight limits, citing, ". . . the lack of technology regarding the effects of heavy loading and frequency on bridge deterioration." Some facts are clear, for example, that bridge deterioration is to some extent accelerated by increased truck traffic, both by numbers of trucks and by higher gross vehicle weights. Higher speeds also increase the rate of damage; Turner *(1)* speculates that the actual stress increase due to dynamic effects on bridge decks may be as much as twice the value anticipated by current design methods. The most significant manifestation of bridge damage due to truck traffic is damage to the deck, with damage rates to other structural components being less significant.

Deck damage may take numerous forms; however, the most important damage mechanisms are transverse cracking and longitudinal cracking. Wheel-load-related deck cracking is worse on structures having lower ratios of dead load to total load. Reinforced-concrete decks on steel I–beams are more susceptible to damage of this type than are decks on prestressed girders, probably because of the inherently greater flexibility of the steel stringer bridges. Overweight vehicle damage to bridges, especially deck cracking, is interrelated with other progressive damage mechanisms (such as corrosion) in a complex manner.

Corrosion of reinforcement is intensified by the increased cracking caused by overloaded vehicles, and spalling of concrete cover resulting from reinforcing steel corrosion is certainly accelerated by traffic. Cady and Weyers *(4)* present a method for estimating the deterioration rate of concrete bridge decks due to corrosive attack, but the method does not involve parameters that depend on traffic density or presence of overloaded vehicles. Damage mechanisms affecting steel floor system members are much better understood than are damage mechanisms affecting concrete beams and girders, and the influence of overloads on steel bridge members is not considered here.

REVIEW OF RECENT RESEARCH

Field Studies of Progressive Damage

In a Texas SDHPT-sponsored study in progress, a preliminary survey of approximately 25 structures was accomplished to identify candidate structures for more detailed study. Structures along routes carrying high levels of heavy truck traffic were surveyed in the preliminary study to identify those structures in which the effects of differential truck traffic could be observed by comparison to control structures. The results of the preliminary study indicated that an observable correlation of some

R. W. James, Texas A&M University, Texas Transportation Institute, College Station, Tex. 77843–3136. R. A. Zimmerman and C. R. McCreary, Jr., Civil Engineering Department, Texas A&M University, College Station, Tex. 77843–3136.

forms of progressive damage induced by heavy trucks could be seen on some of the 25 structures surveyed. In particular, qualitatively higher levels of deck cracking were observed in concrete decks on steel stringer bridges in the structures carrying heavier truck traffic. Other forms of progressive damage were observed, but not so clearly attributable to increased levels of truck traffic.

From the results of the preliminary survey, two candidate structures were selected for further study, along with two control structures. All structures were simple-span bridges, having steel stringers and reinforced-concrete decks. Each candidate structure was of essentially the identical design, construction, and age as the corresponding control structure, and being located on the same route of a divided highway, each candidate structure and corresponding control structure carried approximately the same levels of traffic, with the notable exception of the differential truck traffic from several aggregate quarries located north of the sites. Loaded trucks from these quarries travel southbound to the cities of Ft. Worth and Dallas, and return northbound to the quarries. The candidate structures carrying the southbound lanes experience a significantly higher level of heavy-truck traffic than do the control structures that carry the northbound traffic. This differential truck traffic is heavy, being estimated at approximately 180 veh/hr. This differential traffic is thought to have been experienced by these structures for approximately 26 years. Some of the results of this field study are summarized here.

Procedure

A 12-ft-long section across the width of the span of the US–287 bridge over FM–730 was inspected to investigate the variation in cracking across the width of a span. This 12-ft section represented slightly more than 20 percent of the span length. This area was divided into nine regions, consisting of three regions across the width of the span by three along the length. The regions or panels referred to in the figures are 4-ft lengths across the width of the span. Each region represents a 4-ft-long area between two of the four bridge stringers. The designations left, center, and right refer to the regions between two of the stringers in relation to the flow of traffic.

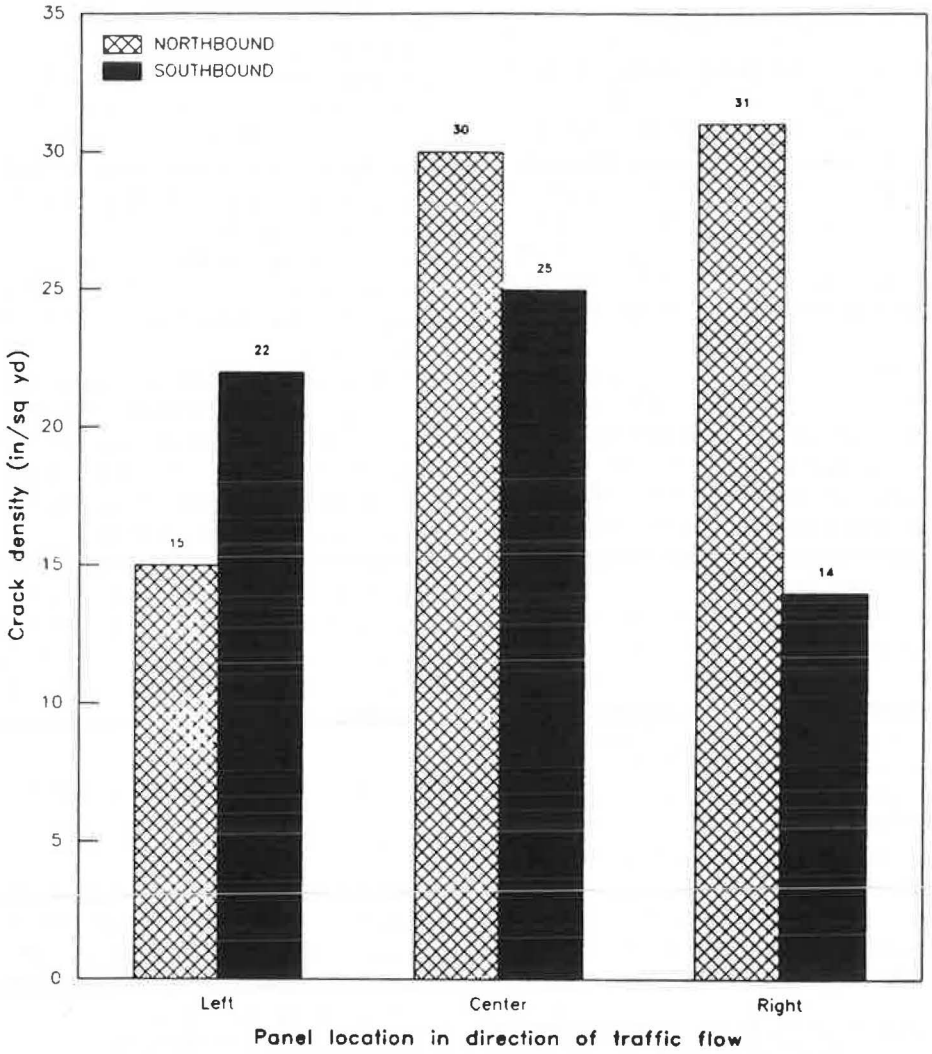

FIGURE 1 Average crack density in reinforced concrete decks subjected to different levels of traffic.

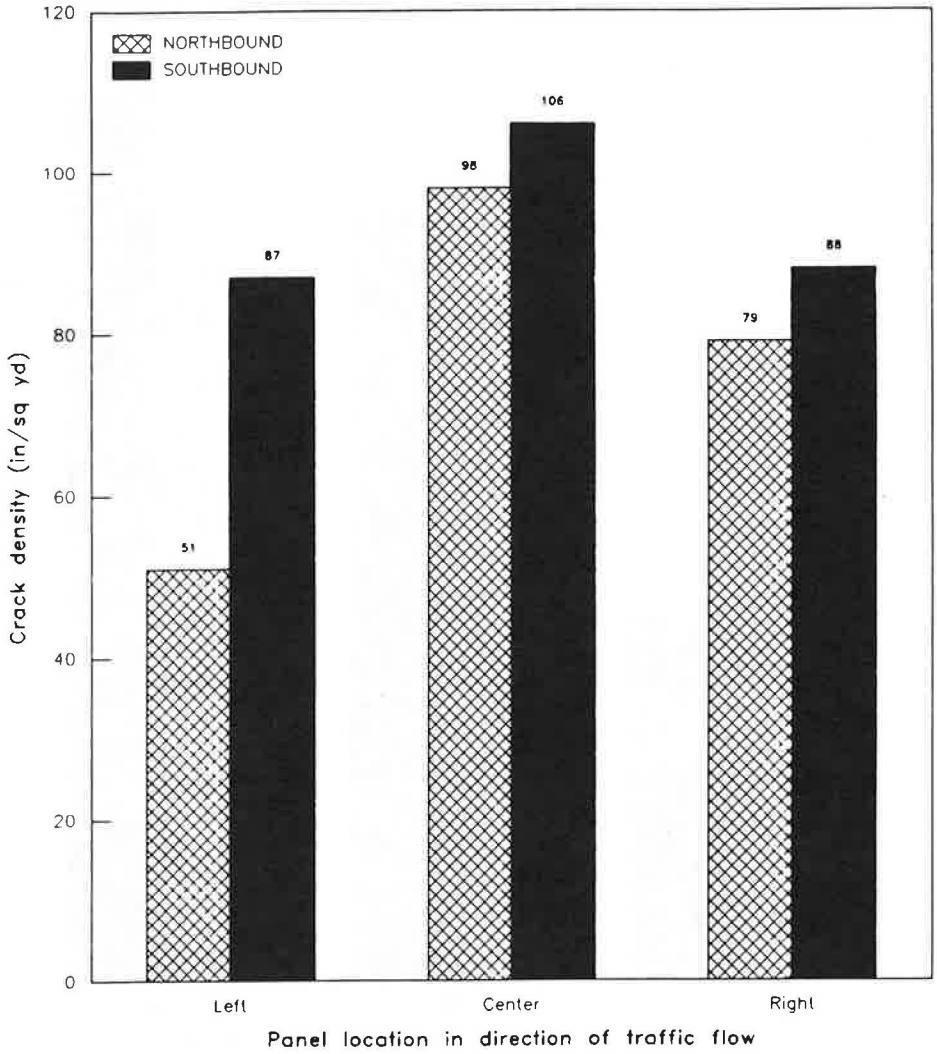

FIGURE 2 Longitudinal crack density in reinforced concrete decks subjected to different levels of traffic.

Cracking on the lower surface of the deck was observed visually and marked by hand. The regions were photographed, allowing office study of the crack patterns. In the analysis of the cracks, cracks oriented within 30 degrees of a line perpendicular to the flow of traffic were denoted transverse cracks, cracks oriented within 30 degrees of a line parallel to the flow of traffic were denoted longitudinal cracks, and all other cracks were denoted diagonal cracks. The crack density reported is the sum of the length of the observed cracks divided by the area of the region of study.

Although both bridges were subject to loading, the southbound bridge, carrying the heavier traffic loads is referred to as the loaded structure, and the northbound bridge is referred to as the unloaded structure. Some of the preliminary observations of crack densities and orientations are summarized in Figures 1–4.

Observations of Total Crack Densities

The observed regions of the loaded bridge almost always exhibited more cracking than the corresponding regions of the unloaded bridge deck. In the loaded bridge, the left regions were always cracked more, by an average of 65 percent, than the left regions of the unloaded bridge deck. The center and the right regions of the loaded bridge usually exhibited greater crack densities, by approximately 6 percent more than the corresponding regions of the unloaded structure.

For both the loaded and unloaded bridges, the center regions always exhibited more cracking than the left regions. On average in the center regions there was 124 percent more cracking for the unloaded bridge and 43 percent more cracking for the loaded bridge. The center regions also usually exhibited more cracking than the right regions in both bridges, averaging 8 percent more for the unloaded bridge and 9 percent more for the loaded bridge. The right regions always exhibited more cracking than the left regions in the unloaded bridge, averaging 107 percent more cracking. In the loaded bridge, the right regions usually exhibited more cracking than the left, averaging 31 percent more cracking.

The difference in crack density between the loaded and unloaded bridges is far greater in the left regions of the bridge deck than in the center or right regions. The more heavily cracked center and right regions have smaller differences between the loaded and unloaded spans.

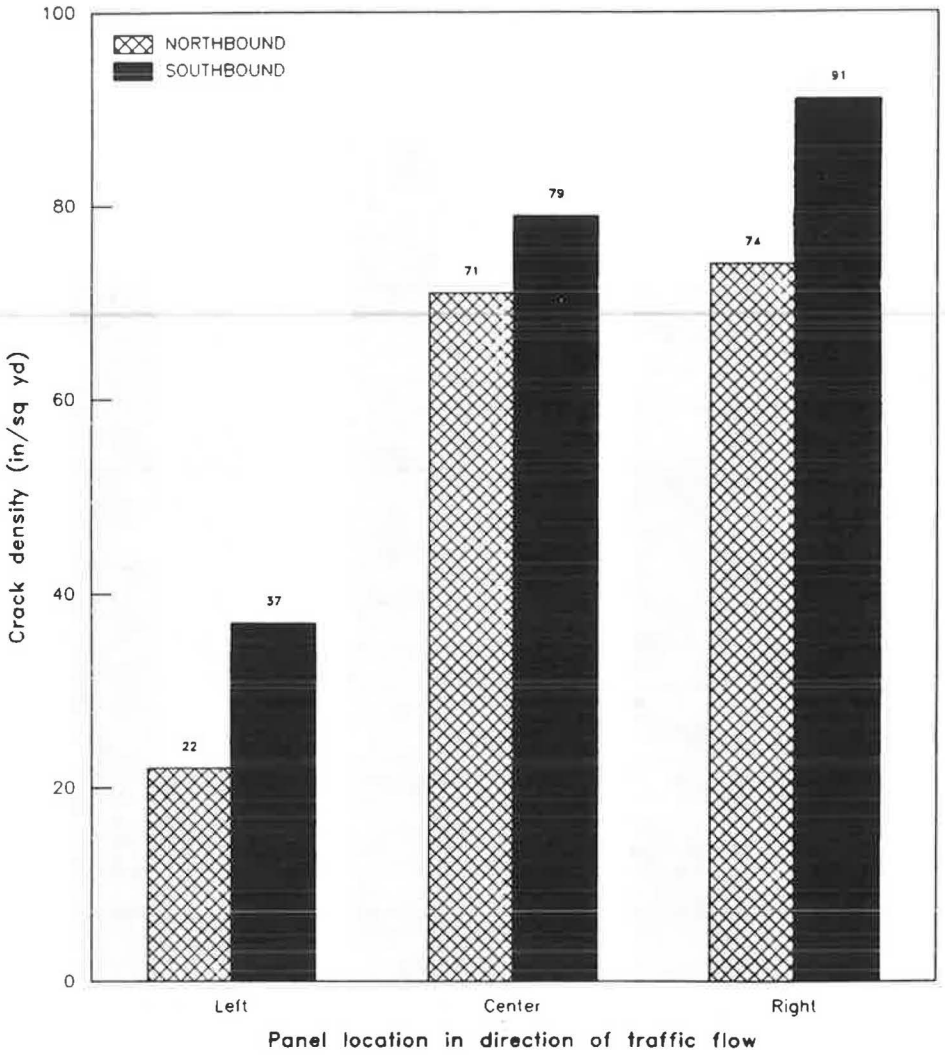

FIGURE 3 Transverse crack density in reinforced concrete decks subjected to different levels of traffic.

Observations of Transverse Cracking

The observed regions of the loaded bridge uniformly exhibited more transverse deck cracking than those of the unloaded bridge by an average of 71 percent in the left regions, 8 percent in the center regions, and 11 percent in the right regions.

For both the loaded and unloaded bridges, the center regions always exhibited more transverse cracking than the left regions. On average, there was 92 percent more transverse cracking in the center regions of the unloaded bridge, and 22 percent more transverse cracking in the center regions of the loaded bridge. The center regions also usually exhibited more transverse cracking than the right regions in both bridges, averaging 24 percent more for the unloaded bridge and 20 percent more for the loaded bridge. For the unloaded bridge, the right regions always exhibited more transverse cracking than the left regions, averaging 55 percent more cracking. For the loaded bridge, there was little difference between the right and left regions.

Observations of Longitudinal Cracking

The loaded bridge always exhibited more longitudinal cracking than the unloaded bridge in the left and right regions. The left regions exhibited an average of 68 percent more longitudinal cracking, and the right regions exhibited an average of 23 percent more longitudinal cracking. The center regions usually exhibited more longitudinal cracking in the loaded bridge, by an average of 11 percent.

For both the loaded and unloaded bridges, the center regions always exhibited more longitudinal cracking than the left regions. On average, there was 223 percent more longitudinal cracking for the unloaded bridge, and 114 percent more longitudinal cracking for the loaded bridge. The right regions always exhibited more longitudinal cracking than the left regions in the loaded bridge, averaging 13 percent more longitudinal cracking. For the unloaded bridge, the right regions usually were cracked more than the center regions by an average of 4 percent. The right regions always exhibited more longitudinal cracking than the left regions in both bridges, averaging 146 percent more cracking in the loaded bridge, and averaging 236 percent more cracking in the unloaded bridge.

Observations of Diagonal Cracking

The loaded bridge usually exhibited more diagonal cracking than the unloaded bridge in the left regions by an average of 47

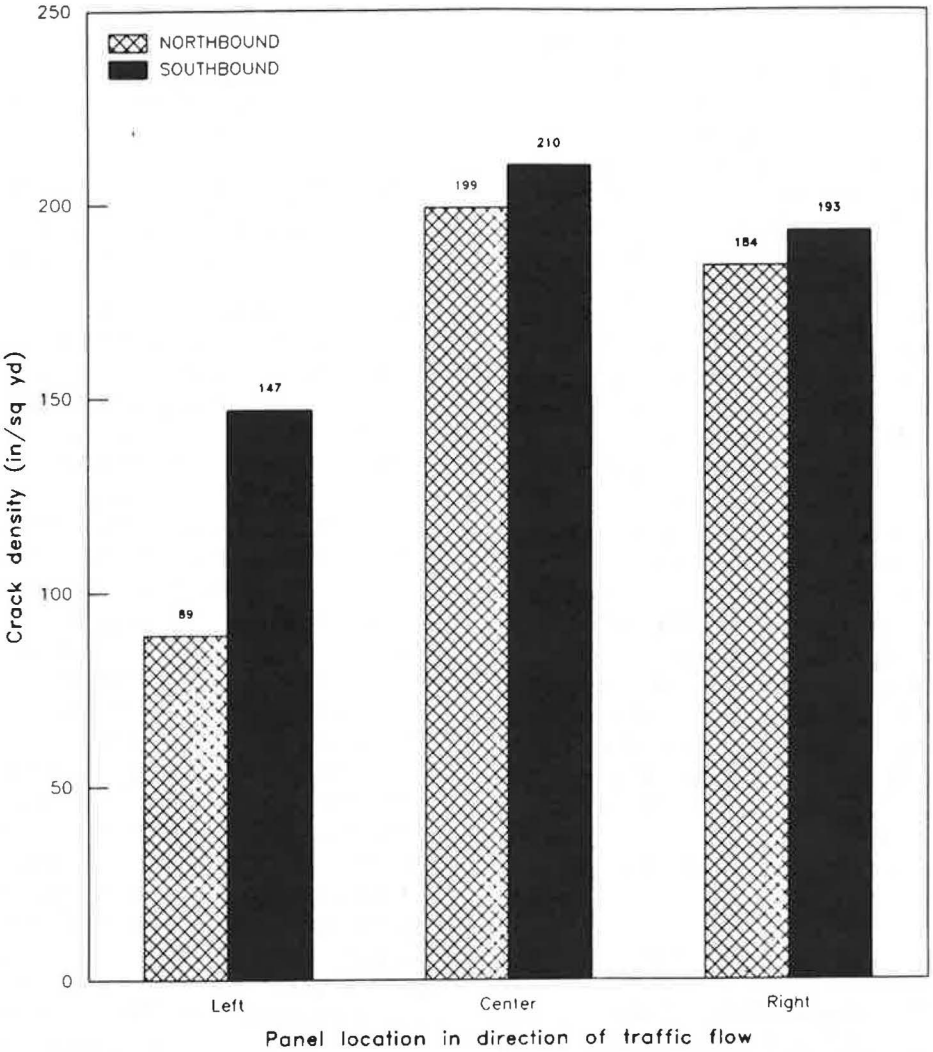

FIGURE 4 Diagonal crack density in reinforced concrete decks subjected to different levels of traffic.

percent. In the more heavily cracked center and right regions, however, an unexpected reversal of this trend was observed. The center regions were usually cracked less for the loaded bridge by an average of 17 percent, and the right regions always exhibited less diagonal cracking for the loaded bridge by an average of 55 percent.

For the unloaded bridge, the center regions always exhibited more cracking than the left regions, averaging 100 percent more cracking. For the loaded bridge, there was an average of 14 percent more diagonal cracking in the center regions than in the left regions. The center regions usually exhibited less diagonal cracking than the right regions in the unloaded bridge, by an average of 3 percent. For the loaded bridge, the center regions always exhibited more diagonal cracking than the right regions, by an average of 79 percent. The right regions always exhibited more diagonal cracking than the left regions in the unloaded bridge, averaging 107 percent more cracking. For the loaded bridge, the right regions usually exhibited less diagonal cracking than the left regions, averaging 36 percent less cracking.

Mechanisms of Overload-Related Damage to Bridge Decks

A finite element model of a steel-concrete composite bridge was applied by Wegmuller *(5)*. The proposed model was an orthotropic layered deck composite with a layered steel I–beam. The concrete, reinforcing steel, and I–beams were modeled as nonlinear materials. Model results were compared to experimental data to demonstrate the successful modeling of such structures in the postelastic regime. The model was limited to short-term, monotonically increasing loads. Tensile cracking of the concrete was treated simply as complete loss of stiffness after a cracking stress is reached. Gradual strain softening, the gradual reduction of normal stress with increasing strains in the postcracking regime as discussed by Bazant *(6)*, was not modeled.

Wegmuller's work *(5)* indicates that successful nonlinear analyses of bridges subject to overloads are possible. Further, he observes that up to about 20 percent overload, the response of the structure can be approximated by modeling the slab as an elastic, perfectly plastic material.

Kostem *(7)* discusses the initiation of deck damage resulting from overloading, drawing conclusions from a parametric investigation using the computer program BOVA *(8)*. Kostem's study is limited to simple-span reinforced or prestressed concrete girders and concrete deck bridges. Kostem considers several vehicles, calculating the gross vehicular weight for each that would induce cracks through the deck of each of

several representative bridge designs. For instance, a 3S2 vehicle is predicted to cause deck cracking in the structures analyzed at gross vehicle weights from 91 to 132 kip, approximately 132 to 193 percent of the current legal gross vehicle weight for the 3S2 vehicle studied. The critical structures for the 3S2 vehicle were 100 ft simple spans using 7 and 8 AASHTO girders and a 7.5-in. deck. The reported results are limited to concrete decks on prestressed girders; however, the method should be applicable to structures of other types.

The earliest indication of overload damage to bridges is expected to be cracking in the slab. Batchelor et al. *(9)* present the results of a series of fatigue tests on 37 panels of five model slabs. Although not conclusive, the results indicate that the fatigue endurance limit punching loads for isotropically reinforced slabs having a reinforcement ratio of 0.2 percent and for slabs conventionally reinforced according to AASHTO specifications are 40 and 50 percent of the static punching failure loads, respectively. The endurance limit for the isotropic slab represents stresses caused by wheel loads approximately four times the design wheel load. Observed fatigue failure modes were predominantly punching shear, with flexural failures observed in some of the slabs having low reinforcement ratios. During the first few cycles of repeated loading, cracking was initiated. The cracks then widened and spread with subsequent repeated loading until a relatively stable period was reached during which little crack growth was observed. Empirical equations are presented that best fit the data. For conventional orthotropic reinforcement, the ratio of the fatigue strength P_f to the punching resistance P_s' is given in terms of the number of cycles to failure N by

$$P_f/P_s' = 1.0 - 0.102 \log N + 0.006(\log N)^2 \quad (1)$$

The observation that fatigue failure of decks is unlikely neglects any interaction of fatigue cracking, which was observed to occur at much lower loads, and corrosion or other environmental effects. Certainly the presence of working cracks in the deck is detrimental to durability, and in many instances the serviceability of the deck is limited by corrosion of reinforcing steel. Cracking of reinforced concrete decks is expected under normal traffic levels.

Maeda et al. *(10)* suggest that slabs under normal service loadings are expected to develop longitudinal and transverse cracking spaced no closer than 1.3 ft, with crack widths of up to 0.008 in., at crack densities of up to 168 in. (linear) of crack per square yard, and exhibiting leaching of calcium hydroxide. More severe cracking, scaling, or spalling of concrete is indicative of abnormal distress, according to Maeda *(10)*. Figure 1 shows that total crack densities considerably greater than the quoted value of 168 in./yd^2 were recorded in the preliminary results of the field study reported here.

The problem of granting overload permit necessitates a more practical approach to the effect of overloads on bridges. White and Minor *(11)* discuss a computerized method of evaluation of bridge overloads that is typical of standard practice by the various state highway agencies. The method described is applied during the permitting process, and consists of a calculation of the maximum moment caused by the overweight vehicle under consideration on the bridge under consideration. An equivalent HS vehicle, some multiple of the HS–20 that causes the same moment, is identified. This vehicle is compared to the operating rating of the bridge, which has been previously catalogued according to AASHTO *(12)* and FHWA *(13)* procedures. The problem with this widely used method of analysis is identified by Kostem *(7)*.

> Any analysis scheme based on linear elastic behavior will . . . lead to conservative results since this approach will ignore the ever present material nonlinearities and the redistribution of stresses in the superstructure.

Other simplifying assumptions used in this and similar methods *(14, 15)* may be unconservative, however. The method reported by White does not check end shear because the only data available to the automated procedure is the rating based only on moment. Still this linear method of analysis, rating, and permitting offers the advantages of automation, economy, and practicality, and any bridges that compute as inadequate are identified for further individual analysis. More rigorous analytical methods can be applied to individual checks of these bridges.

Shanafelt and Horn *(16)* reported the results of a series of tests on a prestressed concrete girder. The purpose of the tests was to determine the effectiveness of various repair techniques applied to damaged girders. Damage representative of impact by overheight vehicles was considered in the series of 10 reported tests; however, Test 1 was a load test of an undamaged girder. Test 1 is helpful in understanding the progressive damage mechanisms that may be a factor in the durability of prestressed concrete girders. Further, this test helps quantify the damage to such girders due to overweight vehicles.

The prestressed concrete girders and composite reinforced-concrete deck design, as represented by this specimen, is among the most durable and overload-resistant designs available to designers; however, the potential for overload-induced progressive damage exists. The test girder was loaded in positive moment as a 60-ft, simply supported beam, by a midspan-concentrated load causing a bending moment equal to 75 percent of the calculated ultimate moment. This moment was equal to 195 percent of the HS–20 LL+I service load moment.

The resulting damage is described as being more severe than anticipated by the researchers. Eight major cracks were created extending from the bottom fiber of the girder to within a few inches of the bottom of the composite slab. In addition, minor cracks were observed between the major cracks. The eight major cracks were spaced 12 to 28 in. over a region approximately 130 in. long at midspan. Crack openings averaged 0.015 in. The stress at crack initiation was significantly less than the value $6\sqrt{f_c'}$. Effects of the conservatism afforded by the AASHTO lateral distribution factors would likely protect such a girder in service; however, if more realistic lateral distribution factors are used, cracking at this loading would be anticipated.

After the initial loading resulted in cracking of the girder, the test was repeated, and the behavior of the girder was different, the load-deflection curve having become nonlinear at a significantly lower load than that required to cause cracking in the initial test. This result could be interpreted as progressive cracking damage, except that a third load cycle resulted in a nearly identical load-deflection relationship. A more credible explanation than progressive damage is suggested by the following. During the first load cycle, the uncracked section

behaves essentially linearly up to the point of crack initiation, at which point the moment of inertia begins to be reduced by the crack, which extends slowly, or at least in small increments, as the load is increased. The continual change in slope of the load-deflection curve indicates that the moment of inertia is continually changing, that is, the crack is continually extending, up to the maximum test load.

During unloading, there is a short elastic unloading portion, followed by a nonlinear unloading portion during which the cracks progressively close and a compression prestress redevelops. On completion of the first loading cycle, a residual strain is apparent. The second load cycle begins to exhibit a nonlinear relationship at a significantly lower load level, as a result of the cracks opening at zero normal stress rather than at the tensile strength of the concrete as in the first cycle. This means the cracks begin to open at a moment of only 75 percent, approximately, of that required to crack the girder in Load Cycle 1. On completion of the second load cycle, there is no additional crack elongation and no significant additional residual deformation because the second load cycle does not reach a greater moment than the first.

The response to the third load cycle is essentially identical to that of the second cycle. Ideally, this behavior might be expected to continue for repeated loadings to the same moment; however, other factors can alter this idealized behavior. The repeated opening and closing of the cracks in the structure can result in propping of the cracks by fines that are displaced from the fracture surfaces, resulting in further increases in residual deformation. Corrosion interacts with this process, accelerating and being accelerated by the repeated opening and closing of the cracks. If loads sufficiently large to initially crack the girder are experienced once and loads sufficiently large to open the cracks occur repeatedly, these mechanisms can serve to cause progressive damage to prestressed concrete bridges.

Prestressed concrete girder bridges are to some extent susceptible to progressive damage mechanisms dependent on the level of the live loads. Such structures are believed to be more resistant to such damage than other structures with a larger ratio of live load to dead load. In a field study in progress, observations of heavily traveled bridges are being compared with observations of less heavily traveled, but otherwise identical, bridges in Texas. Preliminary findings confirm that the decks of some heavily traveled structures clearly exhibit more cracking than the decks of similar but less heavily traveled structures. Also, there is qualitatively a higher level of deck damage in decks supported by steel stringers than in prestressed girder decks. Both of these findings are as expected, however quantified documentation of such progressive damage mechanisms is essential to economic analysis of the effects of changes in truck regulations. Efforts to quantify these observations are in progress.

Fracture Mechanics of Concrete

Although not yet in wide use by the bridge engineering community, numerical fracture mechanics methods are being applied to plain, reinforced, and prestressed concrete structures in other fields, and considerable interest by researchers in this area is evident in the literature. Two distinct methods of modeling fracture of concrete structures are developing. Modeling the crack in a continuum by the use of finite elements having free surfaces along element boundaries where the crack is open, the first approach to have been explored, is perhaps the more straightforward approach. An overview of this method is provided by Ingraffea *(17)*. This method suffers the inherent difficulties associated with the necessity of redefining the mesh as the crack propagates, resulting in significant computational problems, and with the inherent limitation that cracking may occur only on predefined element boundaries. The second, more widely accepted, method, originally proposed by Rashid *(18)*, models the crack by a continuous smeared crack band. This method eliminates the necessity of redefining the mesh as the crack propagates, although the stiffness of the elements involved in the fracture process zone obviously changes with crack propagation. The smeared crack numerical model is in fact believed to be a better physical model of fracture in concrete than the discrete crack model, because in concrete there is a zone of some finite thickness surrounding each crack where physical damage to some extent reduces the stiffness of the continuum.

The applicability of the two methods depends on the scale of the problem, because the fracture of massive structures such as dams and the fracture of smaller structures such as bridge decks in flexure, require significantly different modeling techniques. In the smeared crack band approach, fracture is modeled by a reduction in modulus at integration points where cracking criteria are satisfied. The fracture is therefore manifested in the model by a zone or band of anisotropic material with reduced modulus in the direction normal to the modeled fracture surface.

The constitutive models in use for the concrete vary. A failure of tensile strength and linear strain-softening rule is frequently applied. Its variations include the concepts of crack closing, shear capacity through aggregate interlock, intersecting of cracks, and creep behavior being added under some circumstances. Failure modes of the concrete in compression and biaxial loading are considered in some applications. Reinforcing steel is modeled with associated nonlinear behavior that includes application of yield, rupture, and debonding models.

CONCLUSIONS

1. Based on several observations, cracking of concrete members may occur at tensile stresses below the expected value of $6\sqrt{f_c'}$ or $7.5\sqrt{f_c'}$. Whether residual stresses due to creep or shrinkage are the explanation for this observation is not known. In addition to Shanafelt and Horn *(16)*, who reported cracking at stresses of $2.7\sqrt{f_c'}$ to $4.5\sqrt{f_c'}$, Bonilla et al. *(19)* observed significant cracking in a one-third scale reinforced-concrete deck subjected to negative moments at stresses as low as $3\sqrt{f_c'}$.

2. Concrete bridge decks respond to overloads by exhibiting increased densities of longitudinal and transverse cracking, although normal traffic levels are thought to result in cracking or reinforced concrete decks in some circumstances *(10)*. The increased cracking leads to accelerated corrosive attack and spalling or scaling.

3. Mechanisms exist for progressive overload-induced damage to reinforced-concrete decks and for interaction between mechanical and chemical effects. Models for studying

the rate of deterioration due to these effects and the related economic impact have not yet been developed.

4. Bridge decks supported by steel girders are more susceptible to progressive overload-induced damage mechanisms than are decks on prestressed concrete girders. Preliminary results of field studies in progress indicate that although there is observable damage to decks of both types attributable to heavy-truck traffic, there is a measurably greater extent of damage to decks supported by steel girders when subjected to heavy-truck traffic. A complete quantified measure of the effect of heavy-truck traffic is not yet available, however.

5. Mechanisms exist for progressive damage of cracked prestressed-concrete girders so long as the girder is subject to moments large enough to reopen the initial cracks. Test data *(16)* indicate that the moment necessary to reopen the cracks is significantly lower than the moment causing initial cracking, perhaps only 75 percent of the moment causing initial cracking.

RECOMMENDED FUTURE RESEARCH

Application of rapidly developing technology in the field of fracture of concrete to the problem of progressive mechanical deterioration of concrete bridge decks is a logical extension of the present state of the art in the field of bridge engineering. The establishment of a relationship between mechanical damage (such as that due to wheel loading) and corrosion-induced deterioration is a second problem that should be addressed. Although the solution to the first problem is achievable with current nonlinear finite element technology, the solution to the second problem is more difficult. Further research such as that reported by Cady and Weyers *(4)*, as well as field studies identifying and quantifying the relationships between progressive deterioration and mechanical and environmental loading, are essential for solution of the second problem.

ACKNOWLEDGMENT

These finding are from an ongoing study funded partially by the Texas State Department of Highways and Public Transportation (TSDHPT), for whose support the authors are grateful. The assistance and encouragement of H. L. Furr is acknowledged, as is the assistance of K. Willis of TSDHPT.

REFERENCES

1. F. C. Turner. A Re-Designed Truck to Reduce Highway Damage. Paper presented to joint meeting of the Bridge-Highway Committee of ARTBA at NASHTO Conference, Atlantic City, N.J., 1986.
2. R. W. James, J. S. Noel, H. L. Furr, and F. E. Bonilla. Proposed New Truck Weight Limit Formula. *Journal of Structural Engineering*, ASCE, Vol. 112, No. 7, 1986, pp. 1589–1604.
3. J. L. Brown, D. Burke, F. L. Roberts, and C. M. Walton. *Effects of Heavy Trucks on Texas Highways. Interim Report 231.* Texas State Department of Highways and Public Transportation, Austin, 1978, 63 pp.
4. P. D. Cady and R. E. Weyers. Deterioration Rates of Concrete Bridge Decks. *Journal of Transportation Engineering, ASCE.* Vol. 110, No. 1, 1984, pp. 34–44.
5. A. W. Wegmuller. Overload Behavior of Composite Steel-Concrete Bridges. *Journal of the Structural Division, ASCE.* Vol. 103, No. ST9, 1977, pp. 1799–1819.
6. Z. P. Bazant. Mechanics of Fracture and Progressive Cracking in Concrete Structures. In *Fracture Mechanics of Concrete: Structural Application and Numerical Calculation*, G. C. Sih and A. DiTommaso, eds. Martinus Nijhoff Publishers, Boston, Mass., 1985, pp. 1–94.
7. C. N. Kostem. Overloading of Highway Bridges—Initiation of Deck Damage. In *Transportation Research Record 664.* TRB, National Research Council, Washington, D.C., 1978, pp. 207–211.
8. W. S. Peterson and C. N. Kostem. *User's Manual for Program BOVA.* Report 378B.6A. Fritz Engineering Laboratory, Lehigh University, Bethlehem, Pa., March 1975.
9. B. deV. Batchelor, B. E. Hewitt, and P. Csagoly. An Investigation of the Fatigue Strength of Deck Slabs of Composite Steel/Concrete Bridges. In *Transportation Research Record 664.* TRB, National Research Council, Washington, D.C., 1978, pp. 153–161.
10. Y. Maeda, S. Matsui, I. Shimada, and H. Kato. *Deterioration and Repairing of Highway Bridges in Japan. III. Inspection and Repairing of Cracked Slabs.* Technology Reports of Osaka University, Vol. 31, No. 1599, Osaka, Japan, March 1981, pp. 135–144.
11. K. R. White and J. Minor. Evaluation of Bridge Overloads. *Transportation Engineering Journal, ASCE.* Vol. 105, No. TE1, 1979, pp. 15–21.
12. *Manual for Maintenance Inspection of Bridges—1970.* AASHTO, Washington, D.C., 1970.
13. *Recording and Coding Guide for the Structure Inventory and Appraisal of the Nation's Bridges.* FHWA, U.S. Department of Transportation, 1977.
14. R. R. Johnston, R. H. Day, and D. A. Glandt. *Bridge Rating and Analysis Structural System [BRASS]. Vol. 1. System Reference Manual.* FHWA–RD–73–501. FHWA, U.S. Department of Transportation, 1973, 192 pp.
15. C. O. Hays, Jr. Evaluating Bridge Overloads Using the Finite Element Method. *Proc. of the First International Bridge Conference*, Pittsburgh, Pa., June 1984, pp. 232–238.
16. G. O. Shanafelt and W. B. Horn. *NCHRP Report 280: Guidelines for Evaluation and Repair of Prestressed Concrete Bridge Members.* TRB, National Research Council, Washington, D.C., Dec. 1985, 84 pp.
17. A. R. Ingraffea and V. Saouma. Numerical Modeling of Discrete Crack Propagation in Reinforced and Plain Concrete. In *Fracture Mechanics of Concrete.* Martinus Nijhoff Publishers. Boston, Mass., 1985, pp. 171–225.
18. Y. R. Rashid. Ultimate Strength Analysis of Prestressed Concrete Pressure Vessels. *Nuclear Engineering and Design*, Vol. 7, 1986, pp. 334–344.
19. F. E. Bonilla, R. W. James, R. A. Osegueda, and J. S. Noel. *Composite Action of Precast Panel Bridge Decks in Negative Moment Regions.* Research Report 324–2. Texas Transportation Institute, Texas A&M University, College Station, Tex., 1986, 164 pp.

Publication of this paper sponsored by Committee on Concrete Bridges.

Glass-Fiber-Reinforced Composites in Building Construction

ANDREW GREEN

Glass-fiber-reinforced plastic composites have had limited use as structural components in building construction. To realize the full potential of these materials and increase their use, their outstanding features must be emphasized. In developing composite components, it is essential to combine expertise in the disciplines of plastic and reinforcing materials, structural design, and fabrication techniques. Efficiently designed composite components and a case history are presented to demonstrate typical practical applications.

The unique building shown in Figure 1, the first of its kind, is constructed entirely of glass-fiber-reinforced materials. Because the building is used as a radio-frequency testing station, all components above the ground are required to be nonmetallic so that they do not interfere with electromagnetic waves associated with the operation. Therefore, the components such as rigid frames, columns, purlins and girts, accessories, connections including bolts and nuts, and cladding (building side panels and roof panels) are all made of glass-fiber-reinforced composites. The building is designed like a stressed-skin aircraft structure using torque-box type rigid frames, purlins, and girts.

This unprecedented use of advanced composites as primary structural components met the structural requirements with minimal weight and number of members, thus minimizing overall costs. The composite structures rely on the strengths while recognizing the limitations of the composite materials, without attempting to duplicate standard sections made of rolled or light gauge steels (Figure 2). The structures are designed on the merits of the mechanical properties of the composite material. Control of the stress levels and deflection to within the allowable limits of the composite materials is achieved by the design of the reinforcing scheme, the geometry of the cross section, and the thickness of the skin. The disciplines of structural design, composite materials, and fabrication are linked together to achieve a workable, cost-effective, finished project.

WHY COMPOSITES?

Plastic composites are excellent for corrosion-resistant applications, besides being nonmagnetic and electrically nonconductive. Considering the devastating cost of damage done by corrosion to metal parts in industrial buildings, glass-fiber-reinforced components (e.g., panels, purlins, and girts) are viable, attractive alternatives because of their favorable life-cycle cost. Their light weight reduces installation time and costs. In addition, the degree of light translucency or color tones can be varied.

FIGURE 1 Interior of building made entirely of glass-fiber-reinforced composites.

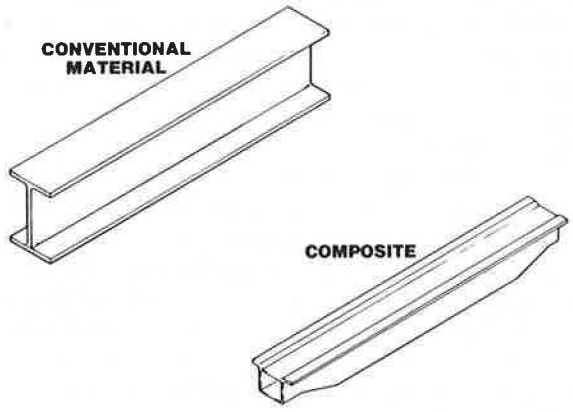

FIGURE 2 While free or unsupported edges in beam design are acceptable with steel shapes, low Young's modulus composite materials require captive elements to resist buckling.

Composite Technology, Inc., 1005 Blue Mound Road, Forth Worth, Tex. 76131.

Currently composites are only used in applications where conventional materials such as steel fail to function effectively.

WHY NOT BEFORE?

The plastic composites industry celebrated its 42nd anniversary at the 42nd SPI Annual Conference and Expo '87 held in Cincinnati, Ohio, in February, 1987. There have been some plastic composites structures built in the past—The Monsanto House of the Future (1957), geodesic domes, shell roofs, and buildings using wide-flange beam shapes and sandwich panels. However, those structures were showcases with little potential for use in the mainstream of the building industry. When it came to meeting the requirements for a standard structure for an industrial building (20- to 25-ft bay spacing and 40- to 60-ft clear spans), none were available. Components suitable for long spans, when feasible, were too expensive because of material and fabrication costs.

Lack of communication between composites industries and building construction industries has caused a great deal of delay in development of composites as building construction materials. In order to build a product such as a preengineered composite building from its conception to final product, expertise in all related disciplines is needed. This requires a designer who works with a stress analyst and composite engineer to come up with the final design for fabrication. Integrating the design of the composite material to the production process is another difficult task. A full-scale test to verify the integrity of the structure is often required (Figure 3). All of these prerequisites, in addition to financial support, are required to make the project a reality.

FIGURE 3 This rigid frame is being tested with an 8,000-lb lateral load at the eave to check for stiffness of the frame and fixity of the base. Box section yields good stiffness in both planes, therefore, lateral support is not needed (a real advantage in erecting operations).

DESIGNING PERFORMANCE INTO THE COMPOSITE

Plastic composites use high-strength fibers, usually glass fibers because of their favorable cost and high tensile strength, for reinforcing components in a plastic-based matrix as a corrosion protective and stress transmission medium. Engineered composites are reliable structural materials that possess desirable inherent characteristics such as high strengths, corrosion resistance, nonelectromagnetism, and integral coloring. Composites for building construction applications require predictable short- and long-term behavior within the expected environments. These characteristics are achieved by using a functional resin system, reinforcement design, and a suitable structural shape (Figure 4).

The plastic resins include polyesters for cost and overall performance, vinyl esters for superior bonding, toughness and greater elongation, and long-term characteristics, and other special-purpose resins for chemical resistance. Various forms of fiber reinforcements include unidirectional rovings for high-unidirectional strength and stiffness; woven rovings for good orthotropic properties; and chopped-strand for continuous-strand mats for semi-isotropic properties, good shear strength, and bulk thickness.

In advanced composites, a reinforcing scheme based on the combination of mats and continuous rovings in relevant directions and positions is used. A plastic resin is selected on the basis of service conditions and its interfacing compatibility with the reinforcing fibers so that the mode of failure is not controlled by the resin, which is the weak or limiting constituent in the composite.

The design of reinforced plastic components for building construction is mainly controlled by deflection limits and stability rather than strengths. Therefore, the structural shapes and fiber placement are designed to obtain the optimum stiffness. The technique is similar to the placement of steel rebars in a reinforced-concrete section. Maximum stress levels are kept relatively lower than those of conventional materials to prevent creep and stress rupture.

HOW TO INCREASE AVAILABILITY OF COMPOSITES

A concerted effort by building construction and composites industries is needed to establish a direction for expanding the use and application of composite materials to take advantage of their primary benefits. Designer engineers in composites are required to be knowledgeable in the disciplines of plastics and reinforcing materials, structural design, and also fabrication techniques. Training provided by engineering schools is essential to optimize performance of these products.

Standard codes of practice for design and applications of plastic composites are urgently needed, or else design efforts will be limited to a small elite group of experts. Codes for

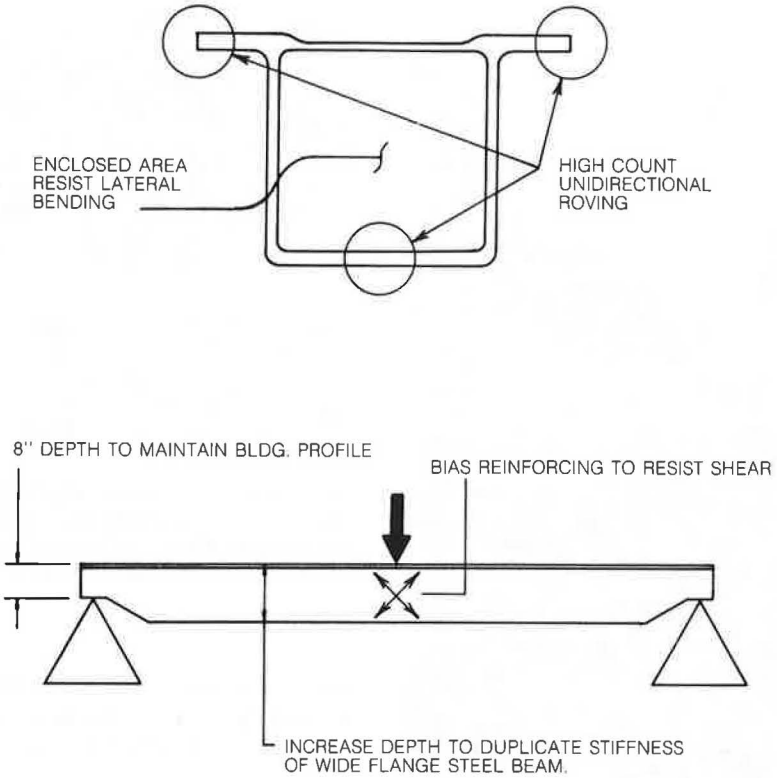

FIGURE 4 Low stress levels and low deflections in beam design are obtained by placing primary reinforcement at maximum distance from the neutral axis and using a large enclosed area for lateral stability.

composites also must be integrated into standard building codes.

Materials used in construction must have reliable data for predictable performance of the products. The properties for which data are needed by designer engineers and fabricators are basic design mechanical properties in relevant directions, joining methods and their allowable loads, creep and stress rupture properties, weathering and aging properties, environmental (corrosion) effects, thermal properties, behavior in resisting fire and spread of flame, and in smoke generation.

The inherent nature of these materials causes combined stress to be more significant than in a homogeneous material. Furthermore, classical linear elastic methods of analysis are not always applicable; therefore, full-scale testing to determine ultimate performance in critical cases is warranted.

At the present time, there is sufficient data to be incorporated into product designs. However, only the small inner circle of specialists can interpret it with confidence and also have the facilities to verify the design from conception through fabrication and large-scale testing. Relevant data must be scientifically gathered and presented in a usable form so that the information can be readily interpreted by structural engineers.

After these needs are remedied, composites can be widely used and designed like other conventional building materials.

FUTURE

Plastic composites will have much wider application when they are accepted as materials in their own right, when they are used in a form that has synergism with their elastic properties and strengths, and when their weaker characteristics are excluded from the design (Figure 5). For example, timber structures and concrete structures are not considered in the same manner or shape as steel structures.

A challenging, new construction material is available and waiting for architects and engineers to cultivate to its full potential. It is not a replacement for conventional materials but an alternative when special situations dictate its use. It has proven itself as a viable, permanent structural material.

The systems and disciplines described here have been in use since 1975. Composite beams, cladding, and decking with sound structural design have experienced a growing acceptance in coastal regions and in industries where building components are exposed to corrosive elements. The long-term structural performance and durability of the materials in numerous installations have demonstrated their suitability for these applications.

CASE STUDY

Required: Electrically nonconductive, nonmagnetic structure for electronic test facility. Elevations of the building to blend in with the countryside and local environment; erection to be simple with as few members as possible.

Solution: A two-piece rigid frame with fixed ends was selected to keep lateral deflections within local codes (Figure 6). The rigid splice (Figure 7) was selected over a knee splice because this area had lower bending moments than the knee.

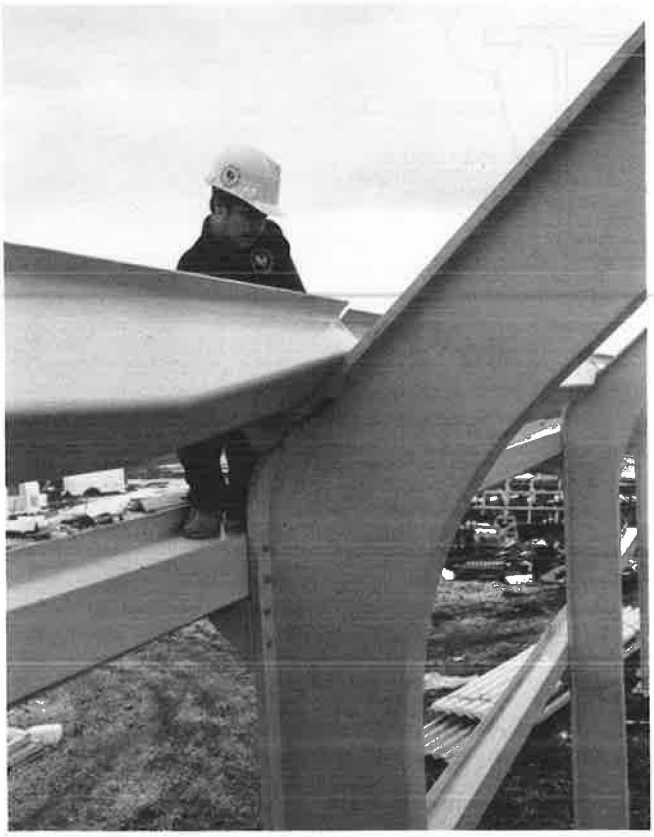

FIGURE 5 Deep rigid-frame knee without splice or connections reduces stress levels and eliminates problem of fasteners at high-moment corner.

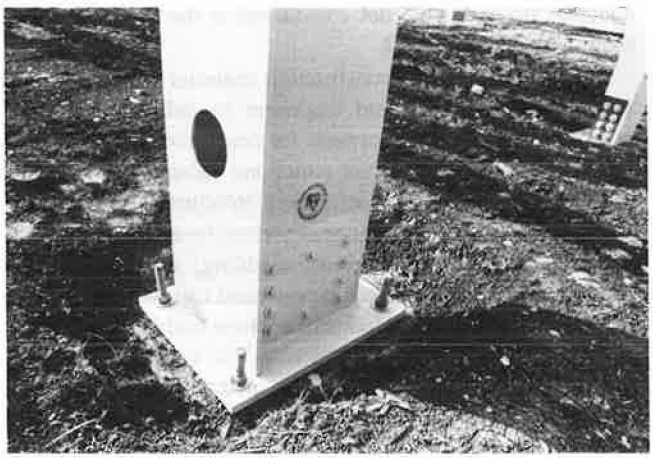

FIGURE 6 Rigid-frame base is fixed to help reduce overall deflection. Rotation of base is resisted by the clamping action of bolts and backing plates bonded on the inside of section. This yields stiff frame with 1 1/8-in. deflection at 16-ft eave height with an 8,000-lb lateral load.

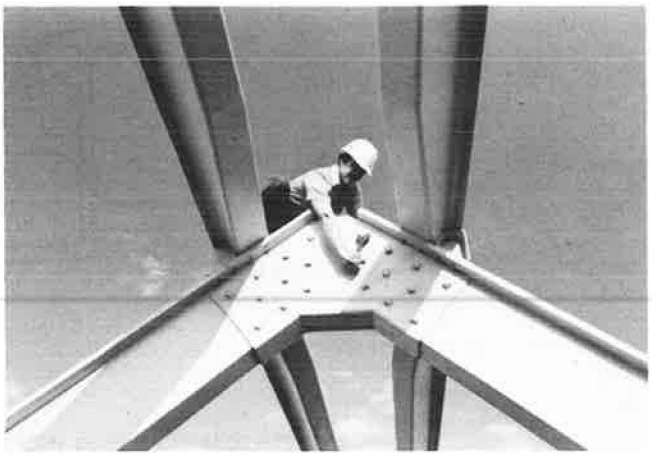

FIGURE 7 Ridge splice showing composite threaded rods and nuts in conjunction with splice plates used exclusively at low-moment joints. High-moment joints are avoided by opting for continuous components.

This choice was important for keeping unit shear stress low in the fiberglass bolts at the ridge splice. Using only two pieces also helps overcome the joining problem by eliminating connections.

The section is a box to increase allowable buckling of flanges and lateral buckling resistance of the frame. Web thickness was increased near the base for shear resistance and to provide resistance to shear buckling.

The rigid frame knee has no joints or splices (Figure 7). Continuous fiberglass rovings maintain uniform strength from one end to the other.

Purlins and girts are 20-ft clear span and use the torque-box system to develop resistance to buckling and lateral bending. No lateral bracing is required.

Fiberglass continuous-strand core and mat skin all-thread rod provides the highest unit strength for fasteners.

Cladding is profiled fiberglas panels that were pigmented beige and coated with an acrylic polymer. The use of nonwoven continuous straight fibers provides low deflection. This property overcomes weakness of high bearing loads on fasteners found on conventional fiberglass panels with large deflection.

Fasteners were tested for torque limits, tensile strength, and shear strength. Cladding was tested to determine its resistance to membrane loads, as well as positive and negative wind loads. All primary structural members were tested to determine stiffness, ultimate strength, and load path at the reaction (Figure 3).

Publication of this paper sponsored by Structures Section.

Fiberglass Tendons for Posttensioning Concrete Bridges

LOTHAR PREIS AND TERRY A. BELL

Glass, if completely oriented in the direction of stress, can withstand forces as well as steel. Combining this strength with light weight and corrosion resistance in a high-quality prestressing tendon is conceivable. Bayer AG, a West German chemical concern with worldwide sales close to $20 billion, has developed a technique that yields unidirectionally oriented fiber-reinforced rods. The product, Polystal, has proven effective in applications where steel-like resistance to stress is required while affording users the advantages of electrical neutrality and corrosion resistance. Over the past 10 years, Bayer AG and Strabag, a West German civil engineering and construction firm, have jointly developed a fiberglass tendon and anchorage system to be used as posttensioning elements for concrete construction. Presently, these elements have been incorporated into a bridge outside of Düsseldorf and their performance is being monitored. In this paper, the development of Polystal as a posttensioning medium and some insight concerning the Ulenbergstrasse Bridge are reviewed.

In July 1986, there was an exceptional event in Düsseldorf; the first road bridge, of span 50 m, was prestressed not by means of steel tendons but using prestressed rods of a high-performance glass fiber composite material. Constructing this bridge is the culmination of nearly one decade of continuous extensive research and development that started in 1978.

DEVELOPMENT OF GLASS FIBER REINFORCEMENT OF CONCRETE STRUCTURES

The idea of using glass fibers to reinforce concrete members is in itself nothing new. The first proposals in this regard were made when glass fibers and glass-reinforced composites were still at an early stage of development, once enough was known about the inherent high tensile strength of these materials *(1)*. Putting the idea into practice, however, was a long and laborious process. Although a number of research engineers, especially in the United States and the Soviet Union, worked on the reinforcement of concrete with glass fibers instead of steel, these pioneers did not succeed in solving all the problems arising in the practical use of these rods. The main obstacle to progress was that they had neither suitable glass fiber reinforcing profiles nor anchors of sufficient load-bearing capacity at their disposal *(2–5)*.

A significant step forward was achieved by Rehm of the Technical University of Stuttgart, who evolved some important theoretical principles of glass fiber prestressing based on discontinuously manufactured high-quality glass fiber composite rods and verified them experimentally.

It was shown, as might be expected, that there was generally no point in reinforcing concrete members with untensioned glass fiber rods in view of their comparatively low modulus of elasticity. The results of Rehm's tests with prestressed elements, however, were so favorable that he was optimistic regarding the technical and economic aspects of glass fiber prestressing, and proposed a broadly based study of the possibilities offered by this method of construction.

This suggestion was taken up by the two firms Bayer AG and Strabag that in 1978 formed a joint venture for development, trial, and application of glass fiber prestressing techniques. Competent research staff from universities also took part, and the project was substantially assisted by the West German Ministry of Research and Technology (BMFT) *(6, 7)*.

It was obvious from the beginning that there were a large number of closely interlinked problems to be solved, demanding close cooperation between basic research, process development, and application technology. It was clear from the complexity of these questions why the original pioneers, working on their own, were unable to achieve a breakthrough in this field.

For his basic research, Rehm had high-quality glass fiber rods with a tensile strength of between 1,400 and 1,700 N/mm^2 that were produced by an elaborate, discontinuous process. For economic reasons, rods of this type were no more suitable for industrial use than the many different types of pultruded profiles that did not normally have sufficiently high strength.

Initially, therefore, the main aim of the project was to develop a process for the continuous, repeatable, industrial-scale manufacture of high-tensile reinforcements from glass fibers and thermosetting resins. With these profiles, the high tensile strength of the glass fibers had to be fully used throughout the service life of the reinforced structure in question.

The second important aspect, which like the manufacturing process was crucial to the success of the whole project, was the development of suitable anchors so that full advantage could be taken of the strength of the glass fiber composite reinforcements under service conditions.

It is rather interesting that, while spectacular success has been achieved in the development of advanced composites based on carbon fibers and the like, there has been a tendency to overlook the fact that the properties of E-glass fibers—which were originally developed for electrical applications more than 40 years ago and are inexpensive and readily available—are fully used in only few applications.

L. Preis, Bayer AG, D–5090 Leverkusen, Federal Republic of Germany. T. A. Bell, Mobay Corp., Pittsburgh, Pa. 15205.

POLYSTAL

Analysis of the conditions necessary for greatest possible advantage to be taken of the fiber properties from both technical and economic points of view shows that the strength of a glass fiber composite material is due almost entirely to the reinforcing fiber. Basically, the only functions of the matrix resin are to hold the fibers together so as to prevent shear between them, to protect them, and to give the composite sufficient dimensional stability over the required range of service temperatures. If the fibers make up approximately 70 percent of the profile by volume, for example, the resin, although it accounts for 30 percent of the cross-sectional area, bears only about 1.5 percent of the load.

In an ideal fiber composite, the load on all the fibers should be equal. This condition is only possible, however, if

- All the fibers are oriented in the direction of the load,
- The fibers are evenly distributed over the cross section so that no stress inhomogeneities can arise, and
- The profile has nearly zero void content.

This, in turn, necessitates a high fiber content. Because stress inhomogeneities can also be caused by air entrapment, every effort must be made to prevent voids from forming when the fibers are impregnated with the matrix resin.

Taking the preceding demands into account, a patented process has been developed by which high-tensile rods can be manufactured continuously on an industrial scale from unidirectionally oriented glass fibers and thermosetting resins. Essential features of these profiles that have been marketed for some time under the trademark Polystal include

- High glass fiber content (80 percent by weight, 65 percent by volume),
- Strictly unidirectional fiber orientation even in the outer layers,
- Uniform fiber distribution over the cross section, and
- Optimum cure.

Some important material data for Polystal profiles are shown in Figure 1, in which the stress-strain curve for Polystal and those for a reinforcing steel (BSt 420/500 RK) and a high-quality prestressing steel (St 1470/1670) are shown for purposes of comparison. This graph is based on Polystal rods of 7.5 mm diameter with a glass fiber content of 83 percent by weight, 69 percent by volume.

The tensile strength—the decisive property as far as prestressed reinforcement is concerned—of Polystal and prestressing steel are similar, although there are considerable differences in the stress-strain behavior of the two materials. Whereas with steel a linear and a plastic range can be distinguished, the curve for Polystal follows Hooke's law exactly until failure. The diagram also shows the relatively large differences between the elasticity moduli of steel and Polystal, which are in the ratio 4:1.

The high elongation at break of over 3 percent and the sudden failure of Polystal when the strength limit is reached show that loads are borne virtually evenly by all the fibers. Any misalignment of the fibers would result in inhomogeneous stress distribution in the rod, that is, in the overloading of certain areas and, therefore, in premature failure at a comparatively low elongation. Further characteristic data for Polystal are given in Table 1.

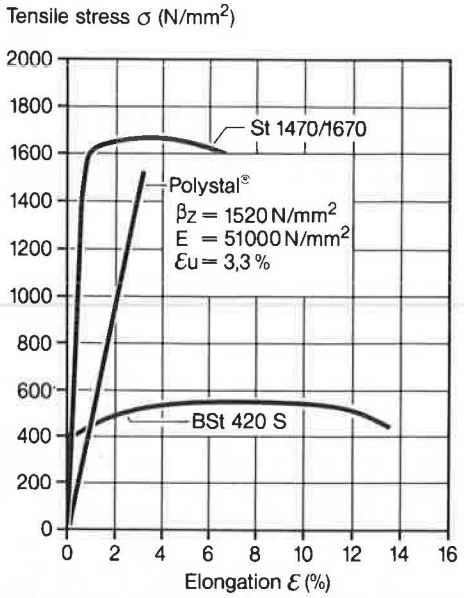

FIGURE 1 Stress-strain curves for Polystal, reinforcing steel, and prestressing steel.

Apart from investigating these fundamental properties, extensive testing has been done to determine the behavior of Polystal under all relevant conditions in connection with its use in construction engineering. Regarding the use of the rods in prestressed concrete, the following factors have to be taken into consideration:

- A small loss of strength (about 4 percent) due to undefined aging effects and
- A drop in tensile strength by 25 to 30 percent compared to the corresponding short-term values as a result of long-term loading (Figure 2).

TABLE 1 MATERIAL CHARACTERISTICS AND COMPARISONS

	Reinforcing Steel BST 420 S	Prestressing Steel ST 1470/1670	Polystal (68% Glass-fibers)	Carbon fibers
Tensile Strength (N/mm²)	> 500	> 1670	1520	2800
Yield Strength (N/mm²)	> 420	> 1470	Not Applicable	Not Applicable
Ultimate Strain (%)	10	6	3.3	0.7
Modulus of Elasticity (N/mm²)	210,000	210,000	51,000	400,000
Specific Tensile (Tensile Density), km	6.4	21.5	72	160
Specific Weight (g/m³)	7.85	7.85	2.0	1.75

*These are typical properties given for information purposes only. They are approximate values and are not necessarily part of the product specification.

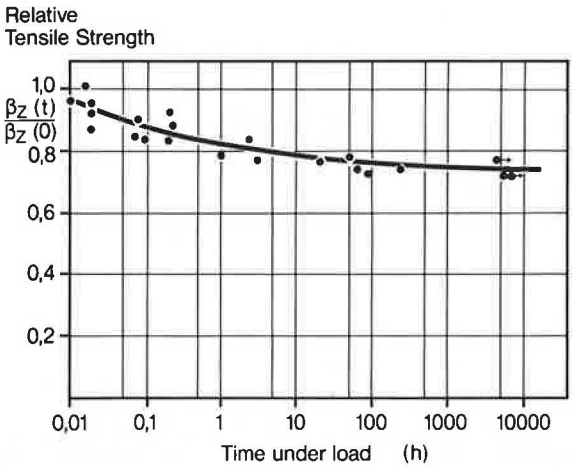

FIGURE 2 Creep strength of Polystal depending on time *(8)*.

Creeping of glass fiber composites as a function of time depends on the fiber content and amounts to approximately 3 percent of the elastic initial elongation (Figure 3). As an extrapolation over a period of 60 years indicates, the loss of tension (relaxation) of a prestressed Polystal rod also amounts to about 3 percent. Moreover, investigations of dynamic behavior have shown that the tolerable stress range of Polystal rods is 34 N/mm² at a base load of 50 percent of the short-term tensile strength and at 33×10^6 cycles.

The glass fibers themselves are less sensitive to high and low temperatures than steel. The resin matrix surrounding them, however, loses some of its strength even at about 100°C. For this reason, all the areas in which its force-transmitting properties are required from the point of view of statics, for example, the anchorage, must be protected from excessive heat. This can

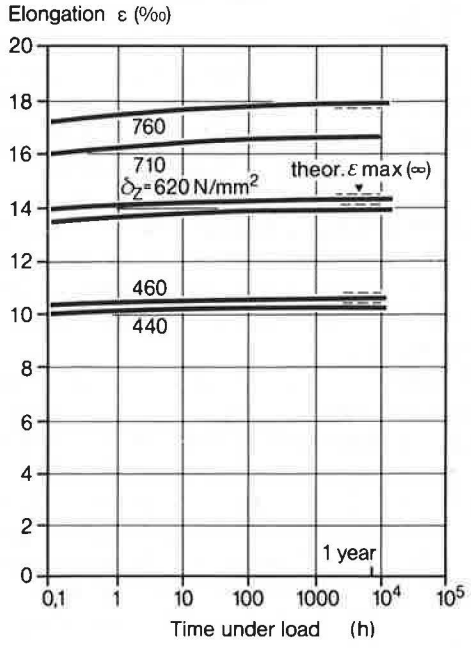

FIGURE 3 Elongation of glass fiber composite rods (56 percent by volume glass fibers) as a function of time *(8)*.

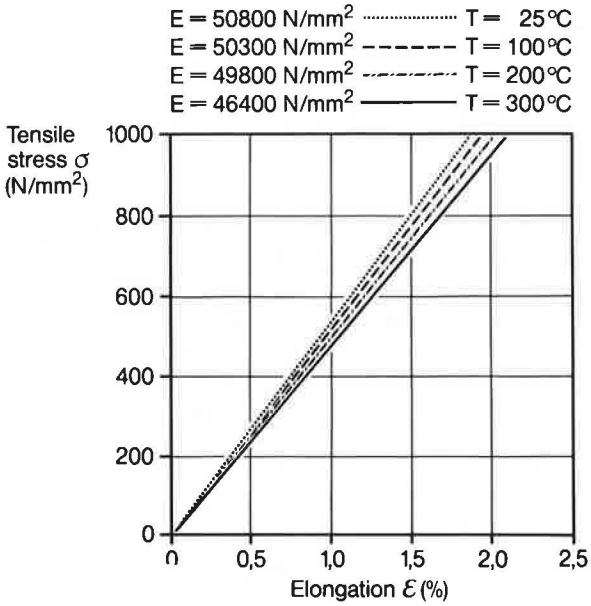

FIGURE 4 Stress-strain curves for Polystal at 25°C, 100°C, 200°C, and 300°C *(10)*.

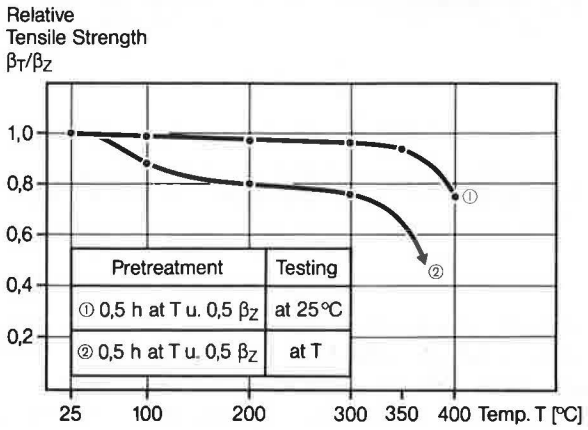

FIGURE 5 Effect of temperature on the short-term strength of Polystal pretreated under various conditions.

be done with a concrete covering, for example. The effect of temperature on the tensile properties of Polystal profiles is shown in Figures 4 and 5.

Reinforcing profiles for use in prestressed concrete must have good long-term chemical resistance to concrete, which is an alkaline medium, and must also be able to transmit large forces to the anchorages. Both these requirements make considerable demands on the base materials and on the processing technology. In retrospect, it turns out that the selection of suitable glass fibers and matrix resins, which was carried out in parallel with process development and optimization, was particularly important regarding the level of technical properties attainable, but also particularly difficult. Special attention has, therefore, been paid to the question of media resistance of the profiles.

Apart from basic laboratory research, methods have been developed for testing prestressed Polystal elements under conditions similar to practice. A so-called "time accelerated test"

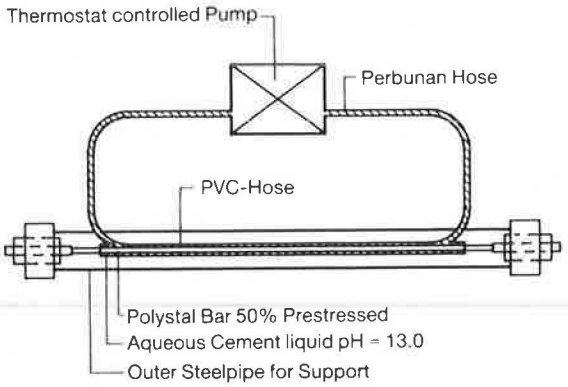

FIGURE 6 Time-accelerated media test of prestressed Polystal rods (60°C, 4 to 14 days) *(11)*.

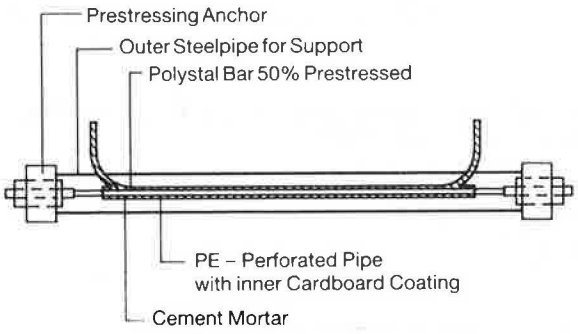

FIGURE 7 Standard media test of prestressed Polystal rods (ambient temperature, 18 to 52 weeks) *(11)*.

(Figure 6) carried out at working load and using aqueous cement liquid (ph = 13) at 60°C continuously circulated by pump allows deduction of the basic serviceability of a profile type relatively quickly (4 to 14 days), while standard tests (Figure 7) characterized by embedding prestressed bars in concrete kept permanently moist, give a more realistic impression of the actual long-term resistance of a certain Polystal type.

As a result of these investigations, a coating based on a highly filled Polyamide has been developed to help the Polystal rods resist chemical attack as well as mechanical damage.

The high strength of Polystal tendons can only be properly exploited in conjunction with anchoring systems in which allowance is made for the extremely anisotropic structure of the composite material. Such anchorage must

- Be highly efficient, so as to make fullest use of the properties of the material;
- Not, if possible, be larger or more expensive than comparable anchoring systems for steel tendons;
- Be easy to handle on site.

In the anchorage areas, the rods are subject to combined longitudinal tensile loads, transverse pressure, and shearing loads, concentrated at certain points. Initially, therefore, the comparatively low interlaminar shear strength of unidirectional

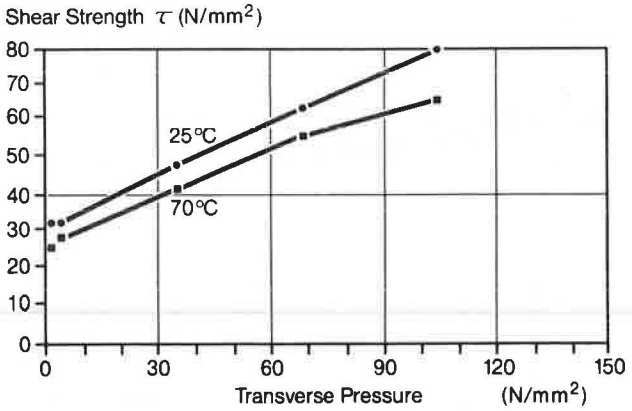

FIGURE 8 Shear strength determined experimentally, as a function of transverse pressure at room temperature and 70°C *(10)*.

fiber composites is likely to result in long anchors. However, Rehm demonstrated experimentally that the interlaminar shear strength can be increased by superimposition of transverse compressive loads (Figure 8). The more concentrically these are transmitted to the cross section of the rod, the larger they can be. This means that the anchors can be made significantly shorter without losing any of their efficiency.

These results are of special importance for clamp and wedge anchors, as well as anchors in which the rods are embedded in polymer concrete; the latter depend on transverse pressure for their effectiveness. In any anchoring system, the shear stress peaks occur where the rods enter the anchors as a result of the incompatibility between the elongations of the composite rods and the anchors. These shear stress peaks must be kept as low as possible.

ULENBERGSTRASSE BRIDGE AT DÜSSELDORF

When a small bridge for the City of Düsseldorf was built early in the research project, various types of anchors could be tested under realistic conditions. This first implementation of glass fiber prestressing occurred in 1980, and demonstrated the fundamental practicability of this new technique, and above all, the suitability of casting type anchors. This bridge supplied much valuable experience that in connection with the results of additional optimization and testing of rods and anchorages as well as tests of construction members encouraged the start of larger constructions.

In 1985, the City of Düsseldorf again made it possible to demonstrate the new prestressing technique in construction of a road bridge for heavy traffic. Before construction of the bridge, competent representatives of science prepared the following expert opinions: "Stability and Durability of the Structure" by Professor König, Frankfurt, "Material and Bonding Characteristics of Polystal in Connection with Prestressing" by Professor Rehm, Stuttgart, and "Judgment on Construction and Anchorage" by Professor Rostasy, Braunschweig (private communications).

Collectively, 59 Polystal prestressing tendons, each composed of 19 7.5-mm-diameter tendon rods, were necessary to

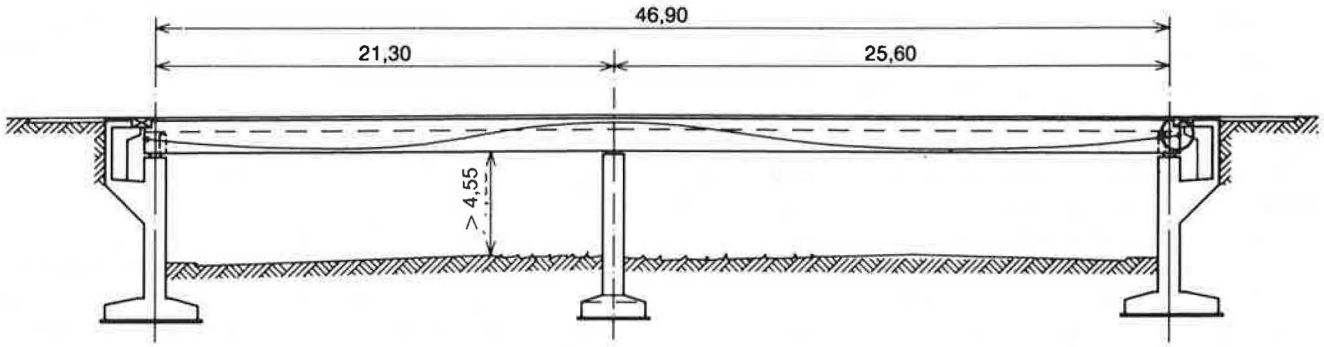

FIGURE 9 Ulenbergstrasse Road Bridge, Düsseldorf, longitudinal section.

produce the calculated initial stressing force of 3,500 tons (60 tons per unit). After prestressing, the cable ducts were filled by an also newly developed resin injection mortar, characterized by excellent flow and outstanding mechanical properties. Technical data for the bridge are summarized in Table 2. Figures 9 and 10 show a longitudinal section and a cross section of the bridge. Figure 11 shows details of the anchorage. Figure 12 shows deflection in a prestressed Polystal test beam.

Practical long-term examinations for different types of soil anchors are underway at this time. The load-bearing capacity of

TABLE 2 TECHNICAL DATA FOR THE BRIDGE

Spans:	L1:L2 = 21.30:25.60 m
Slab width:	15.00 m
Slab thickness:	1.44 m
Clear height:	4.75 m
Loadclass (DIN 1972):	60/30 tons
Degree of prestressing:	partial
Nature of the composite action:	post tensioning with subsequent bond
Bending radius of tendons:	R greater than 32.00 m

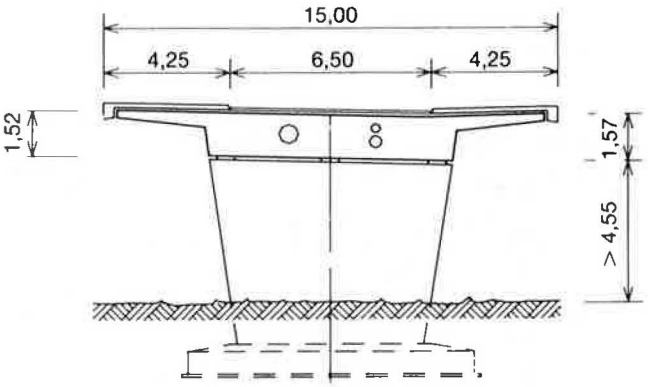

FIGURE 10 Ulenbergstrasse Road Bridge, Düsseldorf, cross section.

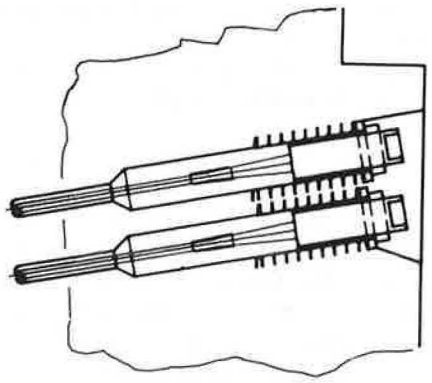

Figure 11 Detail of anchorage.

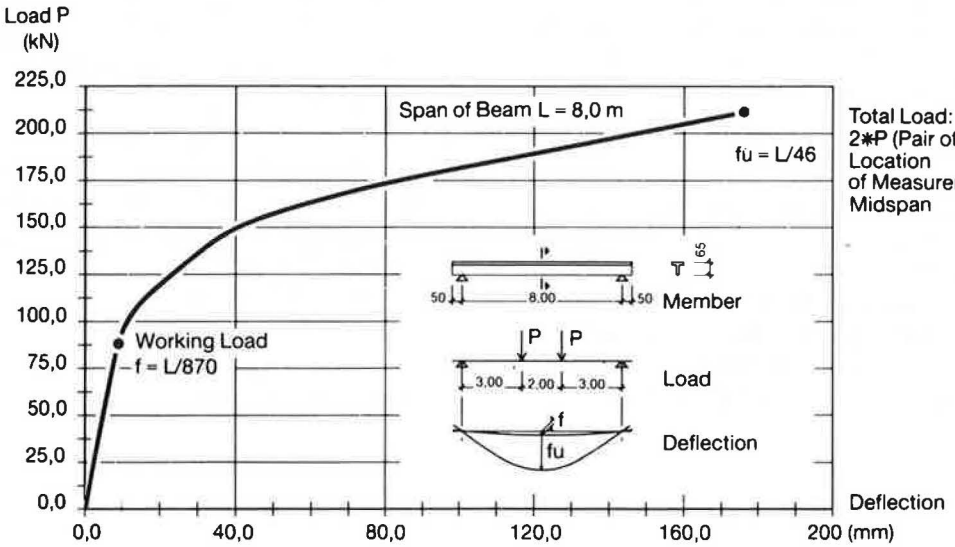

FIGURE 12 Prestressed Polystal test beam (ultimate bending).

such anchors under different load conditions allow for later tests and certification. Another innovation, tested for the first time in prestressed concrete structures, are sensor elements manufactured by integration of optical wave guides into the Polystal rods. Such effects prsage realization of "intelligent" prestressing tendons. With changes in their physical characteristics (e.g., attenuation of light), states of the structural strain may, for example, be detected on any location by those sensors. Significant future progress is expected in this area.

At this point, some comments should be made referring to the fundamental benefits of Polystal with prestressed constructions. One of the special advantages of Polystal in prestressed concrete is its modulus of elasticity, which is only one-quarter that of steel. Although this means initially that the rods have to be stretched four times as much, it also reduces by the same factor the inevitable loss of tensioning forces resulting from shrinkage and from contraction of the concrete due to creep. A further advantage of the low elasticity modulus is that the undesirable flexural stresses caused by curvatures in the rods at intentional deflection points within a structure or when the profiles are wound onto reels for transport and storage are also reduced to one-quarter of the levels of comparable steel rods.

In view of its low elasticity modulus, Polystal is also suitable for prestressing building or other materials having a low elasticity modulus or higher creep values than concrete. Those are applications for which steel cannot be used. Because the density of Polystal is only approximately 2 g/cm^3—about one-quarter that of steel—there are additional advantages in shipment and installation.

In order to demonstrate the break resistance of glass fiber tendons, and then be able to exploit their maximum load-bearing capacity despite the low elasticity modulus, the permissible elongation at the edge of the tensile zone of the concrete at the time of fracture must be increased from 0.5 to 1.0 percent. Whereas the safety theory for steel and prestressed steel reinforcements is based on the assumption that once the yield point is exceeded in the tendons the construction signals its imminent failure through large plastic deformations, glass fiber tendons—which have no yield point or yield zone—are subject to large elastic deformations at the transition from service to failure by virtue of their low elasticity modulus. They give early warning of any impairment of the safety of a structure caused by an error in design; at this point, a glass fiber rod still has a greater load-bearing capacity with which to absorb further increases in the load than does a steel tendon beyond its yield point. This is a distinct advantage of the new material, which could become a technically worthwhile alternative to prestressing steel in nearly all areas and for almost all methods of prestressing.

Its combination of special properties also makes Polystal suitable for numerous applications outside the civil engineering field. Practical experience has already been gained with load-bearing and tensioning members for a high-level antenna; in this application, not only the tensile strength but also the electromagnetic neutrality of the glass fiber rods is of great importance.

Polystal products are already used successfully on a large scale for tension members in fiber-optic telecommunication cables. It is used in this area not only due to its strength properties but also because of its low coefficient of expansion and its absolute insensitivity against electric fields.

The incorporation of Polystal rods in components made from other materials such as glass-reinforced plastic laminates, sheet molding compound, polymer concrete, or cast elastomers may greatly improve the service properties of the components without significantly increasing their weight.

The fortunate combination of rigidity, flexibility, and high abrasion resistance makes Polystal highly suitable for cable insertion devices. These selected examples demonstrate that there are many application areas in which high-strength glass fiber composites such as Polystal have advantages over isotropic materials. Generally, however, they can only be expected to offer solutions to problems from technical and economic points of view where advantage can be taken not only of their high strength but also of other characteristic properties such as low density, corrosion resistance, or electromagnetic neutrality.

REFERENCES

1. I. G. Jackson. Concrete Structural Elements with Reinforced Glass Filament. U.S. Patent 2,425,883. 1947.
2. I. A. Rubinsky and A. Rubinsky. A Preliminary Investigation of the Use of Fiberglass for Prestressed Concrete. *Magazine of Concrete Research*, Vol. 6, 1954, pp. 71–78.
3. S. Kaifasz. Some Tests on Beams Prestressed by Fiberglass Cords. *Magazine of Concrete Research*, Vol. 15, 1963, pp. 91–98.
4. N. F. Somes. Resin-Bonded Glass-Fiber Tendons for Prestressed Concrete. *Magazine of Concrete Research*, Vol. 15, 1963, pp. 151–158.
5. R. Mannfeld. *Application of Glass Fibers as Reinforcement of Concrete.* Thesis, Leipzig, 1967.
6. G. Rehm. *Glass Fiber-Resin Connecting Rods as Reinforcement.* Congress on Concrete in Germany, 1973.
7. G. Rehm and L. Franke. Synthetic-Resin Reinforced Bundled Glass Fiber Rods as Reinforcement in Concrete Construction. *Die Bautechnik*, Vol. 115, 1974, p. 132.
8. G. Rehm and L. Franke. Reinforced GRP-Rods as Reinforcement of Concrete. *Deutscher Auschuss for Stahlbeton*, Vol. 304, 1979.
9. G. Rehm and L. Franke. *Development Trends.* VDI-Berichte, Vol. 384. 1980, pp. 133–140.
10. M. Weise and L. Preis. Synthetic-Resin Reinforced Bundled Glass Fiber Rods—A Corrosion-Resistant Alternative to Prestressed Steel. *Fortschritte im konstruktiven Ingenieurbau*, 1984, pp. 79–85.
11. E. Waaser and R. Wolff. A New Material for Prestressed Concrete—HLV High-Performance Glass Fiber Connecting Rods. *Beton*, Vol. 36, 1986, pp. 245–250.

Publication of this paper sponsored by Structures Section.

Composite Tanker Trucks: Design and Fabrication

JOSEPH M. PLECNIK, A. DIBA, V. KOPPARAM, AND W. AZAR

The use of composite materials is expanding in many industries because of their light weight, corrosion resistance, and strength properties. In this paper, a summary of the design and manufacturing of an all-composite tanker truck is presented. The design is based on the U.S. Code of Federal Regulations for MC–312 tanker trucks, standard design practices for composite pressure vessels, and experience of several composite design engineers. The construction materials include E-glass and vinylester resins. Structural calculations were performed with the SAP IV finite element program for static analysis and the BOSOR IV finite element program for various buckling conditions. The composite tanker truck obtained a U.S. Department of Transportation permit to transport many different hazardous materials.

Composite materials have been successfully used for the past 50 years in a variety of industries including automotive, aerospace, aircraft, chemical processing, recreation, medical, housing, and transportation. For such industries, composites offer advantages such as light weight, high strength-to-weight ratio, high corrosion resistance, and unique mechanical properties. As in reinforced concrete for which R–bars can be placed in a direction of highest stress, fiber composites allow for even greater versatility for optimum design in relation to the type, magnitude, and direction of loading. Current widely used structural applications for composites include aircraft components, entire fiberglass ships up to 200 ft long, emission stacks *(1)*, storage tanks, pipes, and small buildings. For these applications, composites offer unique advantages not available with conventional materials.

In this paper, the basic design and fabrication parameters and the structural design of an all-fiberglass tanker truck with a 5,500-gal (20,820-liter) capacity are discussed. This tanker truck was intended for use in highly corrosive chemical environments for which stainless steel, lined carbon, or aluminum vessels are currently required. Most design parameters are derived from the 1983 U.S. Code of Federal Regulations (CFR) for Motor Carrier Specifications *(1)*. Loading conditions such as dead loads, full vacuum, acceleration, deceleration, and loading and unloading pressures are considered in the design. Because composite materials are not currently recognized in American codes or regulations for the design of tanker trucks, design criteria are presented for allowable stress and strain levels, safety factors against buckling, fatigue design considerations, and allowable displacements.

The tanker truck is manufactured by filament winding technique with the contact molded end heads wound into the shell. Stiffeners are provided on the cylindrical shell for buckling considerations. Loads are transferred from the fiberglass shell into the dual-wheel axles by means of steel saddles wound onto the shell. This article is based on the report *(2)* submitted to the U.S. Department of Transportation for approval or variance for a composite tanker truck. Only E-glass and polyester-type resins were considered in the design. The mechanical properties of composites are a function of many parameters such as fiber and resin type, fiber orientation, and fiber content. The strength of fiberglass composites can vastly exceed that of steel. Relative to bridge components, in addition to strength, fatigue, and creep, environmental degradation and long-term behavior are additional properties of composite materials that must be considered. Many fiberglass tanks, pipes, and boats have been in service up to 30 years. Some specialized structural glass or graphite composite applications such as pressure vessels or aircraft components have also been in service for over 25 years.

ADVANTAGES OF AN ALL FIBER-REINFORCED PLASTIC (FRP) TANKER TRUCK

Although the idea of FRP tanker trucks in the United States is still in its infancy, several European countries and Canada have allowed such trucks on their highways since the early 1960s *(3, 4)*. The primary advantages of composite tanker trucks are lower costs on a life cycle basis, higher strength-to-weight ratios, and superior corrosion resistance of composite materials as compared to steel or aluminum. The light-weight FRP tanker truck results in lower unit transportation costs because of larger payloads, less wear on tires and running gears, and lower maintenance costs (because relining of the tank is not required). Composites are also considered to be thermally insulating materials with thermal conductivity coefficients of 30 to 50 times less than that of steel. Such thermal insulating properties prevent FRP tank contents from reaching their flash point much more effectively than steel or aluminum and allow FRP tankers to maintain their structural integrity much longer under short-duration high-intensity fires that may occur under highway transportation conditions.

However, the resistance to corrosion of composite materials under exposure to various chemicals is the most significant advantage of FRP tanker trucks. Because of the inherent corrosion resistance of composite materials, FRP tanker trucks can be designed to carry most chemicals without the danger of perhaps rapid and undetected degradation or corrosion that can cause potentially dangerous problems in lined or unlined steel

Structures Laboratory, California State University, Long Beach, Calif. 90840.

tanker trucks. For highly corrosive chemicals, steel tanker trucks are normally relined with rubber, epoxies, or fiberglass at a regular frequency of between 1 and 5 years. Based on past performance of above-ground and underground fiberglass tanks and European fiberglass tanker trucks, an all-FRP tanker truck should be able to perform satisfactorily without repair for much longer periods, hence reducing the long-term costs of the FRP tanker truck.

TEMPERATURE AND FIRE EFFECTS

There are two ranges of temperature to which a composite tanker truck may be exposed. The first range is due to ordinary environmental exposure and is taken as around 0°F to 160°F. The second range is due to the significant possibility of fire exposure because of a mishap in the transport of some highly flammable substance such as gasoline or polymers.

Concerning the typical thermal fluctuations of the environment, most mechanical properties of E-glass polyester laminates are not significantly affected. This conclusion is substantiated by numerous research publications *(2)*. However, available experimental test data on the behavior of composite structural components under fire exposure are limited to several reports *(1, 2)*. Numerous test reports are available on the flame spread rate and the nature of the gaseous substances emitted during several standard ASTM tests. None of these tests, however, provide any indication as to the strength properties of composites under fire exposure.

E-glass laminates, although slightly inferior in material properties to other composites, perform well at elevated temperatures. In long-term testing at 225°F, the retention of flexural strength is practically total. In short-term testing, up to 160°F, the retention of tensile strength is total *(2)*. There may be a moderate drop in the tensile modulus of elasticity depending on the particular polyester-type matrix under consideration. Manufacturers' literature indicates that almost all heat distortion temperatures for E-glass composites are greater than 200°F so that heat distortion of E-glass composites in a natural environment should not be a problem for such tanker truck applications.

Limited amounts of experimental data (excluding ASTM D–635 and ASTM E–84 tests) on the behavior of composite structural components under fire exposure are available. However, the available data *(2)* do provide certain generalities that can be extended to composite tanker trucks under fire exposure.

First, short-fiber noncontinuous type of composites (chopped fibers) are severely affected by fire. As the fire burns and the resin pyrolysis process occurs around the short fiber, the fibers may eventually fall off, exposing the short fiber beneath and causing further pyrolysis of the resin. Fortunately, a single woven roving within the laminate can virtually stop this burning process as can continuous-filament construction. In fact, composites manufactured with continuous filaments behave as self-extinguishing materials. In one test, a continuous-filament-wound composite tank of E-glass and isothalic polyester resin subjected to a fire for 30 min was self-extinguished within 5 min. After the resin is pyrolyzed on the surface and to the depth of the exterior glass filament thickness (about 0.020 in.), this exterior fiber acts as an insulator and virtually eliminates the pyrolysis of resin within the composite interior *(2)*.

Second, the resin content of the composite significantly affects the extent and rate of resin pyrolysis within composites, especially for all-chopped-fiber composite construction. The rate of flame spread and pyrolysis appear to increase dramatically when fiber content is less than 30 percent by weight for all-chopped-fiber laminate construction *(20)*. Because filament-wound construction typically contains more than 50 to 60 percent of fiber by weight, the rate and extent of matrix pyrolysis in this type of construction may not be influenced by the percentage of resin content.

Third, most composite materials are thermal insulators, as illustrated by the relative behavior of steel, aluminum, and fiberglass tanker truck tests *(2)*. In the experimental tests, aluminum, steel, and fiberglass vessels were subjected to fire exposure *(1)*. The vessels were filled with gasoline before exposure to fire. Because of the thermally insulating properties of fiberglass, the heat transferred into the vessels was least for the fiberglass vessel. Hence, the aluminum and steel vessels exploded before the fiberglass vessel.

Fourth, glass fibers are considered fireproof materials, that is, they do not support combustion. Also, the melting point of glass exceeds that of steel and aluminum.

Fifth, most unfilled epoxy and polyester resins begin pyrolytic decomposition at temperatures less than 350°F, with rapid decomposition occurring at temperatures greater than 400°F. High-temperature resins (over 600°F) exist, but are not currently used in the composite manufacturing industry because of higher costs or more difficult manufacturing. Pyrolytic decomposition of epoxies or polyesters usually results in the evolution of gases and solids. The gases range from harmless hydrogen to highly toxic carbon monoxide and methane.

At elevated temperatures, the addition of fillers and flame retardants changes the characteristics of resin matrices in a variety of ways such as cost, color, strength, thermal properties, and flame spread. Addition of most fillers results in reduction of strength. Addition of flame retardants reduces the flame spread rate but does not necessarily increase the strength of the resin or composite at elevated temperatures. Because most additives or fillers reduce the critical properties of composites, their use should be limited if possible to several exterior laminas. Selective addition of fillers or additives is feasible in filament-wound or contact molding fabrication techniques.

DESIGN SPECIFICATIONS

Design requirements are provided in the U.S. Code of Federal Regulations (CFR) for various types of motor tanker truck carriers. Well-defined design requirements have been developed from stress and buckling analysis of metals such as steel or aluminum, which are ductile. However, these same requirements cannot be used in the analysis and design of FRP tanker trucks because composite materials are brittle, their stress-strain curves often providing little or no warning of impending failure, and their ductility ratio being close to 1.0. Therefore, the design of the structural members of the FRP tanker truck is based on allowable strain limits included in the following guides:

MAIN STRUCTURE

Capacity:	5,683 gallons
Size:	60" inside dia. x 40' overall length
Shape:	straight cylinder, clean bore
Compartments:	one (Compartment hds. optional)
Code:	MC-312, 35 psi operating pressure
Construction:	
Shell:	½" filament wound to ASTM D3299 ASME Chapter X
Heads:	semi-elliptical, 48" crown radius 8½" knuckle radius, 5/8" solid FRP integral with shell
Ribs:	(13) 4" x 3" rect. foam filled

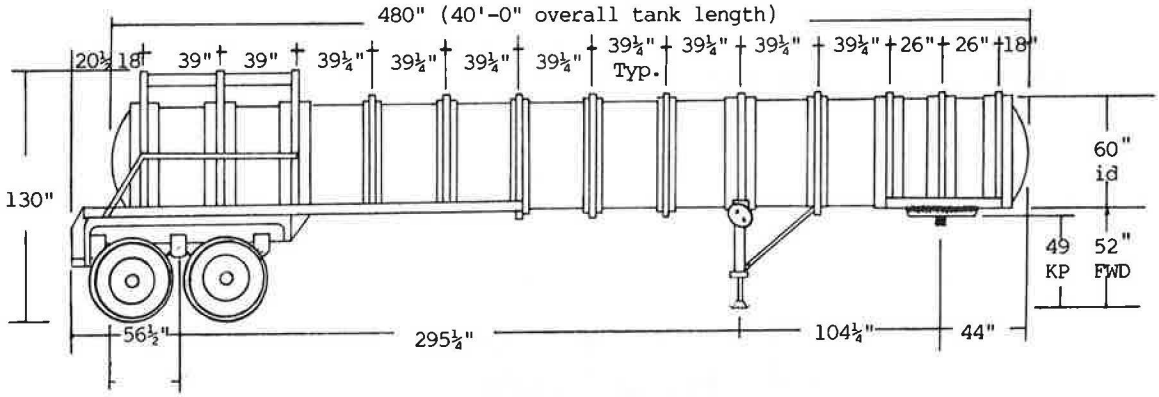

	Trailer Tandem Axles	Tractor Tandem Axles	Steering Axle	Total
Tractor	---	7400	7600	15000
Tank & Gear	7000	2600	400	10000
Payload	27000	24000	4000	55000
TOTAL	34000	34000	12000	80000

FIGURE 1 Design specifications for the FRP tanker truck.

1. ASTM D3299 specification for filament-wound fiberglass tanks *(5)*.
2. NBS PS 15–69 specification for hand-layup fiberglass tanks, pipes, etc. *(6)*.
3. ASME Boiler Code Section X.
4. Design experience with FRP pressure vessels.

A partial list of CFR specifications and dimensions for the FRP tanker truck are provided in Figure 1. The view from the rear of the first prototype is shown in Figure 2. The weight distribution is based on the bridge gross weight formula mandated by the FHWA in 1982. This formula allows for a maximum dual-axle load of 34,000 lb (151,000 N) and a total payload of 55,000 lb (245,000 N). The length and diameter of the tanker truck and the wheel spacings are mandated by this bridge formula. From the viewpoint of structural design, the optimum tanker truck dimensions would result in a tanker truck with a larger diameter and shorter length.

FIGURE 2 End view of the first prototype.

LAMINAR CONSTRUCTIONS

The laminar construction of the shell for the tanker truck is shown in Figure 3 with an interior veil of 0.010 in. (0.025 cm), a chopped glass liner of 0.10 in. (0.25 cm), and filament winding consisting of seven helix cycles and eight laminas of unidirectional fibers in the axial direction. A gel coat was used as a nonstructural exterior surface for environmental and ultraviolet light protection. The end dome heads are of spheroidal geometry with contact-molded laminar construction consisting of 1½-oz (0.417 N) mat and 24-oz (6.67 N) woven roving. As shown in Figure 4, the heads were integrally wound with the shell. The laminar constructions were chosen on the basis of optimum strain and buckling conditions. Premium polyesters and E-glass were used for all laminar constructions. The helical winding angles were optimized with respect to various pressure and flexural load conditions imposed on the shell. The unidirectional fibers were located in the longitudinal directions of the shell to provide increased strength and stiffness for flexural and pressure load conditions. The combination of helical and

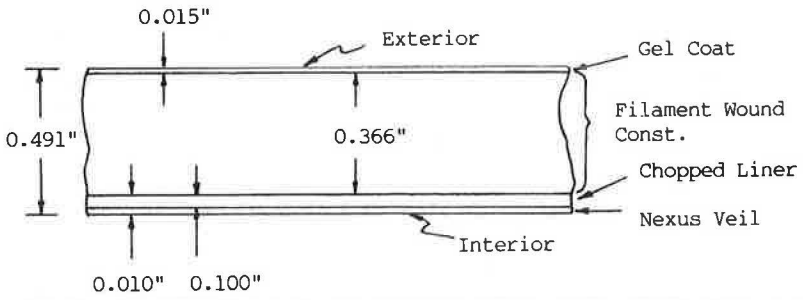

FIGURE 3 Laminar construction for the shell.

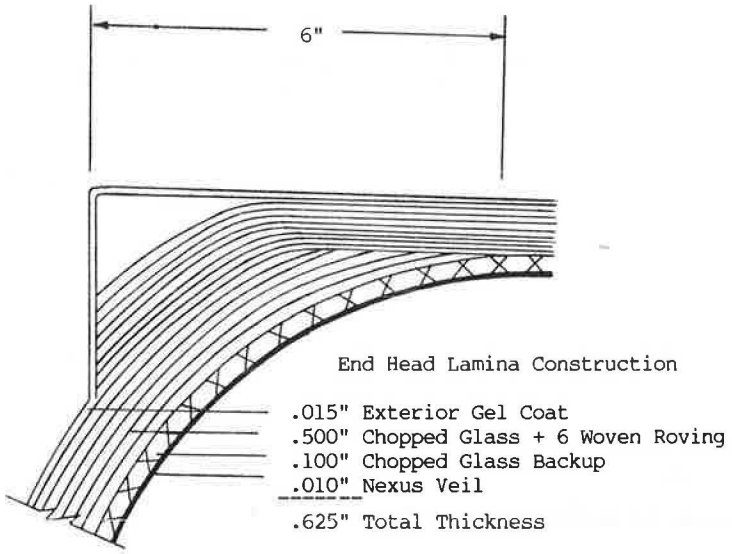

FIGURE 4 End heads wound into shell.

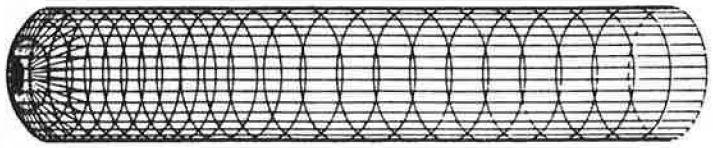

FIGURE 5 Finite element model of half the tanker shell and without saddles.

unidirectional laminas must result in a composite shell with the required strength, stiffness, and most important resistance to the millions of fatigue cycles throughout the life of the tanker truck. The material properties such as moduli, tensile and shear strengths, and ultimate elongations were determined from appropriate ASTM tests on test samples obtained from simulated tanker truck cutouts. These strength values were used in the final design of the tanker truck.

LOAD CONDITIONS AND ANALYSIS TECHNIQUES

The CFR outlines the minimum required design loads for all tanker trucks designed to carry hazardous materials. The design of the FRP tanker truck was based on all of the loads required by the CFR including the following design conditions:

1. Strain and stress levels and buckling for full vacuum.
2. Strain and stress levels and buckling for loading or unloading pressures of 35 psi (241 kPa).
3. Dynamic strains and stresses under horizontal acceleration and deceleration.
4. Dynamic strains and stresses under vertical accelerations.
5. Dynamic strains and stresses generated by surging loads because baffles were not used.

The complete tanker truck assembly was analyzed with several finite element models. The finite element model of half the tanker shell is shown in Figure 5 without the saddles or the axle supports. For the design condition of a fully loaded tanker truck and horizontal accelerations such as collisions, the tanker truck is designed to survive an impact acceleration of 20 g [1 g = 32.2 ft/sec^2 (9.81 m/sec^2)]. The fully loaded tanker truck is also designed to withstand vertical accelerations due to depressions or bumps of up to 9 g before shell buckling occurs. If the tanker truck is fully loaded and under full vacuum conditions, the

safety factor against buckling is only 1.85. Hence, it is recommended that the tanker trucks not be under vacuum condition while on the road. Circumferential ribs were designed for control of buckling and postbuckling behavior as illustrated. The tanker truck has also been designed to withstand the rollover condition (the tanker rolls 180 degrees on its top surface). Sixteen other load and design conditions were also evaluated, with the full vacuum condition the most critical. The stress analysis was performed with the SAP-IV finite element computer program and closed form shell solutions for stress and strains. The buckling analysis was performed with the aid of the BOSOR IV finite element computer program and conventional shell buckling formulas and tabular solutions.

In addition to strain and stress levels and buckling of the various tanker truck components, the fatigue effects on the shell, dome, and bond laminates must also be considered. Fatigue tensile test specimens were fabricated according to ASTM D638 Type III and tested at a stress ratio $R = 0.175$. The tests were performed to 1,000,000 haversine load cycles for specimens in both the hoop and axial directions. The maximum stress level for all fatigue cycles was 10 percent greater than the maximum design stress level. Because of curvature of the hoop direction specimens, these samples were modified so as to avoid large flexural stresses. On completion of the 1,000,000 load cycles, only minor surface cracks were visible without any failure. With regard to the actual number of load cycles that may be experienced by such a tanker truck during its projected lifespan of 10 to 20 years, only a rough estimation is possible. Hence, for safety consideration, the endurance limit of the shell laminar construction should be considered as the highest stress level allowed for load conditions during travel.

CONCLUSIONS

Fiberglass tanker trucks can be designed for extremely complex load and environmental conditions that must be anticipated for transportation of hazardous chemicals on highways. Due to lower dead weights, the payloads for composite tanker trucks are about 8 percent greater than for conventional steel or aluminum tanker trucks. Due to fatigue sensitivity of nonunidirectional composites, the strain limits and the fiber orientations must be optimized to withstand the repeated cyclic loadings and the chemical attack from the various payloads. It is also recommended that the composite tanker trucks be designed at stress levels below the endurance limit because the total number of load cycles at a critical load condition cannot be accurately established.

REFERENCES

1. *U.S. Code of Federal Regulations*, Title 49, CFT 178.0. Dec. 1980.
2. *Application for Exemption in Accordance with 49 CFR, Sections 107.101 and 107.103*. Research and Special Programs Administration, U.S. Department of Transportation, Sept. 1983.
3. G. Belanger. Filament Wound Tank Trailer Popular in Europe and Canada. *Trailer/Body Builders*, March 1972.
4. J. H. Minsker and D. E. Triestram. *Filament Wound Tankers Using Derakane Vinyl Ester Resins*. Dow Chemical Co., Midland, Mich., Feb. 1973.
5. *Standard Specification for Filament-Wound Glass-Fiber Reinforced Polyester Chemical-Resistant Tanks*. Standard D 3299–74. ASTM, Philadelphia, Pa., 1981.
6. *Custom Contact-Molded Reinforced-Polyester Chemical-Resistant Process Equipment*. NBS Voluntary Product Standard PS 15–69. U.S. Department of Commerce, National Bureau of Standards, June 1970.

Publication of this paper sponsored by Structures Section.

Field Study of a Pedestrian Bridge of Reinforced Plastic

FRED C. MCCORMICK

A discussion of the behavior of the superstructure of a pedestrian bridge fabricated with glass-reinforced plastic under a field load test is presented. Experimental measurements of elastic vertical deflections were 1.8 times greater than those predicted by means of a finite element solution. A live load of 3.5 times the dead load of the superstructure and polymer concrete deck was used for the elastic load test. Elastic strains were uniform among the different elements of the superstructure and computed stresses did not exceed 10,000 lbf/in.^{2} at full live load. A residual deflection in the superstructure of 0.10 in. on removal of the live load was concentrated in the supports. Creep deflection and strain measurements recorded over 61 days indicated that negligible creep occurred under a load of 2.6 times the dead load. Air temperature variations produced pronounced changes in deflection and strain readings, but were reversible. The overall structural behavior of the bridge and resistance to handling abuse exceeded expectations.

The design, development, fabrication, and laboratory testing of the components for the pedestrian bridge described in this paper have been discussed in previous publications *(1–5)*. The final configuration of the erected bridge was 16 ft long by 7 ft wide and 18 in. deep. The superstructure consisted of three identical trussed girders placed side by side and attached transversely by pultruded glass-reinforced plastic (GRP) plates bonded to the top flange of each girder. A detailed description of the configuration was presented by McCormick *(1)*. The foundation structure of reinforced concrete consisted of footings, backwalls, and precast seats. The seats were formed to match the triangular shape of the bearing surfaces of each of the bridge girders.

A multiple-layer polymer concrete (PC) overlay was applied to the deck of the bridge to provide a wearing course with a slight crown for drainage. The average depth of the wearing course was approximately ½ in. and weighed approximately 1,000 lb. The total weight of the superstructure was 2,300 lb.

The site chosen for the field study was in Pen Park, one of the municipal recreational areas of Charlottesville, Virginia. The bridge was located across the overflow channel of the primary irrigation pond for a golf course in the park as shown in Figure 1. The intended use of the bridge was for pedestrians and golfers using electric carts weighing approximately 1,000 lb fully loaded. Two months after erecting the bridge, a heavy rainfall in the park caused severe erosion of the region adjacent to the bridge foundation and required removal of the structure. Subsequently, the bridge was moved to the structural testing laboratory of the University of Virginia where an extensive cyclic load fatigue investigation was initiated. The results of the fatigue study will be reported at a later date.

Virginia Department of Transportation, Transportation Research Council, Charlottesville, Va. 22903.

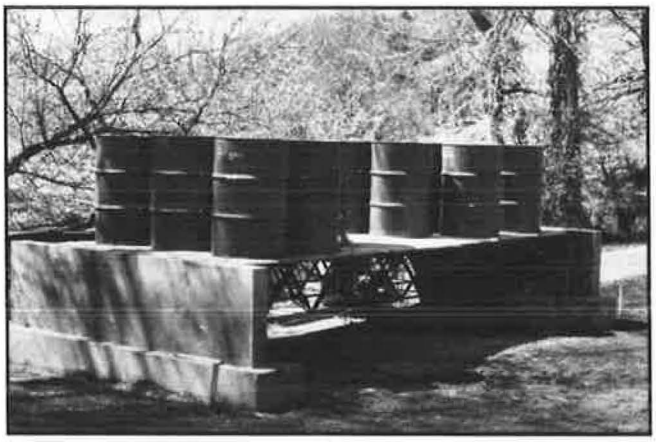

FIGURE 1 Pedestrian bridge in place over the discharge channel of an irrigation pond at Pen Park.

OBJECTIVES

The objectives of the field test were as follows:

1. To measure the elastic behavior of the bridge due to short-term loads.
2. To observe the viscoelastic (creep) behavior of the structure under a constant load applied over several weeks.
3. To assess the effects of weathering and service loads on the structure over a period of years.

Data from both the elastic and viscoelastic tests were obtained and are reported here. Early removal of the bridge from the test site precluded the weathering study.

ERECTION PROCEDURES

The precast concrete bridge seats were positioned on footings and anchored by casting the backwalls against them. Elastomeric (75 durometer neoprene) pads were placed on the bearing surfaces of the seats prior to installing the superstructure. These pads (2 layers, ¼ in. thick) assisted in distributing the bearing pressure uniformly along the contact surface of the pultruded end stiffeners in the girders and also served as shims to adjust the final elevation of the deck surface.

Because of the light weight (1,300 lb) of the bridge before the PC overlay was placed, it was moved manually from a staging area in the park and positioned on the seats without the assistance of mechanical equipment. Approximately 1 hr was required to assemble a crew of 12 workmen, remove the wooden shipping braces, and install the bridge on the seats. Figures 2 and 3 show the sequence of installation.

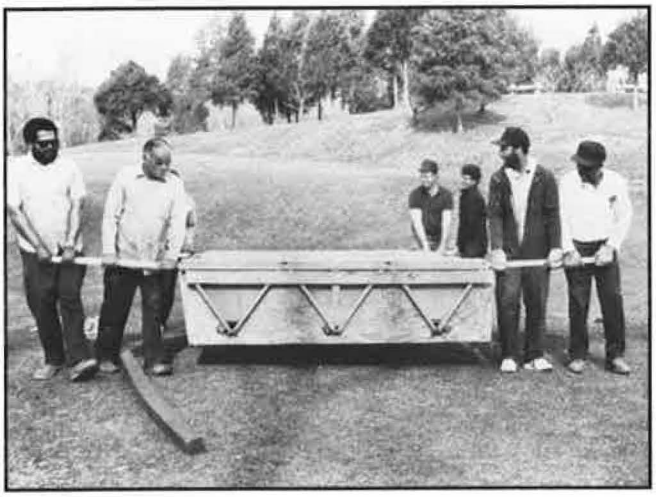

FIGURE 2 Movement of superstructure from staging area to abutments.

FIGURE 3 Lifting superstructure onto the precast concrete seats.

Successive PC layers were applied at intervals of approximately 2 hr to allow sufficient time for the resin binder to cure. Figure 4 shows the hand application of sand at a rate of 2.5 lb/yd^2 to the liquid resin to provide an individual layer thickness of approximately 1/8 in. Excessive amounts of sand were applied to ensure maximum aggregate content in the layer of concrete. The small deck area to be covered did not warrant the use of mechanical equipment for placing the materials. Excess sand was removed after each layer was cured in preparation for the next resin coating. To facilitate water drainage to the sides of the otherwise flat surface, eight layers of sand and resin were applied over various areas of the deck to provide a crown along the center of the deck. Application of the PC in successive

FIGURE 4 Sand aggregate applied to polyester resin to form polymer concrete wearing course.

layers also permitted the buildup of a greater thickness at midspan to compensate for the deflection of the bridge due to its own weight and the weight of the wearing course. The polyester binder used in the concrete was Polylite 92–339 (Reichhold Chemical) and the aggregate was a silica sand from Morie Sand & Gravel. A Morie No. 1 grading was used on layers 1–4 and a Morie No. 2 on layers 5–8. A complete description of the properties of the polymer concrete is given in a report by Sprinkel wherein the resin is designated as Polylite 90–570 *(6)*.

Consideration had been given to placing the PC wearing course on the deck prior to moving the bridge to Pen Park. However, this alternative was rejected because it would increase the weight considerably and because it was questionable if the bond between the concrete and the deck plate would resist the various stresses and deformations caused by handling the bridge. As will be shown later, concern for the integrity of the interfacial bond appeared to be unfounded.

LIVE-LOAD TESTS

Loads were applied by filling 55-gal steel drums with water (≅500 lb total per drum) in the sequence shown in Figure 5. Note that the two center panels of the bridge were not loaded. The progressive manner of loading simulated a load moving from one end of the bridge to the other, which reversed the direction of the shear force in panels 6 and 7 as the load was added to the bridge. The original design with the heavy concrete deck slab precluded a shear reversal in the panels with the application of the design live load, so the diagonal elements in the panels were expected to resist only tensile forces resulting from transverse shears. Consequently, the deck elements (1/2-in.-thick flange, 1/4-in.-thick coverplates, and 1/2-in.-thick PC) were required to transmit the total live shear force from the loaded portion to the centerline of the bridge. Minor buckling of the plates was observed in several of the panels and considerable buckling occurred in the diagonal elements in panels 5 and 6 as the live load was applied successively to the end panels. The diagonals in panel 5 of one of the outside girders remained slightly buckled throughout the load test period. It is probable that the nonuniform application of the live load or

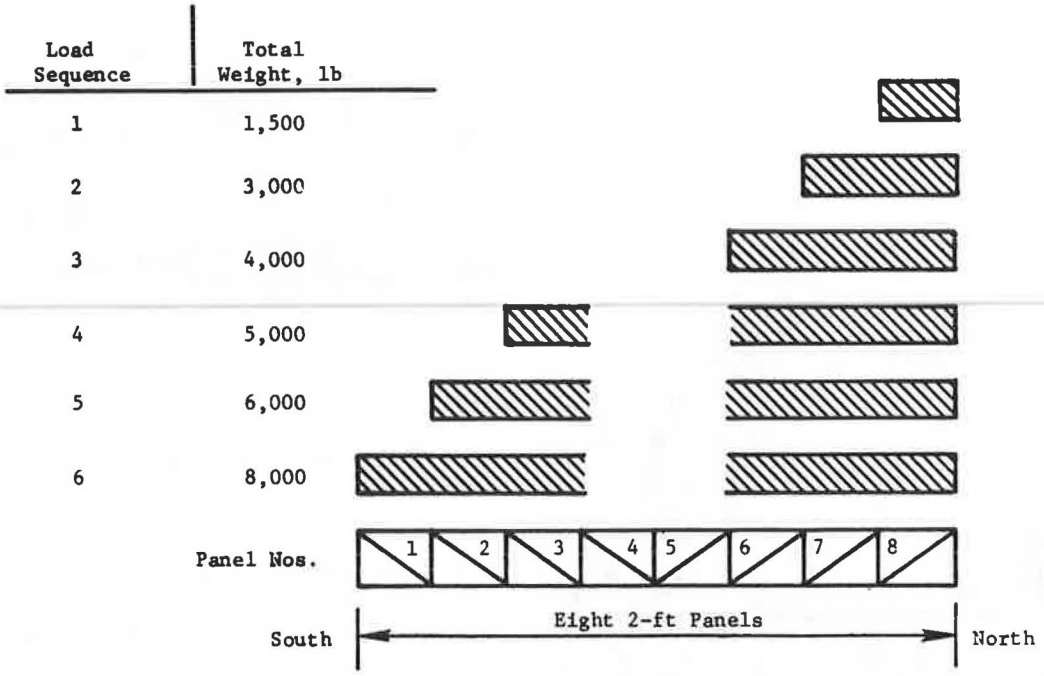

Progressive application of test loads.

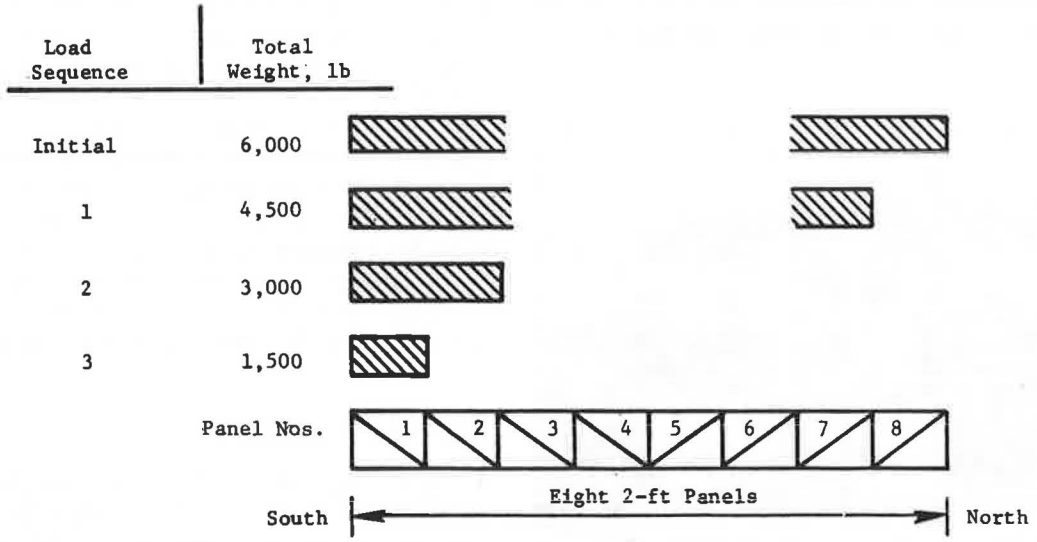

Progressive removal of test loads.

FIGURE 5 Sequence of load application and removal.

slight differences in the end supports induced sufficient torsional distortions into the superstructure to shift the shear forces from one girder to another. Differential distortions of this magnitude were not detectable by the deflection and strain measurements made during the application of the load.

A live load of 8,000 lb on the deck provided an average load of 71.4 lb/ft^2 based on a total surface area of 112 ft^2, or 83.3 lb/ft^2 based on the usable surface of 96 ft^2 between curbs. Because the structure was designed for a live load of 85 lb/ft^2 with the 4-in.-thick portland cement concrete deck in place and acting as the compression flange for the girders, a load of 83.3 lb/ft^2 was considered an overload without the regular concrete deck. The actual contribution of the polymer concrete to the structural behavior of the bridge was unknown, but it was not expected to generate much resistance to compressive flexural forces. An independent determination of a compressive modulus of 1.7×10^6 lbf/in.^{2} for the PC confirmed the expectation that the structural contribution of the wearing surface would be slight, particularly during the long-term creep test of the bridge.

Early evidence of excessive compressive stresses in the flanges was manifested in a slight buckling of the flanges. The maximum amplitude, estimated at 0.10 in., occurred in the end panels in both outside girders. No assessment of buckling was attempted in the interior girder, but it is quite likely that the

behavior was similar to that of the exterior girders. There was concern that the displacements of the flanges would grow and possibly result in a catastrophic failure of the bridge as the ambient temperature increased during the summer months and thereby reduced the effective modulus of the flange and deck material. Consequently, two drums of water were removed from panels 3 and 6 (Figure 5) to reduce the live load to 6,000 lb. This load remained undisturbed on the structure throughout the remaining creep test period of 55 days.

After 61 days under live load, all drums were removed, and rebound deflections of the bridge were measured over a period of 46.5 hr. The unloading sequence for live load removal was depicted in Figure 5. In general, the same progressive load removal sequence was used as was followed for the application of the load to observe the effect of a simulated load passing off of the structure. Some buckling of the diagonals in panels 3 and 4 was observed as the load was removed, but not as much buckling was noticed as occurred in the opposite end of the girders when the load was applied.

Elastic Deflections

Lower chord vertical deflections were measured by dial-gauge indicators with least readings of 0.001 in. located at three positions under the center girder. Because of adverse climatic and other conditions at the site, the dial gauges remained in place for only a short time following the application and removal of the live load. The locations of the gauges beneath the girder and the measured deflections of the lower chord are shown graphically in Figure 6.

All deflection measurements included movement of the end supports in the seats due to compression of the elastomeric

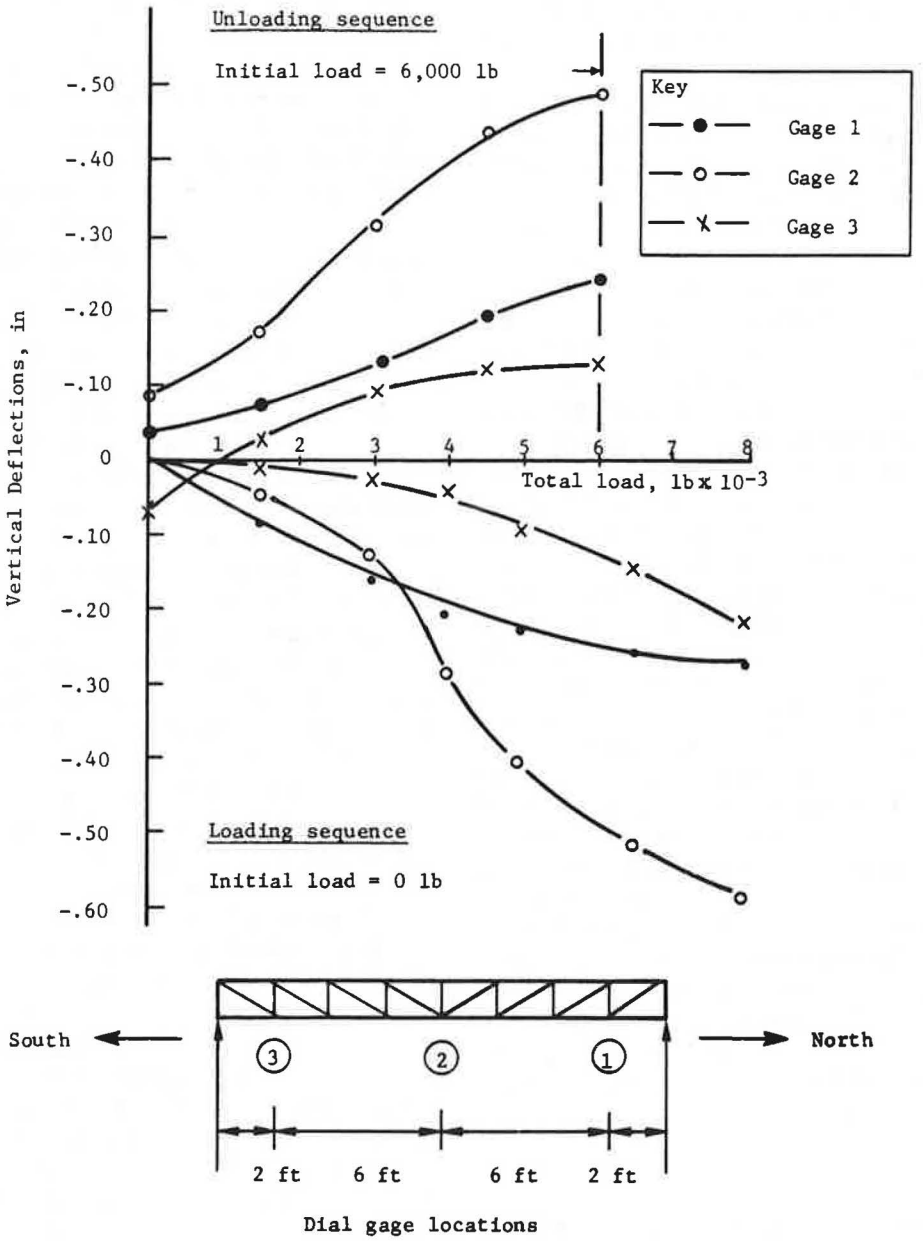

FIGURE 6 Deflections of the lower chord of the center girder as a function of live load.

pads and distortion of the stiffeners in contact with the bearing surfaces. It was not possible to evaluate these components of the measured deflections separately, but they are believed to be a significant part of the values measured by gauges 1 and 3. This supposition is supported by the deck deflection data discussed later. The larger deflection, shown by gauge 1 as compared with that by gauge 3, resulted from the application and removal of the load progressively from the northern end of the bridge to the southern end.

It was expected that the deflection at gauge 3 would reach that of gauge 1 when the full load was applied, because an effort was made to distribute the filled drums symmetrically about midspan. However, a check of the positions of the drums on the deck after they were filled indicated that the loads on the southern half of the bridge were approximately 4 in. closer to the center of the bridge than were loads on the northern half. Thus, it is believed that the off-center loading, plus probable differences in the settlement characteristics of the supports, completely explains the difference of 0.06 in. in the measured deflections.

The difference between the average measured deflections of the end gauges (1 and 3) and gauge 2 was 0.324 in. for the full load of 8,000 lb. If it is assumed that approximately one-half (0.12 in.) of the average deflection (0.24 in.) of the end panels was caused by the settlement of the bearing pads and support stiffeners, the centerline deflection of the girder due to flexural action would be 0.44 in. The estimated center deflection of 0.44 in. results in an L/S value of 435 for a span of 16 ft. This is approximately twice the AASHTO limit for pedestrian bridges. The deflection of 0.44 in. compares with a range of values from 0.25 to 0.30 in. computed from a theoretical analysis of the bridge. McCormick and Alper *(3)* describe the finite element model and solution for the three-girder bridge configuration.

Deflections measured during the unloading cycle of the test mirrored the pattern observed during the loading cycle. Both gauges 1 and 2 indicated a residual net deflection, while gauge 3 showed a greater elastic recovery than that measured during the loading cycle. The residual deflection values recorded when the load was removed were somewhat arbitrary, because the starting values indicated as 6,000 lb in Figure 6 were selected as equal to those measured at 6,000 lb during the loading cycle. The actual deflected positions of the gauge reference points were due to the creep of the bearing pads, temperature-induced distortions, and creep of the trussed girders during the period of loading. The differential deflections between gauge 2 and the average values of gauges 1 and 3 would be affected less by these variables than were the direct readings from the individual gauges. A calculation at zero load for the differential residual deflection indicates a value of 0.11 in. While the exact value of the residual deflection is uncertain, the computed value of 0.11 in. should be an indication of the magnitude of the nonelastic deflection that occurred over the test period. Some of the nonelastic deflection is recoverable, however, as discussed in the following section.

Creep Deflections

Elevations of reference points on the deck were measured periodically to determine the creep deflection of the bridge. The reference points were established by installing brass 1/4-in.-diameter machine bolts through the deck with the heads protruding slightly above the top of the wearing surface. Elevations were measured with a surveyor's precision level and an engineer's scale that was read directly to the nearest 0.05 in. Benchmarks were selected at one point on each abutment, and the deck elevations were computed relative to the benchmarks. A difference of 0.24 in. in the elevation of the benchmarks remained constant throughout the 61 days of readings.

Figure 7 presents the variation in air temperature, the average displacement of the supports, and the average displacement of the midspan of the bridge. Readings of the other four reference points were prevented by the location of the drums.

Initial creep readings taken within 30 min after the final load increment was applied correspond to the zero deflection value at time zero in Figures 7*b* and 7*c*. The deflections shown in Figure 7*b* may be attributed principally to the distortion of the elastomeric bearing pads beneath the supports. The data of Figure 7*c* are plotted as movements of the center span with reference to the benchmarks (solid lines) and also with reference to the supports (dashed lines). Dual data points shown on three different days reflect the reduction of load from 8,000 to 6,000 lb on Day 6 and readings taken in early morning and late evening for temperature fluctuation effects on Days 26 and 54.

In general, the deflection data of the supports and the center span clearly follow the ambient temperature fluctuations—when the temperature increased, the deck rose; when the temperature decreased, the deck fell. As might have been expected, the movement of the midspan was more pronounced than the movement of the supports. The supports were shaded from direct sunlight by the bridge superstructure and the abutments but the deck surface was exposed to heating from the sun during the day and rapid cooling during the night. Because of the continual movement of the deck, it was difficult to determine from the available data whether any viscoelastic creep occurred in the superstructure, but if so, it was not detectable during the 61-day test period.

Figure 8 shows the creep recovery, sometimes referred to as an "elastic aftereffect," of the bridge following removal of the live load. Also indicated is the considerable influence of ambient temperature variations on the deflected position of the lower chord of the bridge. The plotted points indicate gauge readings at times of 0, 24.0, 37.0, 45.5, 46.0, and 46.5 hr. Lines connecting the points are not intended to represent the variation in readings, except for the period from 45.5 to 46.5 hr, when the gauges were monitored continuously. Two phenomena were at work to influence the deflection measurements: creep recovery and temperature variation. Regrettably, a careful record of the ambient temperature was not maintained during the test period, principally because temperature changes were not considered to be such an influential factor as they (in hindsight) apparently were. The effect of temperature was clearly demonstrated by the upward movement of the lower chord over a period of 1 hr (from 7 to 8 a.m.), during which time the ambient temperature increased from 60° to 70°F. Values of 0.02, 0.03, and 0.01 in. occurred at gauges 1, 2, and 3, respectively, during that period of time. The movement due to temperature in 1 hr represents approximately 15 percent of the maximum creep recovery measured in 37 hr. Although the change in geometry of the

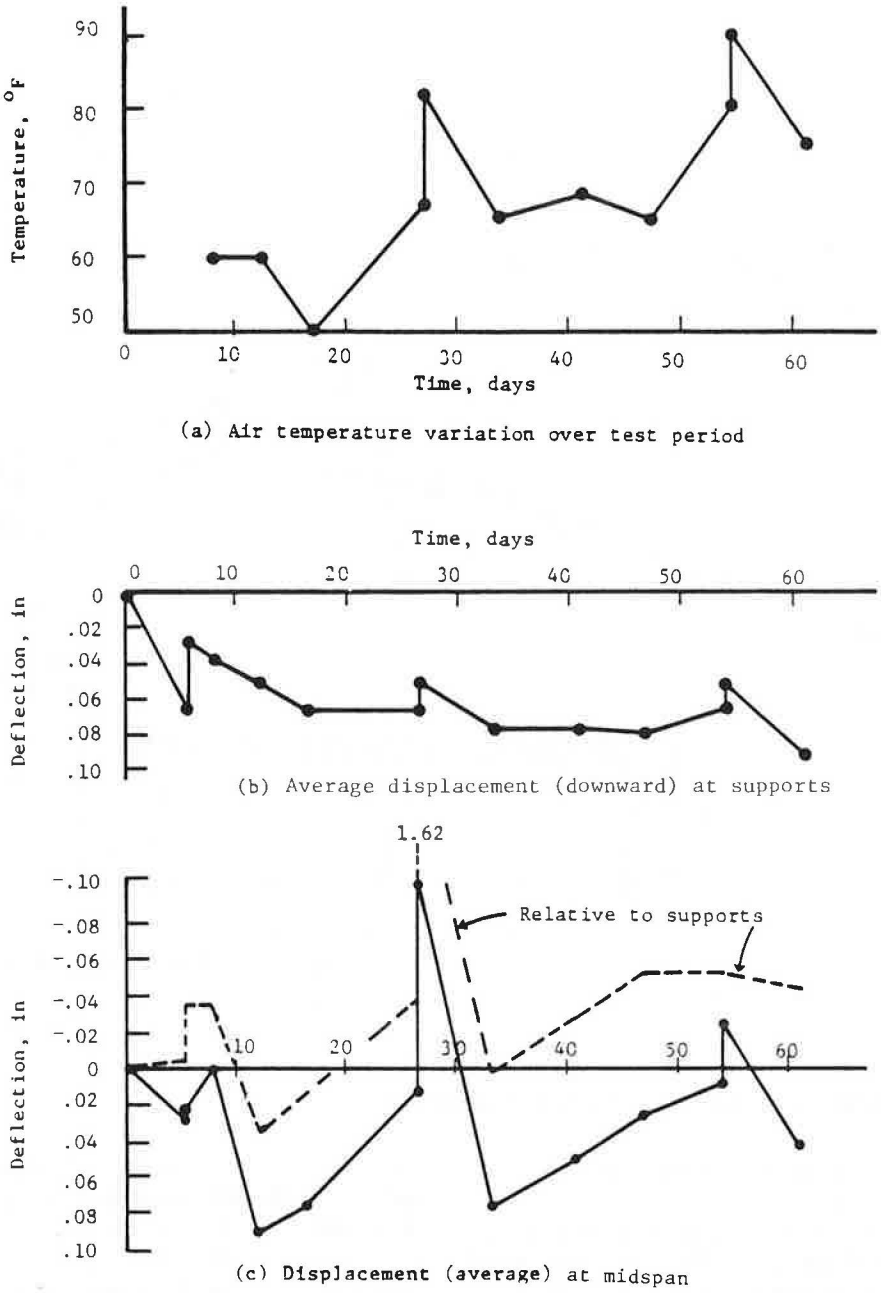

FIGURE 7 *(a)* **Air temperature fluctuation,** *(b)* **Deflections of deck at supports, and** *(c)* **Deflections at midspan.**

structure due to temperature variation is not completely understood, it is believed that the heat absorbed by the deck material when exposed to the sun is the predominating factor for change.

Analyses of the measurements for deflection recovery indicated that essentially all of the movement of the structure occurred at the supports. That is, after allowing for temperature fluctuations, the movement of gauge 2 relative to gauges 1 and 3 was nearly equal over the observation period of 46.5 hr. Therefore, it appears that little, if any, viscoelastic creep occurred in the bridge itself and that the measured rebound of the structure was due to the recovery of the elastomeric bearing pads. A similar observation was made in the creep study of a single girder over a period of 3 months *(1)*.

Elastic Strains

When the structure was built, 20 electrical resistance strain gauges (EA–06–250–BF–350 by Micromeasurements Co.) were bonded to various elements of the deck, web, and lower chord as shown in Figure 9. After 8 years in storage, 18 gauges remained functional and were attached to two portable switching units and one indicator (Bud Co., Model P350).

Strain measurements were recorded during the period of the application of live load and at intervals during the period of the creep test. The strain data obtained during the load test were considered reasonably accurate, but the creep strain data were not considered to be quantitatively correct. Several days after completion of the load test, the switching units were exposed to

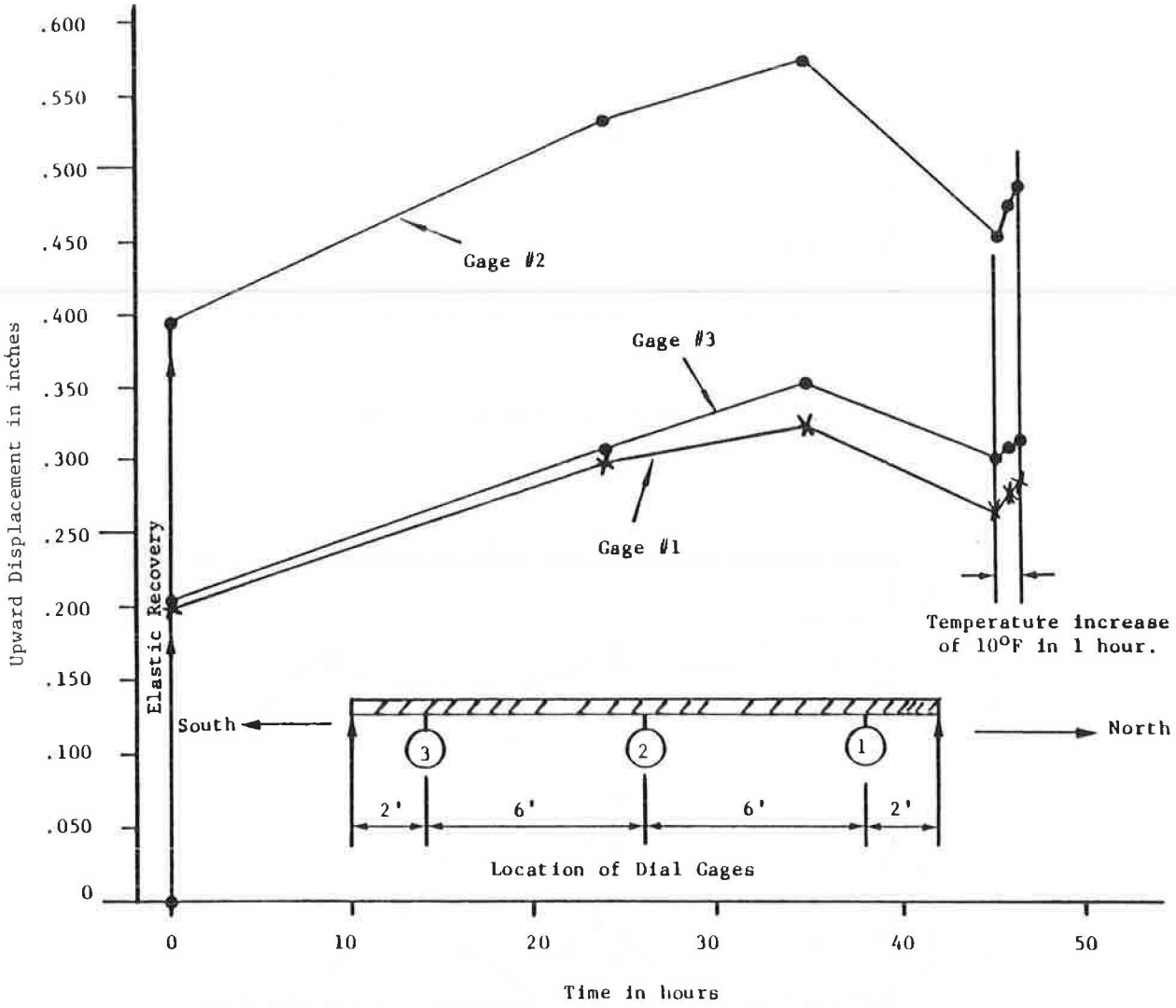

FIGURE 8 Deflection recovery of bridge following load removal.

moisture and an uncontrollable drift in the strain values was noted on subsequent readings.

Figure 10 presents data from six gauges mounted on the inclined web elements. Gages 2, 3, and 4 in the southern end panel tracked each other closely during the period of loading and ranged from 11,000 to 14,000 μin./in. when the total load was applied. These three gauges indicated no reversal of strain increase in the end panel. The difference in strains between gauges 2 and 3 is indicative of a possible load-carrying discrepancy between one of the outside girders and the inside girder, whereas the data from gauges 3 and 4 indicate similar load distributions between the center girder and the other outside girder. Gages 5, 6, and 7 in the second and third panels from the southern end indicated approximately the same increased rate of strain with the application of the load as did gauges 2, 3, and 4 until loads were applied directly to their respective panels. At that time, the strains reversed direction. This change in direction reflected the change in magnitude of the negative shearing force in the interior panels as the load was increased and more uniformly distributed along the length of the bridge.

Figure 11 presents strain data from five gauges mounted on the lower chords. All gauges indicated increasing strain values as the load was increased on the bridge. As expected, a sharp reduction in the strain rate in all five gauges was noted with the application of the last increment of load. As noted previously, the last load increment was applied in the southern end panel and, therefore, should not have affected the flexural stresses in the girders as much as the prior load increments had. Figure 11 shows that a relatively narrow range of strains was measured throughout the four panels and two girders monitored by the gauges, particularly through the application of the first 5,000 lb of load. The narrow range of strain values indicates that the lower chord elements were stressed as uniformly as might be expected with the nonuniform arrangement of the test load. The relative uniformity of stress indicates that the design procedure used to dimension the chord elements produced an efficient structural configuration. Also, the lateral transfer of the load and the interaction between girders during the load test appeared to be satisfactory as indicated by the random variation in strain values in the chords of the inside and outside girders.

Using a tensile elastic modulus value of 7×10^6 lbf/in.^{2} for the lower chord and web elements *(4)*, the strains shown in Figures 10 and 11 may be converted to axial tensile stress in the elements. The inclined web elements, therefore, developed

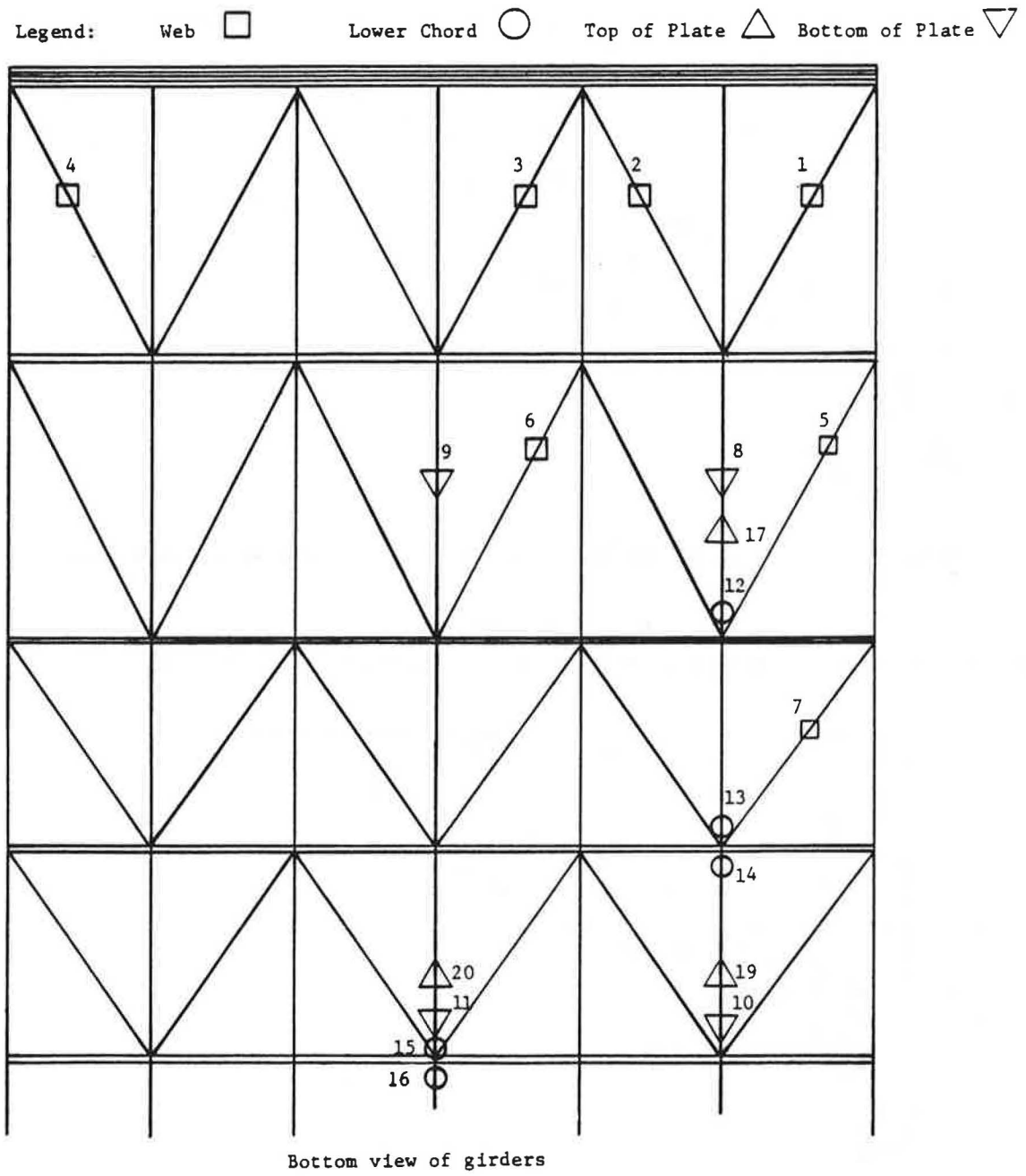

FIGURE 9 Location of electrical strain gauges bonded to elements of the bridge superstructure.

stresses ranging from 4,200 to 9,800 lbf/in.^{2}. Similarly, the lower chord stresses ranged from 3,150 to 6,650 lbf/in.^{2}. With a conservative ultimate strength value for the tensile strands exceeding 50,000 lbf/in.^{2}, the safety factors against tensile failure of the material exceed 5. Obviously, the design limitation of the GRP material system is the deflection of the structure due to the low modulus of the composite or the shear strength of the connections.

Elastic strains monitored in the top flanges and cover plates of the girders were erratic and, therefore, are not discussed further here. It has been noted previously that the thin deck assembly of pultruded plates and polymer concrete overlay deflected locally when the drums were applied to the bridge deck. In addition, slight buckling (both upward and downward) of the plates was observed as the live load was increased across the span. The combination of these two effects accounted for the erratic behavior of the strain gauges.

Creep Strains

Figure 12 presents representative strain data from five active strain gauges and a fixed reference circuit over the duration of the creep test. The reference circuit was fixed at 1,000 μin./in. as a check on the stability of the measuring indicator. As can be seen in Figure 12, the reference circuit remained essentially unchanged for the first 6 days of the creep test. Thereafter, wide fluctuations appeared in the data until, finally, the drift in the reference circuit exceeded the range of the indicator. Also, note

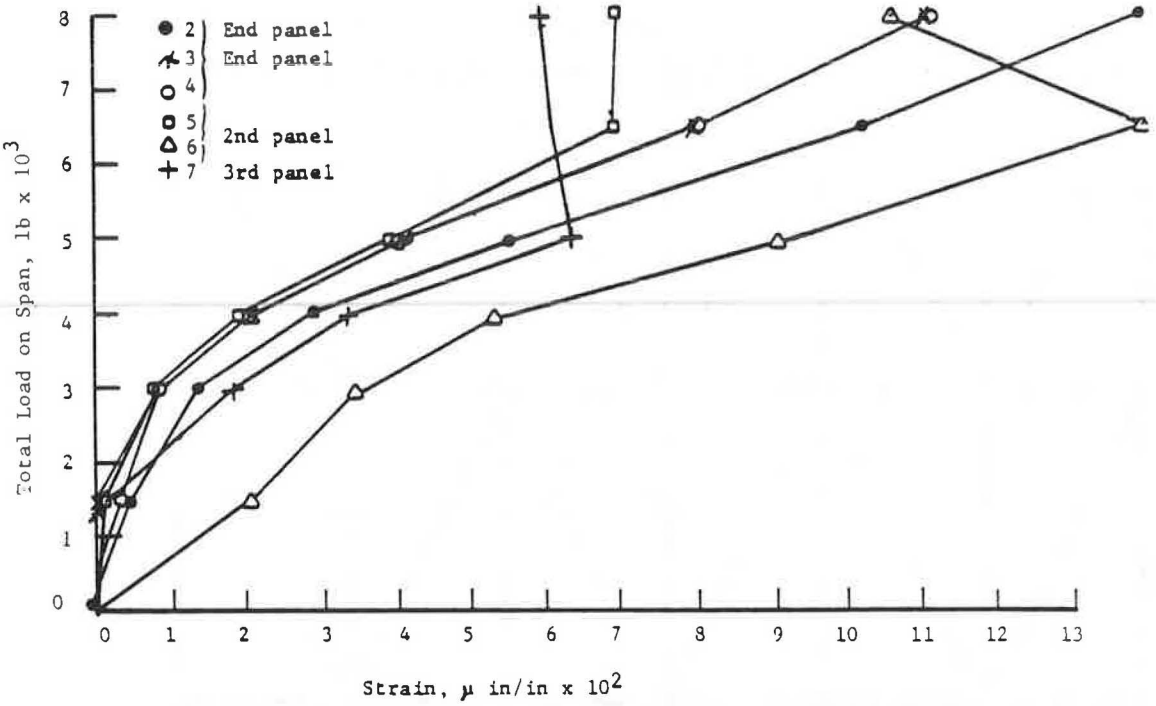

FIGURE 10 Elastic strain in inclined web elements in the girders due to application of loads.

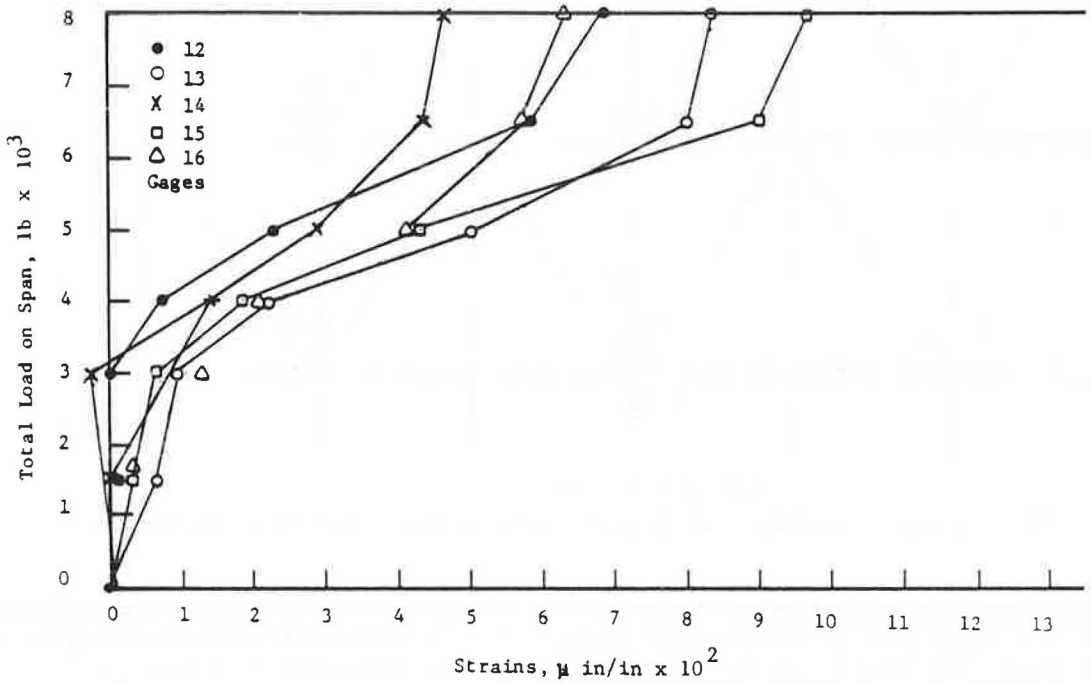

FIGURE 11 Elastic strain in lower chord elements in the girder due to application of loads.

that the magnitude of variations in the reference considerably exceeded those of the measuring circuits, even though the directions of the deviations were the same. Efforts were made to correct the obvious malfunction of the instrument as soon as the deviations were noted, but to no avail. Apparently, moisture penetrated the switching units and altered an internal resistance common to all of the gauge circuits to produce the results obtained. The measurements were discontinued after 54 days.

It is not believed that the fluctuations of the measuring instrument were due to changes in the ambient temperature. The comparison of the strain deviations with the temperature fluctuations shown in Figure 9 indicates little to no correlation. Because of the gross deviations of the measurements, the data are worthless for quantitative use. However, all of the gauges underwent the same magnitude of creep strain, whatever it was. If the first 6 days of the creep strain readings might be

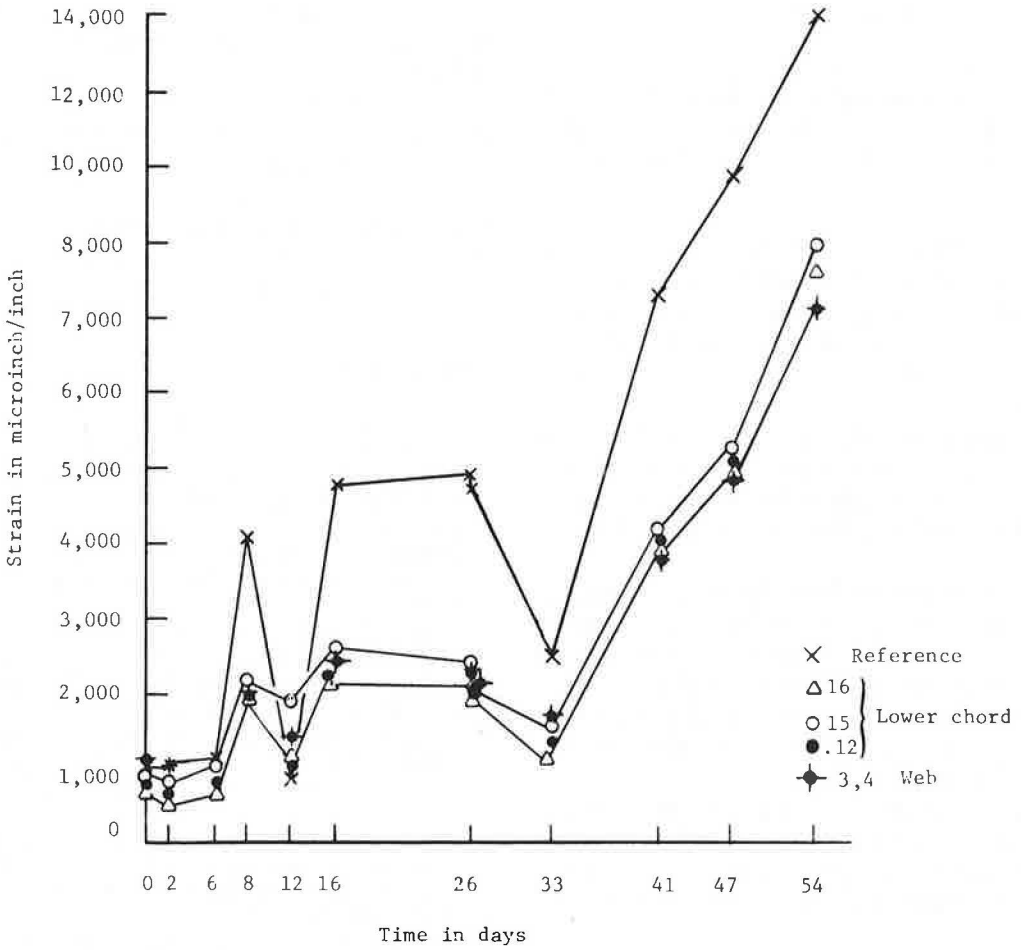

FIGURE 12 Strain in selected elements versus time with full live load.

considered reliable, it appears that no measurable creep occurred in the three lower chord and two web elements shown in Figure 12. The absence of detectable creep strain in the individual elements of the girders corresponds to the deflection measurements of the lower chord and the deck as discussed previously. The relatively low stresses developed in the elements due to the full live load accounts for the absence of creep in the composite material.

HANDLING AND TRANSPORTATION OF BRIDGE

Unexpected but valuable information was obtained when the superstructure was moved to the test site. The bridge was loaded onto a lowboy by means of a front-end loader and transported approximately 8 mi to the erection site. During loading and handling, the outside stiffeners at both ends of the center girder were broken where a lifting chain made contact. The extent of the damage to a stiffener may be seen in Figure 13. Aside from some abrasion on the edge of the cover plate on the deck, no other damage to any of the structural elements was observed. The displaced stiffeners were realigned manually with the lower chord connector and reinforced by cutting and bonding a pultruded GRP plate ½ in. thick to the mating

FIGURE 13 Damaged web stiffener at the end of the center girder.

stiffeners. The repaired members showed no distress during the load tests.

While improper handling of the bridge may have been disastrous, the episode just described turned out to be quite valuable because it provided a test of the toughness of the structure that would not have been conducted intentionally for fear of irreparable damage to the joints and elements.

ASSESSMENT OF PERFORMANCE

The following assessment of the performance of the GRP pedestrian bridge is based on both the qualitative observations made by the project director during the handling and testing of the structure and the quantitative data obtained from the load tests.

1. Elements of the superstructure resisted abuse from lifting and handling better than was anticipated from work with previous laboratory test specimens. Although it was demonstrated that elements could be fractured by highly concentrated forces from lifting chains or bars, the fractures were not extensive and were easily repaired.

2. The bond between the polymer concrete wearing course and the GRP deck plate remained intact throughout the removal of the superstructure from the abutments. No signs of distress or spalling were detected in spite of severe distortion of the deck assembly.

3. The method of supporting the bridge by distributing the bearing pressure from the seats to the faces of the vertical stiffeners at the ends of the girders was quite satisfactory. The elastomeric bearing pad apparently assisted in distributing reactive forces uniformly. However, it was inconvenient from a handling standpoint to be unable to rest the structure temporarily on a horizontal surface.

4. The influence of temperature changes was reversible but pronounced on strains in the elements and deflection of the bridge. The likelihood of large secondary stresses in the superstructure is high if thermal distortions are constrained by supports.

5. Strains appeared to be reasonably uniform along the different elements monitored during both the elastic and creep load tests. Stresses computed from measured strains did not exceed 10,000 lbf/in.^{2} at full live load.

6. Creep deformations in the elements and joints of the superstructure appeared to be nonexistent over the test period of 61 days.

7. The ratio of live to dead load for the creep test was over 3:1 and for the elastic test over 4:1. Even though the replacement of the structural concrete deck in the original design with a nonstructural wearing course reduced the calculated elastic strength capacity of the structure by 98 percent, the deflection of the prototype was less than three times that prescribed by AASHTO specifications.

REFERENCES

1. F. C. McCormick. Laboratory and Field Study of a Pedestrian Bridge Composed of Reinforced Plastic. In *Transportation Research Record 665*, TRB, National Research Council, Washington, D.C., Sept. 1978, pp. 99–107.
2. F. C. McCormick. *Modification Studies for a Bridge Girder of Reinforced Plastics*. VHTRC Report 77–R5. Virginia Highway and Transportation Research Council, Charlottesville, Va., July 1976, 29 pp.
3. F. C. McCormick and H. Alper. *Initial Studies of a Flexural Member Composed of Glass-Fiber Reinforced Polyester Resin*. VHTRC Report 73–R3. Virginia Highway and Transportation Research Council, Charlottesville, Va., July 1973, 28 pp.
4. F. C. McCormick. *Study of a Trussed Girder Composed of a Reinforced Plastic*. VHTRC Report 75–R6. Virginia Highway and Transportation Research Council, Charlottesville, Va., Aug. 1974, 40 pp.
5. F. C. McCormick and H. Alper. *Further Studies of a Trussed-Web Girder Composed of Reinforced Plastics*. VHTRC Report 76–R16. Virginia Highway and Transportation Research Council, Charlottesville, Va., Nov. 1975, 78 pp.
6. M. M. Sprinkel. *Polymer Concrete Overlay on Beulah Road Bridge*. VHTRC Report 83–R28. Virginia Highway and Transportation Research Council, Charlottesville, Va., Feb. 1982, 41 pp.

Publication of this paper sponsored by Structures Section.